Mechanochemical Polymerization and Planarization - A New Route towards Polymers & Graphene Nanoribbons

DISSERTATION

zur Erlangung des akademischen Grades

Doctor rerum naturalium
(Dr. rer. nat.)

vorgelegt

dem Bereich Mathematik und Naturwissenschaften
der Technischen Universität Dresden

von

M. Sc. Sven Grätz

geboren am 25.01.1990 in Nordhausen

Eingereicht am 11.09.2018

Verteidigt am 26.11.2018

Gutachter: Dr. Lars Borchardt

Gutachter: Prof. Dr. Stefan Kaskel

Die Dissertation wurde in der Zeit von 10/2015 bis 09/2018 in der Fakultät Chemie und Lebensmittelchemie, Professur für Anorganische Chemie I angefertigt.

This page is intentionally left blank

1 DANKSAGUNG/ACKNOWLEDGEMENTS

I would like to start with a clarification: the order in which different persons are mentioned here has no indication on the contribution they made during my PhD thesis and this list is by no means exhaustive.

At first, I want to thank Lars, because I would not be at the position I am right now without the help, guidance and the certain amount of warranted critique he gave me during the last three years. But his support started much earlier. It was under him that I started as a research assistant in my first year of studies, where he, together with OM, introduced me into the world of material science and, especially, porous carbon materials. I am very grateful for the freedom Lars gave me in my research, that quickly drifted away from the original goal of porous carbon materials back to my other passion – polymers. I want to also thank Prof. Kaskel for the resources he let me use during these years, the support he gave my application for the travel grant of the graduate school and the insightful discussions.

Irena, Volodymyr and Josch have my thanks for their help with dealing with all of the unexpected malfunctions of the adsorption devices and their help with interpreting the data acquired by this method. Volodymyr also introduced me to the facilities at BESSY and the neutron reactor BER, where he and Simon lay the foundation for our work on in situ methane hydrate investigations and spend many hours, days, nights and weekends together with me. In this context, I also want to thank Dirk and Nico for their experimental support during these times and the help they offered even at the odd hours of night.

While Mirian and En also spent time with me, fighting with the synchrotron in Berlin, I rather want to thank them together with Desi, Tina and Lars for the pleasant travels we had over the years. Whether it was looking for koalas in the trees of Australia, accidentally ordering tripe in Sevilla, trying to find a taxi in the middle of the night in Madrid or going shopping together, every time we travelled, there was fun to be had. Adding to this, I want to also include Sebastian and Erik (also known as Mechanocarb and Friends) in my thanks for their participation in different Mechanocarb group events, barbecuing, rafting, climbing and foremost bathing in

the hot-tub. I could also always count on the two of you in terms of honest opinions and help.

This thesis would not have been possible if I worked alone, therefore, I want to express my thanks to all the people that supported me during my many and sometimes chaotic experiments, mainly the whole AK Kaskel. I especially want to thank Doreen, Valeriya, Jason and Reinhardt for their help in the synthesis and characterisation of nanographenes. Characterization in general was a topic where I heavily relied on other people, for example Sebastian, who had to measure countless samples in the SEM and helped me with the auto-sampler of the pXRD; Elke that constantly had to switch the IR spectrometer back to ATR mode and then had to deal with my colourful samples; Jani and Kai for their help with the UV/Vis and ss UV/Vis respectively; Karl for his CHNS measurements or Ilka for her TGA measurements. I am also grateful for the support on the administrative side of things provided by Chris, Stefanie and Rüdiger.

Another major contribution to this work was brought by the students I had the pleasure of working with, my student assistants Sven, Sebastian Z. and especially Sarah, who spent hours upon hours synthesizing and purifying samples for me. Without their work, maybe half of the experiments presented in this thesis would have never been done. I am, therefore, especially grateful for their help during these three years. I was also lucky in being able to supervise the Master thesis of Bruno, Kensy and the Bachelor theses of Maike and Sebastian Z, all of which also contributed results used in this work.

Putting work aside, I also want to thank the people that helped me with my work-life-balance. I want to thank my friends from school, who stuck with me for the last eight years, leading to a plethora of philosophic discussions, excursions and hunts for, sometimes elusive, geocaches. Another group I held dear over all these years are my friends from the first year of study, Axel, Felix and Matze, with whom I shared time in three different countries and who are together with Olga and Erik also the main lectors of this work, thank you! At last I also want to thank my family who never failed to support me in my endeavours and my wife, who made the years in France enjoyable and never let me down ever since.

2 TABLE OF CONTENTS

LIST OF ABBREVIATIONS

AC	Activated carbon
BET	Brunauer-Emmett-Teller
Ca.	Circa
CV	Cyclic voltammetry
COF	Covalent organic framework
DCM	Dichloromethane
E.g.	Exempli gratia (lat.), for example
Et al.	Et alii (lat.), and others
Equiv.	Equivalents
EtOH	Ethanol
FT	Fourier transform
GPC	Gel permutation chromatography
GTM	"Gas and temperature measurement system" from Fritsch GmbH
IL	Ionic liquid
IR	Infrared
IUPAC	"International Union of Pure and Applied Chemistry"
LAG	Liquid assisted grinding
MALDI	Matrix assisted laser-desorption-ionisation
MAS	Magic angle spinning
MBM	Mixer ball mill (also: vibrational ball mill)
N. a.	Not available
N. s.	Not specified
NLDFT	Non-local density functional theory

NMR	Nuclear magnetic resonance
NPs	Nanoparticles
p/p0	Relative pressure
PA	Poly(azomethine)
PBM	Planetary ball mill
PDI	Polydispersity index
PSD	Pore size distribution
QSDFT	Quenched solid density functional theory
Ref.	Reference
Rpm	Revolutions per minute
RT	Room temperature
Si_3N_4	Silicon nitride, milling material
SEM	Scanning electron microscopy
SSA	Specific surface area
Ss	Solid state
TCCA	Trichloroisocyanuric acid
TEM	Transmission electron microscopy
TOF	Time of flight
TSE	Twin screw extruder
UV/VIS	Ultraviolet/visible
V_{Micro}	Micropore volume
XRD	X-ray diffraction
WC	Tungsten carbide (Element symbols), milling material
Wt%	Weight percent
ZrO_2	Zirconium dioxide, milling material

3 MOTIVATION

"The object of life is not to be on the side of the majority, but to escape finding oneself in the ranks of the insane."

- *- Marcus Aurelius, Roman Emperor*

As the roman emperor and stoic philosopher put it as early as 170 AD, we are condemned to repeat the failures of others if we follow the opinion and beliefs of the majority blindly. According to him, this inadvertently leads to us joining "the rank of the insane". So, what do we have to do to avoid this fate? In a more modern context, this phenomenon is called "thinking outside the box". And it is generally accepted that extraordinary results or breakthroughs happen if people decide to break with the standards and norms in their field. For example, if you are selling furniture and suddenly decide to stop assembling it and sell it to your customer as a giant jigsaw puzzle, your small business expands rapidly and becomes what one knows today as IKEA. This small step broke with the traditions in the field and nowadays this is more or less the standard. What does this imply for us, chemists? In my opinion, we need to stop fixing small problems and min-maxing existing procedures, but instead push towards massive innovations. A quick look at green chemistry nicely illustrates this problem.

The search for the ideal, environmentally friendly and preferably cheap solvent has been a persistent topic in general chemistry.[1,2] In the meantime, the abundant use of solvents in commercial manufacturing inevitably leads to a contamination of our water, soils, and air. In a batch operation in pharmaceutical or fine chemical manufacturing, solvents consistently account for 80 to 90 % of the mass utilization.[3] Facing these challenges, the effort in the development of "green" solvents and processes skyrocketed in the recent past and many consider ionic liquids a potent alternative to classical solvents.[4–6] However, one should keep in mind that not all ionic liquids are environmentally benign and a replacement of solvents does not deal with the problem at hand – it is just a small fix, but not a big innovation. In other situations, hazardous solvents like hexamethylphosphoramide – renowned for its high carcinogenicity – are used purely out of a lack of practical alternatives.[7] These points, among others, led to a mainly negative reception of chemical processes and the chemical industry by the general public.[8] As a matter of fact, the term "chemical"

is associated with health risk, evil and dangerous, however the term "chemical-free" is gaining momentum (17.3 mio. Google hits).

Taking all this into consideration, what is the big innovation needed in chemistry? If one considers solvents as the problem, then the logical step is to simply get rid of them altogether and only as a last resort replace toxic solvents with less toxic ones. Hence, the introduction of solvent-free methods needs to be one of the top priorities of chemists across all fields!

One approach to conduct reactions in the absence of solvents is mechanochemistry. Initiated and/or sustained by mechanical energy, mechanochemical reactions offer a sustainable alternative to many wet-chemical methods.[9] Due to the lack of solvents in mechanochemistry, several of the 12 principles of Green Chemistry are achieved solely by applying this methodology.[10] Innovative uses thereof have made their way into the fields of pharmaceuticals,[11–13] material synthesis[14–18] and, foremost, organic chemistry,[19–21] where the vast potential of this rediscovered field has been demonstrated. However, while mechanochemical reactions have been among the first reaction procedures in history, their full potential has not been explored during the most part of the 20th century, when flask reactions were deemed more sophisticated.[22] Hence, a lot of applications, reactions and mechanism in a ball mill are still left to be discovered or are not well understood yet.

In this context, I have dedicated this thesis to establish mechanochemical protocols for the fields of polymers and nanographenes. Both of those topics are, at the moment, dominated by solution-based synthesis, although the compounds produced are hardly soluble. Hence, solubilizing groups are introduced, in time and resource consuming steps, just to keep the starting materials and products from precipitating. Coming back to Marcus Aurelius, continuing to tackle these syntheses by established chemical procedures bears a sort of irony, in which solubility problems are not solved by avoiding solutions, but by making sure the chemicals stay soluble. This is an inherently futile approach for the ever-larger molecules desired by the community. Instead, stepping outside the comfort zone, developing the procedures necessary and embracing the, sometimes deemed "non-elegant" or "unsophisticated", mechanochemistry can be the impulse needed for these fields to push the materials out of the academic field and into their promising applications.

4 STATE OF THE ART

4.1 MECHANOCHEMISTRY*

Mechanochemistry† describes the field of chemistry in which chemical and physicochemical changes in materials are induced by mechanical energy. The discipline has a long and rich history and, owing to the solvent-free character of the method, is experiencing a renaissance at the moment. In the following chapters, I will discuss the history, theories and models of mechanochemistry, different types of mechanochemical reactors, and upscaling of mechanochemical reactions.

4.1.1 History Or "How Mechanochemistry Became What It Is Today"

Way before elaborate flask and distillation setups were used by the alchemists of the middle ages and renaissance, the mortar was the main tool of alchemy.[23] Scholars in ancient Greece noticed that the pistil not only crushed the substance, but also induced more surprising changes. In 315 B.C. the philosopher and natural scientist Theophrastus of Eresos‡ reported remarkable observation in his book "On Stones" (Περὶ λίθων).[24] While grinding cinnabar (HgS) with vinegar in his copper mortar, he witnessed the formation of mercury. Nowadays, this report is not only the first reported mechanochemical reaction, but also accounts for the first documented isolation of a metal from its ore.

The first systematic studies of a mechanochemical reaction are attributed to Matthew Carey Lea at the end of the 19th century.[25] The American chemist was investigating the influence of different forms of energy on silver halides. In doing

* This chapter was partly translated from German from the book chapter on tribochemical reactors that I wrote for "Handbuch Chemische Reaktoren: Grundlagen und Anwendungen der Chemischen Reaktionstechnik" (Live Reference ISBN 978-3-662-56444-8), which is currently in production.

† While the term mechanochemistry is used commonly for reactions in ball mills, other means of mechanical energy introductions include microwaves, ultra-sonication and anvil. Therefore, the term tribochemistry would be more precise for reactions inside ball mills. However, the distinction is quibbling at best and therefore I am going to utilize the terms interchangeably.

‡ Theophrastos of Eresos was a scholar of Aristotle. For his works on plants he is often considered the father of botany.[214]

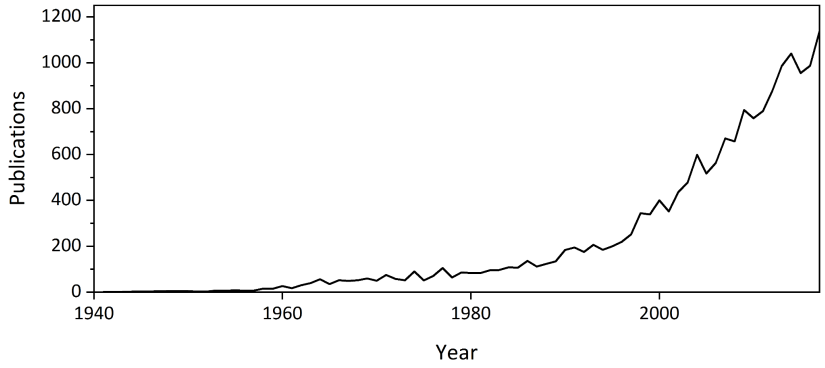

Figure 4.1 Development of the number of publications per year containing the keywords: Mechanochemistry, Mechanosynthesis, Mechanochemical.

this, he discovered several parallels between thermal, radiant and mechanical energy. In the early times of chemistry, however, mechanochemistry played only a marginal role next to the more sophisticated solvent-based chemistry. In 1923, Retsch was the first to introduce a motorized mill.[22] This mill imitated the manual grinding motion. It took until the 60s for a bigger community of mechanochemists to start working together in Eastern Europe and the USSR. They held conferences and focused on the understanding of this "new" method to conduct chemistry. In the following years, the cooperation between scientists from Europe, USSR and Japan was intensified and the first international conference on the topic was held in 1993.[22]

On the other side of the globe, scientists of „The International Nickel Company, Inc." (INCO) were the first to report alloying by the means of mechanochemistry in the late 1960s.[26] As a last resort, they used high energy ball milling to create a fine nanocomposite of nickel and oxides, that was then processed into a bulk material without melting the metal. From this point on, mechanical alloying developed as a separate field and, according to Takacs, "There were no cross-references between the two areas (mechanical alloying and mechanochemistry) for more than 20 years".[22] One main focus was the synthesis of amorphous alloys, where the ball milling methodologies proved to be a viable addition to existing methods.[27] Building on the knowledge acquired over decades, chemists started to mill metal powders in gas atmospheres and successfully created hydrides and nitrides in the process.[26] Therefore, mechanical milling extensively contributed to the field of hydrogen storage materials, where both the tuning of metal and metal alloy microstructures, and the direct synthesis of the hydrides are feasible in the ball mill.[28]

In the last 20 years, mechanochemistry has seen a surge in interest (**Figure 4.1**). Several reasons are behind the renaissance of the field. Besides the scientific potential of an unexplored field and a growing understanding of the processes behind these reactions, the trend towards "green chemistry" and a more sustainable future has led chemists to reconsider their basic tools. While the search for a benign and sustainable solvent is undoubtedly important, the complete absence of a solvent circumvents many entailing problems.[29] The promise of a solvent-free method might have been the spark that carried mechanochemistry at the start but it has since then shown to be more than this. Little by little it became apparent that selectivities in ball mills can differ from classical approaches.[30] In other cases unexpected reactions took place, ones never observed in solvent-based protocols. The reasons for these observations lie within the mechanistic differences between the two methods. An in-depth discussion will be lead in the following section.

4.1.2 The Basis of Mechanochemistry – Theories, Models and Terminologies

Mechanisms of many classical reactions are, by now, well understood. Decades of investigations of activation energies and kinetic behaviors of thermal and photochemical reactions have led us to a point where one can simulate isolated reactions *in silico* and predict a predict a plethora of reaction parameters with astounding precision.[31,32] The processes behind mechanochemical reactions are sadly not that well understood. The nature of massive metal or ceramic milling vessels and their fast movement makes *in situ* investigations challenging. Hence, there are still blanks in our knowledge regarding the precise processes taking place in a ball mill. Nevertheless, several theories have been established.

4.1.2.1 Hot-Spot Theory

One of the first observations made was the fact that mechanochemical reactions proceed in much milder conditions than their classical thermal counterparts. In response, Bowden, Tabor, and Yoffe postulated the so-called "Hot-Spot Theory" in the 50s.[33,34] The core of this theory is the claim that during a collision a small area of the powder (1 μm^2) is experiencing temperatures of over 1000 K for the fraction of a second (10^{-4}-10^{-3} s). This event is supplying the activation energy for the chemical reaction. While temperatures of this order of magnitude have been observed on the tip of propagating cracks in single crystals,[35] the theory itself is heavily disputed nowadays.[36]

4.1.2.2 Magma-Plasma Model

A more in-depth explanation for mechanochemical reactions is given by the so-called "Magma-Plasma Model" by Thiessen.[37] As with the "Hot-Spot Theory", he also assumes high energy densities at the time of the collision. The released energy is capable of forming a so-called triboplasma, which is characterized by the emission of excited particles (**Figure 4.2**). In the plasma, temperatures of 10'000 K are reached for time periods shorter than 10^{-7} s and cause chemical reactions. Even after the subsiding of the plasma, radicals and consecutive processes can trigger further reactions. This approach was the first to mention the possibility that mechanochemical reactions are not governed by just one mechanism but can follow different reaction routes. In addition, the short lifetime of the plasma does not allow

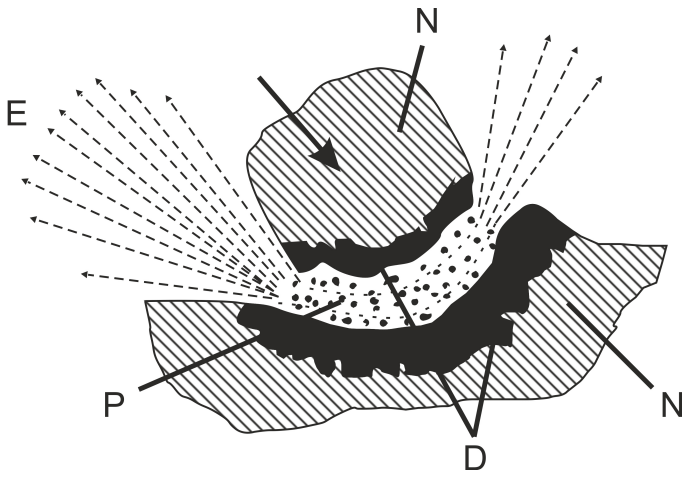

Figure 4.2 "Magma-Plasma Model" reproduced from Thiessen [31] E: excited electrons, N: non-deformed solid D: deformed surface layer, P: plasma.

for equilibration into a Boltzmann distribution. Therefore, chemical processes occurring in this phase may follow other pathways than their solution analoga.[38]

4.1.2.3 **Pseudo-Fluid Model**

Lately, both of the former models have come under severe scrutiny by the mechanochemistry community. *In situ* investigations showed a direct influence of the milling speed and vessel temperature on the reaction kinetics and thermodynamics of different organic reactions. If one assumed one of the older models to be correct, the vessel temperature would be of insignificant relevance, since the reaction is mostly happening as a result of the collision of the milling balls. On the basis of these findings, a new theory was established.[39,40]

$$k = \mathrm{A} * e^{-\frac{E_a}{R*T}} \tag{1}$$

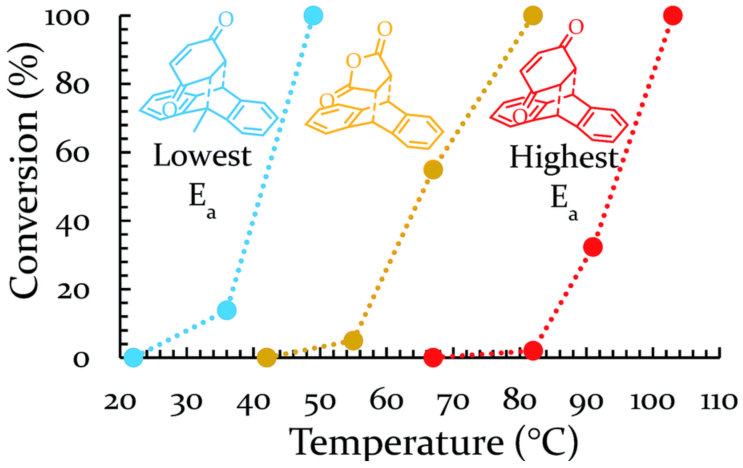

Figure 4.3 Influence of the vessel temperature on the yield of three Diels-Alder reactions with different activation energies. Copied from [40] – Published by The Royal Society of Chemistry.

If these results are evaluated in regards to the Arrhenius equation (**Equation 1**), it appears that the A-term is proportional to the milling speed while the energy term is dependent on the macroscopic temperature of the milling vessel (**Figure 4.3**). The impact energy is decoupled from the reaction enthalpy. The group of Emmerling went as far as to state that the "Magma-Plasma Model" and the "Hot-Spot Theory" play no notable role in the mechanochemistry of soft matter.[41] In this so-called "Pseudo-Fluid Model", the balls play a role smiliar to the solvent in a classical synthesis. Their main task is to ease diffusion and to help mix the reactants. In both functions, ball mills excel especially at high milling speeds. Powders are grinded down in the 100 nm range and every impact is creating a new reactive surface layer and diffusion problems are basically non-existent. Nevertheless, this theory cannot explain the fact that mechanochemical reactions often proceed at temperatures lower than their solvent-based equivalents.

4.1.2.4 **Quantum Chemical Calculations**

Another possible explanation is based on quantum chemical calculations.[42] Shear forces are capable of decreasing the HOMO-LUMO gap in molecules (**Figure 4.4**). This destabilizes the bond. If the mechanical force is big enough, the gap can be completely closed and an athermal reaction occurs. Even if the forces are insufficient to initiate such a reaction, the activation energy of the thermal reaction is lowered nevertheless. These calculations can explain two observations: firstly, the lower temperatures needed for mechanochemical reactions compared to solution-based one, and secondly, the sometimes "counterintuitive" products observed in these reactions.[42]

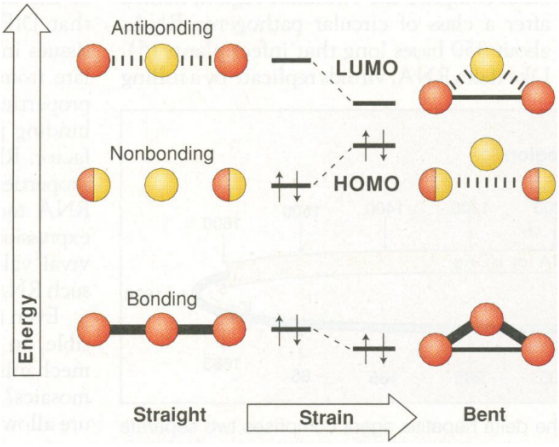

Figure 4.4 Walsh energy-level diagram for H_3^- visualizing the effect of strain on the HOMO-LUMO gap in the molecule. Copied from [42] with permission of "The American Association for the Advancement of Science".

4.1.3 Mechanochemical Reactors

Although ultrasound and microwave are also considered to be mechanical forces capable of influencing chemical reactions, the focus of this chapter will be on different tribochemical reactors, or, in other words, mills. These exist in various types and sizes. They most notably differ in the forces that are applied to the ground material (**Figure 4.5**), and therefore provide different degrees of applicability as mechanochemical reactors. Besides impact, pressure and smashing forces, shearing is of utmost importance if chemical reactions are of interest. Since most of the mills have been developed to reduce the particle size of a given material, it is up to the mechano-chemist to identify promising mills.[36]

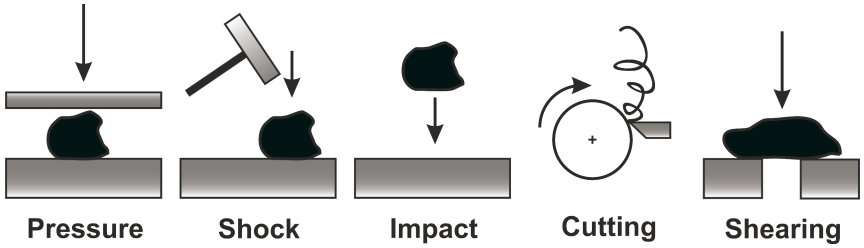

Figure 4.5 Main type of forces present during the milling process in different mills.

4.1.3.1 Vibrational Ball Mills

Vibrational ball mills, often called mixer mills, are one of two dominating mill types in the mechanochemical community. The vessel is subjected to a horizontal, vertical, elliptical, arc or eight-shaped movement. Due to the sudden changes in direction, the milling bodies, usually one to four balls, collide with the walls of the vessel as well as themselves, enabling mechanochemical reactions. For non-linear, elliptic or arc-shaped movement, the balls follow a chaotic pattern, thereby avoiding dead spots. Since the amplitude of the mill is fixed, the energy input is proportional

A B C

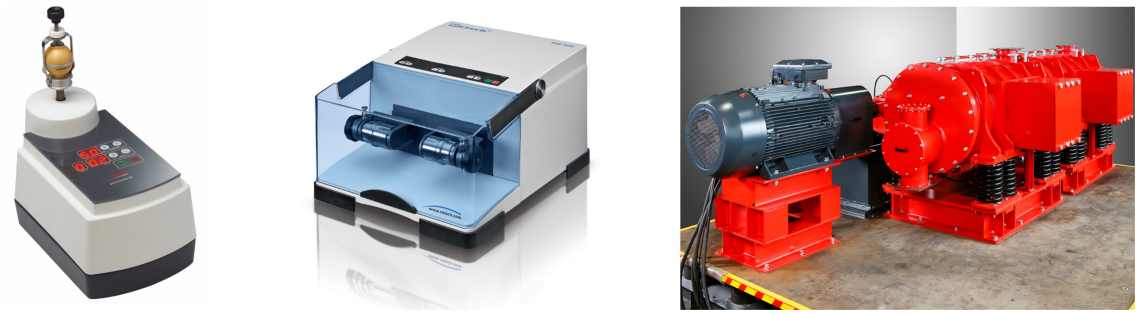

Figure 4.6 A: Mixer mill with vertical movement, Pulverisette 23, Fritsch GmbH. **B:** Mixer mill with horizontal movement, MM-400, Retsch GmbH. **C:** Eccentric vibrational mill, ESM-856-2K, Siebtechnik GmbH.

to the vibrational frequency. With vibrational frequencies, up to 50 Hz accelerations of up to 36 g can be reached in small laboratory mills (**Figure 4.6A,B**). Furthermore, a scale from 0.1 mL for the smallest vessels and up to several thousand liters for industrial eccentric vibrating mills (**Figure 4.6C**) can be covered with this mill type. This is further helped by the fact that industrial mills can usually be operated in a continuous or semi-batch mode.[36]

4.1.3.2 **Planetary Ball Mills**

In rotational ball mills, the vessels are moving in a circle around a fixed point. This causes pressure, impact, and shearing on the ground material. The simplest case, the drum mill is not that common in mechanochemical laboratories, since it lacks the energy necessary to induce or maintain a reaction. In order to achieve higher impact energies, these mills were improved upon resulting in the creation of planetary ball mills. In these mills the vessels are located on a sun-wheel and are rotating counterclockwise around themselves as they traverse the circle in a clockwise fashion (**Figure 4.7A**). The movement of the vessel around the fixed point guides the balls along the walls, whereas its rotation around its own axis detaches them from the wall and collides them with each other.[43] This working principle coupled with a high rotational frequency, creates strong centrifugal forces inside these mills, is resulting in accelerations of 50-100 g. The energy input of planetary ball mills is 100 to 1000-fold higher than for vibrational ball mills. This allows for very fast reactions and furthermore enables reactions that are not possible in mixer ball mills. One major drawback is the fact that this operating principle is hard to scale up in a secure manner and vessel sizes are therefore limited to 500 mL per vessel with a maximum of 4 vessels per mill (**Figure 4.7B**). In addition, it is hard to operate these mills in a continuous or semi-batch fashion. The higher energy variations,

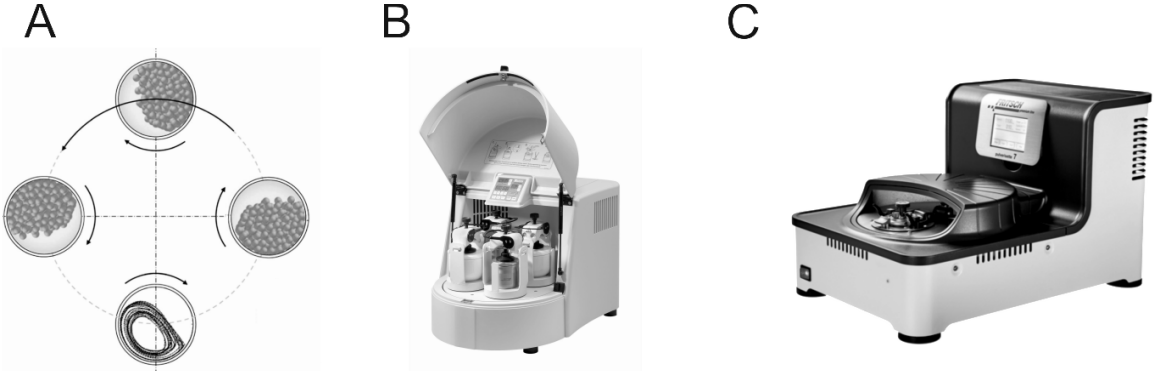

Figure 4.7 A: Principle of movement in a planetary ball mill, taken from [43] with permission of Elsevier. **B:** Planetary ball mill with four vessels, Pulverisette 5, Fritsch GmbH. **C:** High speed planetary ball mill with two vessels, Pulverisette 7, Fritsch GmbH.

however, often operate with only two vessels of smaller capacity (max. 80 mL) (**Figure 4.7C**).

4.1.3.3 **Extruders**

In recent years, ball mills have been accompanied by twin-screw extruders (TSE) as a scalable and continuous tool for mechanochemical reactions. They have been around in the food, pharmaceutical and polymer industries for decades and are commonly used to extrude polymers, cereal products and mix drugs with filler materials.[44–46] In the extruder (**Figure 4.8**), the material is forced into an eight-like motion by continuously being transferred from one screw to the other. In laboratory extruders, rotation speeds between 50 and 1200 rpm can be achieved, thus enabling a wide range of potential residence times and energy inputs. In contrast to a single screw extruder, the material is subjected to strong shear forces while passing inside a TSE.[44] This can be used in combination with heating segments, to conduct chemical reactions. This potential has been explored for several decades in the form of a reactive extrusion of poly(vinyl chloride), which has become a staple process in the polymer industry. Lately, mechanochemists have started to discover this method as a suitable way to scale-up mixer-mill reactions.[47] Processes in TSEs can have time yields of 1 to 6000 $kg \cdot h^{-1}$, depending on the extruder size. Smaller batches (gram-size) are also possible by employing bench-top machines.[48]

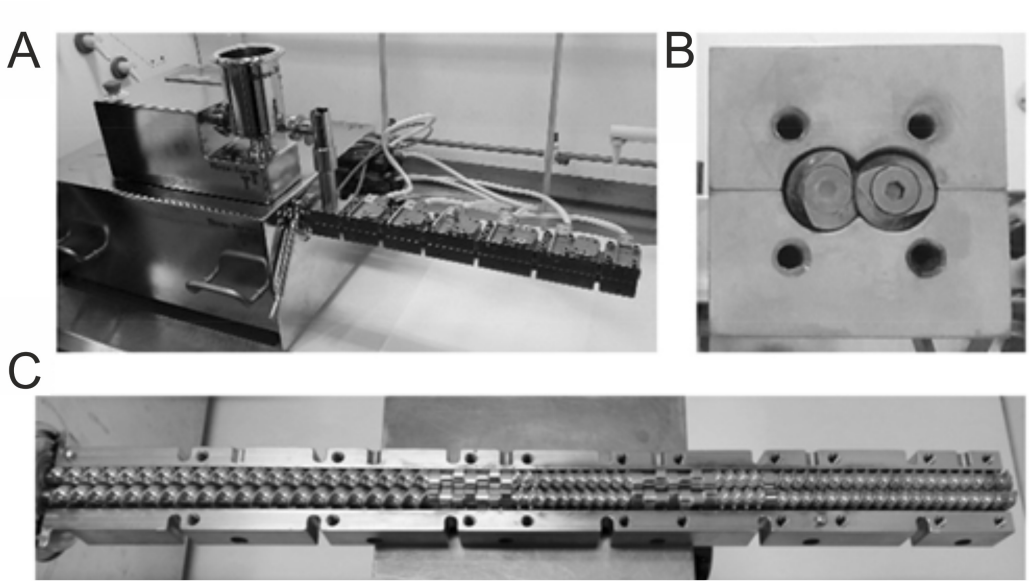

Figure 4.8 A: 12 mm laboratory twin-screw extruder with co-rotating screws and segmented heating jackets. **B:** cross-section of the outlet of said extruder showing the two screws intersecting. **C:** Screw-layout with different regions for mixing and knitting. Copied from [47] – Published by The Royal Society of Chemistry.

4.1.4 Parameters Influencing Mechanochemical Reactions

Mechanochemical reactions possess very different reaction parameters, compared to reactions in solution.[21] The solvent and, in turn, the concentration of reactants plays a minor role, while size and material of the milling balls are of pivotal importance.[49] In the following pages, I am going to discuss the influence of the parameters for vibrational and planetary ball mills, separating them into technological, chemical and process parameters.

4.1.4.1 Technological Parameters

All parameters determined by the milling body material are considered technological parameters, according to Stolle.[49] This includes ball size, count, and material, as well as the type of the ball mill. The material of the milling balls is crucial for the success of a chemical reaction. Besides the density, the Young's modulus is influencing the energy input of the milling process, since the energy of a moving body is proportional to its mass (**Equation 2**).

$$E_{kin} = \frac{1}{2} mv^2 \tag{2}$$

While density is important, other factors, like resistance against chemicals (acidic or basic conditions) and abrasion resistance, are to be considered if one wishes to conduct a reaction inside a ball mill. In the past, several materials have been identified as suitable for this purpose (**Figure 4.9** and **Table 4.1**). Abrasion occurs in all materials and slowly degrades the milling balls by diminishing their size and weight. Therefore, they have to be replaced from time to time, besides the fact that the product can become contaminated with this material. At larger scales, this can be a substantial cost factor. This is why, steel is the material of choice for industrial

Figure 4.9 Milling balls made from different materials and in different sizes. Back row from left to right: tungsten carbide, ZrO_2 (different sizes), silicon nitride. Front row from left to right: steel, copper, brass and nickel.

Table 4.1 Overview of typical milling ball materials and their properties.

Material	Main components	Density / $g \cdot cm^{-3}$	Abrasion resistance
Agate	SiO_2	2.7	Good
Sintered corundum	Al_2O_3	3.8	Moderate
Silicon nitride	Si_3N_4	3.3	Extremely good
Zirconium dioxide	ZrO_2, Y_2O_3	5.7	Very good
Steel, stainless	Fe, Cr, Ni	7.8	Limited
Steel, tempered	Fe, Cr	7.9	Good
Tungsten carbide	WC, Co	14.3	Very good
PTFE	C, F	2.1	Very good

scale applications, while ceramics are a less common alternative. For scientific research, however, zirconium dioxide and tungsten carbide are common milling materials, owing to their high chemical and abrasion resistance.

Alongside the material, the impact energy can also be altered by the size of the milling balls. Due to the fact that smaller balls also lead to a finer ground powder, the milling industry is supplying a wide range of ball sizes. Common sizes range from 0.1 to 30 mm, while mechanochemists typically employ the bigger end of the spectrum (5 to 30 mm) for their reactions. Besides the fact that bigger balls result in a higher energy input, they are also not as prone to sticking to one another if the powder becomes sticky during the milling process.

In addition to the size and material, the ball count is also essential for mechanochemical reactions. It directly influences the energy input of the reaction. While vibrational ball mills can be operated with a single ball, planetary ball mills needs several balls to ensure a sufficient number of collisions. In general, an increase in the number of milling balls leads to an increase in the energy input and thus faster reactions (**Figure 4.10A**).[50] Nevertheless, there are also examples of a decreasing yield with higher impact energies, since organic compounds may also degrade under these conditions. Besides these energetic implications, it is also crucial to maintain a certain free-volume inside the ball mill, where milling balls can be accelerated between collisions. In this context, the mill producers postulated the "1/3 rule", where one-third of the vessel volume should be filled with balls, one third with the powder and the last third should remain free to allow for sufficient ball

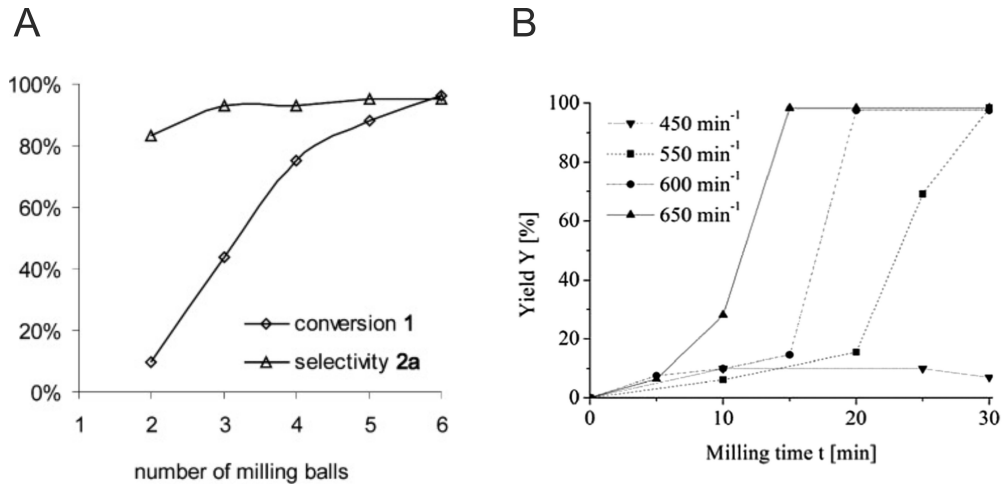

Figure 4.10 A: Influence of the number of milling balls on the reaction of *p*-toluidine (1, 2 mmol) to the corresponding azo compound with $KMnO_4$ as oxidant in a Pulverisette 7 (PBM), using agate balls (15 mm) from [50]. – Published by The Royal Society of Chemistry. **B:** Influence of the rotational frequency on the yield of the Knoevenagel condensation reaction between vanillin and babituric acid in a Pulverisette 6 (PBM) using tempered steel balls (20 mm) copied from [47]. – Published by The Royal Society of Chemistry.

movement. Although this is a generic guideline from the industry, scientific studies found comparable results for the optimal occupation of the milling vessel.[51] These findings also suggest a higher significance of filling the mill with one-third milling balls, to achieve an optimal balance of energy input and ball acceleration space, while the volume of powder used is only of minor importance.

4.1.4.2 **Process Parameters**

Process parameters like milling time and temperature are similar to their counterparts in classical syntheses, reaction time and temperature. For mechanochemical processes, these two are joined by the rotational or vibrational frequency of the mill, as well as the potential pause times in the milling protocol. The frequency is a very influential criterion, since it contributes quadratically to the energy of a milling ball (**Equation 2**, page 12). There are many studies investigating this relationship in regard to the yield and selectivity of tribochemical reactions. Commonly, the conversion increases with the rotational frequency (**Figure 4.10B**), while the selectivity can suffer from a higher energy input. Side reactions and degradation might be accelerated at the same time as the desired process. One major factor here is the increase in vessel temperature with increasing speed, leading to energy dissipation via friction.[52] If tungsten carbide balls are utilized, temperatures as high as 100 °C can be reached inside the vessel within minutes

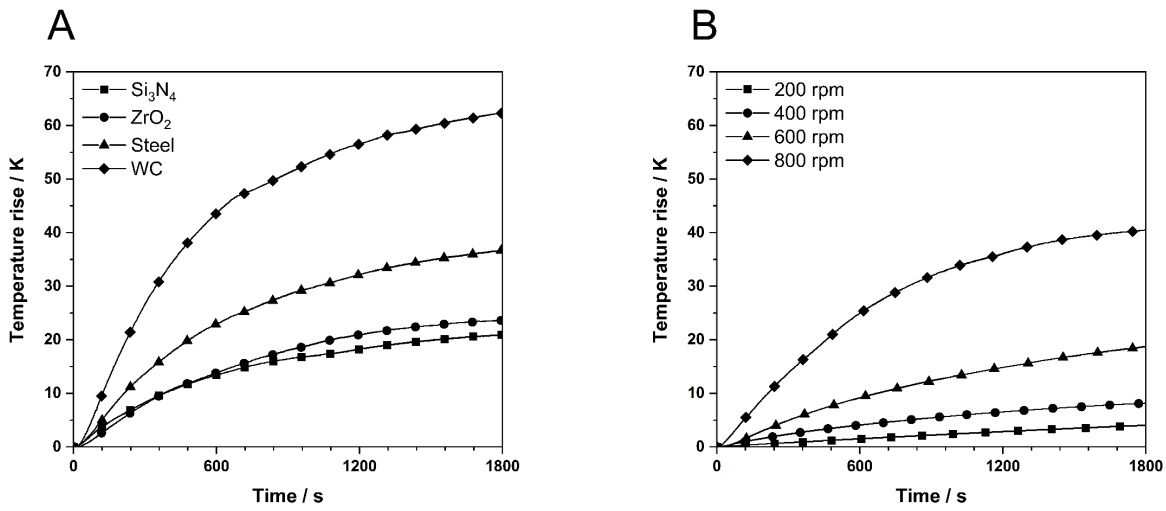

Figure 4.11 A: Influence of the milling material on the temperature inside the milling vessel. Measured in a Pulverisette 7 (PBM) with the GTM system utilizing a 45 mL beaker with 22 zirconium dioxide milling balls à 10 mm while milling potassium carbonate for 30 min. Adapted from [53]. **B**: Influence of the rotational frequency on the temperature inside the milling vessel. Measured in a Pulverisette 7 (PBM) with the GTM system utilizing a 45 mL beaker with 22 milling balls à 10 mm while milling 10 g of iron(III) chloride for 30 min at 800 rpm. Adapted from [52].

(**Figure 4.11**).[53] Considering that these temperatures are measured at the top of the milling vessel, and therefore outside of the chamber, the temperatures on the inside might exceed these measured values.* Furthermore, the thermal conductivity of the vessel material is also influencing these values. In order to avoid this heating, milling at high rotational frequencies as well as using big and dense milling balls should be avoided for sensitive reactants. It is also possible to cool the vessels with liquid nitrogen. This so-called "cryo-milling" is used especially for the grinding of viscoelastic materials.[54] For mechanochemical reactions, however, several studies have found this technique to lead to lower overall yields.[55,56] On the other hand, the vessel can also be heated prior to or during the reaction. This was used to determine the activation energies of a mechanochemical Diels-Alder reaction by Mack and co-workers.[40]

4.1.4.3 **Chemical Parameters**

Chemical parameters like solvent, catalyst or grinding auxiliaries can differ widely from process to process and are hard to discuss out of context. Hence, three important concepts of mechanochemical reactions related to those parameters are going to be introduced here instead.

* Especially planetary ball mills suffer from energy dissipation due to friction. In vibrational ball mills the temperatures reached during the milling process are significantly lower.

Although mechanochemical reactions are generally a solid-state method and do not require the addition of solvents, in some cases a few drops of liquid (<2 $\mu L_{solvent} mg^{-1}_{powder}$, **Figure 4.12**) can greatly accelerate the kinetics of a transformation. This method is called liquid assisted grinding (LAG). In such cases, the solvent is regarded rather as a catalyst than as a reactant.[57] While the mechanism is not completely understood at the moment, James *et al.* postulated that the increase of molecular mobility by small quantities of solvent is the source of this effect.[9] In some cases, even the selectivity of a process can be altered by the introduction of a LAG reagent.[58]

A bulking agent (also filling material) can be regarded as an inert additive to the reaction. The size of the milling jar (20 or 45 mL in our case) requires a minimum volume of reactants in the vessel (ball-to-powder ratio). Otherwise, the milling balls collide without transferring the energy of the collision onto the reactants and suffer enhanced abrasion. I employed an inert bulking agent, such as sodium chloride or an excess of one reagent like potassium carbonate, to gain control over the reaction scale. This method was first described by Konnert *et al.*[59] The bulking reagent can also be chosen to absorb one product, for example water, to avoid a slurrying of the reaction mixture inside the vessel.

Catalyst usage has one major advantage in mechanochemical reactions – they do not need to be soluble. Therefore, simple metal salts can sometimes be utilized instead of organic complexes.[60] Another elegant way of utilizing the milling process as an advantage was introduced by Mack and co-workers.[61] Instead of supplying the copper needed to catalyse a reaction as a powder or salt, they used copper milling balls and vessels in place of inert milling materials. This metal was used to co-catalyse cross-coupling reactions.[61] Thereby, their protocol completely circumvented the need for copper iodide as an co-catalyst in the Sonogashira reaction.

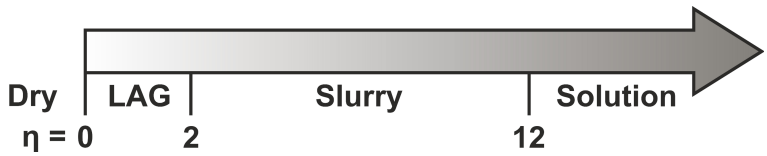

Figure 4.12 Classification of methods in mechanochemistry by the η-value ($\mu L \cdot mg^{-1}$). Most of them are in the range of dry grinding or LAG. Reproduced from [221].

4.1.5 The Versatility of Mechanochemistry

After detailing the history, mechanisms, machinery, and parameters present in mechanochemical reactions, I will use the following chapter to introduce the reader to the colourful and versatile landscape of mechanochemical reactions. Since the sheer number of organic reactions alone fills books, a few examples from several staple disciplines of chemistry have been chosen. For additional interesting ideas and applications please refer to the following reviews and books.[20,21,49,62–66]

4.1.5.1 Inorganic Materials

The most ancient and established field of mechanochemistry is the synthesis of inorganic materials. Faraday himself reduced silver chloride to metallic silver by grinding it inside a mortar as early as 1820.[67] Today, this technique is used to produce intermetallic phases and alloys in a straightforward manner by simply grinding the desired stoichiometric amount of metals inside a ball mill. The milling process frequently leads to the amorphization of the obtained materials. In addition, the required milling times are usually in the range of multiple hours to days. One prominent example is the reaction of the elements nickel, niobium and boron to yield the nanocrystalline $Ni_{75}Nb_{12}B_{13}$ phase under argon atmosphere inside a planetary ball mill (**Equation 3**).[68]

(3)

Reactions can also be observed for metal oxides, nitrides, halogenides, and sulfides. For the first case, binary oxides can be used in analogy to classical high-temperature synthesis of ceramics. Compared to those conditions, inert gases and long reaction times are not required in the ball mill. The synthesis of $NiFe_2O_4$ nanoparticles is only one example for the possibilities of this method (**Equation 4**).[69]

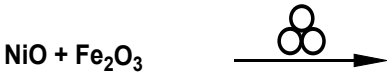

(4)

4.1.5.2 Co-Crystals and Pharmaceuticals

Another hot topic for the application of mechanochemistry on a larger scale is the synthesis of co-crystals. Co-crystals are single phase crystalline materials that

consist of two or more molecular or ionic compounds.[70] Several of the co-crystals synthesised via ball milling have yet to be reported by other means. One example is the co-crystal formed by grinding benzoquinone, bis-β-naphthol, and anthracene reported by Cheung *et al.* (**Equation 5**).[71]

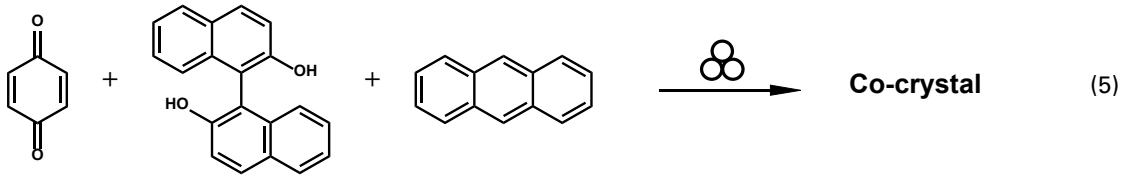

(5)

Co-crystals are of particular interest for the production of pharmaceuticals, where they can increase the solubility of the active pharmaceutical ingredient immensely.[72] As early as 1993, the self-assembly of 9-methyladenine and 1-methylthymine by grinding has been reported (**Equation 6**).[73]

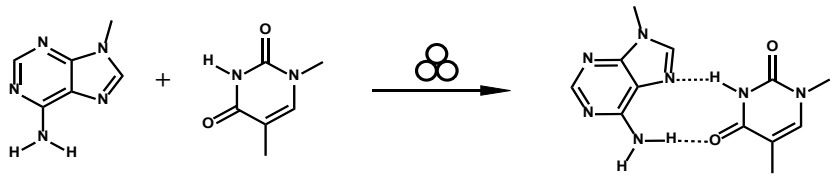

(6)

4.1.5.3 **Organic Synthesis**

Most of the organic reactions in the industry or in the lab are conducted in solution.[74] Especially in the last ten years, mechanochemists have shown that the majority of established reactions can also be transferred into the ball mill without the use of solvents.[49] Amongst these one can find C-C and C-X cross-couplings, metal catalyzed asymmetric transformations, substitutions reactions and many more. The Knoevenagel condensation was shown to proceed inside the ball mill in a matter of minutes as reported by Kaupp *et al.*[75] Furthermore, since this reaction proceeds quantitatively, no further workup is necessary (**Equation 7**).

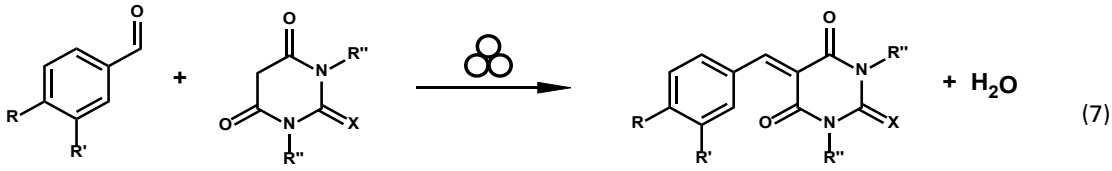

(7)

R = NMe_2, OH; R' = H, OMe; R'' = H, Me, Et; X = O, S

The proline-catalyzed aldol reaction is a common asymmetric organo-catalytic C-C coupling reaction. The group of Bolm has shown that under mechanochemical

conditions this reaction can be carried out with 10 mol% of prolin and produces yields of up to 90 % with high *ee*-values (**Equation 8**).[76]

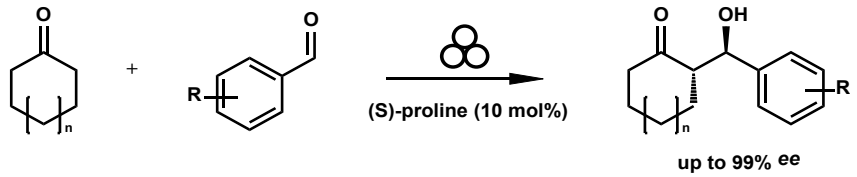

(8)

Another interesting aspect is the possibility to selectively generate reactive species inside the milling vessel and thereby notably reduce the amount of synthetic work. Borwne and co-workers recently demonstrated that an insertion of zinc into aryl or alkyl halogen bonds followed by a Negishi-cross-coupling (**Equation 9**) can be achieved by milling the materials together all at once. Or, as they describe it: "1. Add reagents to milling jar; 2. Screw jar closed (finger tight); 3. Press play".[77]

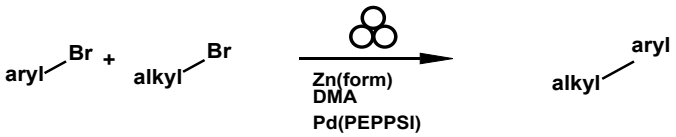

(9)

Sometimes mechanochemical reactions aimed towards replicating a reaction known from solution-based chemistry actually show a different reactivity or selectivity. Wang *et al.* tried to use the ball mill to conduct a hydrocyanation of the fullerene C_{60}. They soon noticed that the result was not the expected compound but rather the dimer C_{120} of said fullerene caused by a 2+2 cycloaddition (**Equation 10**).

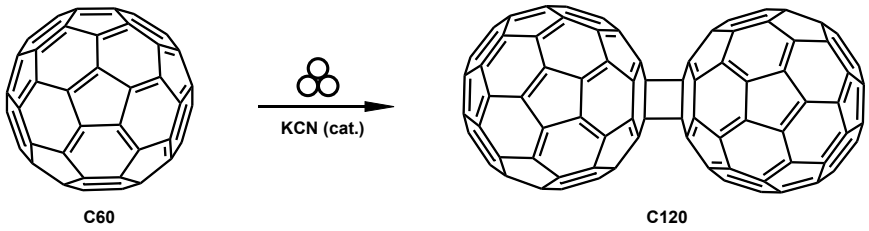

(10)

4.1.5.4 **Metal Complexes**

The synthesis of metal complexes inside the ball mill is closely related to the co-crystal formation discussed earlier. One advantage is the solvent-free nature of the ball milling process. This enables these methods to conserve resources and utilize readily available metal oxides. The group of Stuart James applied the mechanochemical procedure to synthesise zinc-salen complexes in a simple one-step reaction (**Equation 11**).[78]

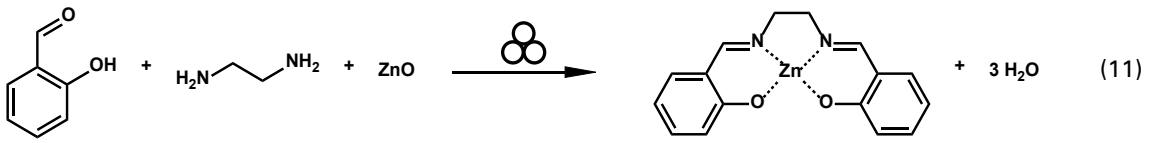

(11)

Another innovative example was published by the group of Friščić. They utilized the common solid state oxidant Oxone® (triple-salt of $KHSO_5$) to oxidize palladium in the presence of sodium halides and ligands to form catalytically active complexes (**Equation 12**).[79] This approach enables the swift upcycling of palladium wastes*.

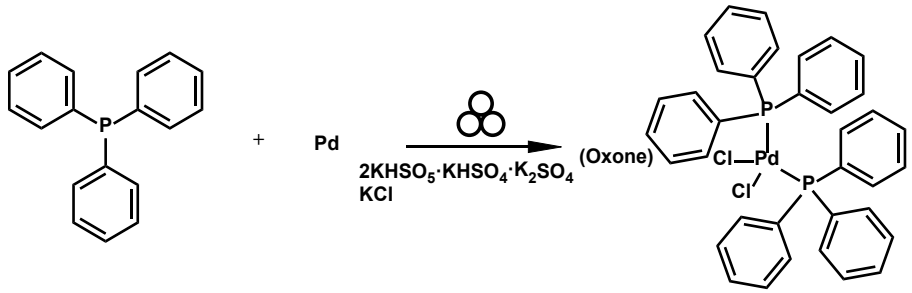

(12)

4.1.5.5 **Polymers**

One of the main focuses of this work was the development of a variety of polymerization reactions in this solvent-free environment. Nevertheless, prior to my research and while this thesis was in process, several methods of mechanochemical polymerizations have been reported by other groups. The first approach was published in 2010 by Posudievsky *et al.*, discussing the synthesis of poly (pyrrole), poly (thiophene) and poly (p-phenylene).[80] The synthesis of the conducting poly (thiophene) was achieved via an oxidative route utilizing ammonium persulfate (**Equation 13**). However, the method presented only yielded oligomers with a degree of polymerization between 6 and 20.

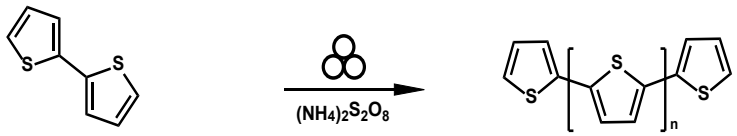

(13)

Yet another successful polymerization was reported by Ohn *et al.* Utilizing a base catalyzed ring opening polymerization, the group produced poly (lactic acid) (PLA) with high molecular weights of up to 100'000 $g \cdot mol^{-1}$.[81] As a biodegradable polymer, PLA is suitable to be produced by this green method (**Equation 14**).

* Palladium waste is commonly accumulated in organic laboratories, due to the fact that most cross-coupling reactions rely on palladium-based catalysts. Only a fraction of this waste is reused and most is discarded alongside other solid waste by-products.[215]

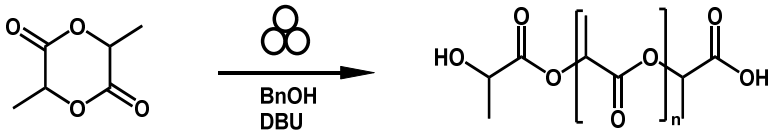

(14)

Coordination polymers are a special subclass of polymers. They consist of organic linker molecules and metal coordination centers.[82] Similarly to their 0D complex analogs, a wide variety of these 1, 2 and 3D materials can be synthesised mechanochemically. In contrast to solution-based protocols, solubility of the metal cluster is not necessary. Emmerling and co-workers published a protocol for several of these compounds, with one example being barium-based polymers with bicarboxylic acid linkers (**Equation 15**).[83]

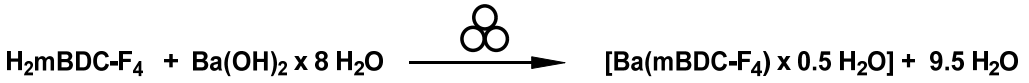

(15)

As a new and promising material class, metal-organic frameworks (MOFs) are sought after for their outstanding adsorption capacities and other adsorption related effects.[84,85] Due to the modular construction principle, many different varieties exist. For a several of them, mechanochemical reaction procedures have been developed in the past years. The group of James, for example, transferred the synthesis of $Cu_3(BTC)_2$ first into the ball mill and later to a twin-screw extruder. This method allows for the economically viable industrial synthesis of this compound (**Equation 16**).[48]

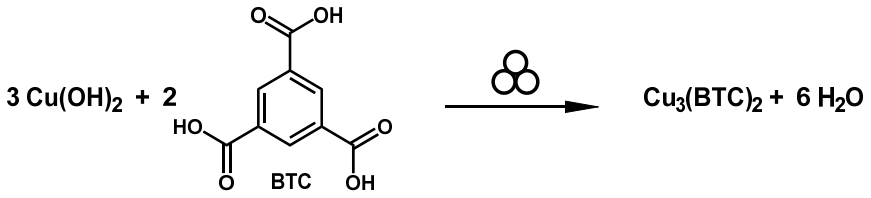

(16)

Porous structures can be built-up by different methods as well. One example is the mechanochemical Friedel-Crafts arylation of carbazole and cyanuric acid described by Troschke *et al.*[86] The so-formed covalent triazine frameworks (CTFs) possess a high thermal stability and surface area, making them the perfect support structures for heterogeneous catalysis (**Equation 17**).

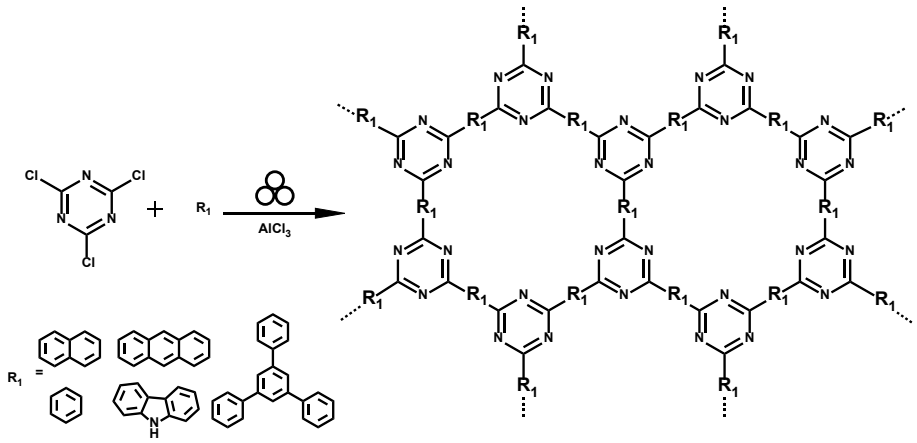

(17)

4.2 OXIDATIVE C-C COUPLING -THE SCHOLL REACTION

4.2.1 History

The Scholl Reaction, a reaction deemed unselective and uncontrollable by the organic chemistry community at the time, has found its true purpose as an intramolecular C-C coupling reaction.[87] It was first reported in the literature in 1873 by Dianin as the intermolecular coupling of 2-naphtol **1** to its dimer 1,1-bi-naphtol **2** in good yield (**Equation 18**).

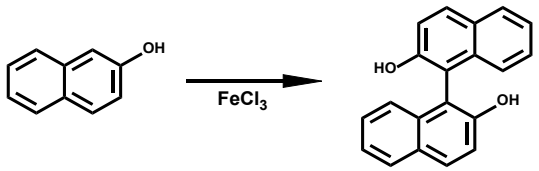

(1) (2), ca. 90 % (18)

Later on, a similar pathway was chosen by Scholl * and Mansfeld.[88] They reported on the planarization of meso-benzdianthron **3** to its π-conjugated counterpart meso-naphthodianthron **4** in an excess of aluminum chloride in less than 60 minutes (**Equation 19**). They point toward the importance of the exact temperature of 140-145 °C in order to avoid side reactions. Scholl and co-workers continued to improve and adapt the reaction and several other manuscripts in this field were published by them in the following years.[89–91]

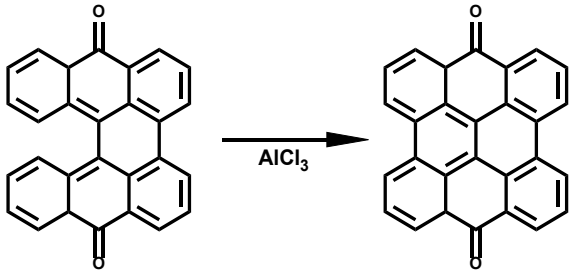

(3) (4), quantitative (19)

Although many changes have been brought to the procedure over the years, the reaction was forth on known as the Scholl reaction, a name still persistent up to this day. In the 1920s the synthesis was applied in an industrial scale to produce the colourant "Vat Green 8" **6** from **5** (**Equation 20**).[92]

* Roland Scholl 30.09.1865 (Zürich) – 22.08.1945 (Dresden); Professor in Karlsruhe (1904-1907), in Graz (1907-1914), in Dresden (1916-1934). Known for the oxidative coupling of PAH, first person to synthesize coronene.

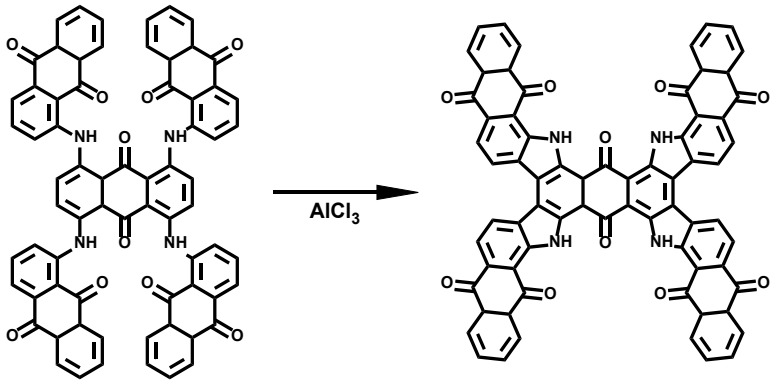

(5) **(6),** quantitative (20)

While the main driver of the research into the oxidative coupling reaction prior to the 2nd world war was in dye research, after 1945 this gradually shifted towards the synthesis of big aromatic hydrocarbons. Synthetically, many changes occurred during this time with the reaction protocol gradually changing from employing solid or low melting $AlCl_3$ compounds to solution-based reactions.[93] The oxidative polymerization of benzene in $AlCl_3$ and $CuCl_2$ introduced yet other conditions,[94] which were later on modified to 25 °C in $AlCl_3$, $Cu(OTf)_2$ and CS_2 by Müllen and co-workers in order to lower the reaction temperature.[95]

Hexa-peri-hexabenzocoronene (HBC, **8**) was first synthesised in 1958 by Clar *et al.*[96,97] Henceforth, a multitude of protocols have been developed, starting from hexaphenylbenzene (HPB, **7**), mediated by $CuCl_2/AlCl_3$, $AlCl_3/Cu(OTf)_2$, $FeCl_3$ or $MoCl_5$, that all lead to an almost quantitative yield. This is especially interesting since six C-C bonds have to be formed in the process.[93] In later years the Scholl reaction has also been successfully employed in the planarization of substituted HBCs (**Equation 21**).[98] Especially $FeCl_3$ seemed to be very tolerant towards bromine functions at the aromatic core.

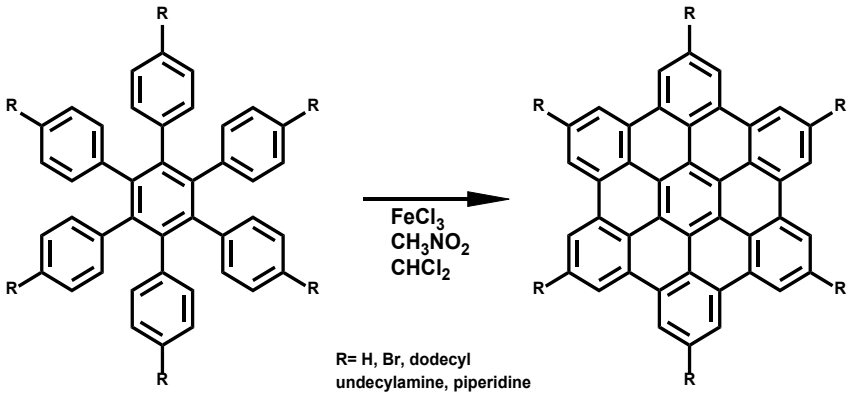

(7) **(8),** (87-93 %) (21)

4.2.2 **Mechanism of the Scholl Reaction**

In general, the cylodehydrogenation reaction can follow two pathways, an oxidative – the Scholl reaction – or a reductive one. For the Scholl reaction, there are two proposed mechanisms that seem to both have merit depending on the molecule and oxidant combination. The first proposed mechanism is closely related to the Friedel-Crafts reaction. Balaban and Nenitzescu even described the Scholl reaction as "the elimination of two aryl-aryl bound hydrogens accompanied by the formation of an aryl-aryl bond under influence of Friedel-Crafts catalysts".[92] Studying the mechanism of the Scholl reaction, two factions formed – one proposing an arenium cation mechanism[99] and the other favoring a radical cation mechanism.[100,101]

The starting point of the arenium cation mechanism (**Figure 4.13**) is the protonation of the aryl species to form an electrophilic σ complex **9'**. This complex is then capable of being attacked by another aromatic ring, forming a new carbon-carbon bond **9''** in the process. The last step is the elimination of dihydrogen to reform the conjugated system **10**.

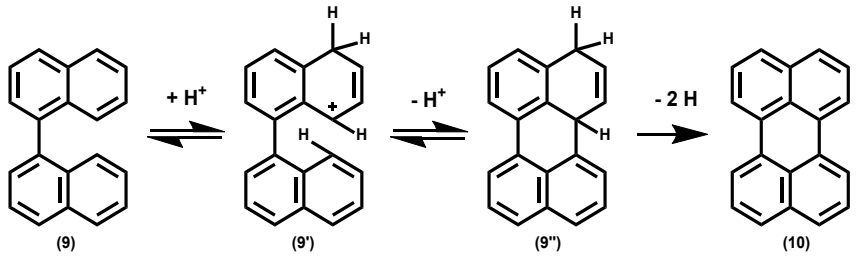

Figure 4.13 The arenium cation mechanism proposed for the Scholl reaction on the example of 1,1'-Binaphthyl (9). Alternatively, Lewis acids can also attach and create the σ complex **9'**.

A lot of experimental evidence supports this mechanism. One major piece of evidence is the observation that besides $FeCl_3$, $AlCl_3$ and other Lewis acids, anhydrous HF[102] or $PhSO_3H$[103] can cause a Scholl reaction. In these media, the radical cations proposed in the other mechanism cannot be formed. Furthermore, modern computational methods have shown that the arenium cation mechanism is thermodynamically favored due to lower energy transition states.[87,104,105]

In contrast, the radical cation mechanism (**Figure 4.14**) postulates the formation of radical cations **9*** in order to form a new carbon-carbon bond **9****. The last step is again the elimination of dihydrogen to reform the aromatic system. A problem in discerning between the two mechanisms is the fact that $FeCl_3$ – the most commonly

used reagent for the Scholl reaction – is a Lewis acid and an oxidant at the same time. Hence, it can cause both pathways to occur. To shed light on the controversy, using the mild DDQ-$MeSO_3H$ system, Rathor and co-workers presented strong evidence for the radical cation mechanism in the triphenylene synthesis.[106] They also point out that the reliance on strong oxidants to support the arenium cation mechanism is contradicted by the observation that even mild oxidants like air or iodine can produce the aromatization.

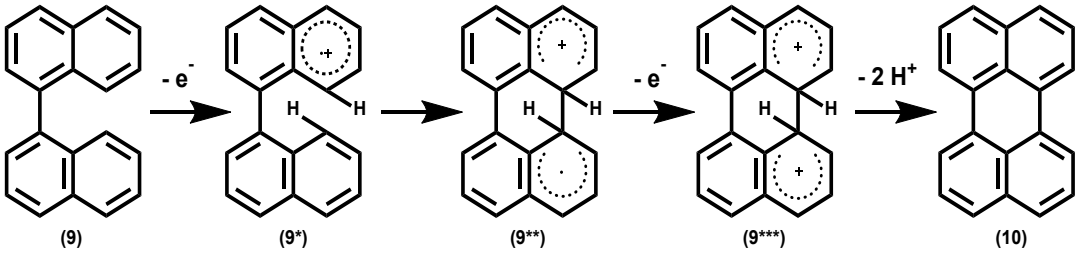

Figure 4.14 The radical cation mechanism proposed for the Scholl reaction on the example of 1,1′-Binaphthyl **9**.

Since both pathways have been reportedly observed – at least for some compounds each – it is valid to say that both of them describe feasible mechanisms for the Scholl reaction. Depending on the conditions, low or high temperature, strong or weak oxidant, the reaction seems to follow different pathways. Grzybowski *et al.* point out, that the high-temperature $AlCl_3$ reaction first described by Scholl is most likely obeying the arenium cation mechanism while the newer, low-temperature pathways, are more likely to progress via the radical cation route.[93]

4.2.3 Applications of the Scholl Reaction

As elaborated above, the Scholl reaction is the method of choice for the planarization of oligophenylenes. While the molecules synthesised in the times of Scholl do not attract as much interest anymore, they paved the way for a completely different chemical discipline. Since the isolation of Graphene in 2004*,[107] several pathways have been explored in order to achieve a controllable and scalable synthesis.[108] Chemists and physicists quickly realized that a defined edge-structure is of utmost importance to enable the use of graphene and graphene nanoribbons in electrical applications.[109] One method of synthesis that has been explored in this context is the bottom-up-approach. And as suggested by the name of this chapter, the Scholl reaction is an integral part of this process. Since most of the pathways towards nanographenes and graphene nanoribbons (**Figure 4.15**) proceed via twisted polymers or molecular precursors, their planarization is usually the last step in their preparation.[110]

Initiated by the fascinating chemistry of PAHs, the bottom-up synthesis of the latter has been investigated thoroughly. These efforts cumulated in the synthesis of the largest graphene molecule to date, the C_{222} – consisting of 222 carbon atoms –

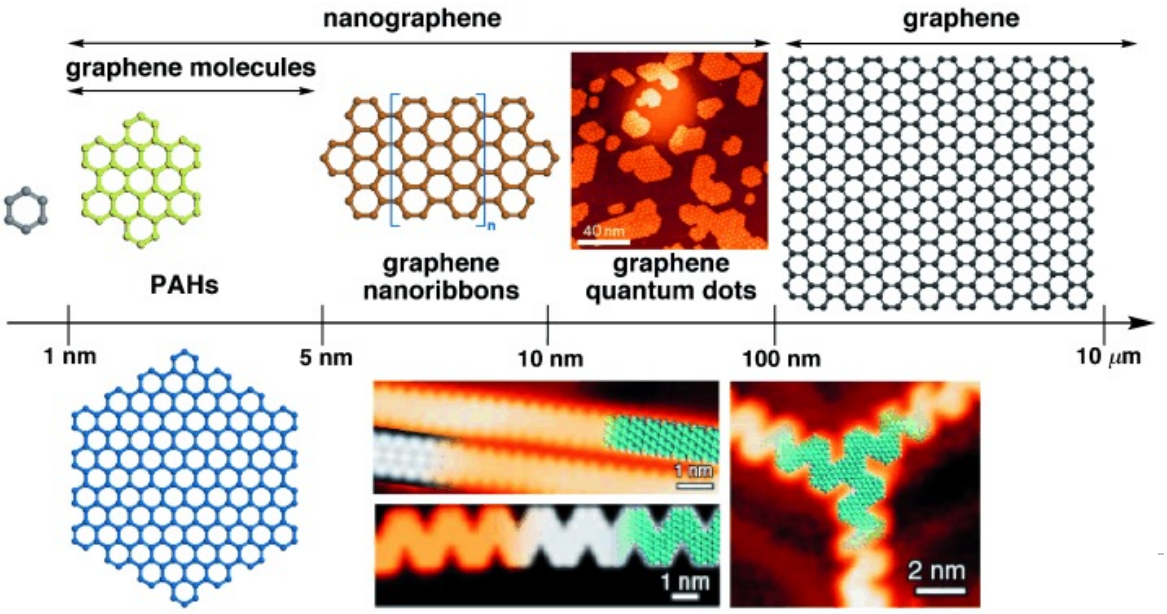

Figure 4.15 Classification of the graphene terminology illustrated over a large size scale. PAH or Graphene molecules make up the smallest sizes between 1 and 5 nm while graphene nanoribbons are strips with a maximum width of 10 nm and a length to width ratio of over ten. Copied from [110] with permission of "Wiley and Sons".

* For the isolation and characterization of graphene Andre Geim and Konstantin Novoselov were awarded with the Nobel Prize in physics in 2010.

with a disc diameter of 3.2 nm (**Figure 4.16**).[95] This molecule proved to be hard to planarize under the common Scholl conditions and a mixture of copper triflate and aluminum chloride in carbon disulphide finally led to the desired graphene molecule. This synthesis also highlights one of the major problems in this research field: while the precursors are twisted and therefore easily soluble, including in the case of C_{222}, the planarized molecules are basically insoluble in common organic solvents. A workaround applied by synthetic chemists is the introduction of solubilizing alkyl chains.[111] Another method reported is the edge-chlorination of these compounds by a post-treatment, as investigated by Tan *et al.*[112]

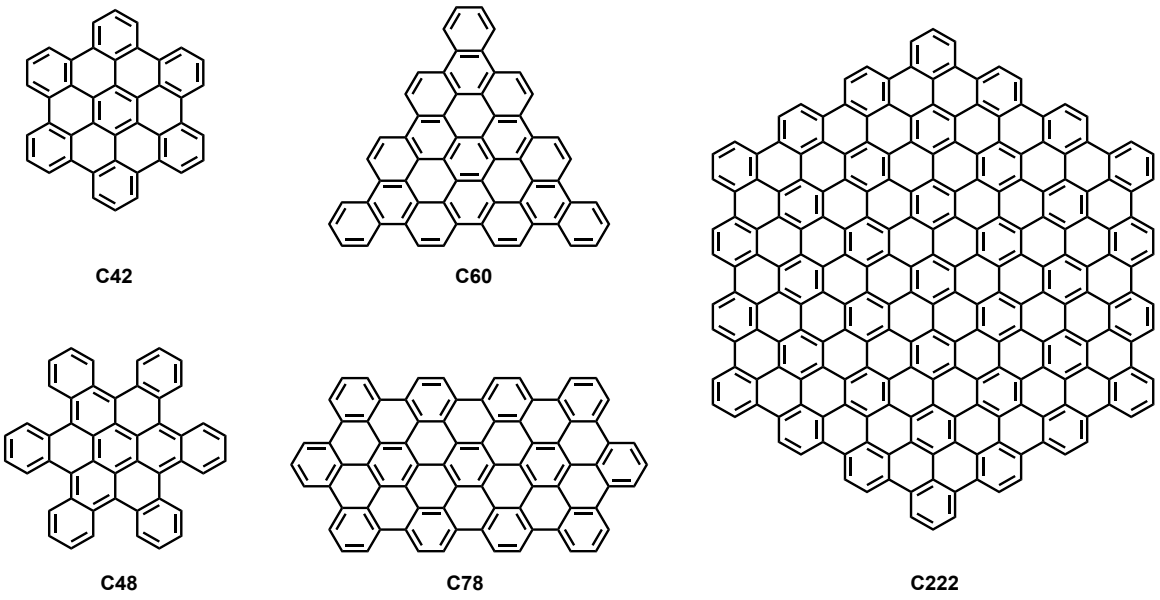

Figure 4.16 Examples of big graphene molecules, ranging from HBC (C_{42}) to C_{222}.

For smaller molecules like HBC, C_{60}, and others (**Figure 4.16**), solubility is still a problem, but their synthesis is generally more versatile allowing a tackling via multiple approaches. Their charm lies in the accessibility of different sizes, symmetries and edge compositions, allowing for the investigation of the latter in terms of energy levels and spin states.[113]

Since a synthesis of even bigger PAH has not been achieved yet – the synthesis of C474 was investigated but the planarization was only partial – the focus has since shifted to other molecules.[111] Graphene nanoribbons are typically synthesised by one of three methods. Besides a similar bottom-up approach, the two most common methods are the surface synthesis in TEMs and the unzipping of carbon nanotubes.[110] While there is a dehydrogenation step in the surface-based method, it

cannot be considered a Scholl reaction since it follows a reductive pathway.[114] In the past, several attempts towards the production of GNR by the bottom-up method have been undertaken but only a few of them led to long, soluble nanoribbons. One of the first approaches by Müllen and co-workers revealed that, although solubilizing dodecyl chains were introduced into the molecules, ribbons with more than 132 carbon atoms in their backbone could not be analyzed because of their lack of solubility.[115]

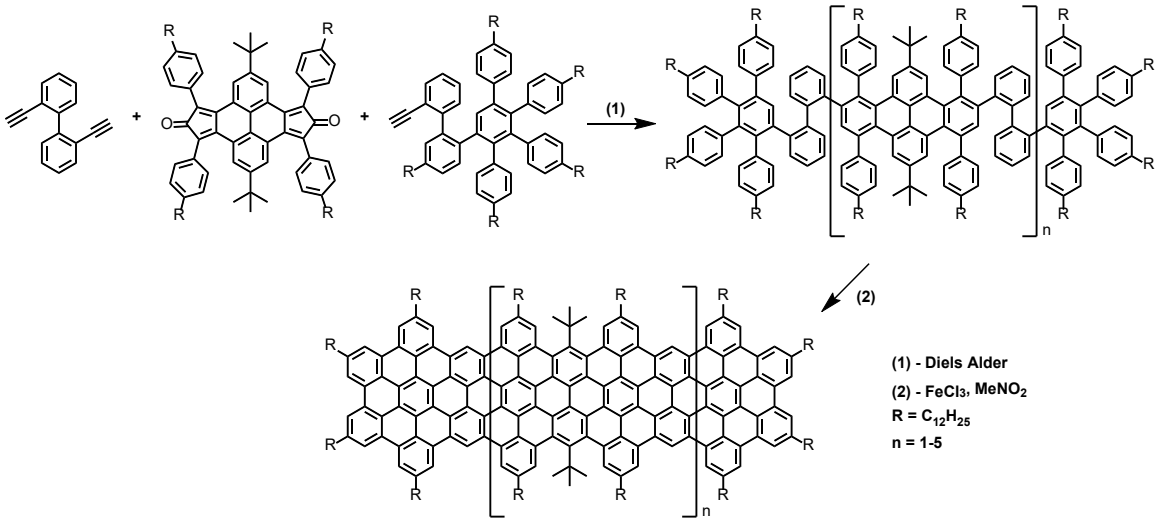

Figure 4.17 Synthesis of a nanoribbon with solubilizing groups. The irreversible Diels-Alder reaction is followed by a Scholl reaction to planarize the polymers. Reproduced from [115].

Consequently, other preparation methods have been proposed. Via the Suzuki polycondensation, ribbons with a length of up to 12 nm could be generated and successfully planarized via the Scholl reaction.[116] Even longer GNRs are accessible by utilizing a zigzag polymer backbone, which enhances solubility by itself, in combination with solubilizing groups. It was again a Suzuki polymerization, where this strategy was successfully implemented. Hereby, 40 nm long ribbons could be achieved.[117]

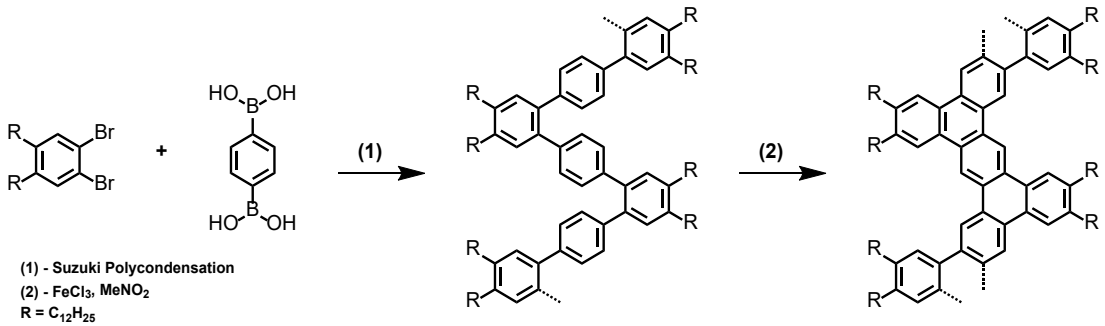

Figure 4.18 Synthesis of a kinked nanoribbon with solubilizing groups. The Suzuki Polycondensation reaction is followed by a Scholl reaction to planarize the polymers. Reproduced from [117].

Although, as outlined above, the Scholl reaction is a versatile tool for the planarization of GNRs, several problems were encountered during the years. One major drawback is that sometimes only partial planarization can be achieved,[118] while in other cases the regio-selectivity is unfavourable.[117] There are also reports of unexpected migrations and rearrangements during the Scholl reaction.[119]

To sum up this chapter, the potential of the Scholl reaction as an easy and relatively well-understood method for the planarization of nanographenes and graphene nanoribbons alike is apparent. One of the main challenges is the solubility of the reaction products, which has led to the extensive introduction of solubilizing groups. Appreciable solubility is usually only achieved in CCl_4 and CS_2, both solvents which should generally be avoided due to their toxicity and environmental impact. Therefore, it would be of considerable interest to develop a method to avoid toxic solvents and solubilizing groups altogether, while maintaining the general feature of high yields for this kind of reaction. For this reason, part II of this thesis is focused on establishing such a pathway.

5 Results and Discussion

5.1 Part I – Mechanochemical Polymerization

Mechanochemical reactions combine several beneficial traits for the synthesis of materials. Offering a fast and cheap way to produce tailored materials on a suitable scale, this methodology can tackle many persistent limitations of material synthesis at once. Especially in polymer syntheses, solubility problems scope and efficiency of viable polymerization reactions and thus the range of accessible materials. Therefore, it makes sense to apply mechanochemistry in this field. There are two main reaction pathways towards porous polymers: metal and non-metal mediated reactions.[120] Many of the underlying organic reactions are known to be accessible in a ball mill but only a few records of actually applying those to polymerization reactions have been reported prior to my entry into this field of research. This chapter is dedicated towards closing this gap by first of all applying known pathways to mechanochemical polymerizations and then expanding these towards "potentially"* porous polymers (**Figure 5.1**). In this context, several metal and non-metal mediated reactions are explored.

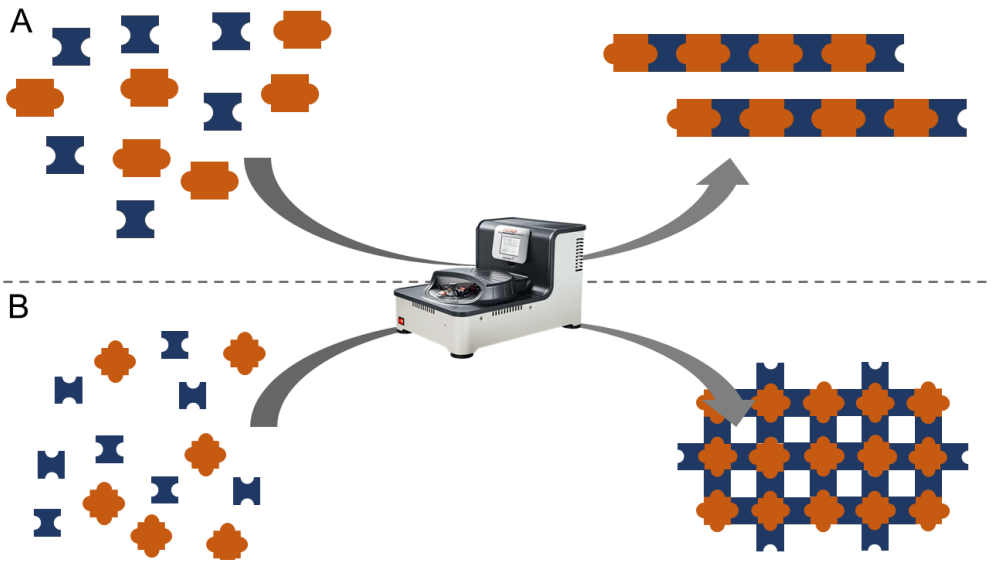

Figure 5.1 Scheme of a mechanochemical polymerization. **A:** A2B2-type polymerization towards a linear polymer. **B:** A4B2 polymerization towards a porous polymer.

* I chose the term potentially because, although the geometry and functionality of the monomers might allow for a porous structure of the resulting polymer, it is known from solution-based protocols that a collapse of the pore structure is sometimes hard to avoid.

5.1.1 Schiff Base Polycondensation*

Since polymerization reactions in ball mills are not well understood at the moment, the first objective was to shed light on how such a reaction is progressing in a ball mill. The phenol resins used by me earlier lacked the accessibility for common analysis methods due to their crosslinked structure. To avoid crosslinking while maintaining the reaction itself is not possible, this is why I switched to an easier controllable process in the form of a Schiff base reaction (**Figure 5.2**). First described by Kaupp and co-workers, the reaction between an aldehyde and an amine is progressing quantitatively in a ball mill.[121] They showed how promising this waste-free approach can be by synthesising twenty different azomethines. From a polymer scientist point of view, this system is prone to be investigated: not only is the reaction fast but the polymerisation by solution methods suffers from the bad solubility of the forming polymer – an issue not relevant for a solid state reaction.[122] To overcome this obstacle, either high temperatures, multi-step reactions or toxic solvents such as hexamethylphosphoramide have been employed in the past.[123] The resulting poly(azomethine)s (PA) are conjugated polymers that show a high thermal stability and photoluminescence.[124] Therefore, they are especially interesting for a potential application as transparent conductors,[125] liquid crystals,[126] aerospace coatings[127] and light emitting diodes.[128,129]

For the synthesis of the poly(azomethine), equal molar amounts of both monomers p-benzoldicarbaldehyde and p-phenylenediamine were mixed together in a zirconium dioxide milling cup (V = 45 mL) with 22 zirconium dioxide milling balls (d = 10 mm) and milled for 30 minutes at 800 rpm in a planetary ball mill. Throughout the study the milling material, speed and duration was varied to obtain insights into the polymerization mechanism.

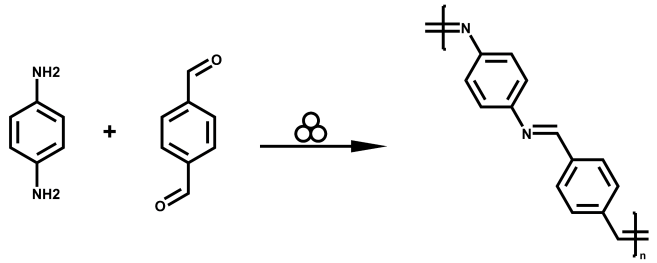

Figure 5.2 Polycondensation reaction between p-benzoldicarbaldehyde and p-phenylenediamine conducted in a planetary ball mill.

* Some passages in this chapter have been quoted verbatim from my publication in RSC Advances[199] – Published by The Royal Society of Chemistry.

5.1.1.1 Characterization of the Polymer

Due to the insolubility of the polymer in common solvents, none of the textbook polymer characterization methods could be applied and I had to resort to other means to follow the reaction. At first, the general success of the reaction was determined by IR spectroscopy (**Figure 5.3A**). The appearance of a vibration of the imine group at 1609 cm^{-1} as well as the fading of the vibrations of the carbonyl and amine groups at 1686 cm^{-1} and 1514 cm^{-1} respectively, prove the formation of an imine group.[130] While small vibrations for the C=O group are still remaining at around 1690 cm^{-1}, the vibrations of the N-H functionality at 1514 cm^{-1} and between 3000 and 3500 cm^{-1}cannot be found in the polymer. This might be due to a slight excess of p-benzoldicarbaldehyde which is caused by impurities in the diamine monomer or monomer getting irreversibly trapped inside the polymer either statistically or through supramolecular association. The high intensity of the C-H out-of-plane bend at 847 cm^{-1} is common for para-substituted phenyl units. In addition, the small bulge in the area between 3000 and 3500 cm^{-1} can be attributed to water released during the condensation reaction.

The polymer was also investigated using solid-state UV/Vis (**Figure 5.3B**). Samples after 1 minute, 5 minutes and 60 minutes were analysed. After only 1 minute of grinding, the formation of the product could already be confirmed by the appearance of the band around 400 nm (π - system) but monomer absorption bands at 259 nm and 305 nm from p-benzoldicarbaldehyde still remained in the spectrum.

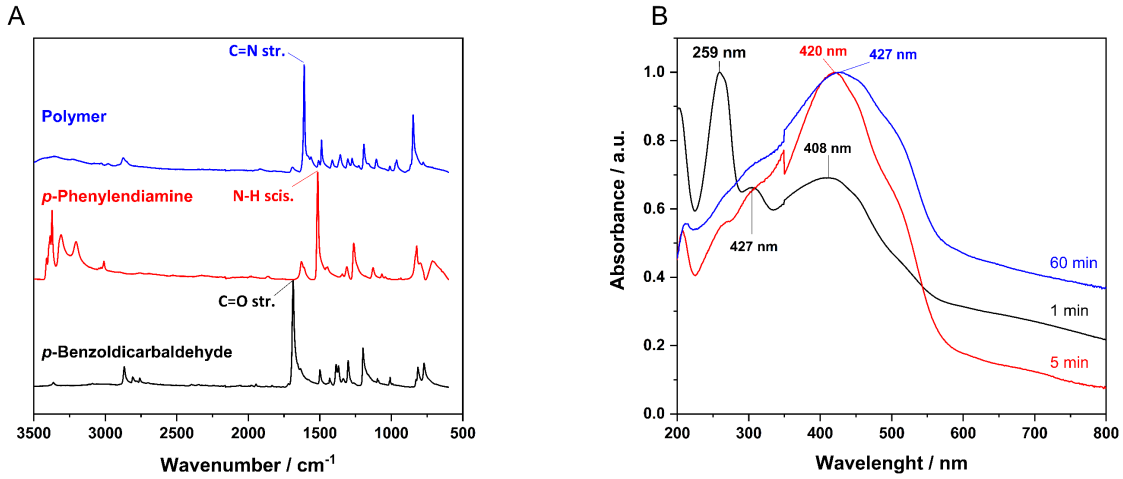

Figure 5.3 A: IR spectra of the monomers and the polymer yielded by ball milling after 40 min with 10 mm ZrO_2 milling balls. Important vibrations are marked. **B:** Changes in the ss-UV/Vis spectrum during the milling with 10 mm ZrO_2 balls at 1, 5 and 40 min. The maxima at 259 nm and 305 nm are from p-benzoldicarb-aldehyde while the ones around 420 nm are due to the π-system of the polymer.

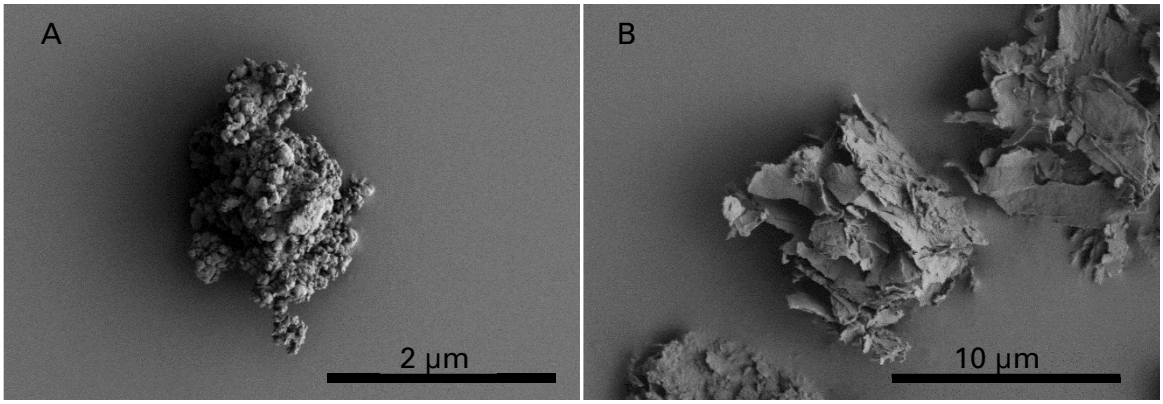

Figure 5.4 SEM micrographs of **A:** Polymer yielded by the mechanochemical reaction with 10 mm ZrO_2 balls after 60 min. **B:** Polymer yielded by solution polymerization.

Interestingly, only 5 minutes into the reaction the monomer peaks had almost disappeared completely and longer reaction times only lead to a bathochromic shift of λ_{MAX} from 420 nm to 427 nm. This is accompanied by a decrease of the optical band gap to 2.19 eV (**Table 5.1** and **Figure Appendix 1A**) – far superior to literature values of 2.50 eV.[130] This change can be attributed to the longer polymer chains and therefore bigger conjugated π-system achieved by the mechanochemical approach.

The morphology of the samples was investigated using SEM. A glimpse onto the SEM micrographs (**Figure 5.4**) showed agglomerated micrometre sized particles with a smooth surface. This contrasts with the reference material, synthesised in a classical solution polymerization, which formed flaky particles. In addition, EDX measurements were also undertaken and showed signs of abrasion for samples milled with either iron or tungsten carbide milling vessels and balls. But neither zirconium dioxide nor silicon nitride showed traces of contamination from the respective milling media.

Differences between the two polymerization methods could also be observed in the thermochemical behaviour of the materials. Investigations via DSC (**Figure 5.5A**) revealed a profound melting peak of the reference material at 375 °C with a melt

Table 5.1 Optical band gaps for polymers created with different milling materials with 10 mm balls and 60 min milling time. Optical band gaps were calculated from the solid state UV/Vis spectra using the Tauc plot.[131]

Material	λ_{MAX} / nm	Optical band gap / eV
Zirconium dioxide	427	2.19
Steel	428	2.21
Tungsten carbide	427	2.23

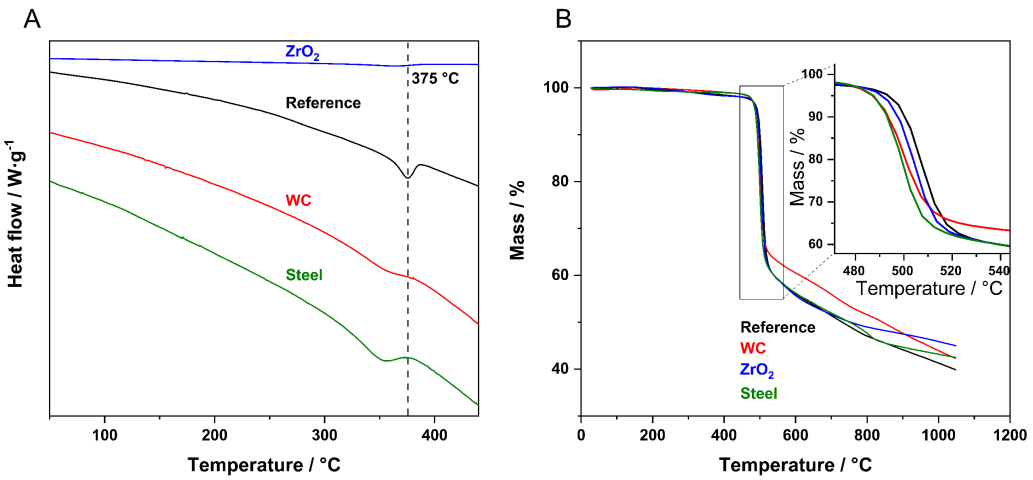

Figure 5.5 A: DSC curves of the polymers obtained with different milling materials and the solution reference. **B:** TGA measurements of the decomposition under argon of polymers obtained with different milling materials and the solution reference. The inlet shows the main degradation step in better detail.

enthalpy of -15.27 J·g^{-1}, while the melting peaks for the products in the ball mill were much broader with enthalpies only half as big and peak temperatures between 350 °C and 360 °C. Both effects are expected for PA with growing chain length and diminishing crystallite size.[132] The thermal resistance of the prepared materials with an onset of decomposition around 490 °C is quite high for polymers (**Figure 5.5B**).[133] The differences between both polymerization methods do not translate into differences in the degradation behaviour of the polymer.

All undertaken analysis methods point towards longer chains created by the mechanochemical approach but the absolute chain length is hard to determine for an insoluble polymer. Standard methods like gel permeation chromatography can only be applied to a soluble sample. I therefore decided to turn towards two different techniques to get a molecular weight for the polymers. At first, the problem was approached with dynamic light scattering. In general polymers tend to coil up in suspensions. The size of this coil is dependent on the molecular weight of the polymer. For an unknown polymer the calibration of this method, however, is impossible, since several samples with known molecular weight must be measured to create a calibration curve. In this case, with a volume mean diameter (determined by dynamic light scattering) of the polymer (**Figure 5.6A**) of 140 nm the ball milled sample is way bigger than the reference sample with 5.5 nm. Furthermore, after one minute the particle diameter of the milled sample is already as big as the solution reference. With longer milling times the value is reaching a plateau around 140 nm. Since the concentrations and dispersion time of the samples have been kept

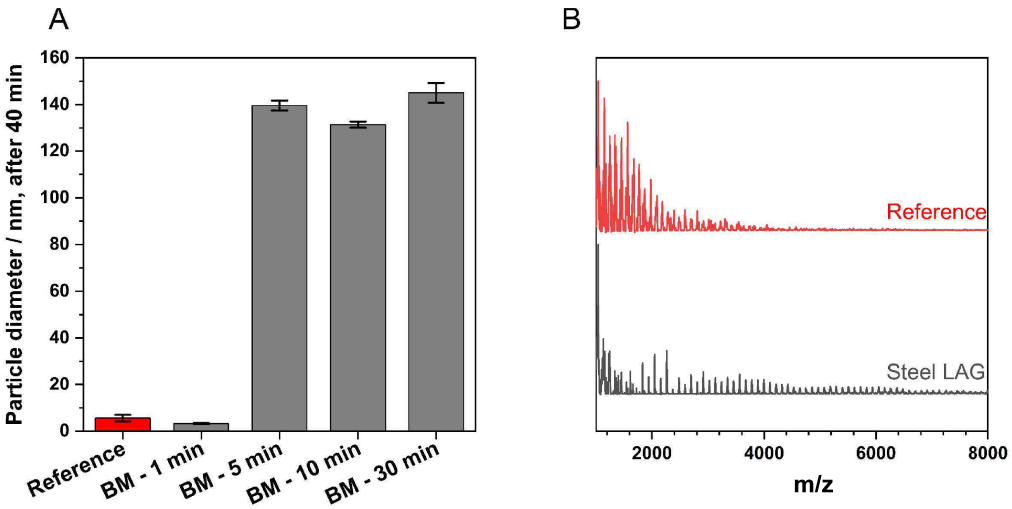

Figure 5.6 A: Particle diameter (volume mean) determined by DLS of the tungsten carbide LAG sample vs the solution polymerised reference (red bar) **B:** MALDI-TOF curves of the reference sample (red) and the Steel LAG sample (black). Dithranol with AgTFA was used as matrix.

constant, these values hint towards a higher molecular weight of the sample created by ball milling.

For further confirmation MALDI-TOF analysis of two samples was also employed (**Figure 5.6B**). Molecular weights were calculated by using the formula for the number average molecular mass (**Equation 22**), were I is the intensity of the MALDI-TOF signal. Here a short oligomeric character (M_n = 1700 g·mol^{-1}; Đ = 1.14) for the solution reference could be observed. The milled sample, however, shows a nearly twice as high molecular weight (M_n = 3010 g·mol^{-1}; Đ = 1.36).

$$M_n = \frac{\sum_{i=1}^{\infty} I_i M_i}{\sum_{i=1}^{\infty} I_i} \tag{22}$$

5.1.1.2 Investigation of the Mechanochemical Polymerization

For an in-depth investigation of the mechanochemical polymerization I focused on the influence of the milling material and the ball size in the second part of the study. In addition to the analysis methods presented in this chapter, the kinetics of the reaction was also studied, to compare said parameters better. Due to the poor solubility of the polymer, textbook methods could not be applied to this system. I resorted to the intensity of the carboxyl group in the infrared spectrum to follow the progress of the polymerization. To compare the integrals with one another, they must be normed to an internal standard. The CH vibration at 2850 cm^{-1} was chosen for this purpose. Since the intensity of a vibration in the IR range is linearly proportional to the concentration of the specific group, the peak areas present an easy way to monitor the reaction (**Equation 23**).

$$Conversion\ (t) = 1 - \left(\frac{A_{C=O}}{A_{C-H}}\right)_t * \left(\frac{A_{C-H}}{A_{C=O}}\right)_0 \tag{23}$$

At first, I was interested in the kinetics of the reaction in a ball mill. With the first experiments it had already been established, that the reaction is proceeding very swiftly. Polymeric products could be observed after as little as 1 minute of milling (cf. **Figure 5.3B**). The sampling intervals were tailored for this fast reaction. After several test runs, a sample was taken every 5 minutes in order to establish proper kinetics for the reaction. However, the biggest changes in the IR spectra can be observed at the beginning of the reaction (cf. **Figure Appendix 1B**). Via integration and normalization, it was established that the mechanochemical polycondensation

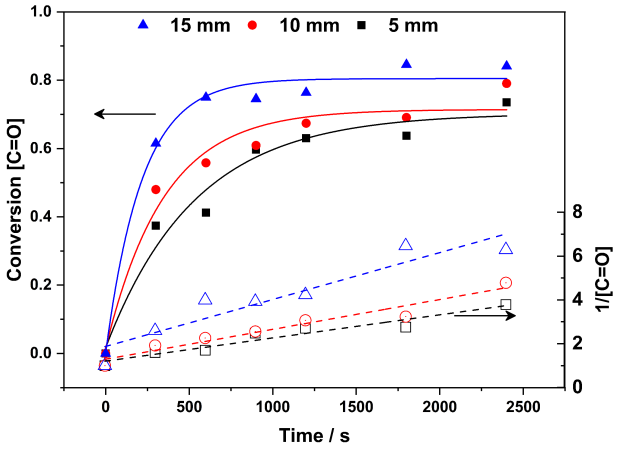

Figure 5.7 Conversion of aldehyde functionalities (full lines and symbols) and 2nd order rate law (dashed lines and empty symbols) in function of the zirconium dioxide ball size.

follows a second order rate law (**Figure 5.7**). This reaction order is to be expected for non-catalysed polycondensation reactions. However, since the processes inside the ball mill are less well understood and, in some cases, widely differ from solution-based analogues, this finding might prove useful in the future. On this basis, the milling ball diameter was varied to observe the differences in the kinetics of the reaction. From the literature it is known that, during the milling process, the ball size has two major influences on the result: first, smaller milling balls lead to a smaller particle size of the resulting powder, hence a bigger surface of reactants is available for the reaction. Secondly, the mass of the balls is proportional to their size and therefore the energy input during the reaction is increasing with bigger balls. The observations made confirm the latter (**Figure 5.7**). With an increasing ball size, one can observe a faster rate of the reaction (slope of the rate law curve). This observation was attributed to the higher collision energies of the bigger balls. In addition, the first statement can also be witnessed in these curves. While a plateau is reached for 15 mm balls after about ten minutes, for both the 10 and 5 mm milling balls the curve seems to be continuing with a different, slower, rate after the initial plateau around 1000 seconds. This effect could partly be due to a reduced "dead volume" (space were the balls cannot reach the powder) with smaller balls. In order to avoid this, another way to investigate the influence of energy input on the reaction had to be established.

Besides the ball size, the ball material is an easy way to vary the energy input in the reaction. In the following experiments a wide range of material densities from 14.89 g·cm^{-3} for tungsten carbide, over 7.9 g·cm^{-3} for steel to 5.7 g·cm^{-3} for zirconium dioxide has been explored. While the slopes in the 2nd order rate law also grow with the density of the material (**Figure Appendix 2A**), a better benchmark for the final polymer was needed. To easily compare the result, the focus was shifted towards the final conversion of aldehyde functionalities, according to IR measurements. This value (p) is of particular interest, since it is linked to the chain length of the polymer ($\bar{X}_n$) via the Carothers equation (**Equation 24**).[134] As it becomes apparent, this equation predicts that only at high conversions long polymer chains are obtained, while oligomers dominate beforehand. Consequently, the goal is to maximize the conversion to obtain polymers with a high degree of polymerization.

$$\bar{X}_n = \frac{1}{1-p} \tag{24}$$

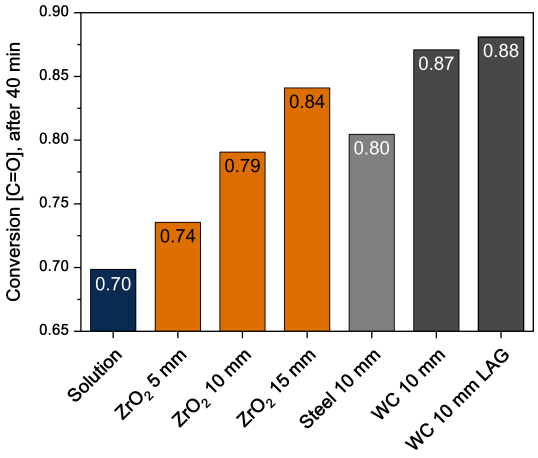

Figure 5.8 Conversion after 40 min for different milling materials, different ball sizes and with the addition of 0.2 µ·Lg^{-1} EtOH (LAG).

The trends observed for the kinetics hold true for the final conversion as well (**Figure 5.8**). The values are the highest for tungsten carbide and are very similar for steel and zirconium dioxide. While the sample milled with 10 mm zirconium dioxide balls is slightly worse than the steel sample, the 15 mm balls lead to a higher conversion and the 5 mm balls only marginally beat the solution-based process. However, all milling materials and ball sizes lead to a higher conversion than the reference sample. In an attempt to increase the conversion further, the influence of small amounts of solvents on the reaction (LAG), was studied as well. As described by Kaitner and co-workers, ethanol has a positive influence on the formation of azomethines.[132] For the mechanochemical polymerization, a similar trend can be observed. The samples created by LAG show a higher and faster conversion than the ones prepared by neat grinding. Moreover, the ethanol is also promoting a crosslinking reaction in the polymer backbone (**Equation 25**).[135,136] Since this is breaking the conjugated π-system and thereby increasing the optical band gap, the crosslinking can be seen in the solid state UV/Vis spectra (**Figure Appendix 2B**).

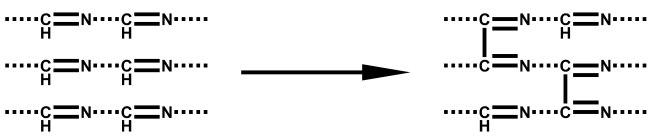

(25)

5.1.1.3 **Conclusion**

Overall, the mechanochemical Schiff base polycondensation reaction can be carried out in a solvent- and catalyst-free manner in a ball mill. The model system of a conjugated PA achieved high conversion in a short time. The polymers showed high thermal stability and low optical bandgaps. In all benchmarks the mechanochemically synthesised sample is outperforming or at least on par with the solution reference. The chain length of the latter is limited by its poor solubility while the solvent-free process is not having these constraints.

Furthermore, the influence of the milling ball size as well as the milling material on the polymerization reaction was investigated. Tungsten carbide milling material lead to the highest conversion but all mechanochemical syntheses yielded higher conversions than the classical solution polymerization. The energy input seems to be the key parameter which can easily be influenced by the milling material, ball size and potentially the milling speed. The reaction itself is progressing following a second order rate law in both systems. The addition of ethanol to the reaction mixture has a positive effect on the conversion. By applying this method to different monomers, these findings can lead to a scalable and sustainable production of PA.

5.1.2 **Suzuki Polycondensation***

After establishing the general possibility of polymerization reactions in a ball mill, a more complex system allowing for the possible synthesis of a broader field of advanced materials such as porous polymers,[137,138] graphene nanoribbons[139] and hyperbranched polymers,[140] was investigated. [141] In the past it has been shown that Sonogashira,[61,142] Mizoroki-Heck[143,144] and Suzuki-Miyaura[145] cross-coupling reactions can indeed be conducted mechanochemically.[146] The influence of base, catalyst and small amounts of solvents have been reported.[60,146,147] However, up to now, no mechanochemical cross-coupling polymerization has been reported. Indeed, such an approach would have an enormous potential in the synthesis of high performance materials.[148–150] Where many state-of-the-art synthetic protocols suffer from economic and ecological problems due to large amounts of toxic solvents and expensive catalysts involved, a mechanochemical approach has neither of those downsides. In this study, the focus was set on the Suzuki cross-coupling reaction as a versatile tool for the synthesis of poly(phenylenes). Poly(para-phenylene) is a conjugated polymer which has been studied intensively in the past,[151,152] for it is a promising material in organic photovoltaics and microelectronics.[153,154] The electrochemical[155–159] and solvent-based[94,160,161] synthetic procedures, however, suffer from low yields and low molar masses of the synthesised polymers. Utilizing a mechanochemical synthesis, one can demonstrate that these limitations can be circumvented. Alongside the linear polymers, hyperbranched polyphenylenes have been in the focus of the scientific community.[153,162,163] They combine the beneficial properties of the aromatic systems like a high temperature resistance with a good solubility and are therefore promising candidates for advanced coating systems and optical applications.[164–166]

In this chapter the influence of the milling material, the milling time and the catalyst concentration is investigated. In addition to the classical A2B2 approach (A2 = dihalogenide and B2 = diboronic acid), an AB (bifunctional, bromide and boronic acid) system is elucidated for a linear and an A2B1 monomer (trifunctional, dihalogenid and boronic acid) for a hyperbranched polymer system.

* Some passages in this chapter have been quoted verbatim from my publication in Green Chemistry.[53] – Published by The Royal Society of Chemistry.This work was further part of the master thesis of Bruno Wolfrum 10/16-03/17 that I supervised. He conducted most of the experiments. For publication the data gathered was interpreted and composed by me.

5.1.2.1 Model Reaction

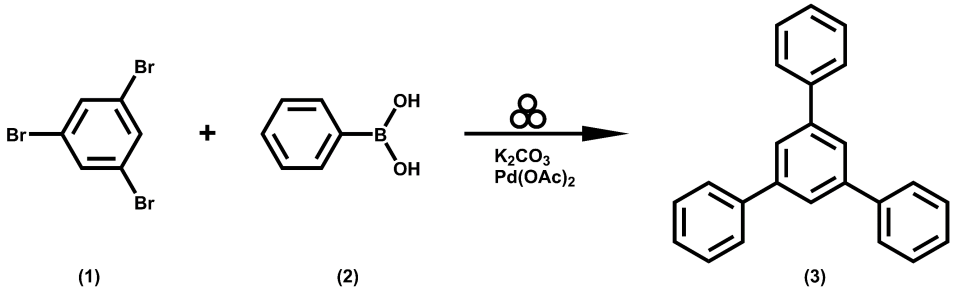

Figure 5.9 Reaction scheme for the model reaction between 1,3,5-tribromobenzene **1** and phenylboronic acid **2** towards 1,3,5-triphenylbenzene **3**.

In advance to the Suzuki polymerization, it was verified whether multiple couplings on the same molecule can be conducted mechanochemically, by utilizing 1,3,5-tribromobenzene **1** and phenylboronic acid **2** as model system (**Figure 5.9**). To achieve the desired product a stoichiometry of 1:3 was chosen. The successful selective multi-coupling was verified by IR spectroscopy and powder X-ray diffraction (**Figure 5.10**). The diffractogram not only reveals the success of the reaction, it simultaneously shows the absence of catalyst and wear debris in the product. The IR spectrum shows coherent results. While the O-H vibration (3260 cm^{-1}) is strong in the spectra of the boronic acid **2**, it is absent in the product. In addition, the C-B vibration (1348 and 1190 cm^{-1}) is disappearing as well, while the C-C (1555 cm^{-1}) and C-H (846 cm^{-1}) vibrations are enhanced. It was therefore concluded that the procedure is suitable to conduct multiple couplings without contamination.

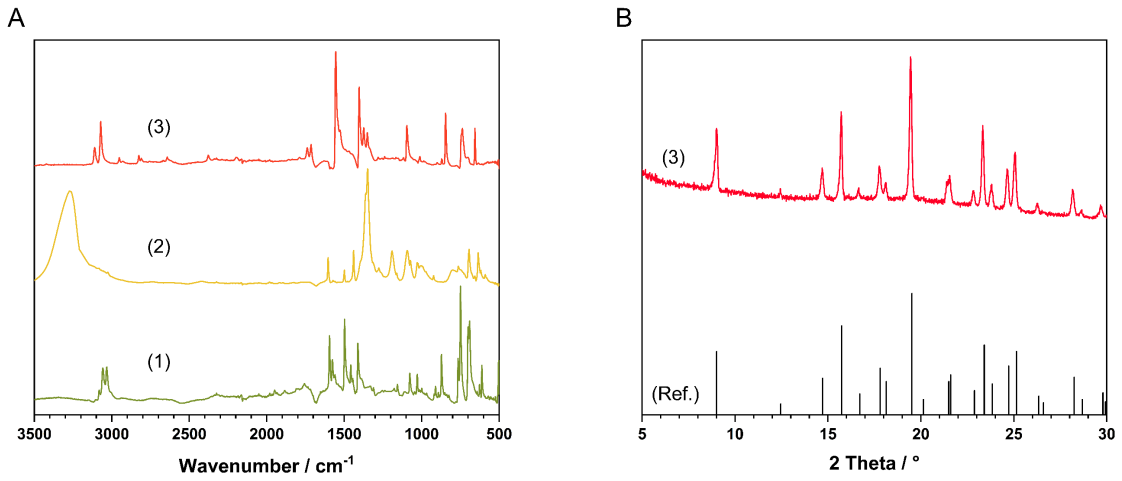

Figure 5.10 A: IR spectra of the substances 1,3,5-tribromobenzene (1) phenylboronic acid (2) and 1,3,5-triphenylbenzene (3) **B:** Diffractogram of **3** compared to a reference from the database (PDF: 33-1943).[222]

5.1.2.2 Linear Polyphenylene

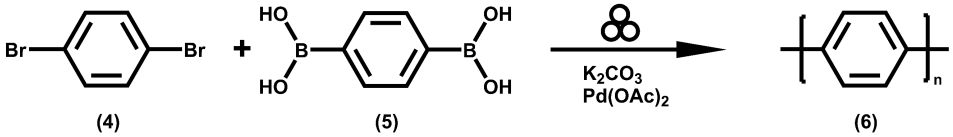

(4) (5) (6)

Figure 5.11 Reaction scheme for the A2B2 polymerization between 1,4-dibromobenzen **4** and 1,4-phenyldiboronic acid **5** towards poly(p-phenylene) **6**.

After the successful model reaction, the simple linear polymerization of the type A2B2 was attempted. In a preliminary investigation of the formation of poly(p-phenylene) (PPP (6)) (**Figure 5.11**) with zirconium dioxide balls, it was found that after 30 minutes a yield of 87 % was reached (**Figure Appendix 3A**). At this time the yield is not changing much anymore. Therefore, these conditions were chosen as the basis for further investigations. The nature of the cross-coupling reaction could be confirmed by the detection of potassium bromide in the mixture after milling. Furthermore, the absence of either base or catalyst in the milling vessel led to no discernible reaction. It is therefore safe to assume that the reaction is indeed a Suzuki polycondensation. Another important aspect to pay attention to prior to parameter investigations are possible side reactions. The selectivity towards polymerization via Suzuki cross-coupling was evaluated by homo-coupling attempts of the boronic acid and for the bromide under the same conditions. While the homo-coupling of the first lead to a 1 % of a polymeric product, no yield could be observed for the bromine. This is further confirmed by the absence of B-O and C-O vibrations at 1330 and 1080 cm^{-1} in the polymer and therefore by-products seem to be neglectable.[167] Consequently, the next challenge was finding an easy and preferably quick and practical way to evaluate the length of the polymer chain. The insolubility of the polymer made text book methods like GPC unfeasible. Once again, the IR spectra

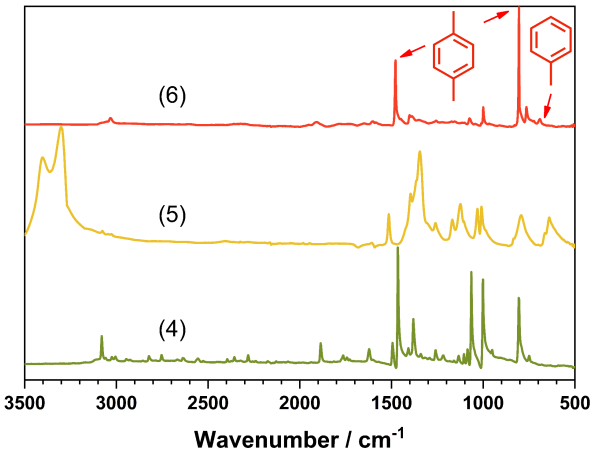

Figure 5.12 IR spectra of 1,4-dibromobenzen (4**)** and 1,4-phenyldiboronic acid (5) towards poly(p-phenylene) (6) Peaks corresponding to terminal and para substituted benzene rings are indicated.

turned out to be the remedy. The IR spectrum (**Figure 5.12**) is characteristic for a PPP, with the principal absorption band at 804 cm^{-1}. The smaller neighbouring bands at 765 and 690 cm^{-1} can be attributed to the vibrations of the terminal phenyl rings. Additionally, no 2,3-substitution (absence of bands between 860 cm^{-1} and 900 cm^{-1}) and no crosslinking (missing band around 1600 cm^{-1}) took place.[159] According to Aeiyach[158] and Lacaze[38] one can use these vibrations to approximate the degree of polymerization (DP) of PPP by utilizing **Equation 26**. Their work was later validated for longer polymers by Trivedi and co-workers.[159] For solution-based procedures DP's lower than 20 have been reported, while electrochemical methods reach values of up to 50 and CVD films have shown the highest value of 150.[168]

$$DP = 2 * \frac{I_{805}}{I_{690}} + 2 \quad (26)$$

By applying this equation to the polymers, the influence of several reaction parameters on the system was investigated. The A2B2 system shows varying yields between the different density materials (**Table 5.2**), with tungsten carbide (14.9 $g \cdot cm^{-3}$) resulting in a complete conversion, while silicon nitride (3.4 $g \cdot cm^{-3}$) only reached 43 % after 30 minutes of milling. For steel (7.9 $g \cdot cm^{-3}$) and zirconium dioxide (5.7 $g \cdot cm^{-3}$) similar yields of 83 and 87 %, respectively can be obtained in the same time. The DP was the highest for the zirconium system with 38, which is higher than conventional solution processes,[159] but still rather low. In addition, only small differences can be seen in the thermal degradation of the polymers (**Figure 5.13**), hinting towards only minor differences between the materials synthesised with different milling materials. Observing this material under the TEM, one can observe a sheet-like structure of the polymer (**Figure 5.13**). Besides the milling material, the halogen function plays a crucial role in a Suzuki cross-coupling reaction. While bromides and iodides are the go-to functionalities in the standard solvent-based procedures, chlorides require special ligands to yield the desired products.[169] For this

Table 5.2 Overview of linear polymer samples synthesised mechanochemically.

Polymerization type	Material	$[Pd(OAc)_2]$ / mol%	Halide	Yield / %	DP
AB3	ZrO_2	14.5	Br	78	-
A2B2	ZrO_2	9.3	Br	87	38
A2B2	Steel	9.4	Br	83	36
A2B2	WC	9.3	Br	100	27
A2B2	Si_3N_4	9.3	Br	43	21

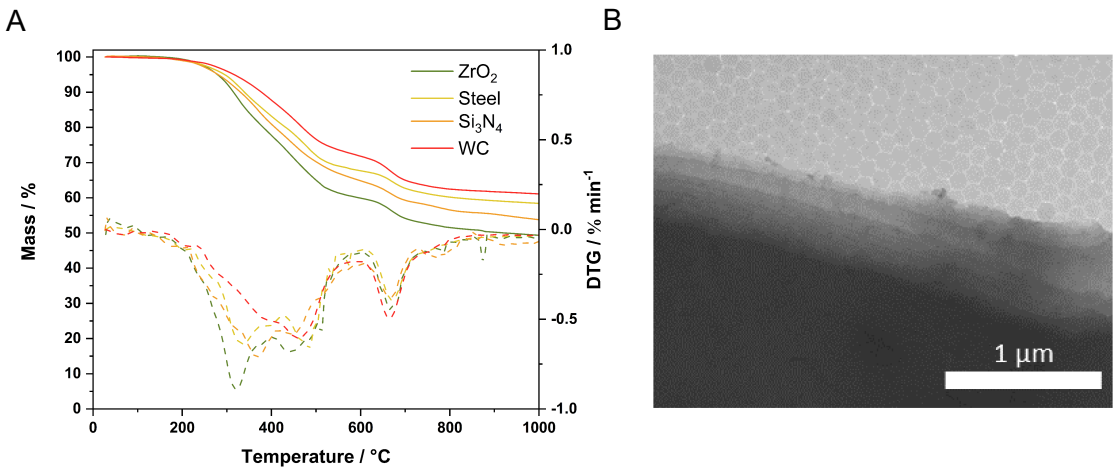

Figure 5.13 A: Comparison of the TGA curves of A2B2 polymers synthesized out of A2 monomers with different halogen functions. **B:** TEM micrograph of A2B2-1 (ZrO_2).

mechanochemical polymerization reaction one can observe a similar trend. While the chloride-based system only afforded a low yield of 10 %, the other halides, bromine and iodine, led to a high yield of 83 % and 86 %, respectively (**Table 5.3** and **Figure 5.14C**). Furthermore, bromide and iodide-based polymers also show similar bands in the IR spectra, whereas the chloride-based polymer in addition also shows bands of leftovers from the boronic acid (**Figure 5.14A)**. The highest DP of 21 could be found for the bromide and the iodide still reaches a DP of 17, while with chloride only 10 phenyl rings are connected after 30 minutes (**Figure 5.14C**). A look at the XRD curves (**Figure 5.14B**) paints the same picture, where the bromide-based sample has four clearly discernible reflexes, and both the iodide and the chloride samples only show very weak signals. The thermal degradation of the polymers (**Figure Appendix 3B**) is also revealing huge differences. Bromide and iodide-based polymers show a similar decomposition, with the iodide one having a delayed onset

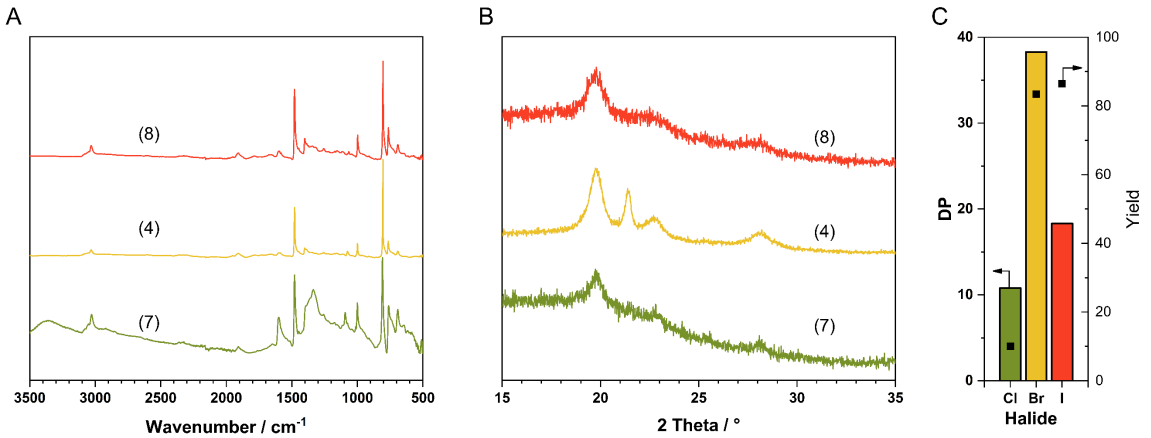

Figure 5.14 Comparison of different halides bromine **4**, chloride **7** and iodide **8** in the reaction with 1,4-phenyldiboronic acid. **A:** IR spectra; **B:** XRD-diffractograms; and **C:** Yield and DP of the different polymers.

Table 5.3 Influence of the halide used for the linear polymer samples synthesised mechanochemically.

Polymerization type	Material	[$Pd(OAc)_2$] / mol%	Halide	Yield / %	DP
A2B2	ZrO_2	9.0	Cl	10	11
A2B2	ZrO_2	9.3	Br	87	38
A2B2	ZrO_2	9.1	I	87	18

of the degradation. The polymer derived from the chloride monomer, however, is exhibiting a complete different behaviour. Form the differences in the spectra and thermal resistance it can be concluded that, due to the lower reactivity of the chloride functionality, the reaction is still unfinished, leading to short oligomers. Taking everything into account, one can state that bromide is the best functional group for the system, leading to the highest DP and yield, while also showing a defined polymer structure. In an additional study, the concentration of palladium catalyst introduced into the system was varied. Starting from 9 mol% as a reference point, it was reduced to 4.6 mol% and further down to 2.2 mol%. In the IR spectra as well as the XRD diffractograms, only small changes can be found (**Figure Appendix 4A,B**). The DPs of the discussed samples are also in a comparable range, between 19 and 38 (**Table 5.4**). As expected, the yield after 30 minutes is lower for the samples with reduced catalyst concentration than for the reference sample. One can therefore decide whether a fast reaction or a reaction with less catalyst is more beneficial for the given application.

Table 5.4 Influence of the amount of catalyst used on the linear polymer samples synthesised mechanochemically.

Polymerization type	Material	[$Pd(OAc)_2$] / mol%	Halide	Yield / %	DP
A2B2	ZrO_2	9.3	Br	87	38
A2B2	ZrO_2	4.6	Br	48	19
A2B2	ZrO_2	2.2	Br	31	27
A2B2	ZrO_2	0	Br	0	-

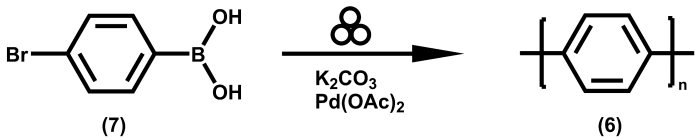

(7) (6)

Figure 5.15 Reaction scheme for the AB type polymerization of 4-bromophenylboronic acid **7** towards poly(*p*-phenylene) **6**.

The DP in polycondensation reactions is very sensitive to small deviations from the correct stoichiometry, as described in the Carothers equation (**Equation 27**).[134] By switching to an AB system (**Figure 5.15**), a perfect stoichiometry can be guaranteed at all points and therefore a higher DP is to be expected. To estimate the influence of this factor, the results obtained with the A2B2 monomer were compared to an AB type monomer (**Figure 5.16**).

$$DP = \bar{X}_n = \frac{1}{1-p} \tag{27}$$

The first observation was that all AB polymerizations lead to a higher DP than their counterpart in the A2B2 system, but in turn the yield was reduced. However, with a DP of 164, the silicon nitride milled sample is surpassing solution or electrochemical processes.[168] Interestingly, samples milled with zirconia balls for 60 minutes feature a lower DP than after 30 minutes. Taking also the rather small DP of samples milled with tungsten carbide and the outstanding DP of samples milled with silicon nitride into consideration, it is safe to assume that the high energy-input of high density milling materials and/or longer milling times cause a degradation of the formed polymer. In order to confirm this theory, SEM pictures of the samples were taken. For the zirconia milled samples (**Figure 5.17A,B**), one can observe mainly

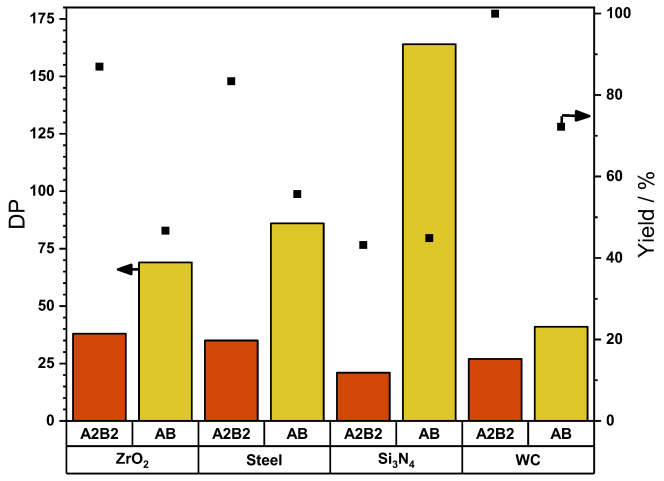

Figure 5.16 Comparison of four different milling materials for the A2B2 and AB approach with DP (bar chart) and yield (points).

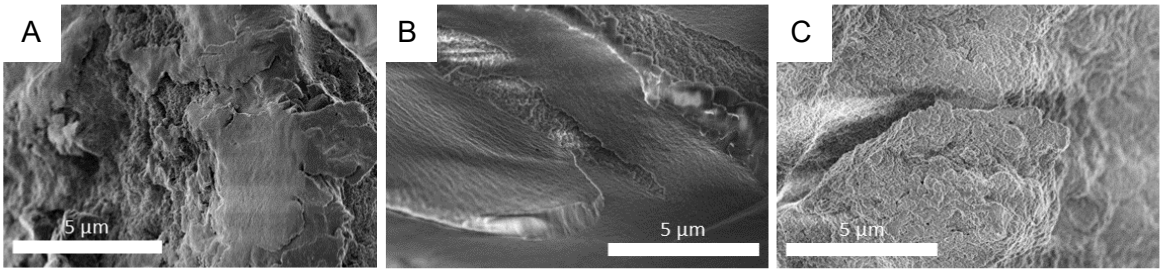

Figure 5.17 A: SEM micrograph of A2B2-1 (ZrO_2); **B:** SEM micrograph of AB-1 (ZrO_2); **C:** SEM micrograph of AB-3 (Si_3N_4); Scale is given for each picture.

sintered particles with smooth surfaces, whereas the silicon nitride sample (**Figure 5.17C**) is presenting smaller particles with rough surface. The powder XRDs shows three wide reflexes (at 19.8°, 22.8° and 28.2°) (**Figure 5.18A**). The tungsten carbide sample, however, only shows remnants of crystallinity, which is in good accordance with the IR results. In the thermal analysis, the main degradation step is shifted upwards by 50 °C, indicating longer chains for the AB system (**Figure 5.18B**). By DSC, no glass transition or melting for any of the polymers could be observed. This finding is in agrement with the literature, where the polymer is described as infusible.[122]

Inherently, the ball milling process imposes steep limitations on *in situ* analysis methods; therefore, the mill is often referred to as a "blackbox" and *in situ* data of reactions is scarce.[170] With a milling system equipped with pressure and temperature sensors (Fritsch, GTM system), however, said properties in the vessel during the milling process can be accessed. The build-up of temperature in the milling vessel can be attributed in part to the energy supplied to the system by the collision of the balls inside the vessels and in part to the enthalpy of the reaction. To eliminate the first factor, the temperature evolution of a background experiment, only involving

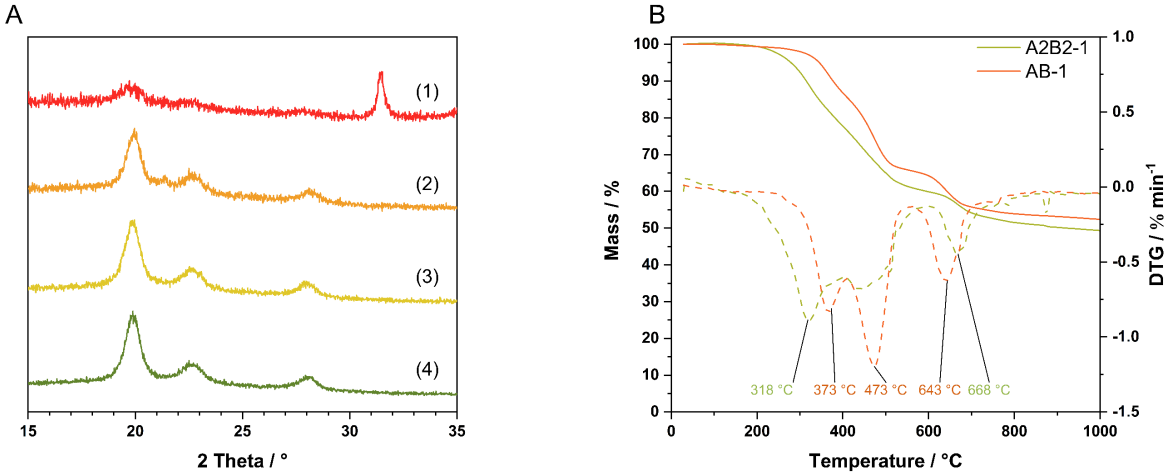

Figure 5.18 A: Comparison of the XRD diffractograms of AB polymers synthesized with different milling materials: WC (1), Si_3N_4 (2), Steel (3), ZrO_2 (4). **B:** Comparison of the TGA curves of A2B2 and AB type polymers synthesized under the same conditions with ZrO_2 balls.

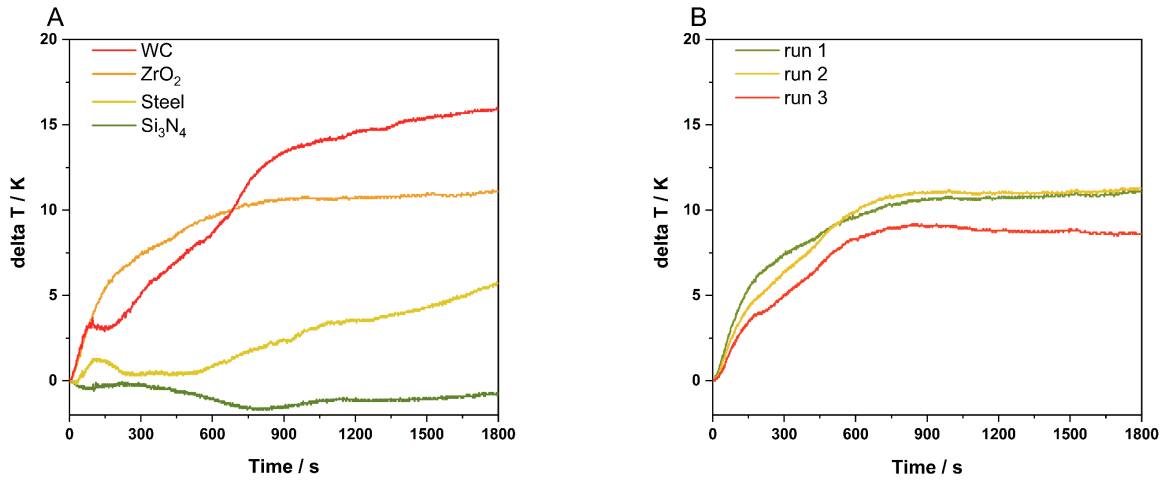

Figure 5.19 A: Development of the vessel temperature during the milling process for the A2B2 type polymerization. A background sample (only K_2CO_3 + milling balls) has been subtracted to eliminate the heat arising from the milling process itself. **B:** Study of the reproducibility of the GTM experiment in the zirconia beaker. Blank reference has been subtracted.

the milling of potassium carbonate (**Figure Appendix 5** and **6**), was subtracted. * After establishing the background, the A2B2 type polymerization was conducted in these different material vessels. Most of the reaction heat is released in the first minute of grinding (**Figure 5.19A**), which is pointing towards a swift reaction. After the majority of monomers have reacted to form short oligomers, the heat released by the condensation towards a long polymer is distributed over a longer time period, leading to a plateau. A notable difference of these plateau temperature differences can be found for tungsten carbide (16 K), zirconium dioxide (11 K) and tempered steel (6 K) as milling materials, while the temperature in the silicon nitride bowl stayed approximately constant. This is likely due to the high heat capacity of the nitride paired with the low density, resulting in an only moderate increase in temperature, although the reaction is still yielding almost 50 % of product. This might also be due to differences in the heat transfer capability between the different materials. In combination with a slightly lower reaction speed, the enthalpy can be dissipated over longer time periods and make detection with a senor challenging. To demonstrate the reproducibility of this method, the zirconium dioxide experiment was repeated three times (**Figure 5.19B**). While the plateau is reached around the same time, the plateau temperature is subject to multiple variables and should be regarded with caution. For example, the use of a slightly above RT milling vessel has a huge influence on the delta T value, due to heat dissipation effects.

* In the literature the use of an inert material to compare to the heat evolvement during a reaction is discussed critically right now.[200] For this reason, I chose the base used in excess in this reaction to avoid the controversy.

5.1.2.3 Hyperbranched Polyphenylene

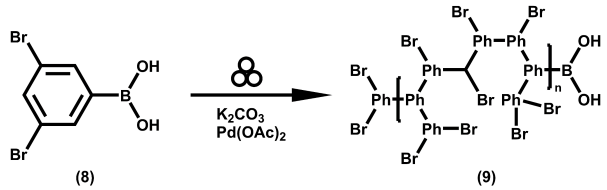

Figure 5.20 Polymerization of 3,5-dibromophenylboronic acid **8** to the hyperbranched polyphenylene **9**.

After demonstrating the feasibility of this approach, the interest in a more thorough analysis of the polymers created by Suzuki polycondensation remained. This task, however, is almost impossible due to the insolubility of the products. To improve the solubility, several modifications can be made. Besides the incorporation of solubilizing groups, the introduction of branching points can lead to an increased solubility.[140] This can be achieved by switching to an A2B1 system as shown by Kim and co-workers (**Figure 5.20** and **Table 5.5**).[163] Utilizing 3,5-bibromophenylboronic acid **8** as A2B1 monomer, one can observe a swift polymerization reaction via IR

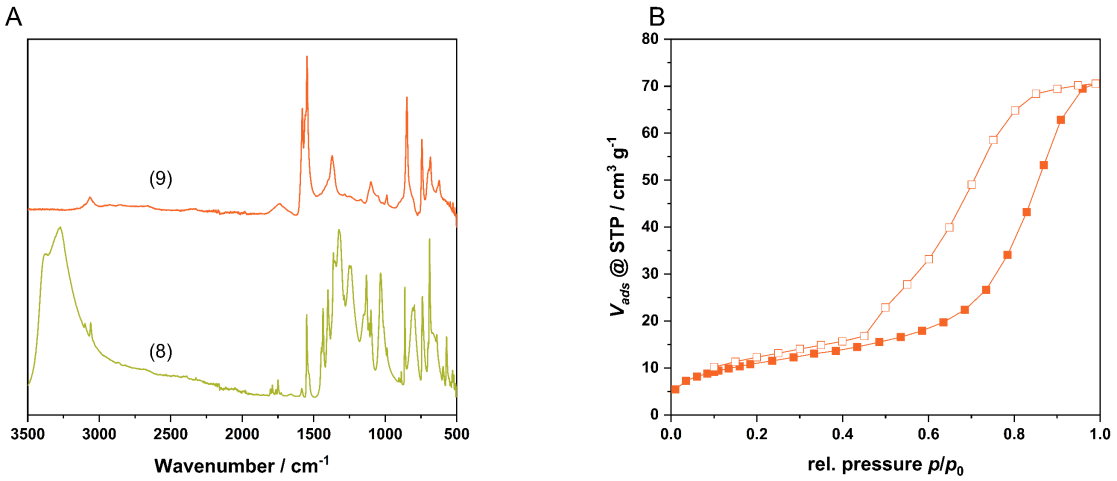

Figure 5.21 A: IR spectra of the monomer (8) and the polymer (9) showing the formation of the hyperbranched polyphenylene **B:** N_2-Physisorption isotherm of the hyperbranched polyphenylene after 30 min of milling.

Table 5.5 Overview of the mechanochemically synthesised hyperbranched polymer samples.

Polymerization type	Material	Time / min	T_g / °C	Rpm	Yield / %
A2B1	ZrO_2	5	209	800	69
A2B1	ZrO_2	30	225	800	79
A2B1	ZrO_2	60	235	800	80
A2B1	ZrO_2	90	261	800	84
A2B1	ZrO_2	120	-	800	80
A2B1	ZrO_2	5	-	200	57

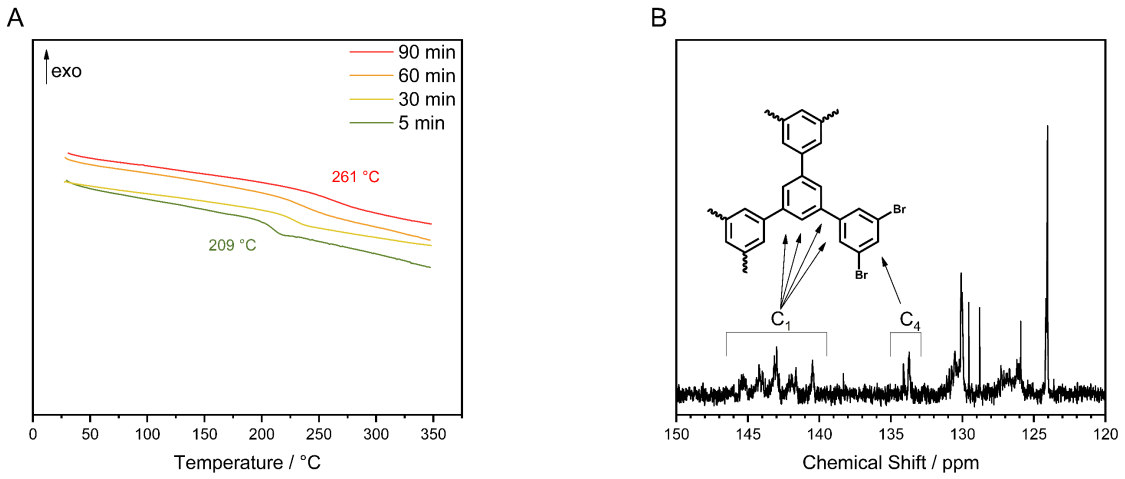

Figure 5.22 A: Comparison of the DSC curves of the hyperbranched polyphenylene formed by the reaction after different times **B:** ^{13}C NMR of the THF-soluble fraction for the A2B1 polymer after 10 min of milling in ZrO_2.

spectroscopy (**Figure 5.21A**). After only one minute, strong aromatic ring vibrations at 1582 and 1548 cm^{-1} are appearing, while the boron-oxygen and boron-carbon vibrations are diminished in intensity.[167] This confirms the growing of a hyperbranched polymer as described in the literature.[163] In the course of the reaction the polymer grows rapidly. The literature suggests that the hyperbranched polymer with a M_n of up to 35000 $g \cdot mol^{-1}$ should be readily soluble in THF and only precipitate when cooled. However, in order to obtain a soluble product, the energy input of the milling process had to be reduced, by reducing the speed to 200 rpm and the reaction time to 5 minutes. According to the GPC-LS measurements, the soluble fraction has a M_n of 5500 $g \cdot mol^{-1}$ and a PDI of 3.2 (**Figure Appendix 8**). One can therefore presume that the insoluble fraction consists of an even higher molecular weight fraction. Further proof is provided by nitrogen physisorption experiments (**Figure 5.21B**), which reveal a mesoporous solid with a specific surface area of 35 $m^2 \cdot g^{-1}$ and a pore volume of 0.1 $cm^3 \cdot g^{-1}$ (**Figure Appendix 7B**). This is a strong indication that the degree of branching and polymerization are both high.

In the past, ^{13}C-NMR has been established as the go-to method for the determination of the degree of branching (DB) of hyperbranched polymers.[140] For polymer (9), the signals between 140 and 146 ppm are caused by the bridging carbon atoms (C_1) and the signals at 133-135 ppm are assigned to the carbon atoms in between two bromine atoms (C_4). According to Kim and co-workers, the deviation of the C_1/C_4 ratio from 0.25 can be understood as the DB.[163] For the polymer **9** (**Figure 5.22B**) the calculated value of 0.74 is close to the literature value of 0.7, underlining similarities between these two approaches.

In contrast to the linear polymers, for all but one of the hyperbranched samples one can observe a glass transition. Kim *et al.* found the T_g to be not influenced by the molecular weight of polymer **9** (for M_n = 2000-35000 g·mol^{-1}) at 238 °C.[163] In this case, however, with increasing reaction time, the T_g is growing from 209 °C at 5 minutes up to 261 °C after 90 minutes of milling. At his point, the glass transition is already becoming barely visible in the DSC curve and for the sample milled for 120 minutes no T_g can be discerned at all (**Figure 5.22A**). These findings also point towards a very high molecular weight of the resulting polymer. Furthermore, the thermal degradation of the hyperbranched polymer in argon can be observed starting at around 450 °C and peaking at 539 °C (**Figure Appendix 7A**). This is in accordance with the literature and only slight variations between the 30 and 120 minute samples can be seen. These are likely due to smaller oligomers still present in the 30 minute sample. The residual mass is around 40 % and 50 % respectively.

5.1.2.4 Green Metrics for the Suzuki Polycondensation

Everybody can claim that their process is greener than established methods and it is hard to evaluate these claims. Thus, in the past, several metrics have emerged to quantify the ecological footprint of chemical processes. These so-called "green metrics" present a useful tool in the evaluation of new reaction pathways.[171,172] While I strongly believe that the mechanochemical process is per se the more benign one, by comparing the solution-based process with the latter it becomes apparent how beneficial the solvent-free approach is (**Table 5.6**). In the following section I am focusing solely on the polymerization reaction and assume that the washing procedures are equivalent for all approaches.

The first metric to be considered was the atom economy. It is a measure of the atoms present in the starting material versus the desired product and is therefore defined by the reaction type (**Equation 28**). The atom economy of the Suzuki reaction is not the most favourable (38 %), while it is the same for both pathways. Potential alternative pathways towards PPP include a Negishi or Kumada coupling, which proceed without palladium and boronic acids and therefore provide a better atom economy.

However, in the Suzuki reaction the conventional solvent-based process additionally entails a very low mass productivity of 1.4 %, mostly due to the solvents present.[163] This value is defined as the inverse of the mass intensity multiplied by 100 (**Equation 30**). It can be visualized as the percentage of mass used in the process that is converted into the final product. For industrial processes a MP between 10 and 40 is desirable.[173] The mass intensity, on the other hand, is defined as the ratio

$$\text{Atom economy (AE)} = \left(\frac{M\,(Product)}{\sum M\,(Educts)}\right) * 100 \tag{28}$$

$$\text{Mass Intensity (MI)} = \left(\frac{Total\ mass\ used\ in\ the\ process)}{Mass\ of\ product}\right) \tag{29}$$

$$\text{Mass productivity (MP)} = (MI)^{-1} * 100 \tag{30}$$

Table 5.6 Overview of the green metrics for the Suzuki polycondensation in different systems.

Type	Atom economy	Mass intensity	Mass productivity	Reaction time
Solvent-based[a]	38	71.4	1.4	6 h
Mechanochemical with bulking material	38	22.0	4.6	30 min
Mechanochemical	38	9.4	10.6	30 min

[a] according to reference [163] in 50 mL Xylene, 5 mL Ethanol and 20 mL K_2CO_3 sat. solution.

of the total mass of the process including solvents, reagents and catalysts and the mass of the final product (**Equation 29**).

The mechanochemical system described here is offering a more than three times higher mass productivity, that can be increased even more by avoiding bulking material, by either reducing the size of the reaction vessel or increasing the amount of monomer per batch. Doing this, an outstanding mass productivity of 10.6 %, suitable for industrial processes, can be obtained. In addition, the mechanochemical approach also offers the benefit of reduced reaction time, which, combined with the energy efficient milling system, leads to a significant decrease of energy consumption of the process. In order to validate this statement, the energy consumption was measured directly at the outlet. The Pulverisette 7 pulls 340 W for 30 minutes (170 W·h), if two zirconium dioxide beakers with 10 mm milling balls are used at 800 rpm. This is a significant energy saving, considering that an oil bath requires 200 W to maintain the temperature of 150 °C. Over six hours, this adds up to 1200 W·h, seven times as much as for the mechanochemical approach.

Another metric one can turn towards is the EcoScale.[174] In this post-synthesis analysis tool, the reaction is evaluated based on yield, cost, safety, conditions and ease of workup. Each procedure is awarded 100 base points and subsequently

Table 5.7 EcoScale calculation for the Suzuki polycondensation of the linear PPP.

Parameter	**Penalty points: (Mechanochemical)**	**Penalty points: (Classic)[a]**
1. Yield: 84 % / 75 %	8	12.5
2. Dibromobenzene	0	0
Phenyldibornicacid	3	3
$Pd(OAc)_2$ / $Pd(PPh)_4$	3	3
K_2CO_3	0	0
Xylene	-	3
Ethanol	-	0
3. Xylene (F)		5
Ethanol (F)	-	5
4. Common setup	0	0
Argon atmosphere	-	1
5. Room temperature, <1 h	0	-
Heating, >1 h	-	3
6. Adding solvent	0	0
Cooling Down	-	0
Simple filtration	0	0
Penalty points total:	**14**	**35.5**

[a] according to reference [163] 50 mL Xylene, 5 mL Ethanol and 20 mL K_2CO_3 sat. solution.

penalty points are subtracted to calculate the EcoScale. Penalty points can be awarded for example: for expensive reactants (3-5) or toxic substances (5-10). A full list of penalty points can be found in the experimental section in **Table 7.2**. Preparations with a EcoScale above 75 are then classified as excellent, between 75 and 50 as acceptable and below 50 as inadequate. In my case, the comparison of the mechanochemical and classical Suzuki polymerisation of the linear PPP is in accordance with the other green metrics (**Table 5.7**). The classical approach is achieving a EcoScale of 64.5, suffering mainly form a low yield, inflammable solvents and the required heating. One the other hand, the mechanochemical process can be classified as "excellent" with a EcoScale of 86.

5.1.2.5 **Conclusion**

Summing up, a new solvent-free Suzuki polycondensation protocol for the synthesis of liner PPP and hyperbranched polyphenylene was developed. The reactions took place in a non-inert, atmosphere without the need of special ligands for the palladium catalyst. The influence of different parameters on the reaction was observed, and it was found that bromide and iodide functionalities both lead to the formation of the desired polymers, in as short as 30 minutes. Furthermore, the utilization of AB type monomers is largely beneficial in the solvent-free environment, generating poly(para-phenylene) with a DP of up to 164 and thereby surpassing solution and electrochemical processes. In addition, the solid-state reaction is proceeding much faster, reaching high yields after only 30 minutes, compared to 12 to 24 hours in solution. For the A2B1 approach, hyperbranched polymers with a good thermal stability could be isolated. It was shown how beneficial the mechanochemical approach can be by the application of green metrics. The mass productivity was found to be by a factor of ten larger compared to the solution-based approach. In combination with the energy and time economy provided by this low temperature approach, the mechanochemical Suzuki polycondensation has been established as a true green alternative to existing procedures.

5.1.3 **Oxidative Polymerisation***

Microporous polymers can be obtained by a wide range of reactions, most commonly Friedel-Crafts alkylations,[175] cross-coupling reactions,[154] Suzuki polycondensation (see 5.1.2), Schiff base reactions[176] (see 5.1.1), cyclotrimerizations,[177] imidisation and amidisation reactions[178] are utilized. Another pathway proposed by Thomas *et al.* is the oxidative coupling of 1,3,5-tris(2-thienyl)benzene to obtain a microporous thiophene polymer (MTP), also referred to as conjugated microporous polymer (CMP-12).[179] Porous organic polymers (POPs) are particularly interesting for the application in organic photovoltaics,[120,180] hydrogen evolution reaction[181] and in catalysis.[15,16]

However, almost all of the microporous polymers suffer from low solubility even at elevated temperatures. Polymerization reactions in solution are thereby inherently flawed and only produce a low degree of polymerization, due to instant precipitation. A common workaround for POPs is the ionothermal synthesis in sealed ampules under harsh conditions.[177] Recently, Troschke *et al.* have presented a mechanochemical pathway for the synthesis of POPs.[86] Inherently a solvent-free method, solubility of neither starting materials nor products has to be taken into account which makes mechanochemistry perfectly suited for the synthesis of POPs.

In this chapter, the focus is on developing a protocol for the solvent-free oxidative polymerisation of 1,3,5-tris(2-thienyl)benzene under mechanochemical conditions (**Figure 5.23**). The influences of oxidant, milling parameters like milling speed, ball-to-powder ratio, milling time, and ball size on the yield and surface area of the polymer are explored. Furthermore, by utilizing an advanced milling setup equipped with in-vessel temperature and pressure sensors, a profound insight into the reaction is gained. The nature and structural properties of the MTP were investigated via ^{13}C CP MAS (Cross Polarization Magic Angle Spinning) NMR spectroscopy, FT-IR, TGA, XRD, elemental analysis, and nitrogen/argon physisorption.

* Some passages in this chapter have been quoted verbatim from my publication in the Journal of Material Chemistry A.[216] – Published by The Royal Society of Chemistry.This work was further part of the bachelor thesis of Maike Oltermann 07/17-10/17 that I supervised. She conducted most of the experiments. For publication the data gathered was interpreted and composed by me.

5.1.3.1 Preliminary Results and Optimization

After conducting preliminary experiments, the resulting polymer already exhibited a surface area of around 1000 $m^2 \cdot g^{-1}$ and FT-IR measurements confirmed the structure of the polymer.[179] Consequently, prior to an in-depth structural characterization, the yield and porosity of the materials were optimized by systematic synthetic screening.

However, the understanding of the influence of different mechanochemical parameters on the reaction product is still rather rudimentary. The sheer number of variables made us turn to a design of experiment approach to determine their influence while keeping the number of experiments in a manageable range. The milling speed, equivalents of $FeCl_3$, milling time, ball size and ball-to-powder ratio were identified as parameters of interest. The impact of the synthesis parameters applied on the mechanochemical oxidative polymerization of 1,3,5-tris(2-thienyl)benzene were studied in a 2^{7-3} factorial design with a resolution of IV with a centre point that was repeated once. The parameters are varied in two levels, as represented in **Table 7.6**. After analysing the obtained data, two major influences become apparent. Fristly, the equivalents of $FeCl_3$ have by far the biggest effect on the surface area of the obtained polymer (**Figure 5.24**). While solvent-based protocols use stoichiometric amounts of iron chloride, the oxidant has to be supplied in excess (at least 2.5 equiv.), in order to obtain a porous material.[179] However, supplying an ever-larger excess of oxidant is does not lead to a higher surface area, levelling out at around 1900 $m^2 \cdot g^{-1}$ for 12 equiv. Secondly, it was also observed that

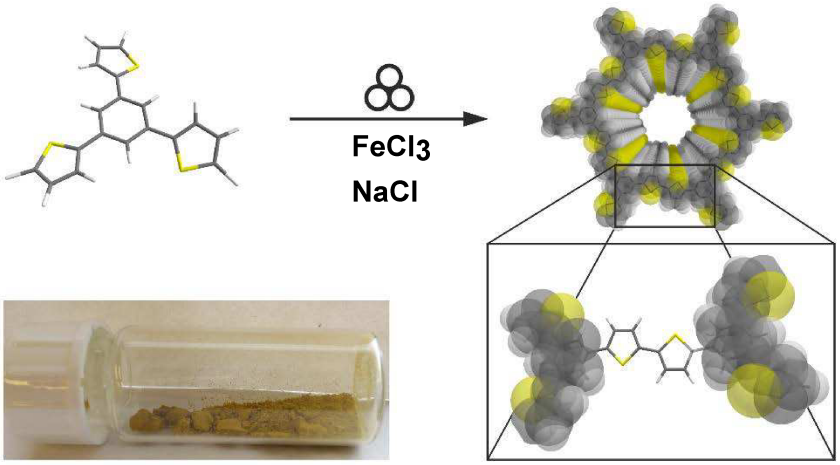

Figure 5.23 The mechanochemical oxidative polymerization of 1,3,5-tris(2-thieneyl) benzene with $FeCl_3$ as oxidant. Colour code: C (grey), H (white), S (yellow) Contrary to the impression of the structure our polymer is amorphous. On the lower left side, one can find a picture of the yellow polymer.

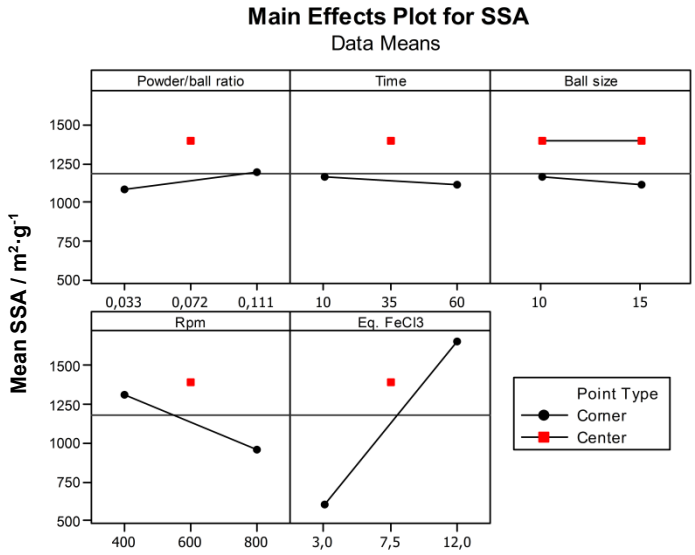

Figure 5.24 Results of the DOE (cf. **Table 7.6**). Visualization of the main effects on the surface area of the MPT polymer. Red dots represent the center point experiments with an average value of each of the parameters.

a decrease of surface area occurs with an increasing milling speed, hinting towards a collapse of the porosity under the high energy milling conditions. Beyond surface area, the yield is also strongly impacted by the $FeCl_3$ equivalents (**Figure 5.25**). Taking the reaction conditions into consideration, it is likely that in the non-inert atmosphere a fraction of the anhydrous $FeCl_3$ transfers into the hexahydrate upon contact with moisture. Thus, the smaller yields and surface area could be explained by the retarded activity of the hydrated $FeCl_3$ in the oxidation reaction.

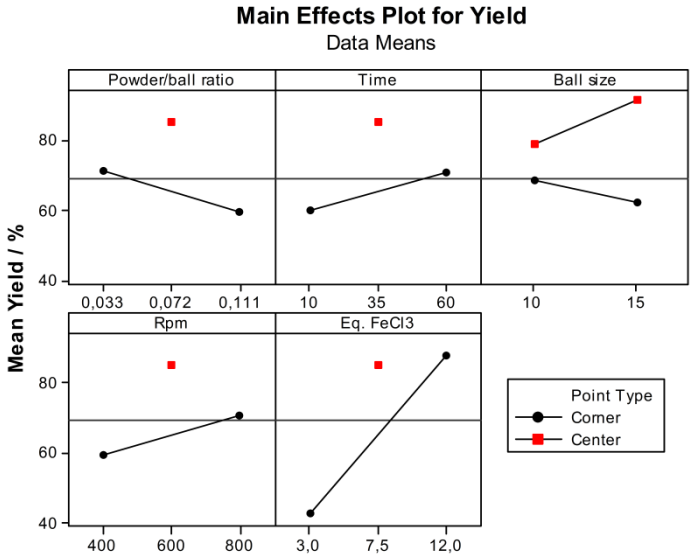

Figure 5.25 Results of the DOE (cf. Table 7.6). Visualization of the main effects on the yield of the MPT polymer. Red dots represent the centre point experiments with an average value of each of the parameters.

5.1.3.2 Structural and Chemical Characterization

After establishing these optimized conditions, the porous nature of the polymer obtained by the latter was investigated (**Table 5.8**). The surface area is an important property of POPs, especially in the context of future applications.[13] While often nitrogen physisorption at 77 K is used to characterize porous materials, it has been shown recently that analyses based on nitrogen adsorption overestimate the surface area and result in inaccurate pore size distribution of polar materials.[184] In this case, the thiophene moieties possess a polar nature and hence argon physisorption at 87 K, as recommended in a recent review, was measured for these samples.[185] The argon isotherm (**Figure 5.26A**) shows a type I shape with an additional contribution of larger macropores, most likely due to interparticular condensation at higher pressures. Surprisingly, the typical swelling behaviour, as in the solvent-based reference (MTP-Sol, **Figure Appendix 9**) or the literature, could not be observed in the ball milled sample.[179] This observation again points to a higher degree of

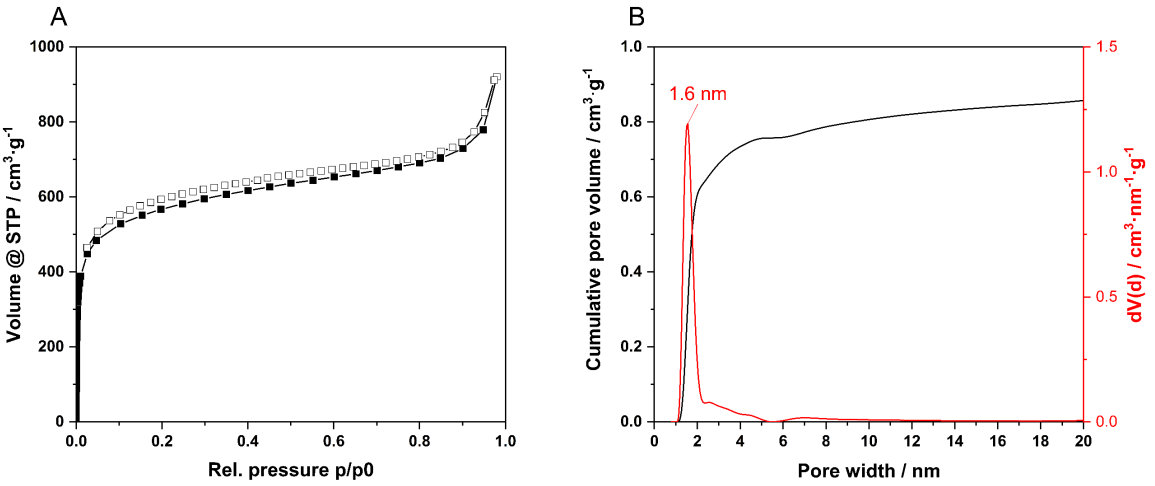

Figure 5.26 A: Low pressure argon isotherm of MPT-1 at 87 K exhibiting a BET surface area of 1850 $m^2 \cdot g^{-1}$ and a pore volume of 0.99 $cm^3 \cdot g^{-1}$ at 0.9 p/p0 **B:** Pore size distribution calculated from A using the QSDFT method. The mainly microporous material possesses a dominant pore at around 1.6 nm.

Table 5.8 Characterization data of MTP-1 from different reaction routes.

Sample	SSA_{BET} / $m^2 \cdot g^{-1}$	Pore Volume / $cm^3 \cdot g^{-1}$	Yield / %
MPT-1[a]	1850	0.95	98
MTP-1-Sol	160	0.13	19
MTP-1-Literature[179]	1060	0.69	-[a]

[a] with optimized reaction conditions; [b] calculated from argon physisorption experiments at 87 K; [c] calculated from nitrogen physisorption at 77 K; [d] determined at p/p0 = 0.9; [e] described as "almost quantitative" and "high" but not quantified in the literature

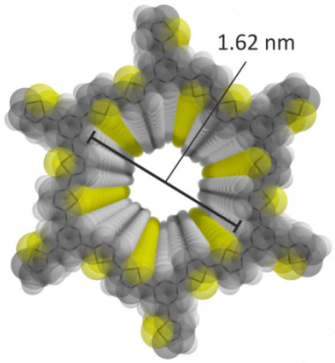

Figure 5.27 Simulated polymer structure with the 1.62 nm pore colour code: C (grey), H (white), S (yellow).

polymerization and crosslinking and therefore a more rigid structure of the polymer. Applying the BET equation results in a specific surface area of about 1850 $m^2 \cdot g^{-1}$ and total pore volume of 0.99 $cm^3 \cdot g^{-1}$ (at 0.9 p/p_0). By the means of QSDFT calculations* the pore size distribution (**Figure 5.26B**) for MTP-1 was established, which shows one dominant pore size at 1.6 nm. This is in good agreement with the literature.[179] Utilizing Material Studio®, the structure of the porous polymer (**Figure 5.27**) based on stacked layers with hexagonal channels perpendicular to the layers was calculated. The channels exhibit a pore diameter of 1.62 nm, which is in agreement with the experimental argon physisorption measurements. Compared to the surface area of 1060 $m^2 \cdot g^{-1}$ reported by Thomas and co-workers for the solution-based protocol, it is apparent that mechanochemistry produces materials with higher surface areas.[179] One possible reason for the lower porosity of the solvent-based polymer is the low solubility of the latter. As described in their paper, the precipitation of yellow polymer can be observed immediately, hinting towards an incomplete network formation.[179]

XRD measurements (**Figure 5.28A,B**) show that MPT-1 is an amorphous polymer. It does not show reflections of either the monomer or the simulated crystal structure of the polymer (**Figure 5.28C**). This observation is in agreement with other polymer networks synthesised under similar conditions.[120,186] While the physisorption experiments point towards the motive of hollow tubes with a diameter of 1.6 nm to be present in the polymer, the diffraction data strongly suggest that these motives possess no long range order of any fashion. Furthermore, the XRD

* I utilized the QSDFT kernel for carbon materials, which is not perfectly suited for this polar polymer. However, due to a lack of alternatives this is common practice in the POP community.

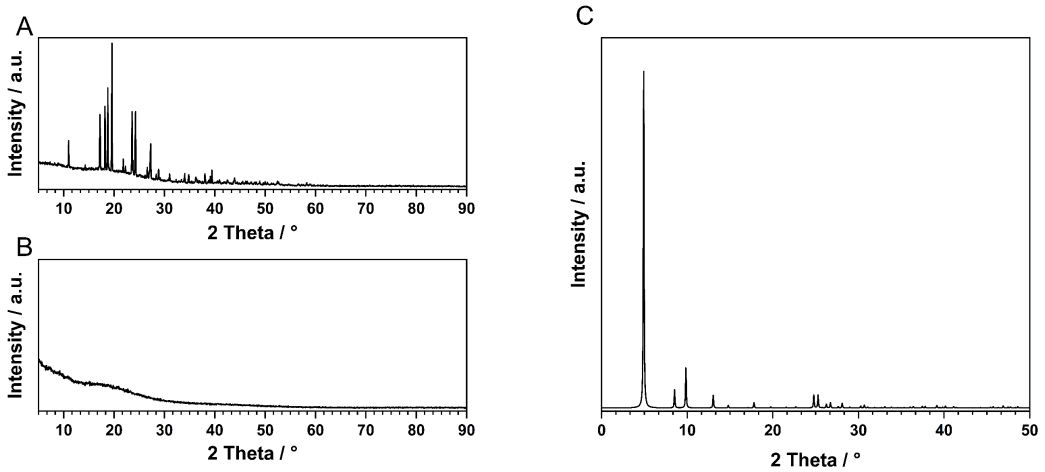

Figure 5.28 X-ray diffraction pattern of **A:** 1,3,5-tris(2-thienyl)benzene B: MPT-1 highlighting the amorphous structure of the polymer. **C:** Simulated powder X-ray diffraction pattern of MPT-1.

diffractograms as well as the energy dispersive x-ray spectroscopy mappings show the absence of crystalline and amorphous iron and zirconia phases. One can therefore rule out a contamination of the polymer with abrasion from the milling balls and leftover oxidant. The purity of the polymer is further confirmed by elemental analysis (**Table 5.9**), indicating high values of sulphur (meas.: 26.74 %, calc.: 29.92 %) in the polymer, as expected from the thiophene moieties.

Furthermore, the ^{13}C CP MAS NMR spectrum of MTP-1 agrees well with the NMR data found in the literature (**Figure 5.29A**).[179] Note that the peak assignment provided

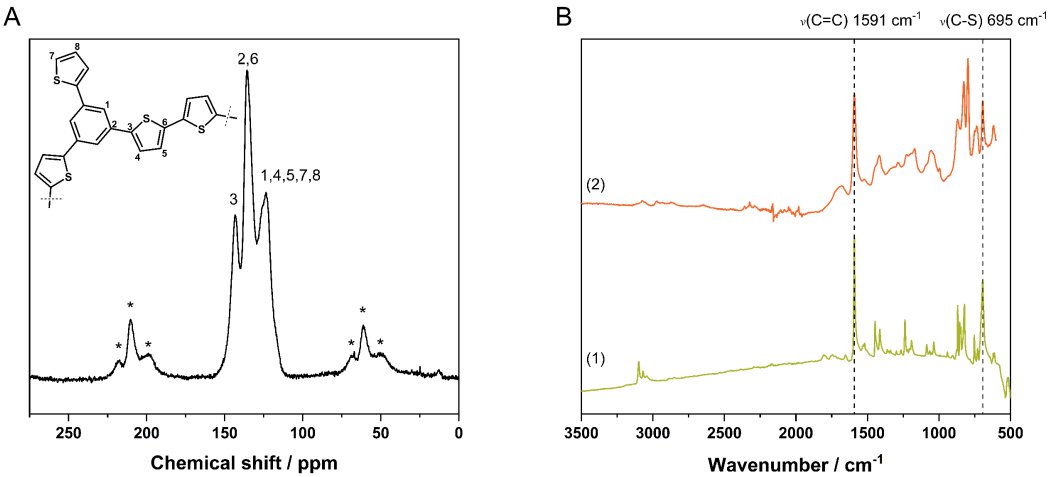

Figure 5.29 A: ^{13}C CP MAS NMR spectrum of MTP-1 with the structure and peak-assignment as an inlay. (* spinning side bands) **B:** FT-IR spectra of MPT-1 (2) and the monomer 1,3,5-tris(2-thienyl)-benzene (1) showing intact C-S vibrations for the polymer.

Table 5.9 Data of the elemental analysis of the mechanochemical and solvent-based MTP-1.

Sample	Found / %				Calculated / %			
	C	H	N	S	C	H	N	S
MPT-1	60.37	2.03	-	26.75	67.25	2.8.	-	29.92
MTP-1-Sol	62.41	2.42	-	26.43				

in the figure was slightly modified based on the simulations of Dr. Paasch, using the program ACD/Labs®. This assignment was confirmed by HETCOR experiments of MTP-1 (**Figure Appendix 10**) and HR (High resolution liquid-state) NMR measurement of the monomer (**Figure Appendix 11**). In addition to the NMR experiments, the incorporation of intact thiophene units into the polymer network is further confirmed by FT-IR spectroscopy (**Figure 5.29B**), showing the C-S vibration remaining at 695 cm^{-1}. Furthermore, MPT-1 shows high thermal stability, decomposing in air (**Figure Appendix 13A**) at around 300 °C. The residual mass of only 0.3 %, confirms the absence of both abrasion and oxidant. In argon atmosphere (**Figure Appendix 13B**), the decomposition proceeds slowly and differential thermal analysis reveals peaks at 577 °C and 767 °C with a leftover mass of 52 % at 1000 °C. Scattering electron microscopy revealed an agglomerated morphology of the samples (**Figure Appendix 12**).

Previously, *in situ* temperature and pressure measurements have been shown to give indications on the progress of a mechanochemical reaction.[52,53,86] While the rise of temperature (**Figure 5.30A**) was not significant, for this reaction one could observe a steep rise of pressure (**Figure 5.30B**) during the milling process. This rise can be attributed to the release of HCl during the reaction. The latter is released as a gas due to the solvent-free nature of the process. The pressure profile reveals the swiftness of the reaction, reaching a small plateau after less than 5 minutes. Afterwards, the increase in pressure is mainly due to the macroscopic heating of the reaction vessel but a minor contribution of the ongoing polymerization reaction cannot be ruled out completely.

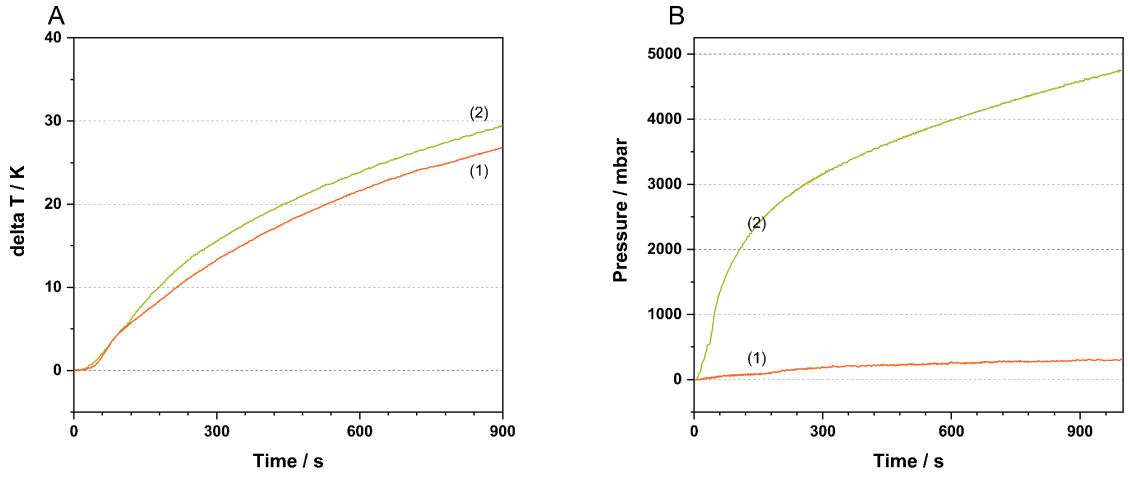

Figure 5.30 A: Development of the relative vessel temperature during the milling process comparison of MPT with a vessel filled with $FeCl_3$ as reference at 800 rpm. **B:** Development of the relative vessel pressure during the milling process comparison of MPT with a vessel filled with $FeCl_3$ as reference.

5.1.3.3 **Carbazole Monomers**

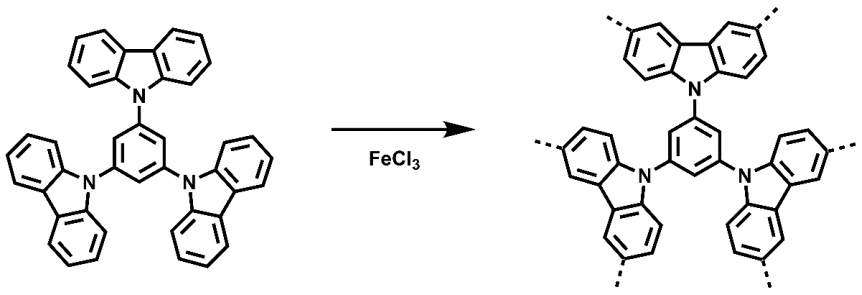

Figure 5.31 Oxidative polymerization of 1,3,5-tri(9-carbazolyl)benzene towards the microporous carbazole polymer.

To prove the generality of the improved synthesis beyond thiophene monomers, the concept was furthermore applied to the synthesis of a microporous carbazole-based polymer (MCP-1). This polymer is starting from 1,3,5-tri(9-carbazolyl)benzene and was previously synthesised by Dai and co-workers in a mixer ball mill (**Figure 5.31**).[187] While Dai and co-workers briefly investigated the influence of the milling parameters and their optimized conditions lead to a polymer with a surface area of 940 $m^2 \cdot g^{-1}$, the protocol at hand produces a polymer with a surface area of 1710 $m^2 \cdot g^{-1}$ (**Figure Appendix 14**) – almost twice as high. The differences between the two procedures are not only in the equivalents of $FeCl_3$ but also the fact that a mixer ball mill was used for the latter. The transfer of protocols between these two mill types bears many challenges. While a direct comparison of these two methods for the production of porous polymers would be of interest, such a study does not exist to the best of our knowledge. These findings demonstrate the versatility of this method, making it applicable in a wide range of polymerization reactions.

5.1.3.4 **Conclusion**

To sum up, a novel pathway for the oxidative polymerisation of the thiophene-derivate 1,3,5-tris(2-thienyl)benzene is described in this chapter. The formation of MTP-1 under ball milling conditions proceeds quantitatively, swiftly and leads to a highly microporous material. By avoiding solubility issues, enhanced crosslinking of the polymer can be achieved, leading to a specific surface area of 1850 $m^2 \cdot g^{-1}$, almost twice as high as the values reported for the solution-based process, and a pore volume of 0.95 $cm^3 \cdot g^{-1}$. The narrow pore size distribution with a uniform pore size of 1.6 nm perfectly fits the simulated structure of the polymer. The successful structure formation is further confirmed via FT-IR and ^{13}C CP MAS NMR spectroscopy. In addition, contamination from the milling material or the oxidant could not be detected in the polymer, confirming the superiority of the mechanochemical approach over solution-based synthesis. Furthermore, it has been demonstrated that this protocol can be extended to other monomers, thus displaying a versatile and potentially easily scalable process for the production of microporous polymers and thereby enabling utilization in an industrial scale for this emerging class of porous materials.

5.2 PART II – GRAPHITIZATION

5.2.1 Scholl Reaction*

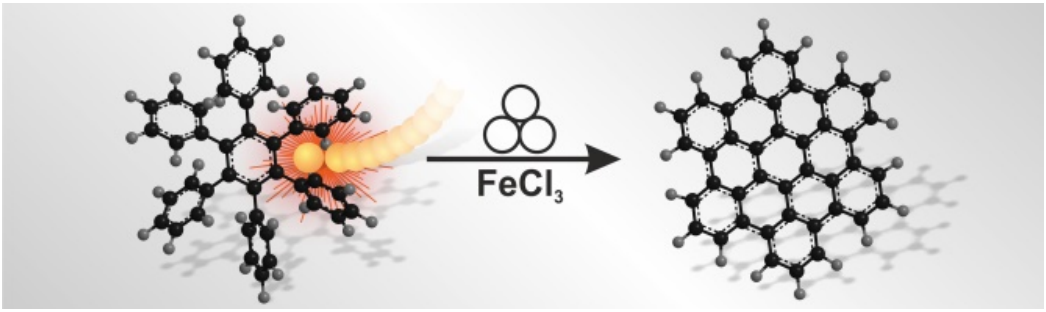

Figure 5.32 Scholl reaction of HPB to HBC.

The Scholl reaction,[87,89,93] a Lewis acid catalysed oxidative cyclodehydrogenation forming aryl-aryl bonds (**Figure 5.32**), is at the heart of the bottom-up synthesis of polycyclic aromatic hydrocarbons (PAHs)[188] or nanographenes and graphene nanoribbons (GNRs).[189] These materials have been studied extensively in the last 20 years, predominantly because of their semiconducting properties and potential applications in organic electronics. In contrast to thermally activated cyclodehydrogenation in on-surface synthesis,[114,150,190] the solution-mediated Scholl reaction is the key transformation to produce fully pi-conjugated („graphitized") materials on the gram scale.[191] Müllen and co-workers, demonstrated that a multitude of nanographenes and GNRs can been produced this way,[95,110,188,189,192–194] culminating in the synthesis of C_{222} - a PAH consisting of 37 benzene rings.[95] A main restriction is the intrinsic low solubility of extended nanographenes and GNRs due to strong aggregation by pi-pi interactions. Especially for the larger monomers solubility is a main concern, but even the smallest planarized hexabenzocoronene (HBC) is barely soluble in common organic solvents even at elevated temperatures. GNRs face the same challenges and a common way to circumvent this is the introduction of solubilizing groups, preinstalled into the monomers.[188,189] This presents not only additional steps in their syntheses but also a bad atom economy for the production of nanoribbons.

*Some passages in this chapter have been quoted verbatim from my publication in Chemical Communications.[52] – Published by The Royal Society of Chemistry.

But where solvent-based chemistry fails, other methods have to step in. As demonstrated throughout this thesis, mechanochemical methodologies have been explored as a powerful tool, offering at least as much flexibility as solvent-based processes.[29,30] While Tanner and co-workers discovered the potential of a Fe(III) catalysed oxidative coupling of 2-naphtol,[195] it was not yet applied to more complex, insoluble systems like nanographenes. After demonstrating that long poly(phenylene)s –which are also the precursors in PAH and GNR chemistry – can be synthesised in a ball mill (Chapter 5.1.2), the missing step towards a completely solvent-free bottom-up fabrication of GNRs lies within the cyclodehydrogenation ("graphitization") of corresponding precursors. In this chapter, I will focus on developing a protocol for the solvent-free Scholl reaction under mechanochemical conditions as a versatile tool for the cyclodehydrogenation, "graphitization" of oligophenylene precursors into benchmark nanographenes such as HBC, triangular shaped $C_{60}H_{42}$ and the massive C_{222}.

The influence of the Lewis acid/oxidizing agent, milling parameters like milling speed, ball-to-powder ratio, milling time and ball size were investigated. Furthermore, a profound insight into the reaction was gained by utilizing an advanced milling setup equipped with in-vessel temperature and pressure sensors. The quality and structural homogeneity of produced nanographenes have been confirmed by MALDI-TOF mass spectrometry and UV/Vis absorption spectroscopy.

5.2.1.1 Scholl Reaction of Hexaphenylbenzene

Starting from hexaphenylbenzene (HPB), a commercially available precursor, the feasibility of the Scholl reaction under mechanochemical conditions in a planetary ball mill was investigated. It was quickly discovered that $FeCl_3$ x 6 H_2O is not promoting the reaction, but anhydrous $FeCl_3$ is. Initial experiments turned out to be very promising, the yield could be quickly raised to 95 % in a 45 mL zirconium dioxide milling vessel with twenty-two 10 mm balls at 800 rpm, adapting the literature known conditions for solution synthesis: 12 equiv. $FeCl_3$ per H atom involved in aryl-aryl bond formation (**Table 5.10**). The experiments were conducted with 0.1 g of the HPB and NaCl as bulking material. MALDI-TOF mass spectrometry of HBC-1 showed the most intense signal at m/z = 522 $g \cdot mol^{-1}$, which represents exactly the target molecule (**Figure 5.33A**). UV/Vis measurements (**Figure 5.33B**) further confirmed the successful synthesis of HBC. The liquid state spectrum shows

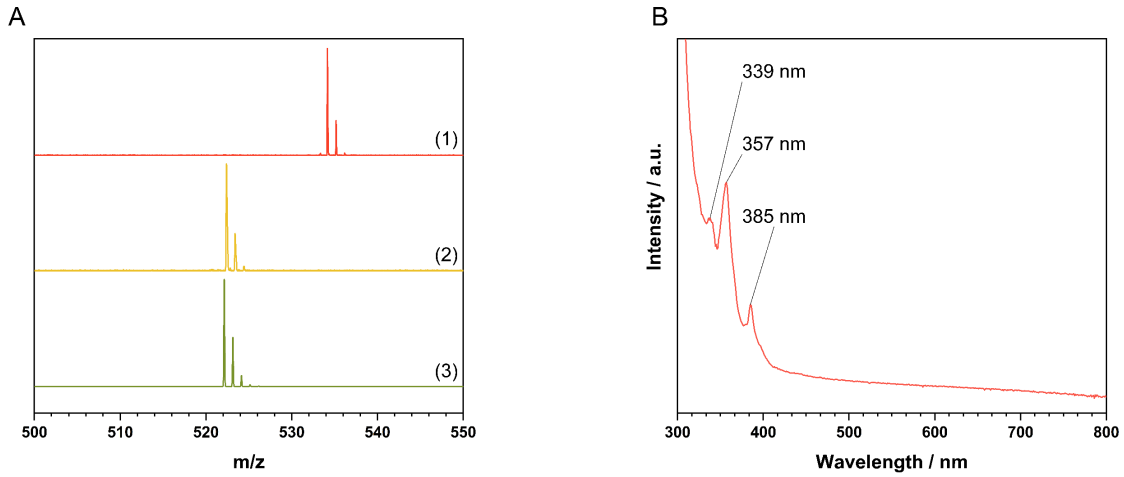

Figure 5.33 A: Scholl reaction of $C_{42}H_{30}$ to $C_{42}H_{18}$, milled with 22x 10 mm zirconium dioxide balls recorded MALDI-TOF spectra of HPB (1), HBC (2), and calculated MALDI-TOF spectra of HBC (3) **B:** UV/Vis measurement of HBC in toluene (c = $1.1 \cdot 10^{-5}$ $mol \cdot L^{-1}$) showing the peaks reported in the literature.

Table 5.10. Reaction conditions and yields of HBC syntheses; Reaction conditions if not stated otherwise: 800 rpm, 22x 10 mm balls, ZrO_2, 12 equiv. $FeCl_3$ per H, NaCl as bulking agent.

Sample	Milling material	Milling time / min	Yield[a] / %
HBC-1	ZrO_2	60	95
HBC-2	Steel	60	-[b]
HBC-3	WC	60	-[b]
HBC-4	Si_3N_4	60	97
HBC-5	ZrO_2	30	92

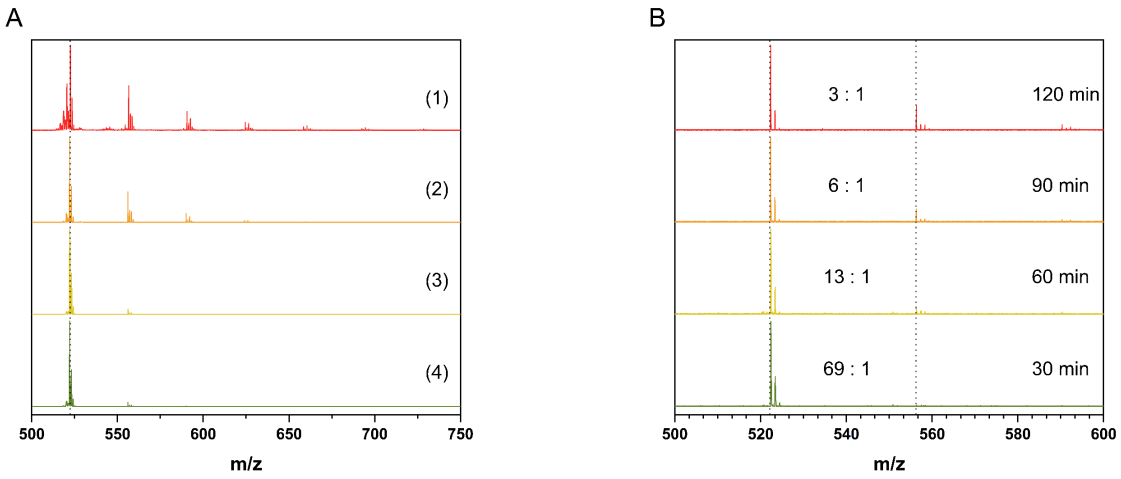

Figure 5.34 A: MADLI-TOF measurements of the HBC system milled with different milling material. Conditions: 800 rpm, 22 balls, 60 min, (1) WC, (2) steel, (3) ZrO_2, (4) silicon nitride. **B:** MADLI-TOF measurements of the HBC system milled for different reaction times. Conditions: 800 rpm, 22 balls, ZrO_2. The ratio between HBC (522.4) and the monochloro adduct (556.3) are given.

distinct peaks at 339, 357 and 385 nm, which is in good agreement with the literature.[196]

After this preliminary result, the influence of different mechanochemical parameters on the reaction were studied. In general, the understanding of how and why they influence the mechanochemical reaction is still in its infancy.[29] Several attempts have been undertaken to illuminate the processes inside the milling vessel.[197,198] A main aspect that these protocols generally share is the dependence on the introduced energy.[198,199] At first, experiments with different milling materials, ranging from silicon nitride (ρ = 3.25 g·cm^{-3}) over zirconium dioxide (ρ = 5.7 g·cm^{-3}) and tempered steel (ρ = 7.9 g·cm^{-3}) to tungsten carbide (ρ = 14.9 g·cm^{-3}), were conducted, to investigate the density influence of the milling material (vessel and balls) and therefore the amount of energy introduced. (**Figure 5.34A**). The formation of HBC could be observed for all four milling materials (samples HBC-1 to HBC-4). However, for tempered steel and tungsten carbide, a large amount of chlorinated side product and abrasion of the milling material could be detected.

Chlorination is a known side effect of the Scholl reaction and is also observed in liquid state approaches. For some applications, chlorination is even wanted, and so additional reactions steps are introduced to this effect. This matter will be further discussed in a separate chapter (5.2.2). For this model reaction, however, a chlorination of the HBC is unwanted. Therefore, further investigations were

continued with the zirconium dioxide system, in order to avoid excessive chlorination and abrasion (**Figure Appendix 15**).

In an additional trial, it was demonstrated that an increase of milling time consequently leads to a higher percentage of chlorinated side products (**Figure 5.34B**). While MALDI-TOF is not a quantitative method, since the tendency towards ionization is different for each substance, it allows us to compare between samples measured in the same setup. While after 30 minutes only traces of the monochlorinated product can be observed, the ratio between those and HBC is steadily growing with increased milling time. After two hours, a 3:1 ratio of HBC and the monochloro adduct can be observed, and the two-times chlorinated adduct is also visible.

Consequently, the reaction protocol was optimized under the aspects of yield, time and side products. The number of variables, however, made us turn to a design of experiment approach to determine their influence while keeping the number of experiments in a manageable range. The milling speed, amount of $FeCl_3$, milling time, ball size and filling degree (ratio of balls to powder) were determined as parameters of interest. This investigation confirmed that, indeed, all these

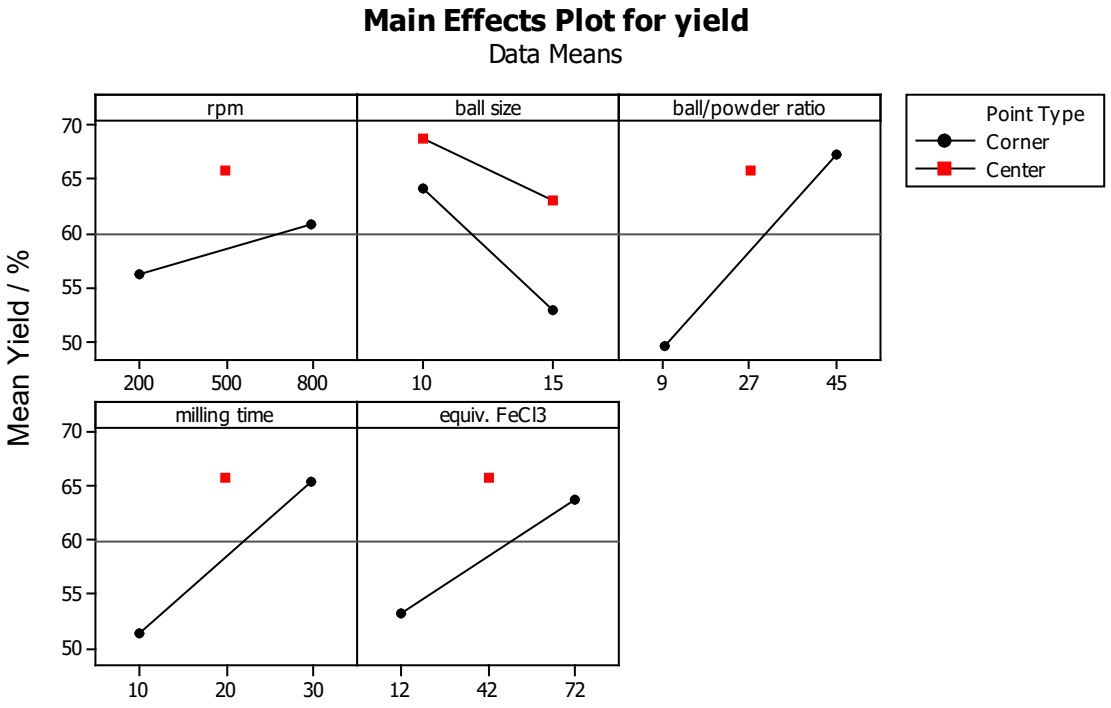

Figure 5.35 Results of the DOE (Table 7.10). The main plots of the parameters: rpm, ball size, ball/powder ratio, milling time and equiv. $FeCl_3$ are presented.

parameters influence the reaction (**Table 7.10**), while, in general, a higher energy input favours a high yield of the reaction.

The main effect plots for the yield of the reaction are given in **Figure 5.35**. These plots can give one an idea of the influence of a single parameter. For the rpm of the ball mill, the influence on the reaction is rather small. The yield at 200 and 800 rpm are varying by around 5 %. The red centre point is at a medium speed, but the influence of other parameters is also taken into account, so it cannot be understood as an influence of the milling speed. For the ball size, however, one can see a big influence on the yield. An increase in ball size is leading to a smaller yield. This is likely due to differences in the milling dynamic: with bigger balls, the impact energy is higher but the number of impacts overall is lower. In addition, to obtain a fine powder, the balls have to be as small as possible, so bigger balls can lead to a decreased surface of the powder during the reaction. The ball to powder ratio (**Figure 5.35** top-right) has big implications for the milling process. It is the weight ratio of the balls (22 balls weight 90 g) to the total powder in the ball mill. If there is less powder, the trajectory of the milling balls is influenced and more energy is transferred to the powder. If too much powder is utilized, the ball movement is hindered, and the transfer of energy is decreased. In the study, a lower amount of powder and, therefore, higher energies seem to favour the reaction. The milling time

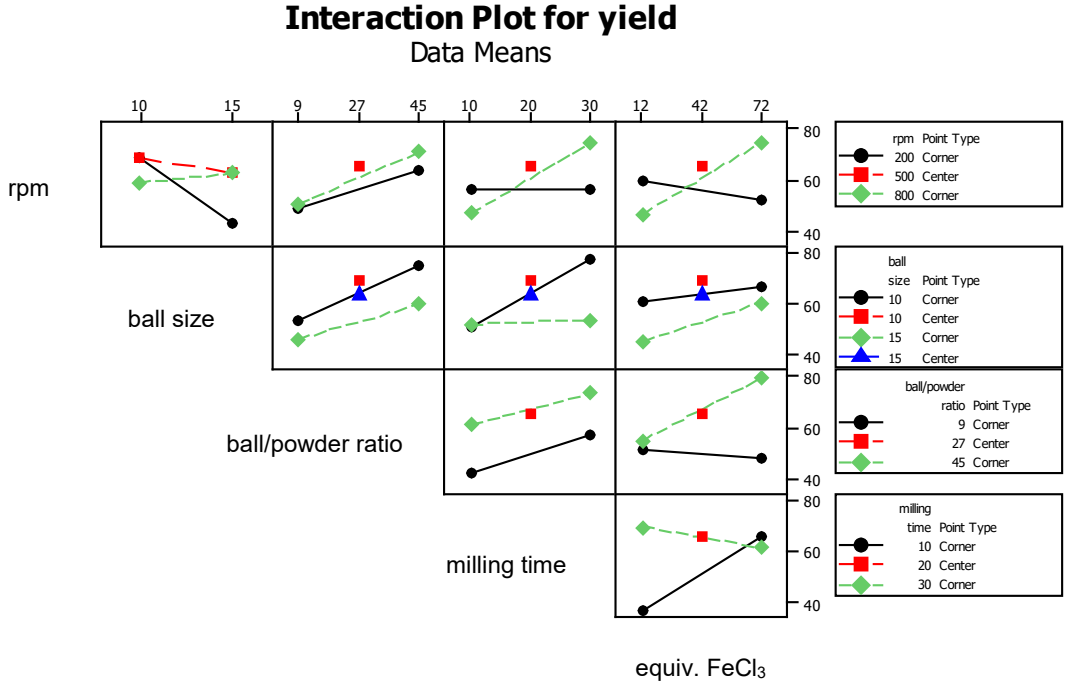

Figure 5.36 Results of the DOE (Table 7.10). The interaction plots of the parameters: rpm, ball size, ball/powder ratio, milling time and equiv. $FeCl_3$ are presented.

and equivalents of $FeCl_3$ have an obvious effect on the reaction, showing an increase in yield with an increase of either one of these parameters. The centre point mentioned earlier seems to be heavily influenced by the last three discussed parameters, which indicates a strongly non-linear behaviour.

In the interaction plot (**Figure 5.36**), the interactions of the different parameters are visualized. If two parameters are independent, the graphs are parallel. If they are interacting, however, the curves are crossing each other. The strongest interaction, can be observed between the reaction time and the equiv. of iron chloride. As it was expected, a bigger amount of reagent is leading to a shorter necessary reaction time. Similarly, the interaction between the rpm and the equiv. of $FeCl_3$ is showing that, at lower speeds, an increase of equivalents of reagent is leading to higher yields. While bigger milling balls have a negative influence on the reaction and the impact of the milling speed is rather low, raising the ball to powder ratio, milling time and equivalents of iron(III) chloride all lead to an increased yield (**Figure 5.35**). Increasing the equiv. of iron(III) chloride, leads to a reduced reaction time until full conversion. The optimized conditions for the mechanochemical Scholl reaction of HPB are: 10 mm milling balls, 800 rpm, a ball to powder ratio of 45, 72 equiv. of $FeCl_3$ and 30 minutes of milling (sample HBC-5, run 18 in the DOE).

Lately, it has been shown that *in situ* temperature measurements can give indications on the progress of a reaction.[41,53,86] The merit of this method is currently being discussed.[200] In the case of the Scholl reaction, however, the temperature rise resulting from the reaction enthalpy is marginal because of the small amount of reactant. Hence, it cannot be used to track the progress in a satisfying manner. Therefore, the *in situ* pressure measurement of the milling vessel, which are much less controversial, was used to elucidate the reaction progression. Applied to this system, one can observe a steep rise of pressure in the first minutes of the reaction (**Figure 5.37A**), caused by the release of HCl during the reaction. This rise occurs in different slopes depending on the milling speed (**Figure 5.37B**). The dependency seems to verify that the reaction is indeed caused by the collision of the milling balls, since the energy increases with the square of the milling speed. As expected, the reaction proceeds the slowest at low energy input, but even at 200 rpm a plateau is reached after as little as 10 minutes. In contrast, for 100 rpm no reaction can be observed at all, indicating a sort of threshold milling speed or minimal energy input

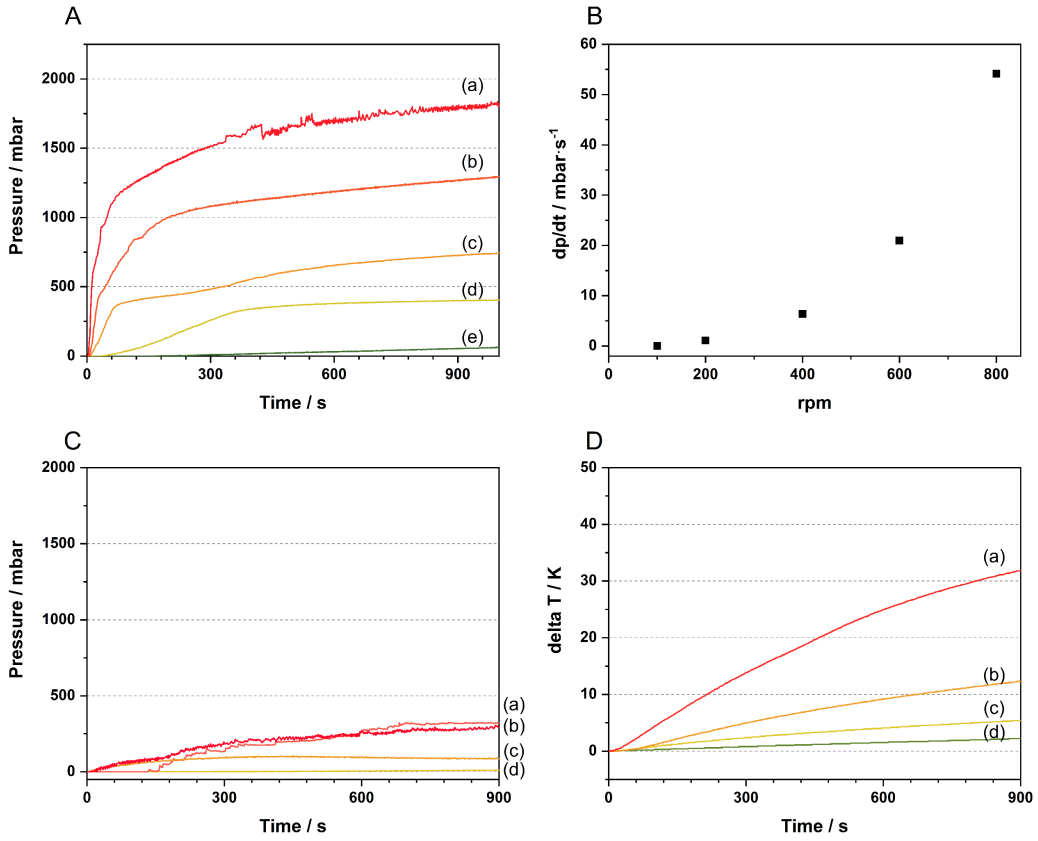

Figure 5.37 A: Development of the vessel pressure during the milling of HPB at different milling speeds. (a) 800 rpm, (b) 600 rpm, (c) 400 rpm and (d) 200 rpm (e) 100 rpm. **B:** Changes in the slope of the pressure rise vs the rpm of the milling vessel. Data extracted from the first minutes of A. **C:** Development of the relative vessel pressure during the milling process without HPB for different milling speeds. **D:** Development of the relative vessel temperature during the milling process of HPB for different milling speeds.

to supply the activation energy for this reaction. This further explains the absence of a reaction when both reagents are subjected to milling inside a mortar. In order to verify these results, experiments without HPB – milling of pure iron chloride – (**Figure 5.37C**) were conducted and one can only observe a neglectable overpressure due to the heating of the vessel.

Regarding the absolute pressure in the vessel after the reaction, one could argue that a higher pressure was due to an increase in released gas, caused by a higher conversion of the precursor. Since the yield is almost unchanged for different milling speeds, this does not seem to be the case. It is rather that the higher absolute pressure for higher milling speeds is caused by the increasing temperatures of the vessels, an effect more profound for higher milling speeds, due to energy dissipation (**Figure 5.37D**).

5.2.1.2 Scholl Reaction of Bigger Nanographenes

While the results for the Scholl reaction of HPB are promising and the insight into the mechanism gained are academically interesting, the real challenge lies in the planarization of bigger nanographenes. In order to establish this method as a versatile alternative to the classical process, it is important to broaden the scope beyond the well-known solution processible HPB. The syntheses towards the triangular shaped C_{60} and the biggest nanographene C_{222} were subsequently investigated in solvent-free conditions as well. During the planarization of C_{60}, it is necessary to forge nine new C-C bonds, and C_{222} requires a whopping 54 new C-C bonds in order to become a nanographene. Surprisingly, no extensive optimization of the reaction parameters was necessary to exceed the solution-based protocols for both systems in terms of yield (**Table 5.11**). The MALDI-TOF spectrum of C_{60} (**Figure 5.38A**) is identical to the simulated one for this compound. On the other hand, the acquisition of the spectra for C_{222} (**Figure 5.38B**) was more complicated, since the compound was harder to ionize in the spectrometer. While the main peak resembles the predicted product peak and no leftover reactant is visible, the intensity is not sufficient to allow for an isotopic resolution.

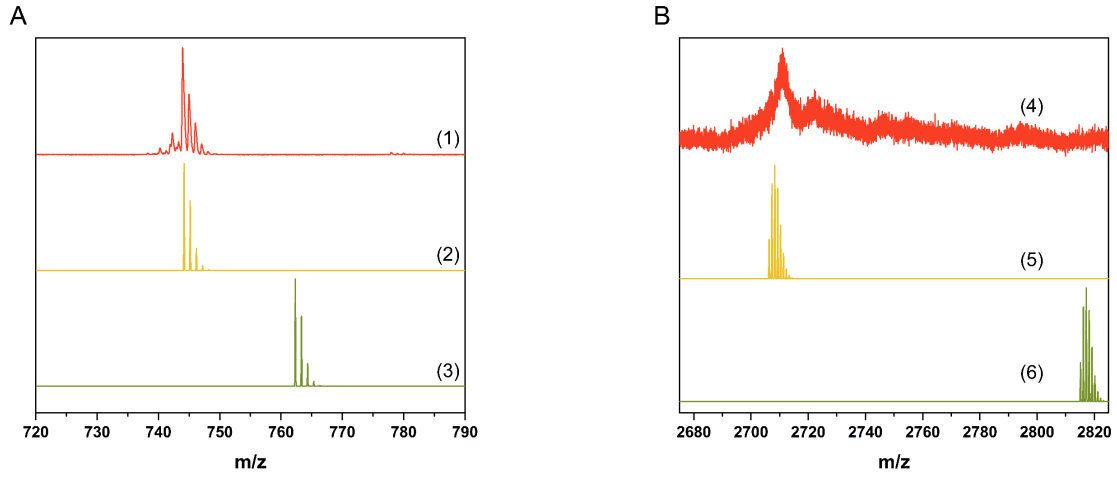

Figure 5.38 A: Scholl reaction of $C_{60}H_{42}$ to $C_{60}H_{24}$, recorded MALDI-TOF spectrum of $C_{60}H_{24}$(1), calculated MALDI-TOF spectra of $C_{60}H_{24}$(2) and $C_{60}H_{42}$(3). **B**: Scholl reaction of $C_{222}H_{150}$ to $C_{222}H_{42}$, recorded MALDI-TOF spectra of $C_{222}H_{42}$(4), calculated MALDI-TOF spectra of $C_{222}H_{42}$(5) and $C_{222}H_{150}$(6).

Table 5.11. Reaction conditions and yields for bigger nanographenes; Reaction conditions: 800 rpm, 22x 10 mm balls, ZrO_2, 12 equiv. $FeCl_3$ per H, NaCl as bulking agent.

Sample	C-C Bonds formed	Milling time / min	Yield / %
$C_{60}H_{42}$	9	60	81
$C_{222}H_{150}$	54	60	89

Furthermore, there is the evidence of a mono-chloro adduct, indicated by the second smaller peak at higher m/z values. Thus far, C_{222} is the largest synthesised nanographene and these difficulties are also faced by solution-based methods.[95] Further characterization was conducted via solid state UV/VIS. In the spectra (**Figure 5.42A**), the maxima show a clear bathochromic shift from 353 nm for HBC to 395 nm for C_{60} and to 717 nm for C_{222}. The *in situ* investigations of these systems reveal that, even for the bigger molecules, the reaction proceeds in a matter of minutes (**Figure 5.42B**). This is especially surprising, since C_{222} is - up to now - the biggest reported PAH with well-defined structure and its planarization took 24 hours under optimised conditions,* whereas this protocol for HPB can be transferred without extensive adaption and, therefore, seems to be independent of precursor size.[95]

* For C_{222}, $FeCl_3$ proved to be insufficient for the planarization in solution and stronger Lewis acids had to be employed to achieve the desired results. Müllen *et al.* used $Cu(OTf)_2$ instead.

5.2.1.1 Scholl Reaction of Different Geometries

Besides those nanographenes typically investigated in this kind of studies, where stable six-membered rings are formed during the planarization reaction, there also exist molecules with different geometries. In fact, a considerable amount of effort was put into the planarization of five-membered rings. This is usually not achievable under standard Scholl conditions.[110] Therefore, chemists tried to substitute the hydrogen in the potential five ring position with halogens, in an effort to introduce a better leaving group.[201]

In the case of nanographenes synthesised by the group of Prof. Feng, especially the "extended HPB **7**", the mechanochemical Scholl reaction led to interesting results (**Figure 5.39**). The solution-based protocol was unable to close the 6 bonds needed to planarize the HBC core, only leading to a partially closed intermediate **7'**. Contrarily, the mechanochemical approach was capable to close the compound completely and yielded the "extended HBC **8**", alongside with chlorinated by-products. Interestingly, traces of the substance with closed 5-rings were also identified amongst these by-products (**Figure Appendix 25**).

Since the molecule is rather hard to synthesise, a suitable substitution was identified in 1,2,3,4-tetraphenyl naphthalene **9**, to study the effect in greater depth. In a series of experiments, the amount of oxidant and the energy input during the milling process was varied in order to establish conditions in which this phenomenon can be observed. Under the optimized mechanochemical Scholl conditions, only a fraction of the product was soluble after the planarization. This was unexpected, since the version with 4 closed six-member-rings is known to be a soluble compound

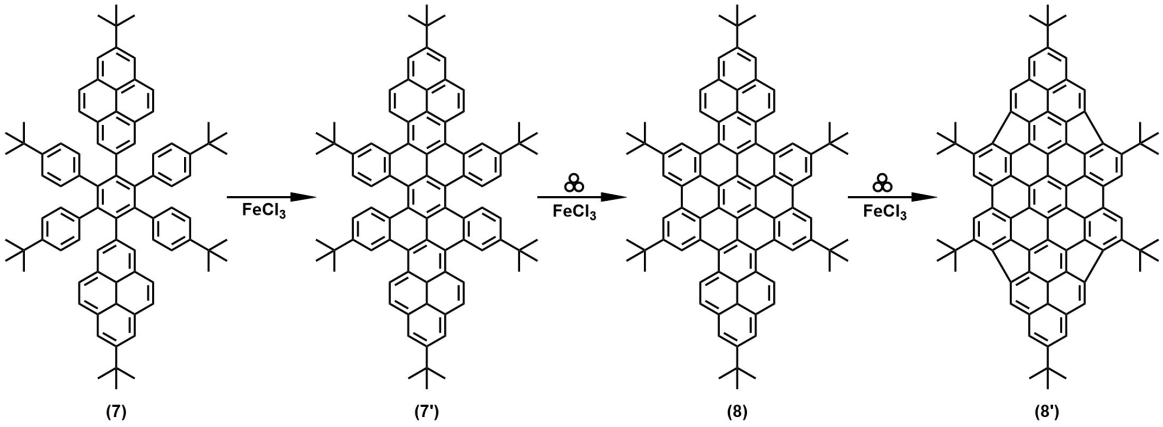

Figure 5.39 The Scholl reaction of extended HPB **7** to yield the extended HBC **8**. In solution only **7'** can be achieved, while the mechanochemical approach also produces **8'** as a side product.

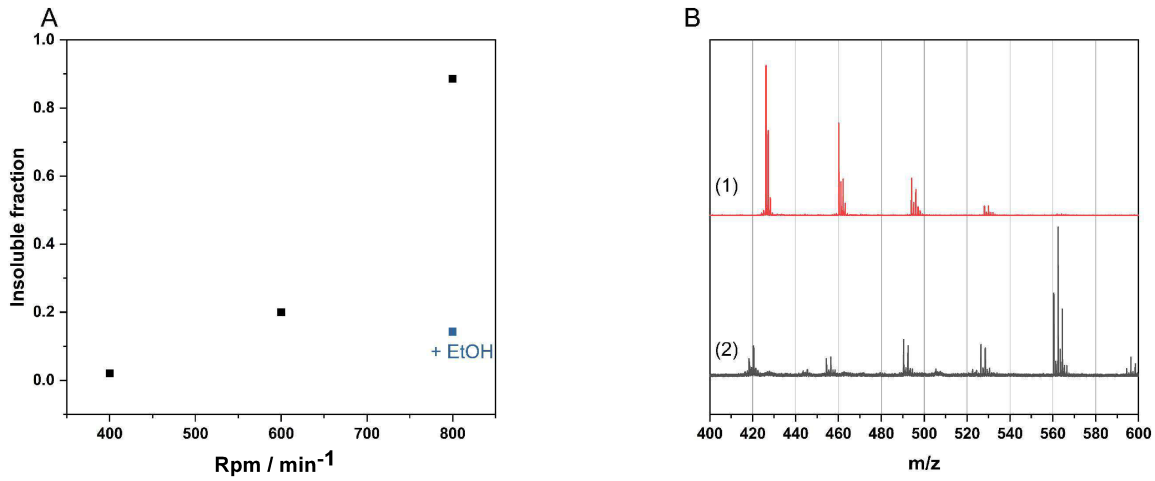

Figure 5.40 A: The amount of insoluble product in the Scholl reaction of 1,2,3,4-tetraphenyl naphthalene in function of the milling speed. **B:** MALDI-TOF spectrum of the soluble fraction (1) and the insoluble fraction (2) of this reaction.

(Hemi-HBC). This insoluble fraction was larger in batches with higher energy input and more iron(III) chloride (**Figure 5.40A**). If one takes a closer look on both fractions produced in the reaction, major differences can be observed. The spectrum of the soluble fraction is dominated by the desired hemi-HBC and mono-, di- and trichloro adduct. On the other hand, in the insoluble fraction, the dominant species is the tetrachloro adduct with one closed five-membered ring (slight shift towards lower m/z).

The same can also be observed for the other peak, which are all shifted by 2 or 4 m/z towards the left. This corresponds nicely to one or two closed five-membered rings. If the chlorination is suppressed, the fraction of insoluble product drastically shrinks and no five-ring formation can be observed, even at high energy inputs. This effect points towards the need of chlorinated species in order to enable this reaction (**Figure 5.41**). DFT calculations seem to agree with this pathway, since the activation energy for a hydrogen abstraction, especially the second one, is relatively high (92 and 201 kJ·mol^{-1}, **Figure Appendix 16**).

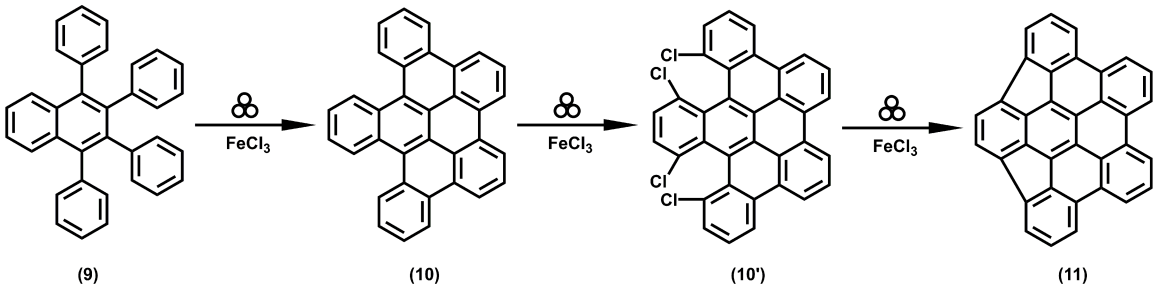

Figure 5.41 The Scholl reaction of 1,2,3,4-tetraphenyl naphthalene **9** to yield hemi-HBC **10**. Under mechanochemical conditions it is further chlorinated **10'** and finally the completely closed species **11** can be observed.

5.2.1.2 **Avoiding Chlorination**

Evident from the results presented on HBC and C_{222}, chlorination is the major side reaction during the planarization process. Although it is also present in solution-based protocols, this pathway should ideally be supressed in order to obtain the cleanest product possible. And as discussed above it can lead to an interesting but undesirable further planarization by five-ring formation. Furthermore, the Scholl reaction leads to a significant increase in vessel pressure, severely hindering the scaleup of this process. Hence, a suppression of vessel pressure and chlorination are both important steps towards a large-scale application. Consequently, measures were taken to deal with the released HCl acid, which is suspected of activating excess $FeCl_3$ and making it capable to chlorinate the nanographenes. A total of four pathways were explored in the process (**Table 5.12**).

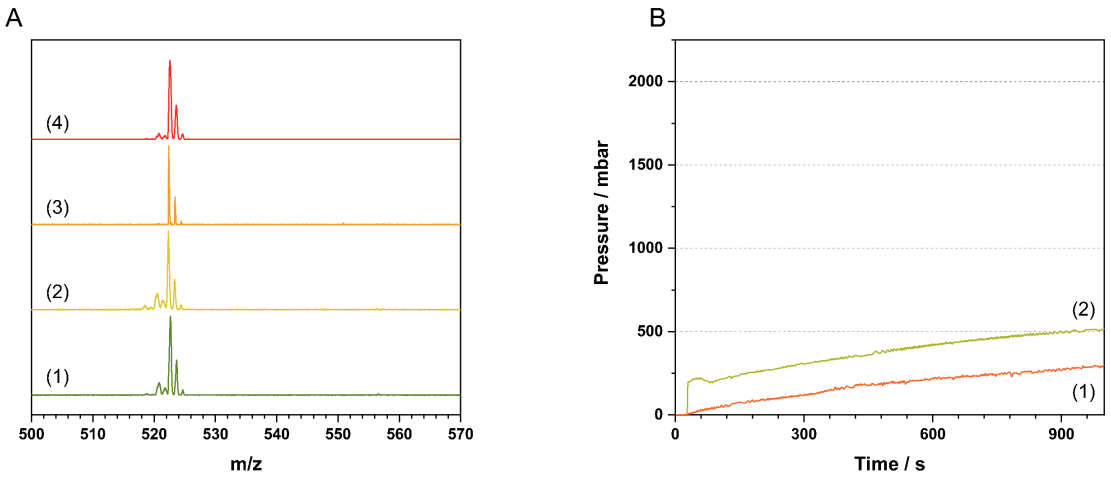

Figure 5.42 A: MADLI-TOF measurements of the HBC system milled with the addition of ethanol (1) and pyridine (2). Only the target mass of 522 m/z can be observed while for (only trace amounts of the mono-chloro adduct are visible. **B:** Development of the relative vessel pressure during the milling process of HBC-EtOH (1) and HBC-Pyridine (2) at 800 rpm.

Table 5.12 Reaction conditions and yields of HBC syntheses while trying to supress chlorination; Reaction conditions if not stated otherwise: 800 rpm, 22x 10 mm balls, ZrO_2, 12 equiv. $FeCl_3$ per H, NaCl as bulking agent.

Sample	Starting material	Milling time / min	Yield / %
HBC-EtOH	HPB[c]	30	45
HBC-EtOH	HPB[c]	60	97
HBC-Pyridine	HPB[d]	30	91
HBC-1.1equiv.[a]	HPB	30	99
HBC-200	HPB	60	95

[a]1.1 equiv. of $FeCl_3$ per H; [b]200 rpm; [c]+1mL EtOH; [d]+1mL pyridine

At first, the gas was dissolved in order to remove it from the reaction. The solubility of the acid is rather good in polar solvents and, while water was excluded from consideration to avoid hydrolysis of the iron chloride, ethanol* was identified as suitable. The LAG approach with this solvent led to a lower yield (45 %) under the conditions optimized before. But, by only increasing the milling time to 60 minutes, full conversion of the HPB could be achieved. This is hinting towards the acceleration of the reaction by the released hydrochloride acid. Probably the same mechanism of activation of the $FeCl_3$ that leads to chlorination is also responsible for the acceleration of the Scholl reaction, or the nature of the LAG process leads to some difficulties in the milling process. Since a clumped-up solid was observed after the milling, compared to a fine powder after dry grinding experiments, the second explanation seems more likely.

To confirm this hypothesis, another route to remove the hydrochloric acid from the milling vessel was investigated. By introducing small amounts of pyridine, which readily reacts with hydrochloric acid and forms solid pyridine hydrochloride, both problems were tackled at once. And indeed, in contrast to the ethanol pathway, the reaction afforded similar yields after only 30 minutes. One can therefore assume that the agglomeration of powder is the main reason for the slower kinetic of the reaction. To prove the absence of chloro adducts, MALDI-TOF measurements of the samples (**Figure 5.42A**) were made. For both samples, only the desired product could be observed, while chlorination seems to be successfully suppressed. In addition, the GTM measurements (**Figure 5.42B**) show the development of significantly less pressure during the milling process, compared to the experiments without additives. In fact, the rise is about as high as for the reference experiments and can therefore be explained solely with the heating of the reactor.

While the two approaches detailed above tackle the release of hydrochloric acid other possible ways of reducing the chlorination are lowering the energy input or reducing the amount of iron chloride to a stoichiometric level. Both ways are indeed successful in supressing the side reaction (**Figure 5.42A**, **Table 5.12**) while maintaining a complete conversion. But, in the course of the milling the vessel pressure is still increasing. Hence, these methods are only suitable if the introduction

* Solubility of HCl in ethanol at 30 °C: 37.52 g / 100 g.[217] The solubility decreases with increasing temperature.

of an additive is not an option from a chemical point of view. On the other hand, both of these workarounds offer interesting prospects in terms of sustainability of the mechanochemical Scholl reaction. If less iron chloride and energy is used, the "greenness" of this pathway is greatly enhanced.

5.2.1.3 **Scholl Reactions in Mixer Ball Mills**

Additionally, a proof-of-principal experiment in a mixer-mill was conducted. Since those mills are generally equipped with smaller milling jars, one can hereby apply this approach to a few mg-scale, suitable for the development of unprecedented, more complex PAHs. Furthermore, the *in situ* techniques reported are all conducted in mills based on this principle.[147,202–206] However, the transfer of protocols between two mill types bears many challenges, and a separate optimization of reaction parameters has to be conducted for mixer mills. The yield after 30 minutes is lower than in the planetary equivalent but an increase in either reaction time or vibration frequency, as well as an adjustment of milling balls (size and number) should produce comparable results in the future.

5.2.1.4 Green Metrics for the Scholl Reaction

Similar to chapter 5.1.2.4, one can also calculate the green metrics for the Scholl reaction (**Table 5.13**). The atom economy of the Scholl reaction of 93 % is excellent for both pathways, due to the nature of the reaction. Differences between the mechanochemical path and its solvent-based analogue become apparent in the mass productivity. Here, the mechanochemical process achieves a mass productivity of 19.4 %, while the solution approach transforms only 0.65 % of its reactants and solvents into product. This is largely due to the need of two different solvents to keep the starting material and the iron(III) chloride in solution. The same picture can be found if both reactions are evaluated based on yield, cost, safety conditions and ease of workup with the EcoScale (**Table 5.13**). The classical approach is limited by the hazardous solvents employed and thus only achieves a value of 67, which ranks the reaction as "acceptable". On the other hand, the mechanochemical Scholl reaction reaches 82.5 points and thus the status of "excellent reaction".

Table 5.13 Overview of the green metrics for the Scholl reaction in different systems.

Type	Atom economy	Mass intensity	Mass productivity	Reaction time
Solvent-based[a]	93	153.85	0.7	1 h
Mechanochemical	93	5.15	19.4	30 min

EcoScale Parameter	Penalty points: Mechanochemical	Penalty points: Solvent-based[a]
1. Yield: 99 % / 98 %	0.5	1
2. FeCl3	0	0
DCM	-	0
Hexaphenylbenzene	5	5
Nitromethane	-	0
Methanol	0	0
3. DCM (T)	-	5
Nitromethane (E, T, F)	-	10
Methanol	10	10
4. Common setup	0	0
Argon atmosphere	-	1
5. Room temperature, <1 h	0	-
Room temperature, <24 h	-	1
6. Adding solvent	0	0
Simple filtration	0	0
Penalty Points	**17.5**	**33**

[a] according to reference [207] in 250 mL DCM and 10 mL nitromethane. For details on the calculations see 5.1.2.4 on page 53 and Table 7.2 on page 100.

5.2.1.5 **Conclusion**

In summary, a novel and innovative mechanochemical process for the Scholl reaction of benchmark nanographenes has been developed. Using $FeCl_3$ in a solvent-free protocol in a planetary ball mill, it could be demonstrated that these reactions proceed in as little as 30 minutes and are limited by neither the solubility nor the size of the PAH. Utilizing MALDI-TOF and solid-state UV/Vis measurements to prove the success of the reaction also lead to the discovery of growing degree of chlorination with increasing reaction time. Based on these findings, the influence of different milling parameters on this reaction was identified and it was found that energy related parameters play a key role. Utilizing *in situ* pressure measurements, the reaction kinetics and energetics were further elucidated and a threshold milling speed for the process could be determined. The chlorination of the nanographenes was suppressed via several pathways, while a high yield and short reaction times were maintained. Furthermore, the protocol was expanded to bigger nanographenes, namely C_{60} and C_{222}. In addition, the process was also transferred into a mixer ball mill, enabling the scalability to few mg scales. This new reaction route paves the way towards larger extended nanographenes in spite of their low solubility, and therefore renders the introduction of solubilizing groups obsolete.

5.2.2 Edge Chlorination

In the last chapter, the planarization of nanographenes using the mechanochemical Scholl reaction was discussed.[52] For these materials, solubility is one of the major concerns and, therefore, the solvent-free pathway is offering an inherent advantage. For a number of applications, however, solution-based processing cannot be completely avoided and a simple method to introduce solubilizing groups post-synthesis is highly sought after. In our work on the planarization, we also noticed a partial chlorination as a side reaction - especially under high energy conditions. The focus of this chapter is to push this side reaction to a full chlorination of the nanographenes - or at least to a point where they become soluble. That mechanochemical aromatic substitution reactions to form aryl halides are indeed possible was first reported by Ondruschka and co-workers.[208] They utilized oxone and the corresponding sodium halide to successfully functionalize mesitylene with bromide and chloride groups. During their research, they observed that the reaction proceeds sequentially and multiple substitutions can be achieved if the ratio of the halides is adjusted. However, only small organic molecules and a maximum of three substitutions have been investigated.[208]

In this study, the focus was set on developing a protocol for the solvent-free edge-chlorination under mechanochemical conditions for the same benchmark nanographenes as in the prior chapter (HBC, triangular shaped $C_{60}H_{42}$ and C_{222}). The influence of different pathways on the chlorination is studied (**Figure 5.43**). Furthermore, the quality and structural homogeneity of produced nanographenes have been confirmed by MALDI-TOF mass spectrometry, UV/Vis absorption and IR spectroscopy.

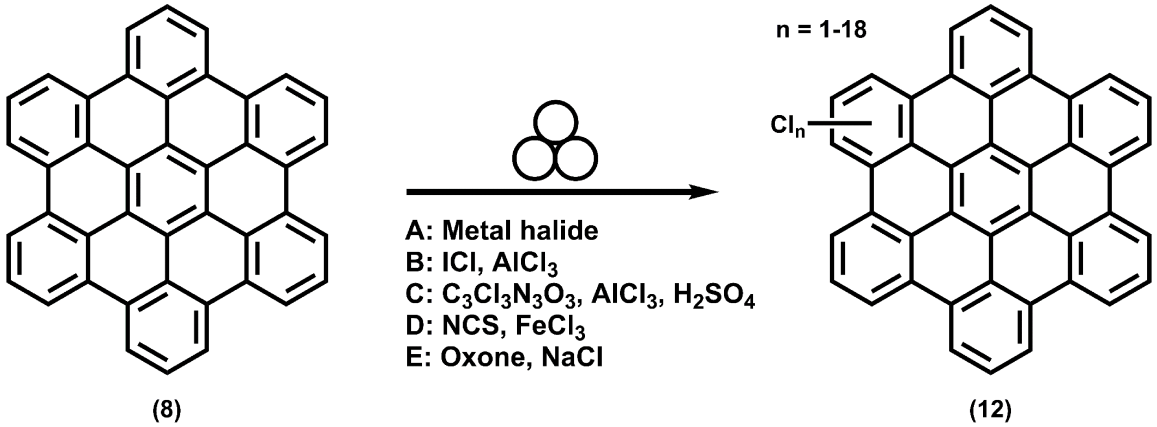

Figure 5.43 Different pathways for the edge-chlorination of HBC **8** to yield the partially or fully chlorinated HBC **12** presented in this chapter.

5.2.2.1 Edge Chlorination of Hexaphenylbenzene

While several chlorination methods are known to work in solution, only two approaches have been employed in solid-state up to now. One of the most common chlorination protocols is the so-called BMC* procedure. The reaction between thionyl chloride and sulfur monochloride, in combination with aluminum chloride as a Lewis acid, creates the extremely reactive species $SCl_3^+AlCl_4^-$, which can pretty much chlorinate every organic molecule.[209] However, experiments with this reagent only yielded completely insoluble, uncharacterizable, mixtures of products. Thus, this method is omitted from further discussion.

After failure of the BMC pathway, the first approach was to force the existing Lewis acid system towards a higher degree of chlorination. The key factors in avoiding chlorination was the reduction of energy input and reaction time. It is, therefore, to be expected that a high energy input for a longer period of time enhances the chlorination reaction. The major problem with this kind of approach is that, as was recently published, Friedel-Crafts reactions are thriving under similar conditions.[86] Thus, the result was a large amount of insoluble oligomerization and

Table 5.14 Reaction conditions and yields of the chlorinated HBC syntheses; Reaction conditions if not stated otherwise: 800 rpm, 10x 10 mm balls, ZrO_2, 60 min.

Entry	Method	Time / min	Soluble Fraction / %	Yield[a] / %
1	A – $FeCl_3$	60	81	49
2	B	60	33	21
3	C	60	49	33
4	D	60	37	20
5	E	60	83	43
6	A – $CuCl_2$	60	8	5
7	A – $AlCl_3$	60	1	0.5
10	A – $MoCl_5$	60	11	15
11	A – $FeCl_3$	720	22	22
12	A – $AlCl_3$	720	1	0.5

[a] yield calculated for the soluble fraction in regard to perchlorinated HBC

* The BMC method is named after the initials of its developers: Manuel **B**allester, Carlos **M**olinet and Juan **C**astañer. It was developed in the 60's and has since been used for the chlorination of organic compounds.[218]

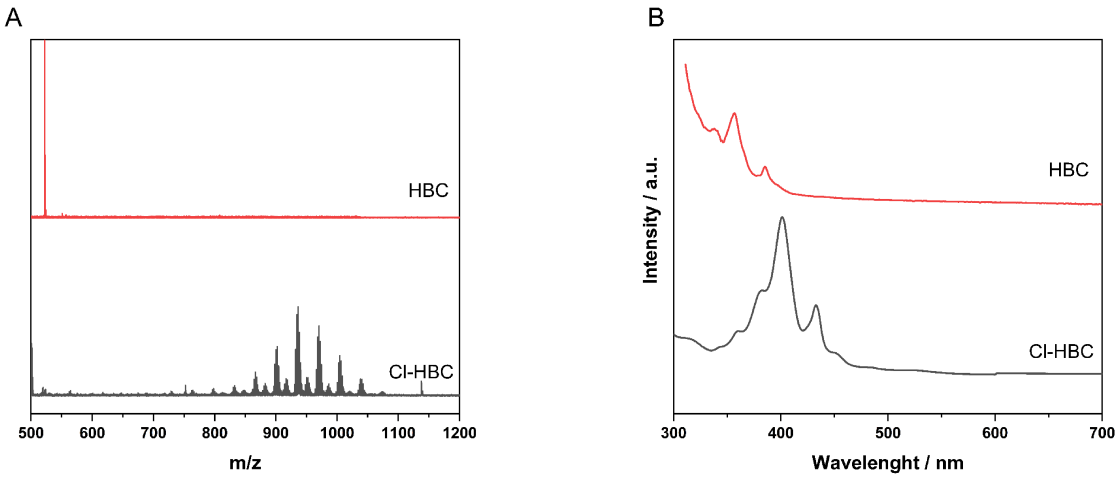

Figure 5.44 A: MALDI-TOF spectrum of chlorinated and pristine HBC by approach A ($FeCl_3$). **B:** UV/Vis spectra of these compounds in toluene.

polymerization products, instead of a fully chlorinated nanographene. It is therefore important to keep the reactions times and energy input on a moderate level, while still enabling the chlorination reaction. The resulting procedure was able to produce roughly 80 % of soluble chlorinated HBC with a mixed amount of chloride atoms per molecule (**Table 5.14**, Entry 1). This mixture can be observed directly in the MALDI-TOF spectrum (**Figure 5.44A**), where everything between 5 and 16 chlorine atoms per molecule are detected, with the majority being around 11 (**Figure 5.45A**). The chlorination can also be clearly observed in the UV/Vis spectra of the substances, where it leads to a strong bathochromic shift of about 50 nm (**Figure 5.44B**). The obtained spectra are in close agreement with the literature.[112]

An increase in reaction time led to the aforementioned oligomerisation instead of an increase of perchlorinated product. Therefore, other pathways were explored

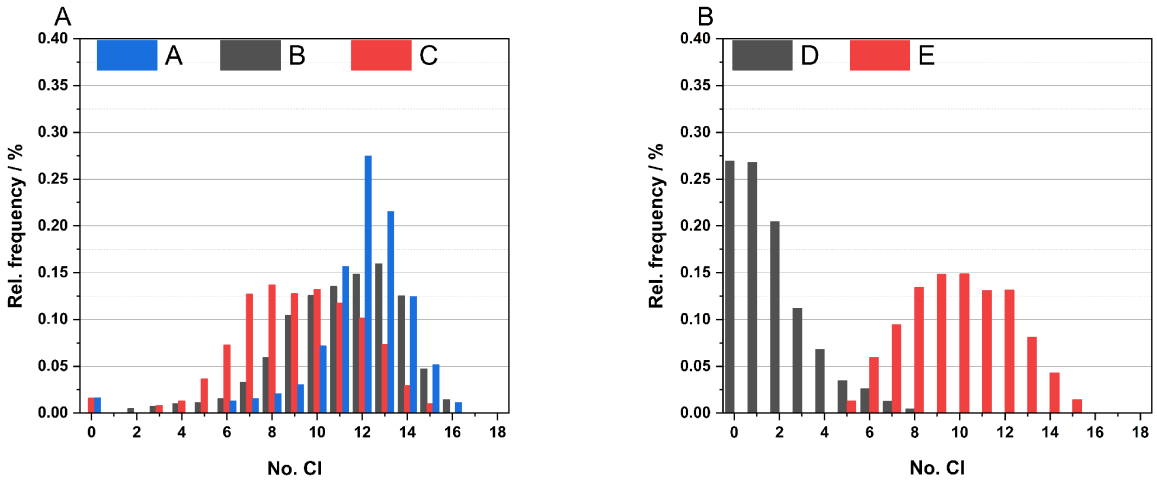

Figure 5.45 A: Representation of the varying degree of chlorination for the methods A: $FeCl_3$, B: ICl, $AlCl_3$, C: $C_3Cl_3N_3O_3$, H_2SO_4. **B:** Representation of the varying degree of chlorination for the methods. D: NCS, E: Oxone.

to achieve this goal. The first idea was to simply adapt the solution-based protocol for the chlorination of nanographenes reported by Tan *et al*.[112] However, the results were inferior in both soluble amount of product and degree of chlorination (**Table 5.14**, Entry 2). This might be due to the fact that iodine monochloride as a liquid is hindering an effective mechanochemical reaction by dissipating a major fraction of the impact energy. Furthermore, the approach led to a clumped-up texture of the powder after the reaction, thus impeding an efficient mixing.

In another attempt to raise the amount of chlorine introduced to the nanographenes, a mixture of trichloroisocyanuric acid (TCCA)* and sulfuric acid was used, according to a protocol for chlorination by Duncan and coworkers.[210] This system yielded slightly better results than the iodine monochloride system but also suffered from the liquid (H_2SO_4) added for the activation of the TCCA (**Table 5.14**, Entry 3). It achieved slightly inferior chlorination results after one hour then the pure Lewis acid system. A more common approach to chlorination in organic chemistry is the use of N-chlorosuccinimide.[211] While this approach suffers from a low atom economy of the reaction, it was nevertheless tried out for the nanographenes. Transferring this method into the ball mill led to a maximum of eight chlorine atoms introduced (**Table 5.14**, Entry 4).

As mentioned earlier, Ondruschka and co-workers utilized Oxone† in combination with sodium halides to achieve chlorination of simple aromatic molecules.[208] It is likely that this approach leads to an *in situ* formation of the halogen gas (Cl_2) or hypochlorite, which consequently chlorinates the aryls. In the chlorination of HBC, this approach leads to results comparable to those obtained for than iron(III) chloride. However, the MALDI-TOF data suggest additional species beside the ones expected from chlorination. This might be due to additional sulfonation or oxidation caused by the peroxysulfate.

---

* TCCA is used as an algicide and bactericide in swimming pools and as a dye in the textile industry and is therefore a cheaply available chemical.[219]

† Oxone is the triple salt ($KHSO_5$ 0.5·$KHSO_4$ 0.5·K_2SO_4). It has a higher stability than pure potassium peroymonosufate and is commonly used as an oxidant in organic chemistry.[220]

5.2.2.2 One-Pot Planarization and Edge Chlorination

While the development of a fast and non-toxic chlorination pathway for nanographenes is interesting on its own, as discussed earlier the "side reaction" of chlorination had to be suppressed during the planarization of said molecules.[52] In the context of this study it would be desirable to enhance the chlorination during the planarization in order to achieve a one-pot planarization and chlorination of nanographene precursors (**Figure 5.46**). This would eliminate the need for additional processing steps and lead directly to soluble molecules.

The results, from the investigation of the Scholl reaction, gave a clear picture whether it is possible to achieve this one-pot process with iron chloride alone. While the use of tungsten carbide milling balls achieved a high degree of chlorination for some molecules, the yield was very low (<10 %). Increasing the equivalents of iron(III) chloride further (1000:1) also had no positive effect. Consequently, the mixtures used for the edge-chlorination of HBC were milled with hexphenylbenzene instead of HBC. As a matter of fact, it seems that the hydrochloride acid released

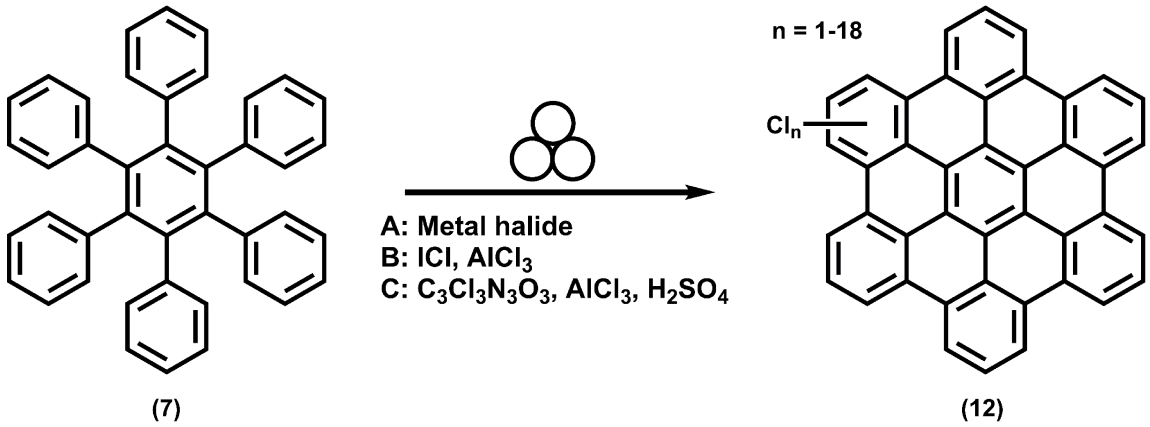

Figure 5.46 Different pathways for the one-pot planarization and edge-chlorination of HPB **7** to yield the partially or fully chlorinated HBC **12** presented in this chapter.

Table 5.15 Reaction conditions and yields of the one-pot chlorinated HBC syntheses; Reaction conditions if not stated otherwise: 800 rpm, 10x 10 mm balls, ZrO_2, 60 min.

Entry	Method	Time / min	Soluble Fraction / %	Yield[a] / %
1	A – $FeCl_3$	60	8	4
2	B	60	50	43
3	C	60	31	28

[a] yield calculated for the soluble fraction in regard to perchlorinated HBC

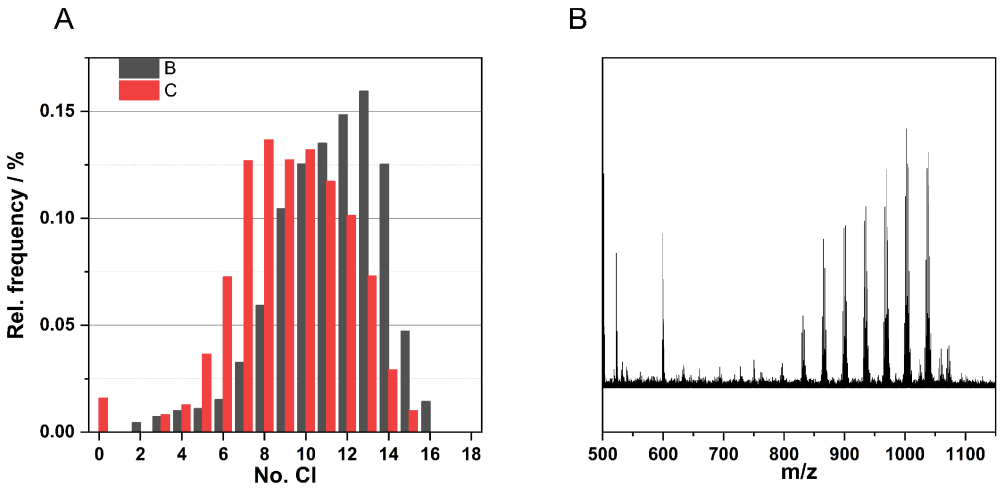

Figure 5.47 A: Representation of the varying degree of chlorination for the methods B: ICl, $AlCl_3$, C: $C_3Cl_3N_3O_3$, $FeCl_3$. **B:** MALDI-TOF spectrum of chlorinated and soluble HBC by approach B.

during the planarization reaction has a catalysing effect on the two methods for edge-chlorination presented above. For the TCCA approach this is in line with the literature, were acids are commonly used as catalysts.[210] For the iodine monochloride method, the effect probably stems from the activation of the aluminium chloride present in the slurry. Both of these methods lead to a partially soluble product after as little as 60 minutes. In the direct comparison, the iodine monochloride pathway shows a higher yield and higher degree of chlorination (**Figure 5.46A** and **Table 5.15**). Interestingly, compared to the edge-chlorination performed from HBC, the MALDI-TOF pattern is shifted towards a higher degree of chlorination (**Figure 5.46B**).

5.2.2.3 **Conclusion**

In this chapter, the chlorination reaction observed during the Scholl reaction was investigated more thoroughly. While several chlorination reagents produced a fair quantity of soluble chlorinated HBC, the best results could be obtained with iron(III) chloride and a mixture of Oxone and sodium chloride. Several other Lewis acids were also investigated, but resulted in worse yields, and side-reactions like oligomerisation were difficult to avoid completely. Standard chlorination procedures from solution-based chemistry, generally, performed poorer in the solvent-free environment. Compared to those methods, the mechanochemical chlorination protocol does not rely on overly toxic solvents like carbon disulfide or tetrachloromethane. The reaction time is also significantly shorter, requiring only one hour instead of several days. It has also been demonstrated that the planarization and chlorination reaction can be conducted in a one-pot manner. The hydrochloric acid formed during the planarization seems to be beneficial to the chlorination reaction and thus higher degrees of chlorination could be achieved with this approach. By combing the two reactions one can obtain a considerable fraction of soluble nanographenes, from scratch, in as little as 60 minutes.

6 SUMMARY AND OUTLOOK

The aim of this thesis was the adaptation of different polymerisation reactions and the synthesis of nanographenes to the solvent-free environment of a ball mill. As stated in the previous chapters, this has overall been a resounding success. The developed mechanochemical protocols, are not only on par with solution-based analogues but outperform them in most cases. Not only were reaction time and energy consumption considerably lower for mechanochemical reaction, yields and polymerization degrees could be raised as well.

The first part of this work focused on the development of mechanochemical polymerization procedures. The first pathway chosen by me, adapted the procedure of Kaupp and co-workers for the reaction between an aldehyde and an amine to difunctional monomers, in order to obtain a linear poly(azomethine).[121] The reaction proceeded in a matter of minutes, producing the infusible polymer in quantitative yields. The polymer synthesised by this approach is outperforming the solution-based reference in all benchmarks. This can be attributed to the poor solubility of the polymer: whereas it is leading to an almost instant precipitation and thus an end of the polymerization reaction in solution, the solvent-free approach is not having such constraints. This reaction was also used for a first, although rudimentary, study of the milling parameters. It was quickly found that a higher energy input, in the form of tungsten carbide balls, led to a higher degree of polymerization. The addition of small amounts of ethanol pushed the conversion of aldehyde groups even further. While the linear polymers are only of limited use, the azomethine formation is a staple reaction for the construction of covalent organic frameworks (COF). It has been recently shown that a mechanochemical reaction can also produce these promising porous materials. While I conducted preliminary experiments to synthesise porous COFs, the results so-far have been underwhelming. The key towards these is most likely the use of appropriate porogenes and a moderate amount of energy to avoid a collapse of the porosity. Therefore, more experiments have to be conducted in order to establish conditions to produce COFs with a permanent porosity inside the ball mill.

Another basic reaction of organic chemistry is the Suzuki cross-coupling. This metal-catalysed reaction has been used for decades to synthesise poly(phenylenes).

The mechanochemical variant of this reaction has been reported for several organic molecules.[145] After verifying that several couplings at once were possible, I went on to synthesise a linear and hyperbranched poly(phenylene) via this reaction. The results for the linear poly(para-phenylene), a polymer renowned for its infusibility and insolubility, were especially noteworthy. By adopting an AB approach, the degree of polymerization could be raised to exceed every other synthesis method, including chemical vapor deposition. Adding to this, the long polymer, with 164 repeating benzyl rings, can be produced in as little as 30 minutes, while using palladium acetate and in a non-inert atmosphere. Compared to 12 to 24 hour syntheses in solution, needing expensive ligands, this is a major improvement. The hyperbranched polymer showed a good thermal stability and a porous structure. Alike to the poly(azomethine) procedure, the Suzuki reaction can be used to produce COFs. Similarly, preliminary reactions towards these 3D materials have been unsuccessful so far. However, the strengths of this cross-coupling lie within the synthesis of graphene nanoribbon precursors. In this topic, a cooperation with the group of Prof. Feng was initiated. A major advantage of the mechanochemical approach is, once again, the indifference towards solubility. Therefore, longer chains and in turn longer nanoribbons might be build-up using this approach in the future.

Finishing the first part of this thesis is an oxidative polymerization approach. In contrast to the two polymerizations investigated before, this had already been used for the synthesis of linear polymers. In fact, it was the first polymerization reaction reported inside a ball mill.[80] By changing the monomer to a trifunctional one, this reaction was used to synthesise a porous polymer instead of a linear one. The material obtained is highly microporous thiophene polymer with a monodisperse pore size of 1.6 nm, which perfectly fits the structural simulation. Furthermore, the typical polymeric swelling behaviour cannot be observed and thus the network seems to be highly interconnected. The *in situ* monitoring equipment allowed to follow this reaction through the release of hydrochloric acid. The data supports the swiftness of the reaction with a plateau after 15 minutes. By applying a design of experiments approach, the amount of oxidant was found to govern the yield and the porosity of the material. Under optimized conditions, the surface area of the polymer (1850 $m^2 \cdot g^{-1}$) is almost twice as high as the values reported in the literature for the solution-based reference. In combination with the also high pore volume of 0.95 $cm^3 \cdot g^{-1}$ and a quantitative yield this polymer is promising for applications as

catalyst support or for the hydrogen evolution reaction.[120] The latter is recently being explored in a cooperation with the group of Prof. Thomas. Besides thiophene monomers, carbazole based monomers can also be polymerised using this protocol. In the future, it might be beneficial to widen the scope even further by using pyrrole- or pyridine-containing monomers with adequate doping for the synthesis of conducting porous polymers.

The second part of this thesis was concerned with an oxidative C-C coupling reaction – the Scholl reaction. In the area of nanographenes, solubility is always a major concern. For many molecules, solubilizing groups are introduced to keep them in solution after planarization. I could show that the Scholl reaction is proceeding in the ball mill in as little as 30 minutes, with quantitative yields and is limited neither by the solubility nor the size of the nanographenes. Once again, the reaction could be followed by using an *in situ* pressure measurement, due to the released hydrochloric acid. This way, a threshold milling speed, from which the reaction proceeds, could be determined. Afterwards, a design of experiment approach was applied to optimize the yield of the reaction. Especially when using a high energy input or long reaction times, chlorination of the products could be observed as a side reaction. Consequently, four different workarounds were developed to suppress this. While the reduction of the amount of iron chloride was the most straightforward way, the addition of small amounts of ethanol also completely suppressed the pressure rise, inside the vessel. Hence, the scale-up of this planarization can be simplified. In addition, the reaction was expanded to bigger nanographenes, namely C_{60} and C_{222}, and adapted to a mixer ball mill. Interesting results were obtained for molecules with potentially closable five-membered rings. Here the side reaction of chlorination seems to play a role in the formation of said five-rings. The closing of these cannot be achieved by solution-based protocols in one step. At the moment, I am working on expanding the Scholl reaction to its main purpose: the planarization of graphene nanoribbons. Together with the group of Prof. Feng, this challenging topic is being investigated, with the bottleneck being the synthesis of suitable molecules in quantities necessary for the ball mill. In the future, the planarization of other geometries like seven-membered rings, might also be attainable. Another possible improvement is the utilization of a reductive pathway, with copper instead of iron chloride. First reactions have been very promising in this

regard, leading to a full conversion to HBC, but requiring reaction times exceeding 12 hours.

On a last note, the chlorination reaction observed during the Scholl reaction, was further investigated. I found that, by using iron(III) chloride as chlorination agent, an almost completely soluble nanographene could be obtained. This is especially interesting since the mechanochemical chlorination protocol does not rely on overly toxic solvents like carbon disulphide or tetrachloromethane. The reaction time is also significantly shorter, requiring only one hour instead of several days. While studying this reaction, I noticed that some of the reagents used are also present in the Scholl reaction. Thus, a combination of the two separate reactions led to a one-step procedure for the production of partially chlorinated nanographenes. This protocol could be potentially applied to the graphene nanoribbons as well. Hence, a one-step planarization and chlorination reaction, not requiring solubilizing groups, seems to be a highly probable prospect.

At this point, I would like to return to the motivation, where I stated: “Hence, a lot of applications, reactions and mechanisms in a ball mill are still left to be discovered or are not well understood.” In the course of this thesis I demonstrated the potential that mechanochemistry has in the fields of polymer synthesis and nanomaterials. I strongly believe that the field of mechanochemistry is only at the beginning of its renaissance, and, with the concept slowly being picked up by more and more chemists and the industry, this process will be accelerated. Therefore, mechanochemical synthesis will enable us to make green chemistry a reality across all fields and many applications.

7 EXPERIMENTAL SECTION

7.1 PART I – MATERIALS AND METHODS

7.1.1 Materials

Table 7.1 Chemicals used in this thesis.

Chemical	CAS-number	Supplier	Purity
1,2,3,4-tetraphenylnaphthalene	751-38-2	Sigma Aldrich	97 %
1,3,5-tris(2-thienyl)benzene	15509-95-2	TCI	> 98 %
1,3,5-tris(N-carbazolyl)benzene	148044-07-9	Sigma Aldrich	> 97 %
1,3,5-tribromobenzene	626-39-1	TCI	> 98 %
1,4-benzenediboronic acid	4612-26-4	TCI	97 %
1,4-benzenediboronic acid bis(pinacol) ester	99770-93-1	TCI	> 98 %
1,6-dibromopyrene	27973-29-1	Carbosynth	> 97 %
1,4-dibromobenzene	106-37-6	ABCR	99 %
3,5-dibromophenylboronic acid	117695-55-3	TCI	97 %
4-biphenylboronic acid	5122-94-1	Activate Scientific	98 %
4-bromophenylboronic acid	5467-74-3	TCI	97 %
5,6,11,12-tetraphenylnaphthacene	517-51-1	Sigma Aldrich	> 98 %
Acetone	67-64-1	BCD Chemie	98 %
Acetonitrile	75-05-8	ABCR	99 %
Aluminium chloride	7446-70-0	ABCR	99 %
Bis-(4-bromophenyl acetylene)	2789-89-1	Fisher Scientific	97 %
2-Bromoacetophenone	70-11-1	TCI	> 98 %
Chloroform	67-66-3	Fisher Scientific	> 98 %
Copper(I) iodide	7681-65-4	Strem Chemicals	98 %
Copper(II) bromide	7789-45-9	Sigma Aldrich	99 %
Trifluoromethansulfonic acid	1493-13-6	Sigma Aldrich	98 %
Copper(II) chloride	7447-39-4	ABCR	98 %
Copper(II) fluoride	7789-19-7	Sigma Aldrich	98 %
Dichlorobis(triphenylphosphine)palladium(II)	13965-03-2	Strem Chemicals	99.9 %
Dichloromethane	75-09-2	VWR Chemicals	> 98 %
Dicobalt octacarbonyl	10210-68-1	Strem Chemicals	95 %
Ethanol	64-17-5	VWR Chemicals	> 98 %
Ethynyltrimethylsilane	1066-54-2	Sigma Aldrich	98 %

Chemical	CAS-number	Supplier	Purity
Hexaphenylbenzene	992-04-1	TCI	98 %
Iodine monochloride	7790-99-0	ABCR	n.a.
Iodine trichloride	865-44-1	Sigma Aldrich	97 %
Iron(III) chloride, anhydrous	7705-08-0	ABCR & Sigma Aldrich	> 98 %
Magnesium sulfate	7487-88-9	Grüssing	99 %
Methanol	67-56-1	VWR Chemicals	> 98 %
Molybdenum(V) chloride, anhydrous	10241-05-1	ABCR	99.6 %
N-chlorosuccinimide	128-09-6	Sigma Aldrich	98 %
N,N-dimethylformamide	68-12-2	Fisher Scientific	> 98%
O-terphenyl	84-15-1	Sigma Aldrich	99 %
OXONE®, monopersulfate compound	70693-62-8	Sigma Aldrich	n.a.
Palladium acetate	3375-31-3	Sigma Aldrich	98 %
P-phenylendiamin	106-50-3	ABCR	97 %
Phenylboronic acid	98-80-6	Sigma Aldrich	95 %
Potassium carbonate	584-08-7	Grüssing	> 98 %
Sodium chloride	7647-14-5	Grüssing	> 98 %
Terephthalaldehyde	623-27-8	ABCR	98 %
Tetrahydrofuran	109-99-9	VWR Chemicals	> 97%
Tetrakis(4-aminophenyl)methane	60532-63-0	Sigma Aldrich	> 90%
Tetraphenylcyclopentadienone	479-33-4	Fisher Scientific	99 %
Toluene	108-88-3	Sigma Aldrich	> 99 %
Trichloroisocyanuric Acid	87-90-1	TCI	> 95 %
Trifluoromethansulfonic acid	1493-13-6	Sigma Aldrich	98 %
Triphenylene	217-59-4	Sigma Aldrich	98 %
Triphenylphosphine	603-35-0	Sigma Aldrich	99 %
Tetrakis(triphenylphosphine)palladium(0)	14221-01-3	Strem Chemicals	99 %
Hydrochloric acid (37 % in H_2O)	7647-01-0	VWR Chemicals	n.a.

Zirconium dioxide (Type ZY-S) milling balls with a diameter of 5 mm were purchased from Fritsch GmbH. The average weight of one milling ball is 0.41 ± 0.01 g.

Zirconium dioxide (Type ZY-S) milling balls with a diameter of 10 mm were purchased from Sigmund Lindner GmbH. The average weight of one milling ball is 3.19 ± 0.05 g.

Zirconium dioxide (Type ZY-S) milling balls with a diameter of 15 mm were purchased from Sigmund Lindner GmbH. The average weight of one milling ball is 11.4 ± 0.5 g.

Tempered steel (1.4125, AISI 440C) milling balls with a diameter of 10 mm were purchased from TIS Wälzkörpertechnologie GmbH. The average weight of one milling ball is 4.02 ± 0.02 g.

Tempered steel (1.4125, AISI 440C) milling balls with a diameter of 15 mm were purchased from TIS Wälzkörpertechnologie GmbH. The average weight of one milling ball is 13.77 ± 0.01 g.

Tungsten carbide (YG6X, G10 surface) milling balls with a diameter of 10 mm were purchased from Zhuzhou Good Cemented Carbide Co., Ltd. The average weight of one milling ball is 7.20 ± 0.26 g*.

Tungsten carbide (YG6X, G10 surface) milling balls with a diameter of 15 mm were purchased from Zhuzhou Good Cemented Carbide Co., Ltd. The average weight of one milling ball is 26.21 ± 0.01 g.

Silicon nitride (Type SNCB5) milling balls with a diameter of 5 mm were purchased from Fritsch GmbH. The average weight of one milling ball is 1.95 ± 0.01 g.

* The balls measured had already been used to a different degree, this explains the big variations (standard deviation) in the mass per ball.

7.1.2 Methods

Argon physisorption measurements were performed at 87 K on an Autosorb-IQ-C-XR (Quantachrome Instruments). High purity gases were used for physisorption measurements (Ar: 99.999 %). Specific surface areas (SBET) were calculated using the equation from Brunauer, Emmet and Teller (BET) in a relative pressure range that fits to the consistency criteria proposed by Rouquerol and Llewellyn.[212] Pore size distributions were calculated using the Quenched Solid Density Functional Theory (QSDFT) method for carbon (slit pores, equilibrium kernel) on the adsorption branch. Total pore volumes were determined from the adsorption branch at $p/p_0 = 0.95$. Prior to physisorption experiments, all samples were activated at 423 K for 24 h under vacuum.

Ball milling was conducted in two Pulverisette 7 premium line planetary ball mills of Fritsch GmbH with the original milling vessels. The details ball size, material etc. are given at the individual experiment. In some cases, a MM-400 of the Retsch GmbH was used as a mixer ball mill instead. These instances are marked separately.

Dynamic light scattering (DLS) was measured at an MALVERN Zetasizer Nanosizer in quartz cuvettes. The sample was dissolved in concentrated sulfuric acid and filtered through a 0.2 µm PTFE filter. Per sample 3 measurements with 11 runs each were conducted in backscattering mode. The attenuator and measurement position were determined automatically.

Dynamic scanning calorimetry (DSC) was performed on a Mettler Toledo DSC1 STARe System using aluminum crucibles under argon stream with the heating rate of 10 K min^{-1}. The results were analyzed using the STARe SW 11.00 software. The samples were cycled from RT to 450 °C, then cooled down to RT again afterwards a second cycle was done with the same conditions. For the integrations the second heating curve was utilized.

Elemental analysis was carried out on a vario MICRO cube Elemental Analyzer by Elementar Analysatorsysteme GmbH in CHNS modus.

Infrared spectroscopy (IR) was carried out on a BRUKER Vertex 70 with a Specac Golden Gate ATR unit. A resolution of 2 cm^{-1} was utilized and the resulting spectra were treated with ATR-correction by the OPUS 6.5 software. Each sample was

measured five times and the average of the integrals was taken in order to reduce effects caused by inhomogeneities.

Gel permeation chromatography (GPC) was performed with a AGILENT TECHNOLOGIES series 1200 HPLC pump, and 1 PL MIXED-C separation column 300x 7,5 mm and 5 µm PSgel, a Fa. BURES RI and viscosity detector and a WYATT TECHNOLOGY MiniDAWN-LS detector. THF (stabilized with 0.0025 wt% BHT) was used as an eluent with a flow rate of 1mL·min^{-1}.

Matrix assisted laser desorption ionization time of flight mass spectroscopy (MALDI-TOF) was carried out on a Bruker Autoflex Speed spectrometer using a 337 nm nitrogen laser with dithranol + AgTFA or TCNQ as matrix.

Proton Nuclear magnet resonance spectroscopy (^{1}H NMR) was recorded in deuterated Dichlormethane (CD_2Cl_2) solution at room temperature, using a BRUKER AC 300 P instrument.

Nitrogen physisorption measurements were performed at 77 K on a Quantachrome Quadrasorb apparatus. High purity gases were used for physisorption measurements (N_2: 99.999 %). Pore size distributions were calculated using the Quenched Solid Density Functional Theory (QSDFT) method for carbon (slit/cylinder/sphere pores, adsorption kernel) on the adsorption branch. Prior to physisorption experiments, all samples were activated at 423 K for 12 h under vacuum.

Powder X-ray diffraction (PXRD) patterns were collected in transmission geometry (Mythen 1K detector) with a Stoe Stadi P diffractometer operated at 40 kV and 30 mA with a Ge monochromator using Cu-Kα1 radiation.

Scanning electron microscopy (SEM/EDX) images were obtained using a Hitachi SU8020 SEM equipped with a secondary electron (SE) detector. Prior to the measurement the samples were prepared on an adhesive carbon pad and sputtered with gold to obtain the necessary electron conductivity.

Solid state ^{13}C CP-MAS NMR experiments were performed on a Bruker Ascend 800 spectrometer operating at 201.2 MHz for ^{13}C using a commercial double resonance 3.2 mm MAS NMR probe. Ramped ^{1}H-^{13}C cross-polarization (CP, contact time: 4 ms, pulse repetition time: 3 s) and SPINAL ^{1}H-decoupling was applied. The

MAS frequency was 15 kHz. The ^{13}C chemical shifts were referenced with adamantane. Peak assignment was done utilizing ACD Labs*.

Solid state UV/Vis measurements were conducted on a VARIAN Cary 4000 with a HARRICK Praying Mantis unit. The step width was set to 1 nm and the sources were switched at 350 nm. The crude samples were mixed with an excess of $BaSO_4$ prior to measuring.

Thermogravimetric analysis (TGA) was performed on a NETZSCH STA 409 PC/PG system using alumina crucibles under argon stream with the heating rate of 10 $K \cdot min^{-1}$.

Transmission electron microscopy (TEM) was recorded using a Carl Zeiss Libra 120.

1 * ACD/C+H NMR Predictors and DB 2017.1.3, *Advanced Chemistry Development*, Inc., Toronto, ON, Canada, www.acdlabs.com, 2017.

7.1.3 Green Metrics

Table 7.2 Penalty points in the EcoScale metric.

Parameter	Penalty points:
1. Yield	(100 - % yield)/2
2. Price of reaction components (to obtain 10 mmol of product)	
Inexpensive (<$10)	0
Expensive (>$10 and <$50)	3
Very expensive (>$50)	5
3. Safety	
N (dangerous for environment)	5
T (toxic)	5
F (highly flammable)	5
E (explosive)	10
F+ (extremely flammable)	10
T+ (extremely toxic)	10
4. Technical setup	
Common setup	0
Funnel, syringe pump, gas pressure regulator	1
Unconventional activation technique	2
Pressure equipment, >1 atm	3
Any additional special glassware	1
(Inert) gas atmosphere	1
Glove box	3
5. Temperature/time	
Room temperature, <1 h	0
Room temperature, <24 h	1
Heating, <1 h	2
Heating, >1 h	3
Cooling to 0 °C	4
Cooling, <0 °C	5
6. Workup and purification	
None	0
Cooling to room temperature	0
Adding solvent	0
Simple filtration	0
Removal of solvent with bp < 150 °C	0
Crystallization and filtration	1
Removal of solvent with bp > 150 °C	2
Solid phase extraction	2
Distillation	3
Sublimation	3
Liquid-liquid extraction	3
Classical chromatography	10

7.2 PART II – POLYMERIZATION

7.2.1 Schiff Base Polycondensation

Mechanosynthesis of PPI by neat grinding

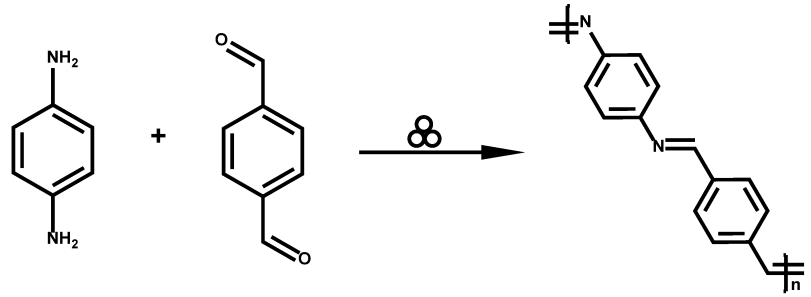

For the NG experiments equimolar quantities of p-benzoldicarbaldehyde (4.963 g, 37 mmol) and p-phenylenediamine (4.001 g, 37 mmol) were placed in a 45 mL zirconium dioxide grinding jar with twenty-two 10 mm diameter zirconium dioxide grinding balls. The mixture was then milled for 40 minutes in a Fritsch Pulverisette 7 premium line planetary ball mill operating at a rotation speed of 800 rpm. The samples were analysed as made. (Yield: 99 %)

Mechanosynthesis of PPI by liquid assisted grinding

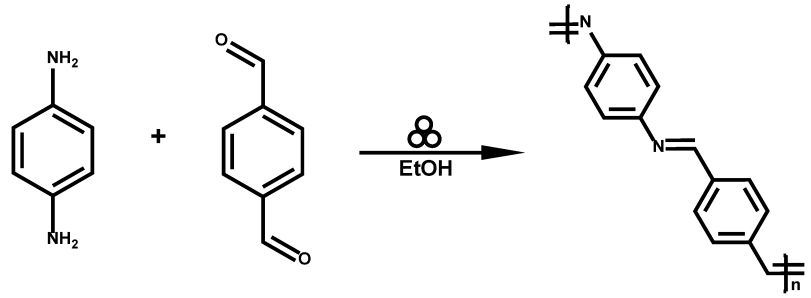

For the LAG experiments equimolar quantities of p-benzoldicarbaldehyde (4.963 g, 37 mmol) and p-phenylenediamine (4.001 g, 37 mmol) were placed in a 45 mL zirconium dioxide grinding jar with twenty-two 10 mm diameter zirconium dioxide grinding balls. Then 0.2 $\mu l \cdot g^{-1}_{monomer}$ ethanol was added to the mixture. This mixture was then milled for 40 minutes in a Fritsch Pulverisette 7 premium line planetary ball mill operating at a rotation speed of 800 rpm. The samples were analysed as made. (Yield: 100 %)

Other milling materials were tungsten carbide and tempered steel. If balls other than 10 mm were used, the same weight of grinding balls was utilized. (15 mm: 7 balls; 5mm: 180 balls)

Solution polymerization of PPI as a reference material

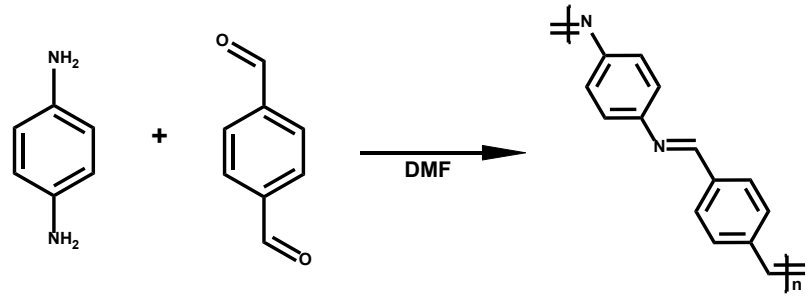

For the reference experiment equimolar quantities of p-benzoldicarbaldehyde (2.478 g, 18.5 mmol) and p-phenylenediamine (2.000 g, 18.5 mmol) were placed in a 250 mL round bottom flask with 100 mL DMF. The mixture was heated to 170 °C and was refluxed for 2 hours. Afterwards the hot mixture was filtrated and the solid was washed with EtOH and dried over night at 80 °C. (Yield: 90 %)

Overview of the conducted experiments

Table 7.3 Overview of linear polymer samples synthesised mechanochemically. All samples were milled for 40 min in a 45 mL vessel with 90 g of milling balls of the respective material and size.

Sample	Milling material	Ball size / mm	LAG	Conversion [C=O] / %	Yield / %
PPI-1	ZrO2	10	-	78	93
PPI-2	Steel	10	-	80	99
PPI-3	WC	10	-	87	n.a[a]
PPI-4	ZrO2	10	1 mL EtOH	81	n.a[a]
PPI-5	Steel	10	1 mL EtOH	82	100
PPI-6	WC	10	1 mL EtOH	88	98
PPI-7	ZrO2	5	-	74	85
PPI-8	ZrO2	10	-	79	93
PPI-9	ZrO2	15	-	84	n.a[a]
PPI-L[b]				70	90

[a] impurities of abrasion led to a yield above 100 %, [b] solution reference

7.2.2 Suzuki Polycondensation

Mechanosynthesis of 1,3,5-triphenylbenzene; AB3 approach

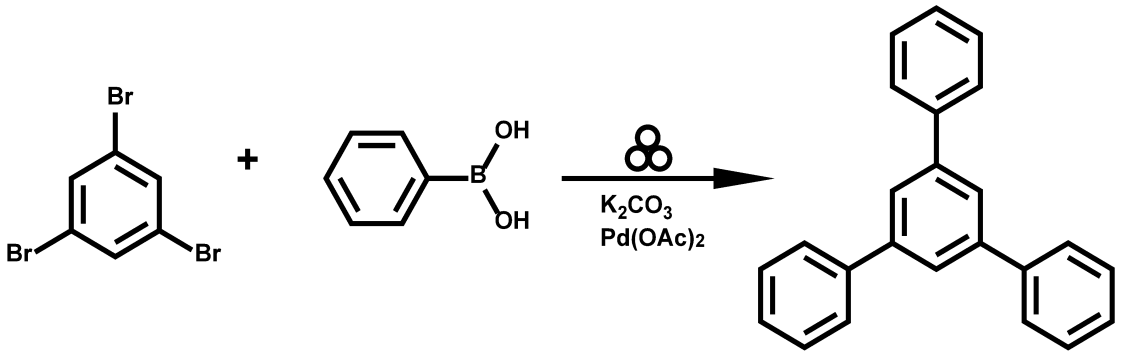

For the experiment equimolar quantities of 1,3,5-tribromobenzene (1.177 g, 3.7 mmol), phenylboronic acid (1.368 g, 11.2 mmol), palladium acetate (113 mg, 13.5 mol%) and potassium carbonate (7.455 g, 53.9 mmol) were placed in a 45 mL zirconium dioxide grinding jar with twenty-two 10 mm diameter zirconium dioxide grinding balls. The mixture was then milled for 30 minutes in a Fritsch Pulverisette 7 premium line planetary ball mill operating at a rotation speed of 800 rpm. The samples were washed with water, 10 wt% hydrochloric acid, ethanol and acetone and then dried over night at 80 °C.

Mechanosynthesis of linear PPP by neat grinding; A2B2 approach

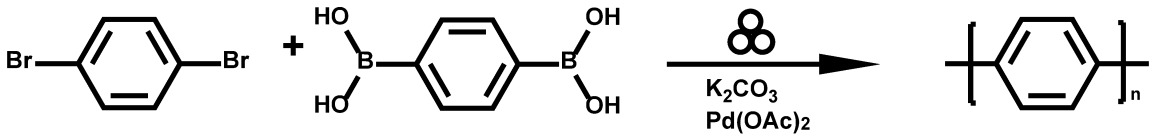

For the experiment equimolar quantities of 1,4-dibromobenzene (0.813 g, 3.44 mmol), 1,4-phenyldiboronic acid (0.569 g, 3.44 mmol), palladium acetate (69 mg, 9.3 mol%) and potassium carbonate (8.549 g, 61.86 mmol) were placed in a 45 mL zirconium dioxide grinding jar with twenty-two 10 mm diameter zirconium dioxide grinding balls. The mixture was then milled for 30 minutes in a Fritsch Pulverisette 7 premium line planetary ball mill operating at a rotation speed of 800 rpm. The samples were washed with water, 10 wt% hydrochloric acid, ethanol and acetone and then dried over night at 80 °C.

Mechanosynthesis of linear PPP by neat grinding; AB approach

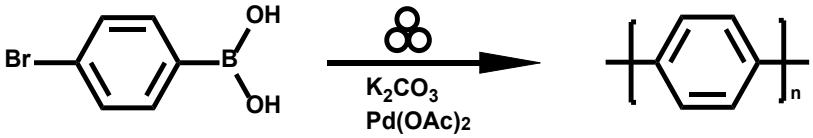

For the experiment 4-bromophenylboronic acid (1.451 g, 7.23 mmol), palladium acetate (139 mg, 9.3 mol%) and potassium carbonate (8.41 g, 60.85 mmol) were placed in a 45 mL zirconium dioxide grinding jar with twenty-two 10 mm diameter zirconium dioxide grinding balls. The mixture was then milled for 30 minutes in a Fritsch Pulverisette 7 premium line planetary ball mill operating at a rotation speed of 800 rpm. The samples were washed with water, 10 wt% hydrochloric acid, ethanol and acetone and then dried over night at 80 °C.

Mechanosynthesis of hyperbranched polyphenylene by neat grinding; A2B1 approach

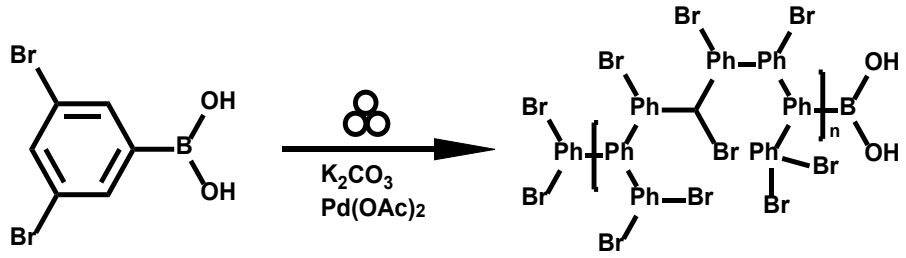

For the experiment 3,5-dibromophenylboronic acid (1.400 g, 7.23 mmol), palladium acetate (101 mg, 9.3 mol%) and potassium carbonate (8.499, 61.50 mmol) were placed in a 45 mL zirconium dioxide grinding jar with twenty-two 10 mm diameter zirconium dioxide grinding balls. The mixture was then milled for 30 minutes in a Fritsch Pulverisette 7 premium line planetary ball mill operating at a rotation speed of 800 rpm. The samples were washed with water, 10 wt% hydrochloric acid, ethanol and acetone and then dried over night at 80 °C.

Overview of the conducted experiments

Table 7.4 Overview of linear polymer samples synthesised mechanochemically. All samples were milled for 30 min in a 45 mL vessel with 22 milling balls of the respective material. 4.5 mol% of catalyst was used per bromide if not state otherwise.

Sample	Reagent	Milling material	Type	Yield / %
Model-1	1,3,5-tribromobenzene + phenylboronic acid	ZrO_2	AB3	78
Model-2		WC		78
PPP-1	1,4-dibromobenzene + 1,4-phenyldiboronic acid	ZrO_2	A2B2	87
PPP-2		Steel		83
PPP-3		WC		100
PPP-4		Si_3N_4		43
PPP-5	4-bromophenylboronic acid	ZrO_2	AB	47
PPP-6		Steel		56
PPP-7		WC		72
PPP-8		Si_3N_4		45
PPP-1-Br	1,4-dibromobenzene + 1,4-phenyldiboronic acid	ZrO_2	A2B2	87
PPP-1-Cl	1,4-dichlorobenzene + 1,4-phenyldiboronic acid			10
PPP-1-I	1,4-diiodobenzene + 1,4-phenyldiboronic acid			87
PPP-Cat-1[a]	1,4-dibromobenzene + 1,4-phenyldiboronic acid	ZrO_2	A2B2	87
PPP-Cat-2[b]				48
PPP-Cat-3[c]				31
PPP-Cat-4[d]				0

[a] 4.5 mol% $Pd(OAc)_2$ per Br; [b] 2.25 mol% $Pd(OAc)_2$ per Br, [c] 1.1 mol% $Pd(OAc)_2$ per Br, [d] no $Pd(OAc)_2$

Table 7.5 Overview of hyperbranched polymer samples synthesised mechanochemically. All samples were milled in a 45 mL vessel with 22 zirconium dioxide milling balls. 4.5 mol% of catalyst was used per bromide if not state otherwise.

Sample	Reagent	Time / min	Type	Yield / %
H-PP-5	3,5-dibromophenylboronic acid	5	A2B1	69
H-PP-30		30		79
H-PP-60		60		80
H-PP-90		90		84
H-PP-120		120		80
H-PP-5-200[a]		5		57

[a] milled at 200 rpm

7.2.3 Oxidative Polymerization

Synthesis of the microporous thiophene polymer (MTP-1)

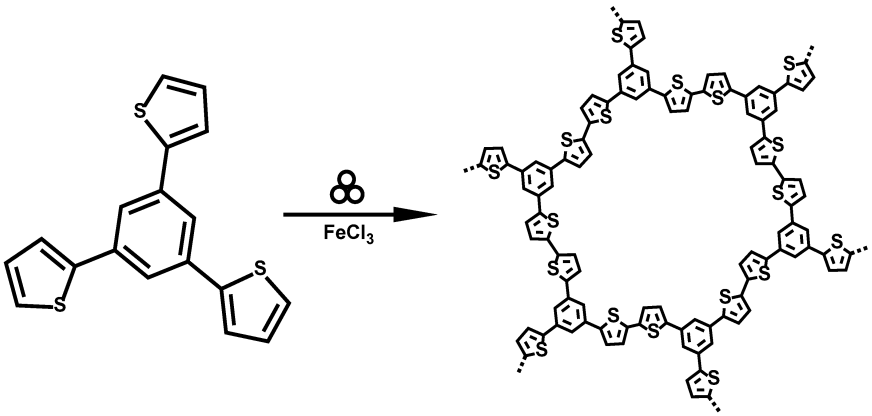

In the optimized mechanochemical synthesis of MTP-1, 0.3 g of 1,3,5-tris(2-thienyl)benzene (0.925 mmol), 1.8 g iron(III) chloride (11.1 mmol, 12 equiv.) and the inert bulking material 0.9 g sodium chloride were transferred into a 45 mL grinding jar with twenty-two 10 mm diameter grinding balls. The reactants were then milled for 60 minutes at 400 rpm in a Fritsch Pulverisette 7 premium line planetary ball mill. After the reaction, the grinding jar was opened and the reaction mixture was poured into water. The crude product was consequently washed with water and soxhlet extracted with water and THF before it was dried at 70 °C. MTP-1 was obtained as a yellowish powder (290 mg, yield: 98 %).

Synthesis of the solvent-based microporous thiophene polymer (MTP-1-sol)

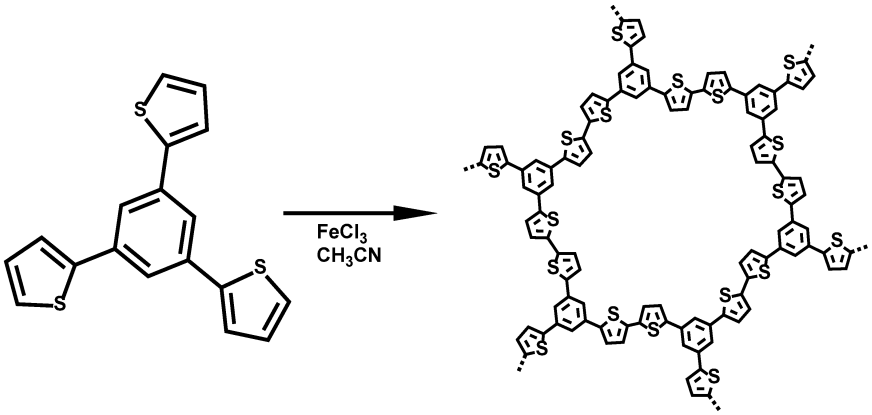

In the solution-based reference synthesis of MTP-1-Sol, 0.45 g iron(III) chloride (2,774 mmol, 3 equiv.) were dissolved in 25 mL of CH_3CN at -20 °C. Then 0.3 g of 1,3,5-tris(2-thienyl)benzene (0.925 mmol) in 10 mL of CH_3CN were slowly added to

the iron chloride solution. The mixture was stirred for one hour before the precipitate was filtered off. The crude product was consequently washed with methanol, hydrochloric acid and THF and afterwards dried at 80 °C. MTP-1-Sol was obtained as a greenish-yellowish powder (51 mg, yield: 19%).

Synthesis of the microporous carbazole polymer (MCP-1)

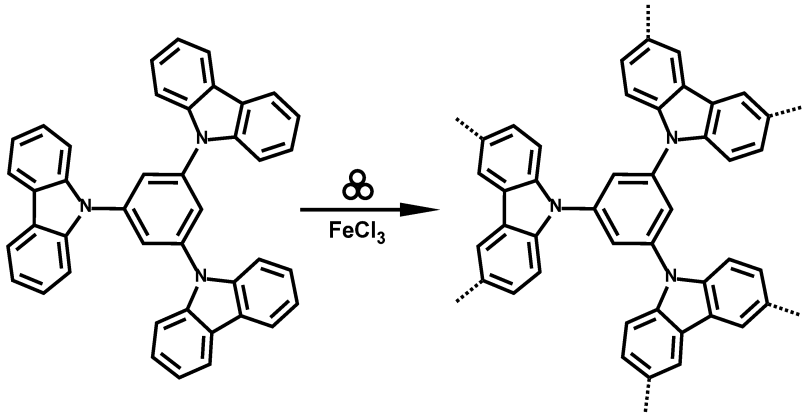

For the synthesis of MCP-1, 0.3 g of 1,3,5-tri(N-carbazolyl)benzene (0.521 mmol), 1.02 g iron(III) chloride (6.25 mmol, 12 equiv.) .and the inert bulking material 8.68 g sodium chloride were transferred into a 45 mL grinding jar with twenty-two 10 mm diameter grinding balls. The reactants were then milled for 60 minutes at 400 rpm in a Fritsch Pulverisette 7 premium line planetary ball mill. After the reaction, the grinding jar was opened and the reaction mixture was poured into water. The crude product was consequently washed with water and soxhlet extracted with water and THF before it was dried at 70 °C. MCP-1 was obtained as a beige powder (150 mg, yield: 50 %).

7.2.3.1 **Design of Experiments Matrix**

Design of experiments describes a methodological variation of parameters in order to get the most information out of a minimum number of experiments. The data is therefore collected and a regression function is calculated in order to fit the investigated result (e.g. yield) with the chosen parameters in order to determine their influence. Since it is a statistical approach the variance of the experiment is taken into consideration as well. This can be accomplished by repeating certain experiments. It is beneficial to repeat the centre points that are introduced into the set-up to detect non-linear behaviour because their all parameters are at under non-

extreme conditions. The choice of parameters and their step size is crucial for precise results. It should be noted that it is in general better to choose them in such a matter as to obtain maximum effects, to better differentiate the effects from the normal variance. Furthermore, the runs are conducted in a randomized order to spread influence from random disturbances (different batches of starting material, lab temperature, etc.) evenly over all experiments.

The impact of the synthesis parameters applied on the mechanochemical oxidative polymerization of 1,3,5-tris(2-thienyl)benzene were studied in a factorial 2^{7-3} factorial design with a resolution of IV with a centre point that was repeated once. The parameters are varied in 2 levels, as represented in (**Table 7.6**).

Table 7.6 2 level, fractional DOE layout with center points, randomized order for the synthesis of MTP-1.

Run order	Equiv. $FeCl_3$	Ball/powder ratio	Ball size / mm	Milling time / min	Rpm	Yield / %	SSA_{BET}[a] / $m^2 \cdot g^{-1}$
1	12.0	0.033	15	60	400	98	2002
2	12.0	0.033	10	60	400	88	1989
3	12.0	0.111	10	60	400	96	1927
4	3.0	0.033	10	60	400	36	582
5	7.5	0.072	15	35	600	97	1552
6	7.5	0.072	10	35	600	73	1384
7	3.0	0.111	15	60	400	31	850
8	3.0	0.033	15	10	400	22	898
9	3.0	0.111	15	10	800	32	675
10	12.0	0.033	15	10	800	91	1092
11	12.0	0.111	15	10	400	72	1469
12	12.0	0.111	10	10	800	86	1894
13	3.0	0.033	10	10	800	51	477
14	3.0	0.033	15	60	800	81	266
15	12.0	0.033	10	60	800	93	1378
16	7.5	0.072	15	35	600	85	1227
17	7.5	0.072	10	35	600	85	1412
18	3.0	0.111	10	10	400	26	842
19	12.0	0.111	15	60	800	69	1585
20	3.0	0.111	10	60	800	61	250

[a] calculated from nitrogen physisorption

Simulation of structural model for MPT-1

A model of the crystal structure of MPT-1 was established by using Material Studio 5*. The structure was initially modelled in a hexagonal unit cell with space group P3a symmetry common in hexagonal COFs. The geometry and unit cell parameters were optimized by using the forcite module with default settings. The final unit cell parameters are 20.7305 Å and 3.5891 Å for a/b and c, respectively. Due to the low crystallinity of MPT-1 no structural refinement of the diffraction pattern could be performed further validating the proposed model.

* Material Studio 5.0 (Accelrys Software Inc., San Diego, USA, 2009)

7.3 PART III – GRAPHITIZATION

7.3.1 Scholl Reaction

7.3.1.1 Precursor Synthesis*

1,3,5-tris(2-bromophenyl)benzene **(1)**

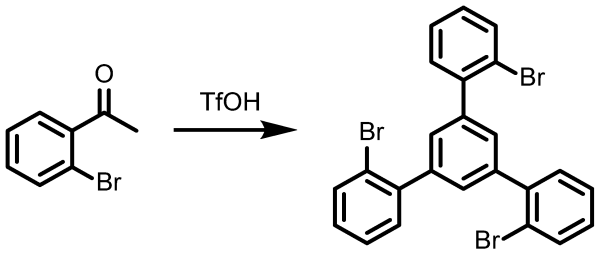

1

The condensation reaction under strongly acidic conditions was performed according to the literature procedure.[118,213] A round bottom flaks was charged with 5 g of 2-bromoacetophenone (25.1 mmol, 1 equiv.) and 10 mol% of trifluoromethanesulfonic acid. The mixture was heated up to 130 °C and stirred until completion (7 h). The cold reaction mixture was quenched with water and extracted with dichloromethane. The collected organic phase was washed with brine and dried over magnesium sulphate. The remaining reaction residue after solvent evaporation was cleaned by silica gel chromatography, using dichloromethane/iso-Hexane 1:6 as eluent to afford the desired compound **1** as bright yellow solid (2 g, yield: 15 %). ^{1}H NMR (CD_2Cl_2, 300 MHz): 7.72-7.69 (dd, 3H), 7.53 (s, 3H), 7.50-7.39 (m, 6H), 7.28-7.22 (m, 3H). The spectroscopic data of compound **1** are consistent with those described in literature.[118]

* The precursor molecules were synthesized by Doreen Beyer. The procedures are nevertheless included in my thesis in order to give the complete picture of the synthesis protocol of the bigger nanographenes.

1,3,5-tris(2-1,1':4',1''-Terphenyl)benzene **(2)**

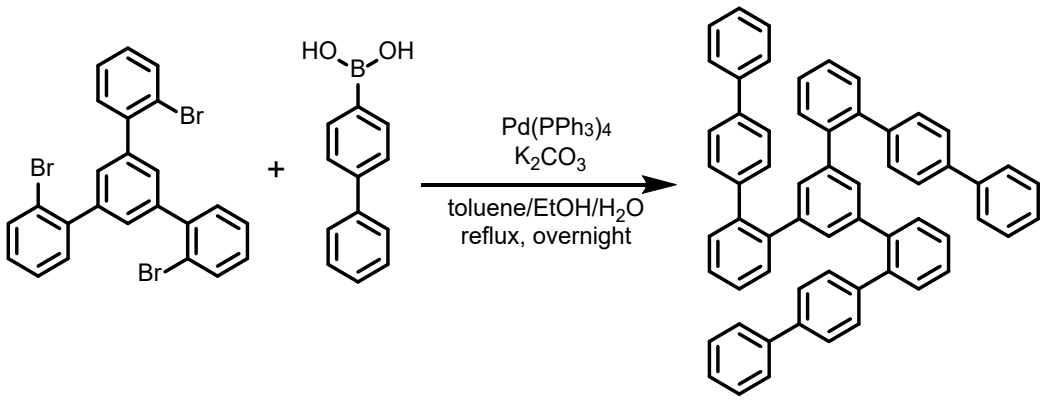

1 **2**

The Suzuki cross-coupling reaction was performed according to the literature procedure.[118,213] In a Schlenk flask 25 mL toluene, 6 mL EtOH and 6 mL water were mixed and 420 mg (773 µmol, 1 equiv.) 1,3,5-tris-2'-bromophenylbenzene and 919 mg (4.6 mmol, 6 equiv.) 4-biphenylboronic acid were added. The mixture was degassed with argon for at least 20 minutes. Afterwards the catalyst was added in one portion and the mixture was refluxed overnight. After standard workup procedure the remaining crude compound was purified by silica gel chromatography, using dichloromethane/iso-hexane 1:6 as eluent. The title compound **2** was separated as white solid (920 mg, yield: 66 %). ^{1}H NMR (**Figure Appendix 17**) (CD_2Cl_2, 300 MHz): 7.42-7.33 (m, 27H), 7.26-7.20 (m, 3H), 6.99-6.96 (m, 9H); 6.81 (s, 3H). The spectroscopic data of compound **1** are consistent with those described in literature.[118] MALDI-TOF (TCNQ): 762.35, calc. 763.00.

4,4'-Bis[(trimethylsilyl)ethynyl]tolane **(3)**

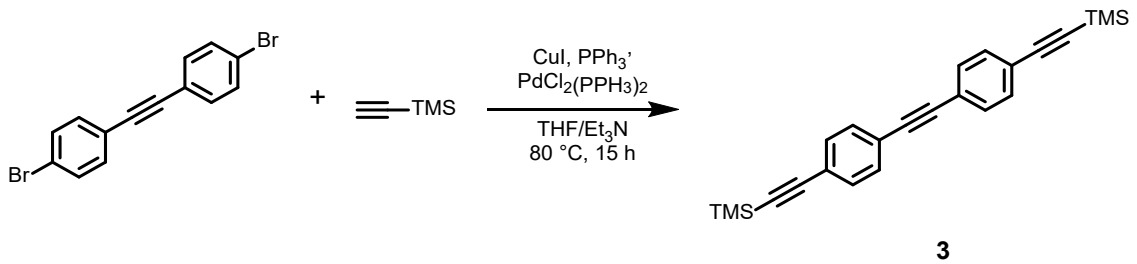

3

A Schlenk flask was charged with 4.5 g (13.4 mmol, 1 equiv.) Bis(4-bromophenyl acetylene), 510 mg (2.7 mmol, 0.2 equiv.) Copper(I) iodide and 351 mg (1.3 mmol, 0.1 equiv.) Triphenylphosphine. To these 50 mL dry Tetrahydrofuran and 50 mL dry

Triethylamine was added. Afterwards 3.95 g (40.1 mmol, 3 equiv.) Ethynyltrimethylsilane and 375 mg (536 µmol, 0.04 equiv.) Dichloro(triphenylphosphine)palladium(II) were added quickly. The resulting reaction mixture was stirred at 80 °C for 15 h. The cold solution was quenches with deionized water and 5 M HCl, extracted with Ethyl acetate, washed with brine and dried over magnesium sulphate. The crude product was further cleaned by silica gel chromatography with Ethyl acetate/iso-Hexane 1:9 as eluent. Title compound **3** was obtained as light grey solid (4 g, yield: 81 %). ^{1}H NMR (**Figure Appendix 18**) (CD_2Cl_2, 300 MHz): 7.49-7.42 (m, 8H), 0.26 (s, 18H). The spectroscopic data of compound **3** are consistent with those described in literature.[95]

4,4'-Diethynyltolan **(4)**

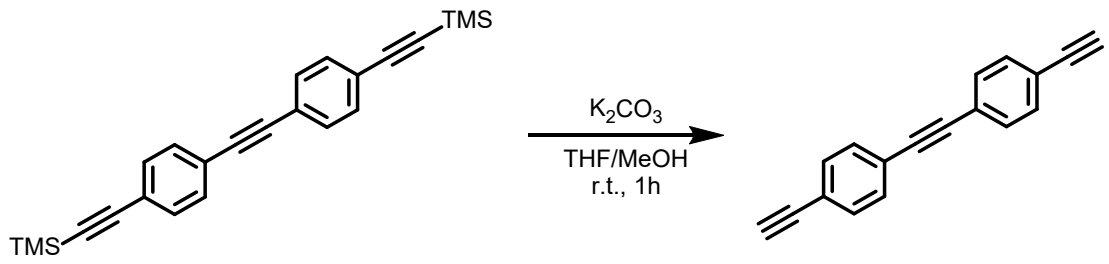

3 **4**

In a round bottom flask, containing a 1:1 mixture of Methanol and Tetrahydrofuran (30 mL:30 mL), was charged with 1.72 g (5.7 mmol, 2.2 equiv.) Potassium carbonate and intensively degassed with argon. Compound **3** (2.1 g, 5.7 mmol, 1 equiv.) was added in one portion and the solution was maintained at room temperature for 1 h until completion. The reaction mixture was quenched with deionized water, extracted with Ethyl acetate, washed with brine and dried over magnesium sulphate. After standard workup procedure the resulting crude target compound **4** (720 mg, yield: 56 %) was directly used without further purification for the next step. ^{1}H NMR (**Figure Appendix 19**) (CD_2Cl_2, 300 MHz): 7.46 (d, J = 19.2 Hz, 8H), 3.26 (s, 2H) ppm. The spectroscopic data of compound **4** are consistent with those described in literature.[95]

4,4'-(2,3,4,5-Tetraphenylbenzene)tolan **(5)**

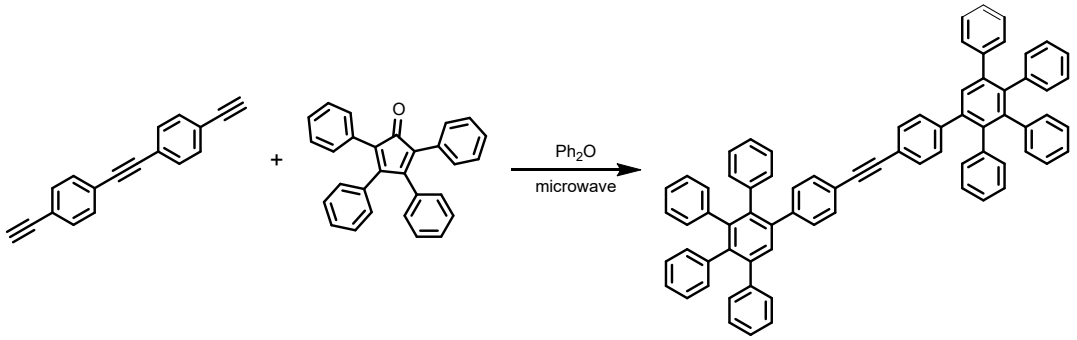

4 5

300 mg (1.3 mmol, 1 equiv.) of compound 4 and 1.13 g (2.9 mmol, 2.2 equiv.) tetraphenylcyclopentadienone were dissolved in 5 mL diphenyl ether. The microwave-assisted Diels-Alder reaction was performed under inert conditions with the mono-mode microwave reactor "Discover SP-D" from CEM. Implemented microwave conditions: 250 °C, 300 W, power max: *on*, stirring speed: *medium*, 12 h. The obtained reaction mixture was precipitate in 200 mL *iso*-Hexane. The light brown precipitate was filtered and washed with Methanol to afford compound **5** as brownish solid (650 mg, 52 %). ^{1}H NMR (**Figure Appendix 20**) (CD_2Cl_2, 300 MHz): 7.52 (s, 2H), 7.35-6.79 (m, 48H) ppm. The spectroscopic data of compound **4** are consistent with those described in literature.[95]

1,2,3,4,5,6-Hexakis(4',5',6'-triphenyl-1,1':2',1''-terphenyl) benzene **6**

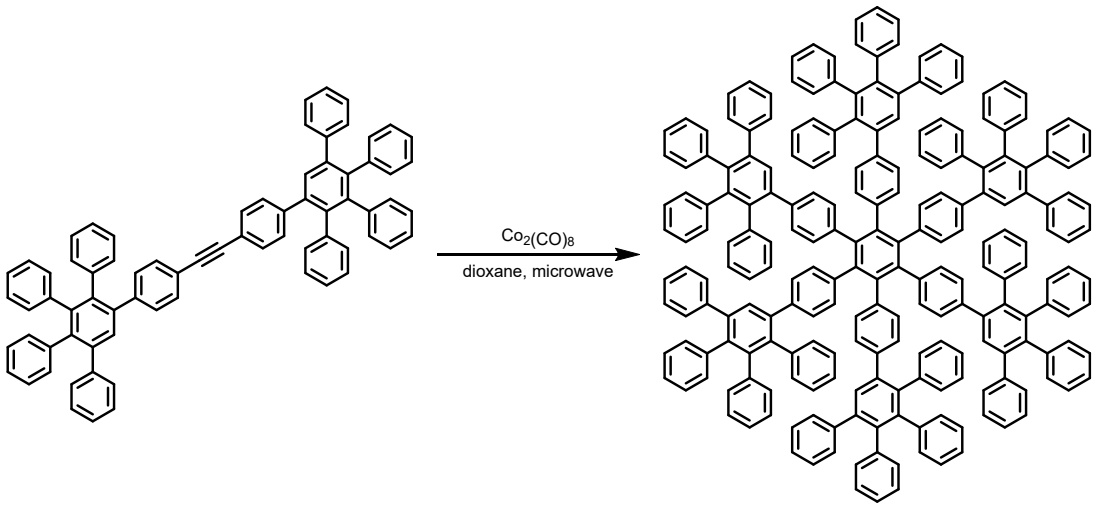

5 6

100 mg (106 µmol, 1 equiv.) of compound **5** and 8.5 mg (25 µmol, 0.7 equiv.) Cobalt carbonyl were dissolved in 1.5 mL Dioxane and intensively degassed with

argon. The microwave-assisted cyclotrimerization reaction was performed at 160 °C, 300 W, power max: *on*, stirring speed: *medium*, 4 hours. The reaction mixture was precipitate in 10 mL *iso*-hexane. Afterwards the crude solid was purified by silica gel column, using ethyl acetate/iso-Hexane 1:4 as eluent. Title compound **6** was obtained as off-white solid (350 mg, yield: 44 %). ^{1}H NMR (**Figure Appendix 21**) (CD_2Cl_2, 300 MHz): 7.40 (s, 6H), 7.14 (s, 30H), 7.01-6.70 (m, 90H), 6.63 (d, J = 8.3 Hz, 12H), 6.37 (d, J = 8.3 Hz, 12H) ppm. The spectroscopic data of compound **4** are consistent with those described in literature.[95] MALDI-TOF (DCTB): 2820.69, calc. 2817.18.

7.3.1.1 **Planarization experiments**

Hexabenzocoronene **(8)**

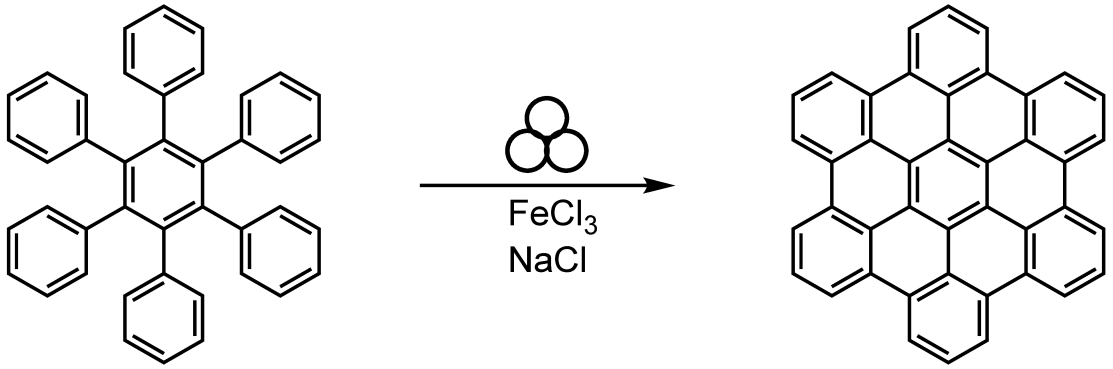

7 **8**

In a typical synthesis, 0.1 g HPB **7** (0.187 mmol), 2.184 g iron(III) chloride (13.5 mmol, 72 equiv.) and the inert bulking material 7.716g sodium chloride were transferred into a 45 mL zirconium dioxide grinding jar with twenty-two zirconium dioxide 10 mm diameter grinding balls (3.19 g each). The reactants were then milled for 60 minutes at 800 rpm in a Fritsch Pulverisette 7 premium line planetary ball mill. After the reaction, the grinding jar was opened and the reaction mixture was poured into water. The crude product was consequently washed with water, methanol and ethanol before it was dried at 80 °C. HBC **8** was obtained as a red solid (93 mg, yield: 95 %). MALDI-TOF (**Figure Appendix 22**) (TCNQ): 522.40, calc. 522.14.

C_{60} **(9)**

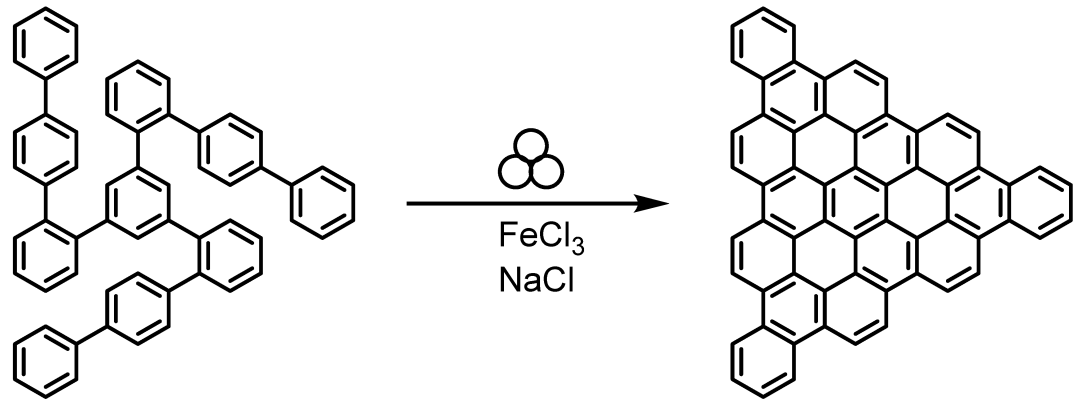

2 **9**

For C_{60} the protocol was changed in the following manner: 0.1 g of 1,3,5-tris(2-1,1':4',1''-terphenyl) benzene **2** (0.131 mmol), 2.295 g iron(III) chloride (14.1 mmol)

and the inert bulking material 7.605 g sodium chloride were transferred into a 45 mL grinding jar with twenty-two 10 mm diameter grinding balls. The reactants were then milled for 60 minutes at 800 rpm in a Fritsch Pulverisette 7 premium line planetary ball mill. After the reaction, the grinding jar was opened and the reaction mixture was poured into water. The crude product was consequently washed with water, methanol and ethanol before it was dried at 80 °C. C_{60} **9** was obtained as a red solid (79 mg, yield: 81 %). MALDI-TOF (**Figure Appendix 23**) (TCNQ): 743.95, calc. 744.19.

C_{222} **(10)**

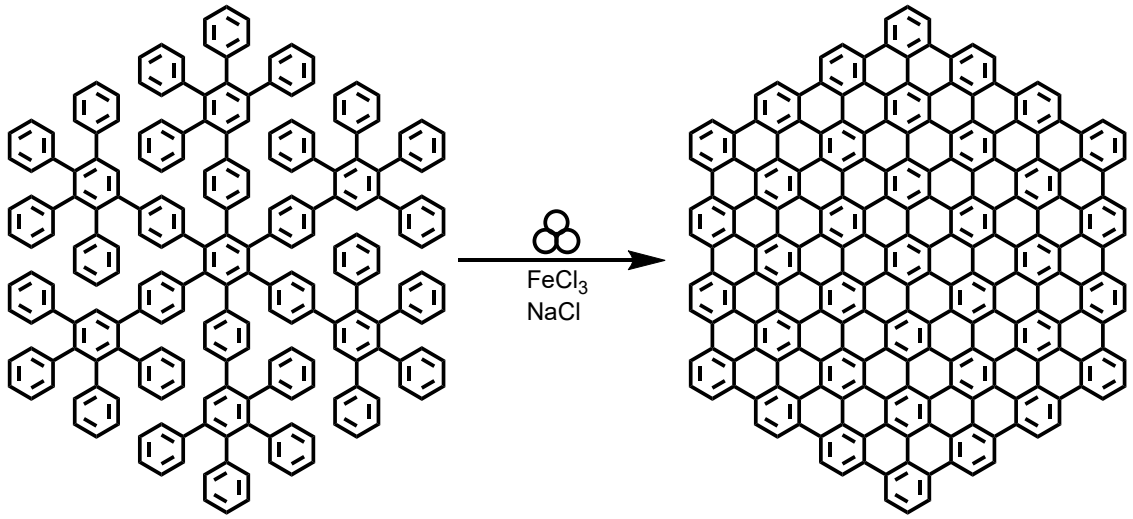

6 **10**

For C_{222} the protocol was changed in the following manner: 0.05 g of 1,2,3,4,5,6-Hexakis(4′,5′,6′-triphenyl-1,1′:2′,1′′-terphenyl)benzene **6** (0.018 mmol), 1.865 g iron(III) chloride (11.5 mmol) and the inert bulking material 8.085 g sodium chloride were transferred into a 45 mL grinding jar with twenty-two 10 mm diameter grinding balls. The reactants were then milled for 60 minutes at 800 rpm in a Fritsch Pulverisette 7 premium line planetary ball mill. After the reaction, the grinding jar was opened and the reaction mixture was poured into water. The crude product was consequently washed with water, methanol and ethanol before it was dried at 80 °C. C_{222} **10** was obtained as a black solid (43 mg, yield: 89 %). MALDI-TOF (**Figure Appendix 24**) (TCNQ): 2711.02, calc. 2708.34.

Overview of the conducted experiments

Table 7.7 Investigation of the milling material. All experiments were conducted with HPB, at 800 rpm, with 22x 10 mm balls, a milling time of 60 min and 12 equiv. of FeCl3 per H.

Sample	Milling material	Yield[a] / %	Comment
HBC-1	zirconium dioxide	95	-
HBC-2	tempered steel	-[b]	excessive abrasion
HBC-3	tungsten carbide	-[b]	excessive abrasion
HBC-4	silicon nitride	97	-

[a] yield after purification, [b] abrasion of the milling material in combination of excessive chlorination lead to abrasion of the milling material in combination of excessive chlorination makes the determination of a yield of HBC impossible

Table 7.8 Investigation of the milling time (HPB-t) and speed (HPB-s). All experiments were conducted, with HPB, 22x 10 mm zirconium dioxide balls, and 12 equiv. of $FeCl_3$ per H.

Sample	Rpm	Milling time / min	Yield[a] / %
HBC-t-30	800	30	95
HBC-t-60	800	60	95
HBC-t-90	800	90	-[b]
HBC-t-120	800	120	88
HBC-s-100	100	60	12[c]
HBC-s-200	200	60	95[c]
HBC-s-400	400	60	94[c]
HBC-s-600	600	60	99[c]
HBC-s-800	800	60	95[c]

[a] yield after purification, [b] MALDI-TOF TOF measured from a small sample of the 2 h synthesis taken after 1 h, [b] Conducted in a GTM vessel for *in situ* investigation

Table 7.9 Scope of the starting materials, capture of HCl (HPB-lp) and transfer to the mixer ball mill (HPB-mm). All experiments were conducted, 22x 10 mm zirconium dioxide balls, and 12 equiv. of FeCl3 per H if not state otherwise.

Sample	Starting material	Milling material	Rpm	Milling time / min	Yield[a] / %
C_{60}	$C_{60}H_{42}$ **2**	zirconium dioxide	800	60	81[b]
C_{222}	$C_{222}H_{150}$ **6**	zirconium dioxide	800	60	89[b]
HBC-lp-1	HPB + Pyridine	zirconium dioxide	800	30	91[b]
HBC-EtOH-1	HPB + Ethanol	zirconium dioxide	800	30	45[b]
HBC-EtOH-2	HPB + Ethanol	zirconium dioxide	800	60	99[b]

Sample	Starting material	Milling material	Rpm	Milling time / min	Yield[a] / %
HBC-200	HPB	zirconium dioxide	200	60	95 [b]
HBC-1.1eq[c]	HPB	zirconium dioxide	800	30	99 [b]
HBC-mm	HPB	tempered steel	25 Hz	30	58 [d]

[a] yield after purification, [b] conducted in a GTM vessel for *in situ* investigation, [c] only 1.1 equiv. of $FeCl_3$ per H, [d] mixer ball mill: 0.1 g HBP, 2.184 g $FeCl_3$, 4x 10 mm balls

7.3.1.2 Design of Experiments Matrix

Table 7.10 2 level, fractional DOE layout with centre points, randomized order.

Run order	Rpm	Ball size / mm	Ball/powder ratio	Milling time / min	Equiv. $FeCl_3$	Yield / %
1	200	15	45	30	12	45
2	800	10	45	30	12	80
3	800	15	9	10	72	64
4	200	10	9	30	12	89
5	500	10	27	20	42	70
6	200	15	45	10	72	70
7	200	15	9	30	72	15
8	500	10	27	20	42	67
9	800	15	9	30	12	63
10	200	10	45	10	12	63
11	800	10	45	10	72	80
12	800	10	9	10	12	12
13	800	15	45	10	12	31
14	200	15	9	10	12	42
15	200	10	9	10	72	48
16	200	10	45	30	72	76
17	800	10	9	30	72	63
18	800	15	45	30	72	92
19	500	15	27	20	42	59
20	500	15	27	20	42	67

7.3.2 Edge Chlorination of Nanographenes

7.3.2.1 Chlorination of Hexaphenylbenzene

Method A: Metal chloride

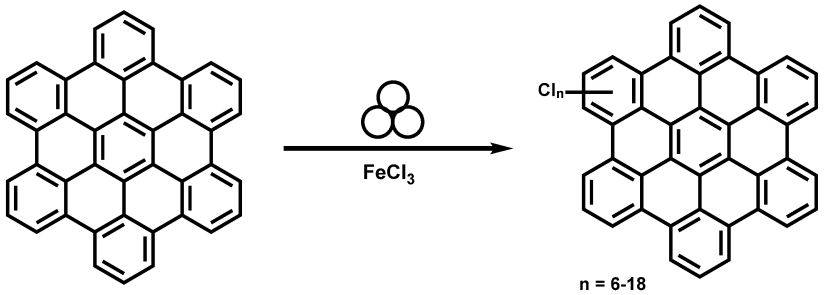

8 12

In a typical synthesis, 0.1 g HBC **8** (0.192 mmol) and an excess of 1.9 g metal chloride (e.g. iron(III) chloride (11.75 mmol, 61 equiv.)) were transferred into a 20 mL zirconium dioxide grinding jar with ten zirconium dioxide 10 mm diameter grinding balls (3.19 g each). The reactants were then milled for 60 minutes at 800 rpm in a Fritsch Pulverisette 7 premium line planetary ball mill. After the reaction, the grinding jar was opened and the reaction mixture was poured into water. The crude product was consequently washed with water, methanol and ethanol. The soluble fraction was extracted with $CHCl_3$ which was consequently evaporated and the solid was dried at 80 °C. Chlorinated HBC **8** was obtained as a dark red solid (108 mg, yield: 49 %). MALDI-TOF **(Figure Appendix 26)**.

Other metal chlorides used with the same mass ratio: $CuCl_2$ (11 mg, yield: 5 %), $AlCl_3$ (1 mg, yield: 1 %), $MoCl_5$ (25 mg, yield: 11 %)

Method B: ICl

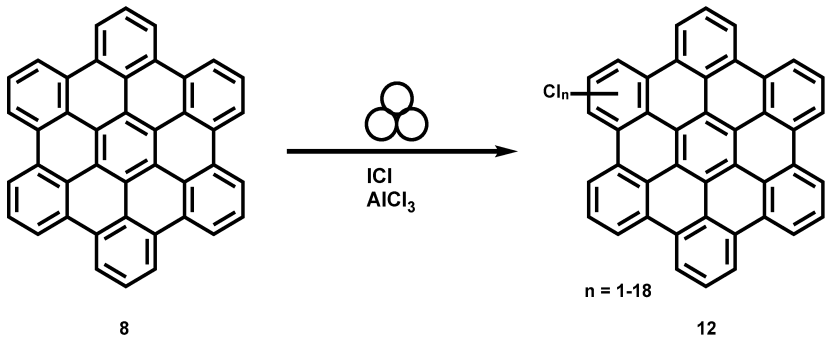

8 12

In a typical synthesis, 0.03 g HBC **8** (0.057 mmol) and an excess of 0.563 g aluminium chloride (4.133 mmol, 72 equiv.) and 1.62 g iodine monochloride (0.5 mL, 9.98 mmol, 174 equiv.) and 1,4 g of sodium chloride as bulking material were transferred into a 20 mL zirconium dioxide grinding jar with ten zirconium dioxide 10 mm diameter grinding balls (3.19 g each). The reactants were then milled for 60 minutes at 800 rpm in a Fritsch Pulverisette 7 premium line planetary ball mill. After the reaction, the grinding jar was opened and the reaction mixture was poured into water. The crude product was consequently washed with water, methanol and ethanol. The soluble fraction was extracted with $CHCl_3$ which was consequently evaporated and the solid was dried at 80 °C. Chlorinated HBC **8** was obtained as a dark red solid (14 mg, yield: 21 %). MALDI-TOF **(Figure Appendix 27)**

Method C: $C_3Cl_3N_3O_3$

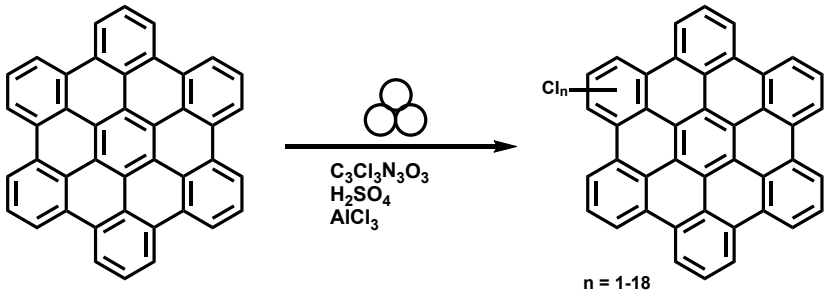

8 **12**

In a typical synthesis, 0.1 g HBC **8** (0.192 mmol) and an excess of 1.017 g aluminium chloride (7.463 mmol, 39 equiv.) and 0.881 g trichloroisocyanuric acid (3.789 mmol, 19.8 equiv.) were transferred into a 20 mL zirconium dioxide grinding jar with ten zirconium dioxide 10 mm diameter grinding balls (3.19 g each). The reactants were then milled for 60 minutes at 800 rpm in a Fritsch Pulverisette 7 premium line planetary ball mill. After the reaction, the grinding jar was opened and the reaction mixture was poured into water. The crude product was consequently washed with water, methanol and ethanol. The soluble fraction was extracted with $CHCl_3$ which was consequently evaporated and the solid was dried at 80 °C. Chlorinated HBC **12** was obtained as a dark red solid (36 mg, yield: 33 %). MALDI-TOF **(Figure Appendix 28)**

Method D: NCS

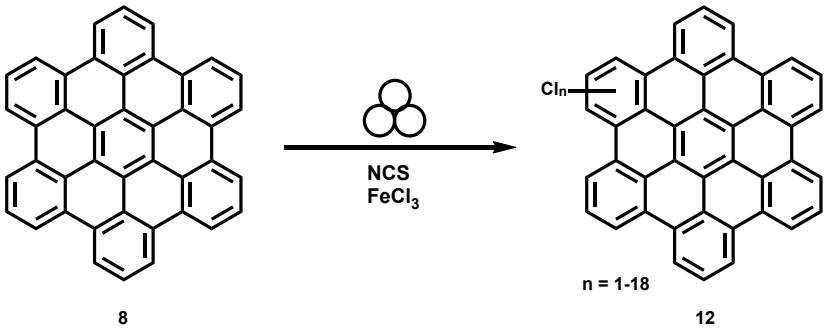

8 12

In a typical synthesis, 0.03 g HBC **8** (0.057 mmol) and an excess of 0.335 g iron(III) chloride (2.067 mmol, 36 equiv.) and 0.276 g N-chlorosuccinimide (2.067 mmol, 36 equiv.) and 1,4 g of sodium chloride as bulking material were transferred into a 20 mL zirconium dioxide grinding jar with ten zirconium dioxide 10 mm diameter grinding balls (3.19 g each). The reactants were then milled for 60 minutes at 800 rpm in a Fritsch Pulverisette 7 premium line planetary ball mill. After the reaction, the grinding jar was opened and the reaction mixture was poured into water. The crude product was consequently washed with water, methanol and ethanol. The soluble fraction was extracted with $CHCl_3$ which was consequently evaporated and the solid was dried at 80 °C. Chlorinated HBC **12** was obtained as a dark red solid (13 mg, yield: 20 %). MALDI-TOF **(Figure Appendix 29)**

Method E: Oxone

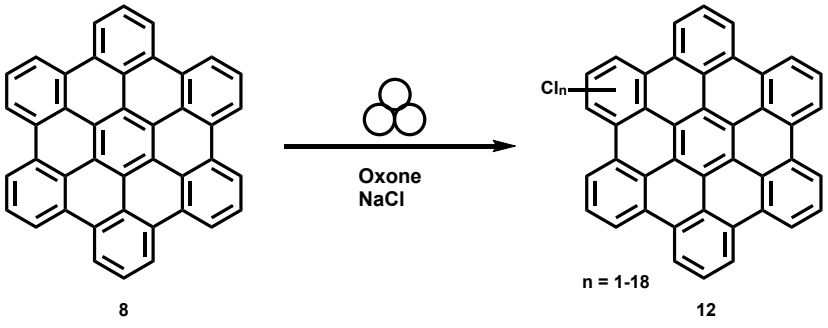

8 12

In a typical synthesis, 0.1 g HBC **8** (0.192 mmol) and an excess of 1.413 g Oxone ($KHSO_5 \cdot 0.5\ KHSO_4 \cdot 0.5\ K_2SO_4$) (4.596 mmol, 24 equiv.) and 0.487 g sodium chloride (8.338 mmol, 44 equiv.) were transferred into a 20 mL zirconium dioxide grinding jar with ten zirconium dioxide 10 mm diameter grinding balls (3.19 g each). The reactants were then milled for 60 minutes at 800 rpm in a Fritsch Pulverisette 7 premium line planetary ball mill. After the reaction, the grinding jar was opened and

the reaction mixture was poured into water. The crude product was consequently washed with water, methanol and ethanol. The soluble fraction was extracted with $CHCl_3$ which was consequently evaporated and the solid was dried at 80 °C. Chlorinated HBC **12** was obtained as a dark red solid (115 mg, (95 mg soluble in $CHCl_3$), yield: 43 %). MALDI-TOF **(Figure Appendix 30)**

7.3.2.2 One-Step Planarization and Edge-Chlorination Procedure

Method A: $FeCl_3$

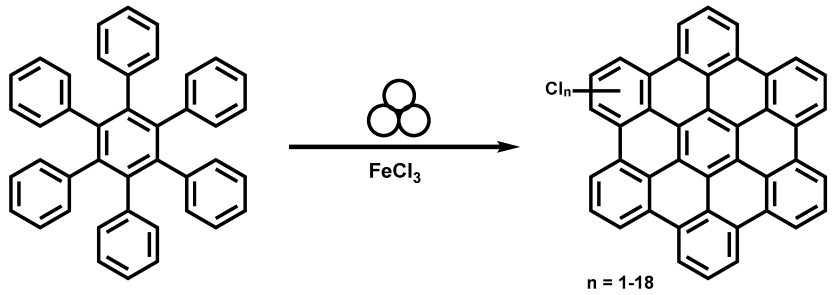

7 12

In a typical synthesis, 0.1 g hexaphenylbenzene **7** (0.191 mmol) and an excess of 9.1 g iron(III) chloride (56 mmol, 294 equiv.), were transferred into a 45 mL tungsten carbide grinding jar with 22 tungsten carbide 10 mm diameter grinding balls. The reactants were then milled for 60 minutes at 800 rpm in a Fritsch Pulverisette 7 premium line planetary ball mill. After the reaction, the grinding jar was opened and the reaction mixture was poured into water. The crude product was consequently washed with water, methanol and ethanol. The soluble fraction was extracted with $CHCl_3$ which was consequently evaporated and the solid was dried at 80 °C. Chlorinated HBC **8** was obtained as a dark red solid (8 mg, yield: 4 %).

Method B: ICl

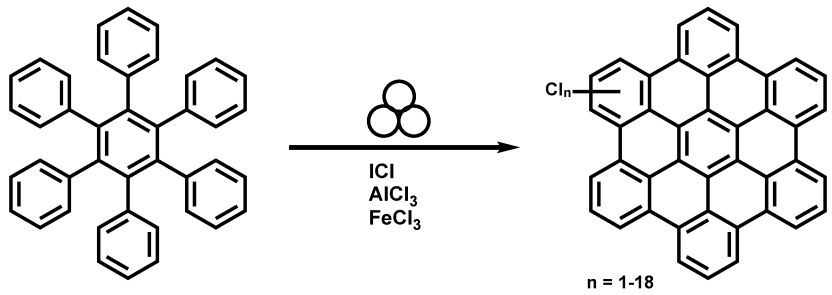

7 12

In a typical synthesis, 0.1 g hexaphenylbenzene **7** (0.191 mmol) and an excess of 0.939 g aluminium chloride (6.889 mmol, 36 equiv.),1.120 g iron(III) chloride (6.889 mmol, 36 equiv.) and 1.118 g iodine monochloride (0.35 mL, 6.889 mmol, 36 equiv.) were transferred into a 20 mL zirconium dioxide grinding jar with ten zirconium dioxide 10 mm diameter grinding balls (3.19 g each). The reactants were then milled for 60 minutes at 800 rpm in a Fritsch Pulverisette 7 premium line planetary ball mill. After the reaction, the grinding jar was opened and the reaction mixture was poured

into water. The crude product was consequently washed with water, methanol and ethanol. The soluble fraction was extracted with $CHCl_3$ which was consequently evaporated and the solid was dried at 80 °C. Chlorinated HBC **8** was obtained as a dark red solid (91 mg, yield: 43 %). MALDI-TOF (**Figure 5.47B**).

Method C: $C_3Cl_3N_3O_3$

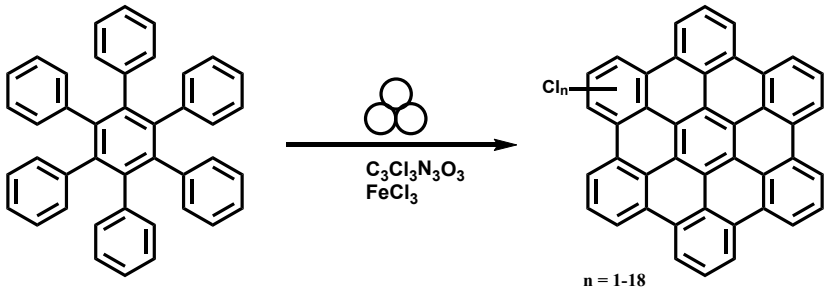

7 12

In a typical synthesis, 0.1 g hexaphenylbenzene **7** (0.187 mmol) and an excess of 1.092 g iron(III) chloride (6.889 mmol, 36 equiv.) and 0.808 g trichloroisocyanuric acid (3.553 mmol, 18.6 equiv.) were transferred into a 20 mL zirconium dioxide grinding jar with ten zirconium dioxide 10 mm diameter grinding balls (3.19 g each). The reactants were then milled for 60 minutes at 800 rpm in a Fritsch Pulverisette 7 premium line planetary ball mill. After the reaction, the grinding jar was opened and the reaction mixture was poured into water. The crude product was consequently washed with water, methanol and acetone. The soluble fraction was extracted with $CHCl_3$ which was consequently evaporated and the solid was dried at 80 °C. Chlorinated HBC **12** was obtained as a dark red solid (60 mg, yield: 28 %). MALDI-TOF (**Figure Appendix 31)**

8 REFERENCES

1 J. M. DeSimone, *Science*, 2002, **297**, 799–803, DOI: 10.1126/science.1069622.
2 R. A. Sheldon, *Green Chem.*, 2005, **7**, 267–278, DOI: 10.1039/b418069k.
3 D. J. C. Constable, C. Jimenez-Gonzalez and R. K. Henderson, *Org. Process Res. Dev.*, 2007, **11**, 133–137, DOI: 10.1021/op060170h.
4 N. V. Plechkova and K. R. Seddon, *Chem. Soc. Rev.*, 2008, **37**, 123–150, DOI: 10.1039/b006677j.
5 R. D. Rogers and K. R. Seddon, *Science*, 2003, **302**, 792–793, DOI: 10.1126/science.1090313.
6 C. Capello, U. Fischer and K. Hungerbühler, *Green Chem.*, 2007, **9**, 927–934, DOI: 10.1039/b617536h.
7 J. A. Zapp, *Science*, 1975, **190**, 422–422, DOI: 10.1126/science.190.4213.422-a.
8 E. Fu, A. Fitzpatrick, C. Connors, D. Clay, et al., *Public attitudes to chemistry*, London, 2015.
9 S. L. James, C. J. Adams, C. Bolm, D. Braga, et al., *Chem. Soc. Rev.*, 2012, **41**, 413–447, DOI: 10.1039/C1CS15171A.
10 P. T. Anastas and J. C. Warner, *Green chemistry: theory and practice*, Oxford University Press, Oxford, 2000.
11 F.-J. Wang, H. Xu, M. Xin and Z. Zhang, *Mol. Divers.*, 2016, **20**, 659–666, DOI: 10.1007/s11030-016-9666-y.
12 K. Lien Nguyen, T. Friščić, G. M. Day, L. F. Gladden, et al., *Nat. Mater.*, 2007, **6**, 206–209, DOI: 10.1038/nmat1848.
13 C. Mottillo and T. Friščić, *Chem. Commun.*, 2015, **51**, 8924–8927, DOI: 10.1039/C5CC01645B.
14 K. Užarević, T. C. Wang, S.-Y. Moon, A. M. Fidelli, et al., *Chem. Commun.*, 2016, **52**, 2133–2136, DOI: 10.1039/C5CC08972G.
15 A. L. Garay, A. Pichon and S. L. James, *Chem. Soc. Rev.*, 2007, **36**, 846–855, DOI: 10.1039/b600363j.
16 V. Šepelák, A. Düvel, M. Wilkening, K. D. Becker, et al., *Chem. Soc. Rev.*, 2013, **42**, 7507–7520, DOI: 10.1039/c2cs35462d.
17 S.-E. Zhu, F. Li and G.-W. Wang, *Chem. Soc. Rev.*, 2013, **42**, 7535–7570, DOI: 10.1039/c3cs35494f.
18 P. Baláž, M. Baláž and Z. Bujňáková, *Chem. Eng. Technol.*, 2014, **37**, 747–756, DOI: 10.1002/ceat.201300669.
19 G. Kaupp, J. Schmeyers and J. Boy, *Chemosphere*, 2001, **43**, 55–61, DOI: 10.1016/S0045-6535(00)00324-6.
20 A. Stolle, T. Szuppa, S. E. S. Leonhardt and B. Ondruschka, *Chem. Soc. Rev.*, 2011, **40**, 2317–2329, DOI: 10.1039/c0cs00195c.
21 G. W. Wang, *Chem. Soc. Rev.*, 2013, **42**, 7668–7700, DOI: 10.1039/c3cs35526h.
22 L. Takacs, *Chem. Soc. Rev.*, 2013, **42**, 7649–7659, DOI: 10.1039/c2cs35442j.
23 A. J. Lynch and C. A. Rowland, *The History of Grinding*, Society for Mining, Metallurgy, and Exploration Inc., Littleton, CO, 2015.
24 L. Takacs, *J. Miner. Met. Mater. Soceity*, 2000, **52**, 12–13, DOI: 10.1007/s11837-000-0106-0.
25 L. Takacs, *J. Mater. Sci.*, 2004, **39**, 4987–4993, DOI: 10.1023/B:JMSC.0000039175.73904.93.
26 M. S. El-Eskandarany, *Mechanical alloying for fabrication of advanced engineering materials*, Noyes Publications, Norwich, NY, 2001.
27 B. S. Murty and S. Ranganathan, *Int. Mater. Rev.*, 1998, **43**, 101–141, DOI: 10.1179/imr.1998.43.3.101.
28 J. Huot, D. B. Ravnsbæk, J. Zhang, F. Cuevas, et al., *Prog. Mater. Sci.*, 2013, **58**, 30–75, DOI: 10.1016/J.PMATSCI.2012.07.001.
29 J.-L. Do and T. Friščić, *Synlett*, 2017, **28**, 2066–2092, DOI: 10.1055/s-0036-1590854.

30 J. G. Hernández and C. Bolm, *J. Org. Chem.*, 2017, **82**, 4007–4019, DOI: 10.1021/acs.joc.6b02887.
31 E. Soriano and I. Fernández, *Chem. Soc. Rev.*, 2014, **43**, 3041–3105, DOI: 10.1039/c3cs60457h.
32 P. Geerlings, S. Fias, Z. Boisdenghien and F. De Proft, *Chem. Soc. Rev.*, 2014, **43**, 4989–5008, DOI: 10.1039/c3cs60456j.
33 F. P. Bowden, Y. D. Yoffe and A. D. Yoffe, *Initiation and Growth of Explosion in Liquids and Solids*, Cambridge University Press, Cambridge, 1952.
34 F. P. Bowden and D. Tabor, *The friction and lubrication of solids*, Clarendon Press, Oxford, 1958.
35 R. Weichert and K. Schönert, *J. Mech. Phys. Solids*, 1974, **22**, 127–133, DOI: 10.1016/0022-5096(74)90018-0.
36 P. Baláž, *Mechanochemistry in Nanoscience and Minerals Engineering*, Springer, Berlin, Heidelberg, 2008.
37 P. A. Thiessen, K. Meyer and G. Heinicke, *Grundlagen der Tribochemie*, Akademie-Verlag, Berlin, 1967.
38 G. Heinicke, *Tribochemistry*, Akademie-Verlag, Berlin, 1984.
39 F. Fischer, K.-J. Wenzel, K. Rademann and F. Emmerling, *Phys. Chem. Chem. Phys.*, 2016, **18**, 23320–23325, DOI: 10.1039/C6CP04280E.
40 J. M. Andersen and J. Mack, *Chem. Sci.*, 2017, **8**, 5447–5453, DOI: 10.1039/c7sc00538e.
41 H. Kulla, M. Wilke, F. Fischer, M. Röllig, et al., *Chem. Commun.*, 2017, **53**, 1664–1667, DOI: 10.1039/C6CC08950J.
42 J. J. Gilman, *Science*, 1996, **274**, 65–65, DOI: 10.1126/science.274.5284.65.
43 C. Burmeister, L. Titscher, S. Breitung-Faes and A. Kwade, *Adv. Powder Technol.*, 2018, **29**, 191–201, DOI: 10.1016/j.apt.2017.11.001.
44 H. F. Giles, J. R. Wagner and E. M. Mount, *Extrusion:The Definitive Processing Guide and Handbook*, Elsevier Science, Amsterdam, 2008.
45 M. N. Riaz, *Extruders in Food Applications*, CRC Press, Boca Raton, FL, 2000.
46 M. M. Crowley, F. Zhang, M. A. Repka, S. Thumma, et al., *Drug Dev. Ind. Pharm.*, 2007, **33**, 909–926, DOI: 10.1080/03639040701498759.
47 D. E. Crawford and J. Casaban, *Adv. Mater.*, 2016, **28**, 5747–5754, DOI: 10.1002/adma.201505352.
48 D. Crawford, J. Casaban, R. Haydon, N. Giri, et al., *Chem. Sci.*, 2015, **6**, 1645–1649, DOI: 10.1039/C4SC03217A.
49 A. Stolle, *Ball Milling Towards Green Synthesis*, Royal Society of Chemistry, Cambridge, 2014.
50 R. Thorwirth, F. Bernhardt, A. Stolle, B. Ondruschka, et al., *Chem. - A Eur. J.*, 2010, **16**, 13236–13242, DOI: 10.1002/chem.201001702.
51 A. Stolle, R. Schmidt and K. Jacob, *Faraday Discuss.*, 2014, **170**, 267–286, DOI: 10.1039/C3FD00144J.
52 S. Grätz, D. Beyer, V. Tkachova, S. Hellmann, et al., *Chem. Commun.*, 2018, **54**, 5307–5310, DOI: 10.1039/C8CC01993B.
53 S. Grätz, B. Wolfrum and L. Borchardt, *Green Chem.*, 2017, **19**, 2973–2979, DOI: 10.1039/C7GC00693D.
54 C. Suryanarayana, *Mechanical alloying and milling*, CRC Press, Boca Raton, FL, 2004.
55 A. Jayasankar, A. Somwangthanaroj, Z. J. Shao and N. Rodríguez-Hornedo, *Pharm. Res.*, 2006, **23**, 2381–2392, DOI: 10.1007/s11095-006-9110-6.
56 D. C. Waddell and J. Mack, *Green Chem.*, 2009, **11**, 79–82, DOI: 10.1039/B810714A.
57 N. Shan, F. Toda and W. Jones, *Chem. Commun.*, 2002, **0**, 2372–2373, DOI: 10.1039/b207369m.
58 A. V. Trask, W. D. S. Motherwell and W. Jones, *Chem. Commun.*, 2004, **0**, 890–891, DOI: 10.1039/b400978a.
59 L. Konnert, A. Gauliard, F. Lamaty, J. Martinez, et al., *ACS Sustain. Chem. Eng.*, 2013, **1**, 1186–1191, DOI: 10.1021/sc4001115.
60 Z.-J. Jiang, Z.-H. Li, J.-B. Yu and W.-K. Su, *J. Org. Chem.*, 2016, **81**, 10049–10055, DOI: 10.1021/acs.joc.6b01938.

61 D. A. Fulmer, W. C. Shearouse, S. T. Medonza and J. Mack, *Green Chem.*, 2009, **11**, 1821–1825, DOI: 10.1039/b915669k.
62 E. Boldyreva, *Chem. Soc. Rev.*, 2013, **42**, 7719–7738, DOI: 10.1039/c3cs60052a.
63 S. L. James and T. Friščić, *Chem. Soc. Rev.*, 2013, **42**, 7494–7496, DOI: 10.1039/c3cs90058d.
64 J. Andersen and J. Mack, *Green Chem.*, 2018, **20**, 1435–1443, DOI: 10.1039/c7gc03797j.
65 J. L. Howard, Q. Cao and D. L. Browne, *Chem. Sci.*, 2018, **9**, 3080–3094, DOI: 10.1039/C7SC05371A.
66 J. L. Do and T. Friščić, *ACS Cent. Sci.*, 2017, **3**, 13–19, DOI: 10.1021/acscentsci.6b00277.
67 M. Faraday, *Q. J. Sci. Lit. Arts*, 1820, **8**, 374–376.
68 L. M. Kubalova, V. I. Fadeeva, I. A. Sviridov and S. A. Fedotov, *J. Alloys Compd.*, 2009, **483**, 86–88, DOI: 10.1016/j.jallcom.2008.07.167.
69 H. Yang, X. Zhang, W. Ao and G. Qiu, *Mater. Res. Bull.*, 2004, **39**, 833–837, DOI: 10.1016/j.materresbull.2004.02.001.
70 A. D. Bond, *CrystEngComm*, 2007, **9**, 833–843, DOI: 10.1039/b708112j.
71 E. Y. Cheung, S. J. Kitchin, K. D. M. Harris, Y. Imai, et al., *J. Am. Chem. Soc.*, 2003, **125**, 14658–14659, DOI: 10.1021/ja030506s.
72 N. Shan and M. J. Zaworotko, *Drug Discov. Today*, 2008, **13**, 440–446, DOI: 10.1016/j.drudis.2008.03.004.
73 M. C. Etter, S. M. Reutzel and C. G. Choo, *J. Am. Chem. Soc.*, 1993, **115**, 4411–4412, DOI: 10.1021/ja00063a089.
74 R. Breslow, in *Handbook of Green Chemistry*, Wiley-VCH Verlag GmbH & Co. KGaA, Weinheim, Germany, 2010.
75 G. Kaupp, M. Reza Naimi-Jamal and J. Schmeyers, *Tetrahedron*, 2003, **59**, 3753–3760, DOI: 10.1016/S0040-4020(03)00554-4.
76 B. Rodríguez, T. Rantanen and C. Bolm, *Angew. Chemie*, 2006, **118**, 7078–7080, DOI: 10.1002/ange.200602820.
77 Q. Cao, J. L. Howard, E. Wheatley and D. L. Browne, *Angew. Chemie Int. Ed.*, 2018, **57**, 11339–11343, DOI: 10.1002/anie.201806480.
78 M. Ferguson, N. Giri, X. Huang, D. Apperley, et al., *Green Chem.*, 2014, **16**, 1374–1382, DOI: 10.1039/C3GC42141D.
79 J.-L. Do, D. Tan and T. Friščić, *Angew. Chemie*, 2018, **130**, 2697–2701, DOI: 10.1002/ange.201712602.
80 O. Y. Posudievsky, O. A. Goncharuk and V. D. Pokhodenko, *Synth. Met.*, 2010, **160**, 47–51, DOI: 10.1016/J.SYNTHMET.2009.09.031.
81 N. Ohn, J. Shin, S. S. Kim and J. G. Kim, *ChemSusChem*, 2017, **10**, 3529–3533, DOI: 10.1002/cssc.201700873.
82 P. J. Hagrman, D. Hagrman and J. Zubieta, *Angew. Chemie Int. Ed.*, 1999, **38**, 2638–2684, DOI: 10.1002/(SICI)1521-3773(19990917)38:18<2638::AID-ANIE2638>3.0.CO;2-4.
83 A.-A. Al-Terkawi, G. Scholz, F. Emmerling and E. Kemnitz, *Solid State Sci.*, 2018, **79**, 99–108, DOI: 10.1016/j.solidstatesciences.2018.03.013.
84 S. Kitagawa, R. Kitaura and S. Noro, *Angew. Chemie Int. Ed.*, 2004, **43**, 2334–2375, DOI: 10.1002/anie.200300610.
85 H. Furukawa, N. Ko, Y. B. Go, N. Aratani, et al., *Science*, 2010, **329**, 424–428, DOI: 10.1126/science.1192160.
86 E. Troschke, S. Grätz, T. Lübken and L. Borchardt, *Angew. Chemie*, 2017, **129**, 6963–6967, DOI: 10.1002/ange.201702303.
87 B. T. King, J. Kroulík, C. R. Robertson, P. Rempala, et al., *J. Org. Chem.*, 2007, **72**, 2279–2288, DOI: 10.1021/jo061515x.
88 R. Scholl and J. Mansfeld, *Berichte der Dtsch. Chem. Gesellschaft*, 1910, **43**, 1734–1746, DOI: 10.1002/cber.19100430288.
89 R. Scholl, C. Seer and R. Weitzenböck, *Berichte der Dtsch. Chem. Gesellschaft*, 1910, **43**, 2202–2209, DOI: 10.1002/cber.191004302175.
90 R. Scholl and C. Seer, *Justus Liebig's Ann. der Chemie*, 1912, **394**, 111–177, DOI: 10.1002/jlac.19123940202.
91 R. Scholl, E. Schwinger and O. Dischendorfer, *Berichte der Dtsch. Chem. Gesellschaft*,

1919, **52**, 2254–2261, DOI: 10.1002/cber.19190521116.
92 A. T. Balaban and C. D. Nenitzescu, in *Friedel –Crafts and Related Reactions*, Wiley, New York, 1964, pp. 979–1047.
93 M. Grzybowski, K. Skonieczny, H. Butenschön and D. T. Gryko, *Angew. Chemie Int. Ed.*, 2013, **52**, 9900–9930, DOI: 10.1002/anie.201210238.
94 P. Kovacic and A. Kyriakis, *J. Am. Chem. Soc.*, 1963, **85**, 454–458, DOI: 10.1021/ja00887a019.
95 C. D. Simpson, J. D. Brand, A. J. Berresheim, L. Przybilla, et al., *Chem. - A Eur. J.*, 2002, **8**, 1424–1429, DOI: 10.1002/1521-3765(20020315)8:6<1424::AID-CHEM1424>3.0.CO;2-Z.
96 E. Clar and C. T. Ironside, *Proc. Chem. Soc. London*, 1958, **5**, 150–150.
97 E. Clar and J. F. Stephen, *Tetrahedron*, 1965, **21**, 467–470, DOI: 10.1016/S0040-4020(01)82216-X.
98 S. Ito, M. Wehmeier, J. D. Brand, C. Kübel, et al., *Chem. - A Eur. J.*, 2000, **6**, 4327–4342, DOI: 10.1002/1521-3765(20001201)6:23<4327::AID-CHEM4327>3.0.CO;2-7.
99 G. Baddeley, *J. Chem. Soc.*, 1950, **0**, 994–997, DOI: 10.1039/JR9500000994.
100 J. Kenner, *J. Soc. Chem. Ind.*, 1933, **42**, 469–470.
101 J. J. Rooney and R. C. Pink, *Proc. Chem. Soc. London*, 1961, **Apr**, 142–144.
102 J. Simons and R. McArthur, *Ind. Eng. Chem.*, 1947, **39**, 364–367, DOI: 10.1021/ie50447a626.
103 C. D. Nenitzescu and A. Balaban, *Chem. Ber.*, 1958, **91**, 2109–2116, DOI: 10.1002/cber.19580911016.
104 P. Rempala, J. Kroulik and B. T. King, *J. Org. Chem.*, 2006, **71**, 5067–5081, DOI: 10.1021/jo0526744.
105 P. Rempala, J. Kroulík and B. T. King, *J. Am. Chem. Soc.*, 2004, **126**, 15002–15003, DOI: 10.1021/ja046513d.
106 L. Zhai, R. Shukla, S. H. Wadumethrige and R. Rathore, *J. Org. Chem.*, 2010, **75**, 4748–4760, DOI: 10.1021/jo100611k.
107 K. S. Novoselov, A. K. Geim, S. V Morozov, D. Jiang, et al., *Science*, 2004, **306**, 666–669, DOI: 10.1126/science.1102896.
108 R. Ruoff, *Nat. Nanotechnol.*, 2008, **3**, 10–11, DOI: 10.1038/nnano.2007.432.
109 Y.-M. Lin, C. Dimitrakopoulos, K. A. Jenkins, D. B. Farmer, et al., *Science*, 2010, **327**, 662–662, DOI: 10.1126/science.1184289.
110 L. Chen, Y. Hernandez, X. Feng and K. Müllen, *Angew. Chemie Int. Ed.*, 2012, **51**, 7640–7654, DOI: 10.1002/anie.201201084.
111 J. Wu, W. Pisula and K. Müllen, *Chem. Rev.*, 2007, **107**, 718–747, DOI: 10.1021/cr068010r.
112 Y.-Z. Tan, B. Yang, K. Parvez, A. Narita, et al., *Nat. Commun.*, 2013, **4**, 2646, DOI: 10.1038/ncomms3646.
113 J. Wu, L. Gherghel, M. D. Watson, J. Li, et al., *Macromolecules*, 2003, **36**, 7082–7089, DOI: 10.1021/ma0257752.
114 M. Treier, C. A. Pignedoli, T. Laino, R. Rieger, et al., *Nat. Chem.*, 2011, **3**, 61–67, DOI: 10.1038/nchem.891.
115 Y. Fogel, L. Zhi, A. Rouhanipour, D. Andrienko, et al., *Macromolecules*, 2009, **42**, 6878–6884, DOI: 10.1021/ma901142g.
116 Xiaoyin Yang, Xi Dou, Ali Rouhanipour, Linjie Zhi, et al., *J. Am. Chem. Soc.*, 2008, **130**, 4216–4217.
117 L. Dössel, L. Gherghel, X. Feng and K. Müllen, *Angew. Chemie Int. Ed.*, 2011, **50**, 2540–2543, DOI: 10.1002/anie.201006593.
118 X. Feng, J. Wu, V. Enkelmann and K. Müllen, *Org. Lett.*, 2006, **8**, 1145–1148, DOI: 10.1021/ol053043z.
119 X. Dou, X. Yang, G. J. Bodwell, M. Wagner, et al., *Org. Lett.*, 2007, **9**, 2485–2488, DOI: 10.1021/ol0708018.
120 N. Chaoui, M. Trunk, R. Dawson, J. Schmidt, et al., *Chem. Soc. Rev.*, 2017, **46**, 3302–3321, DOI: 10.1039/C7CS00071E.
121 J. Schmeyers, F. Toda, J. Boy and G. Kaupp, *J. Chem. Soc. Perkin Trans. 2*, 1998, **4**,

989–994, DOI: 10.1039/a704633b.
122 M. Grigoras and C. O. Catanescu, *J. Macromol. Sci. Part C Polym. Rev.*, 2004, **44**, 131–173, DOI: 10.1081/MC-120034152.
123 T. Miyaji, C. Azuma, E. Asaoka and S. Nakamura, *J. Polym. Sci. Part A Polym. Chem.*, 2000, **38**, 1064–1072, DOI: 10.1002/(SICI)1099-0518(20000401)38:7<1064::AID-POLA3>3.0.CO;2-2.
124 A. Iwan and D. Sek, *Prog. Polym. Sci.*, 2008, **33**, 289–345, DOI: 10.1016/j.progpolymsci.2007.09.005.
125 C. L. Liu, F. C. Tsai, C. C. Chang, K. H. Hsieh, et al., *Polymer*, 2005, **46**, 4950–4957, DOI: 10.1016/j.polymer.2005.03.059.
126 J. M. Adell, M. P. Alonso, J. Barberá, L. Oriol, et al., *Polymer*, 2003, **44**, 7829–7841, DOI: 10.1016/j.polymer.2003.10.032.
127 N. Chantarasiri, C. Chulamanee, T. Mananunsap and N. Muangsin, *Polym. Degrad. Stab.*, 2004, **86**, 505–513, DOI: 10.1016/j.polymdegradstab.2004.06.002.
128 M. Bruma, E. Hamciuc, B. Schulz, T. Köpnick, et al., *Macromol. Symp.*, 2003, **199**, 511–521, DOI: 10.1002/masy.200350942.
129 A. Kimoto, J.-S. Cho, M. Higuchi and K. Yamamoto, *Macromolecules*, 2004, **37**, 5531–5537, DOI: 10.1021/ma0499674.
130 C. Yang and S. A. Jenekhe, *Chem. Mater.*, 1991, **3**, 878–887.
131 J. Tauc, *Mater. Res. Bull.*, 1968, **3**, 37–46, DOI: 10.1016/0025-5408(68)90023-8.
132 D. Cinčić, I. Brekalo and B. Kaitner, *Chem. Commun.*, 2012, **48**, 11683–11685, DOI: 10.1039/c2cc36357g.
133 P. M. Hergenrother, *Angew. Chemie Int. Ed.*, 1990, **29**, 1262–1268, DOI: 10.1002/anie.199012621.
134 W. H. Carothers, *Trans. Faraday Soc.*, 1936, **32**, 39–43, DOI: 10.1039/tf9363200039.
135 K. Suematsu, K. Nakamura and J. Takeda, *Polym. J.*, 1983, **15**, 71–79, DOI: 10.1295/polymj.15.71.
136 A. Padwa, W. Bergmark and D. Pashayan, *J. Am. Chem. Soc.*, 1969, **91**, 2653–2660, DOI: 10.1021/ja01038a043.
137 F. Vilela, K. Zhang and M. Antonietti, *Energy Environ. Sci.*, 2012, **5**, 7819–7832, DOI: 10.1039/c2ee22002d.
138 D. Wu, F. Xu, B. Sun, R. Fu, et al., *Chem. Rev.*, 2012, **112**, 3959–4015, DOI: 10.1021/cr200440z.
139 K. T. Kim, J. W. Jung and W. H. Jo, *Carbon N. Y.*, 2013, **63**, 202–209, DOI: 10.1016/j.carbon.2013.06.074.
140 C. Gao and D. Yan, *Prog. Polym. Sci.*, 2004, **29**, 183–275, DOI: 10.1016/j.progpolymsci.2003.12.002.
141 A. D. Schlüter, *J. Polym. Sci. Part A Polym. Chem.*, 2001, **39**, 1533–1556, DOI: 10.1002/pola.1130.
142 R. Thorwirth, A. Stolle and B. Ondruschka, *Green Chem.*, 2010, **12**, 985–991, DOI: 10.1039/c000674b.
143 V. Declerck, E. Colacino, X. Bantreil, J. Martinez, et al., *Chem. Commun.*, 2012, **48**, 11778–11780, DOI: 10.1039/c2cc36286d.
144 E. Tullberg, D. Peters and T. Frejd, *J. Organomet. Chem.*, 2004, **689**, 3778–3781, DOI: 10.1016/j.jorganchem.2004.06.045.
145 N. Miyaura and A. Suzuki, *Chem. Rev.*, 1995, **95**, 2457–2483, DOI: 10.1021/cr00039a007.
146 F. Bernhardt, R. Trotzki, T. Szuppa, A. Stolle, et al., *Beilstein J. Org. Chem.*, 2010, **6**, No. 7, DOI: 10.3762/bjoc.6.7.
147 F. Schneider, T. Szuppa, A. Stolle, B. Ondruschka, et al., *Green Chem.*, 2009, **11**, 1894–1899, DOI: 10.1039/b915744c.
148 M. Y. Han, B. Özyilmaz, Y. Zhang and P. Kim, *Phys. Rev. Lett.*, 2007, **98**, 206805, DOI: 10.1103/PhysRevLett.98.206805.
149 X. Li, X. Wang, L. Zhang, S. Lee, et al., *Science*, 2008, **319**, 1229–1232.
150 J. Cai, P. Ruffieux, R. Jaafar, M. Bieri, et al., *Nature*, 2010, **466**, 470–473, DOI: 10.1038/nature09211.
151 P. Kovacic and M. B. Jones, *Chem. Rev.*, 1987, **87**, 357–379, DOI: 10.1021/cr00078a005.

152 G. K. Noren and J. K. Stille, *J. Polym. Sci. Macromol. Rev.*, 1971, **5**, 385–430, DOI: 10.1002/pol.1971.230050105.

153 A. A. J. Berresheim, M. Müller and K. Müllen, *Chem. Rev.*, 1999, **99**, 1747–1786, DOI: 10.1021/cr970073+.

154 C. Li, M. Liu, N. G. Pschirer, M. Baumgarten, et al., *Chem. Rev.*, 2010, **110**, 6817–6855, DOI: 10.1021/cr100052z.

155 S. Aeiyach, J. E. Dubois and P. C. Lacaze, *J. Chem. Soc. Chem. Commun.*, 1986, **0**, 1668–1669, DOI: 10.1039/c39860001668.

156 M. Satoh, K. Kaneto and K. Yoshino, *J. Chem. Soc. Chem. Commun.*, 1985, **0**, 1629–1630, DOI: 10.1039/c39850001629.

157 A. F. Shepard and B. F. Dannels, *J. Polym. Sci. Part A-1 Polym. Chem.*, 1966, **4**, 511–518, DOI: 10.1002/pol.1966.150040305.

158 S. Aeiyach and P. C. Lacaze, *J. Polym. Sci. Part A Polym. Chem.*, 1989, **27**, 515–526, DOI: 10.1002/pola.1989.080270212.

159 S. Geetha and D. C. D. Trivedi, *Synth. Met.*, 2005, **148**, 187–194, DOI: 10.1016/j.synthmet.2004.09.017.

160 P. Kovacic and F. W. Koch, *J. Org. Chem.*, 1963, **28**, 1864–1867, DOI: 10.1021/jo01042a031.

161 T. Yamamoto, Y. Hayashi and A. Yamamoto, *Bull. Chem. Soc. Jpn.*, 1978, **51**, 2091–2097.

162 Z. B. Shifrina, M. S. Averina, A. L. Rusanov, M. Wagner, et al., *Macromolecules*, 2000, **33**, 3525–3529, DOI: 10.1021/ma991369f.

163 Y. H. Kim and O. W. Webster, *Macromolecules*, 1992, **25**, 5561–5572, DOI: 10.1021/ma00047a001.

164 I. A. Khotina, L. S. Lepnev, N. S. Burenkova, P. M. Valetsky, et al., *J. Lumin.*, 2004, **110**, 232–238, DOI: 10.1016/j.jlumin.2004.08.014.

165 K. Xu, H. Peng, Q. Sun, Y. Dong, et al., *Macromolecules*, 2002, **35**, 5821–5834, DOI: 10.1021/ma020365z.

166 F. Morgenroth and K. Müllen, *Tetrahedron*, 1997, **53**, 15349–15366, DOI: 10.1016/S0040-4020(97)00967-8.

167 A. P. Côté, A. I. Benin, N. W. Ockwig, M. O'Keeffe, et al., *Science*, 2005, **310**, 1166–70, DOI: 10.1126/science.1120411.

168 V. M. Kobryanskii, in *Proc. of SPIE*, 2001, p. 161, DOI: 10.1117/12.429380.

169 A. F. Littke and G. C. Fu, *Angew. Chemie Int. Ed.*, 2002, **41**, 4176–4211, DOI: 10.1002/1521-3773(20021115)41:22<4176::AID-ANIE4176>3.0.CO;2-U.

170 T. Friščić, I. Halasz, P. J. Beldon, A. M. Belenguer, et al., *Nat. Chem.*, 2013, **5**, 66–73, DOI: 10.1038/nchem.1505.

171 D. J. C. Constable, A. D. Curzons and V. L. Cunningham, *Green Chem.*, 2002, **4**, 521–527, DOI: 10.1039/B206169B.

172 P. Anastas and N. Eghbali, *Chem. Soc. Rev.*, 2010, **39**, 301–312, DOI: 10.1039/B918763B.

173 A. Lapkin and D. J. C. Constable, *Green Chemistry Metrics: Measuring and Monitoring Sustainable Processes*, John Wiley & Sons, Ltd, Chichester, UK, 2009.

174 K. Van Aken, L. Strekowski and L. Patiny, *Beilstein J. Org. Chem.*, 2006, **2**, 3, DOI: 10.1186/1860-5397-2-3.

175 C. F. Martín, E. Stöckel, R. Clowes, D. J. Adams, et al., *J. Mater. Chem.*, 2011, **21**, 5475–5483, DOI: 10.1039/c0jm03534c.

176 P. Pandey, A. P. Katsoulidis, I. Eryazici, Y. Wu, et al., *Chem. Mater.*, 2010, **22**, 4974–4979, DOI: 10.1021/cm101157w.

177 P. Kuhn, M. Antonietti and A. Thomas, *Angew. Chemie Int. Ed.*, 2008, **47**, 3450–3453, DOI: 10.1002/anie.200705710.

178 N. Ritter, I. Senkovska, S. Kaskel and J. Weber, *Macromol. Rapid Commun.*, 2011, **32**, 438–443, DOI: 10.1002/marc.201000714.

179 J. Schmidt, J. Weber, J. D. Epping, M. Antonietti, et al., *Adv. Mater.*, 2009, **21**, 702–705, DOI: 10.1002/adma.200802692.

180 C. Gu, N. Huang, Y. Chen, L. Qin, et al., *Angew. Chemie Int. Ed.*, 2015, **54**, 13594–13598,

DOI: 10.1002/anie.201506570.
181 R. S. Sprick, B. Bonillo, R. Clowes, P. Guiglion, et al., *Angew. Chemie Int. Ed.*, 2016, **55**, 1792–1796, DOI: 10.1002/anie.201510542.
182 R. R. Haikal, X. Wang, Y. S. Hassan, M. R. Parida, et al., *ACS Appl. Mater. Interfaces*, 2016, **8**, 19994–20002, DOI: 10.1021/acsami.6b05031.
183 A. B. Soliman, R. R. Haikal, Y. S. Hassan and M. H. Alkordi, *Chem. Commun.*, 2016, **52**, 12032–12035, DOI: 10.1039/C6CC06773E.
184 F. Rouquerol, J. Rouquerol, K. S. W. Sing, P. Llewellyn, et al., *Adsorption by Powders and Porous Solids Principles, Methodology and Applications*, Academic Press, Amsterdam, 2014.
185 M. Thommes, K. Kaneko, A. V Neimark, J. P. Olivier, et al., *Pure Appl. Chem.*, 2015, **87**, 1051–1069, DOI: 10.1515/pac-2014-1117.
186 V. Nguyen and M. Grünwald, *J. Am. Chem. Soc.*, 2018, **140**, 3306–3311, DOI: 10.1021/jacs.7b12529.
187 X. Zhu, C. Tian, T. Jin, K. L. Browning, et al., *ACS Macro Lett.*, 2017, **6**, 1056–1059, DOI: 10.1021/acsmacrolett.7b00480.
188 A. Narita, X.-Y. Wang, X. Feng and K. Müllen, *Chem. Soc. Rev.*, 2015, **44**, 6616–6643, DOI: 10.1039/C5CS00183H.
189 A. Narita, X. Feng and K. Müllen, *Chem. Rec.*, 2015, **15**, 295–309, DOI: 10.1002/tcr.201402082.
190 L. Talirz, P. Ruffieux and R. Fasel, *Adv. Mater.*, 2016, **28**, 6222–6231, DOI: 10.1002/adma.201505738.
191 T. H. Vo, M. Shekhirev, D. A. Kunkel, M. D. Morton, et al., *Nat. Commun.*, 2014, **5**, 3189, DOI: 10.1038/ncomms4189.
192 A. Narita, X. Feng, Y. Hernandez, S. A. Jensen, et al., *Nat. Chem.*, 2013, **6**, 126–132, DOI: 10.1038/nchem.1819.
193 M. D. Watson, A. Fechtenkötter and K. Müllen, *Chem. Rev.*, 2001, **101**, 1267–1300, DOI: 10.1021/cr990322p.
194 C. D. Simpson, G. Mattersteig, K. Martin, L. Gherghel, et al., *J. Am. Chem. Soc.*, 2004, **126**, 3139–3147, DOI: 10.1021/ja036732j.
195 M. O. Rasmussen, O. Axelsson and D. Tanner, *Synth. Commun.*, 1997, **27**, 4027–4030, DOI: 10.1080/00397919708005446.
196 W. Hendel, Z. H. Khan and W. Schmidt, *Tetrahedron*, 1986, **42**, 1127–1134, DOI: 10.1016/S0040-4020(01)87517-7.
197 T. Szuppa, A. Stolle, B. Ondruschka and W. Hopfe, *ChemSusChem*, 2010, **3**, 1181–1191, DOI: 10.1002/cssc.201000122.
198 T. Szuppa, A. Stolle, B. Ondruschka and W. Hopfe, *Green Chem.*, 2010, **12**, 1288–1294, DOI: 10.1039/c002819c.
199 S. Grätz and L. Borchardt, *RSC Adv.*, 2016, **6**, 64799–64802, DOI: 10.1039/C6RA15677K.
200 K. Užarević, N. Ferdelji, T. Mrla, P. A. Julien, et al., *Chem. Sci.*, 2018, **9**, 2525–2532, DOI: 10.1039/C7SC05312F.
201 A. K. Dutta, A. Linden, L. Zoppi, K. K. Baldridge, et al., *Angew. Chemie Int. Ed.*, 2015, **54**, 10792–10796, DOI: 10.1002/anie.201503553.
202 S. Haferkamp, F. Fischer, W. Kraus and F. Emmerling, *Beilstein J. Org. Chem.*, 2017, **13**, 2010–2014, DOI: 10.3762/bjoc.13.197.
203 L. Batzdorf, F. Fischer, M. Wilke, K.-J. Wenzel, et al., *Angew. Chemie Int. Ed.*, 2015, **54**, 1799–1802, DOI: 10.1002/anie.201409834.
204 P. A. Julien, I. Malvestiti and T. Friščić, *Beilstein J. Org. Chem.*, 2017, **13**, 2160–2168, DOI: 10.3762/bjoc.13.216.
205 K. S. McKissic, J. T. Caruso, R. G. Blair and J. Mack, *Green Chem.*, 2014, **16**, 1628–1632, DOI: 10.1039/c3gc41496e.
206 R. Schmidt, H. Martin Scholze and A. Stolle, *Int. J. Ind. Chem.*, 2016, **7**, 181–186, DOI: 10.1007/s40090-016-0078-8.
207 F. Cataldo, O. Ursini, G. Angelini and S. Iglesias-Groth, *Fullerenes, Nanotub. Carbon Nanostructures*, 2011, **19**, 713–725, DOI: 10.1080/1536383X.2010.494787.
208 R. Schmidt, A. Stolle and B. Ondruschka, *Green Chem.*, 2012, **14**, 1673–1679, DOI:

10.1039/c2gc16508b.
209 C. Glidewell, *Inorganica Chim. Acta*, 1986, **117**, L7–L8, DOI: 10.1016/S0020-1693(00)88051-2.
210 E. C. Juenge, D. A. Beal and W. P. Duncan, *J. Org. Chem.*, 1970, **35**, 719–722, DOI: 10.1021/jo00828a039.
211 K. Tanemura, T. Suzuki, Y. Nishida, K. Satsumabayashi, et al., *Chem. Lett.*, 2003, **32**, 932–933, DOI: 10.1246/cl.2003.932.
212 J. Rouquerol, P. Llewellyn and F. Rouquerol, in *Studies in Surface Science and Catalysis*, Elsevier, Amsterdam, 2007, pp. 49–56.
213 X. Feng, J. Wu, M. Ai, W. Pisula, et al., *Angew. Chemie*, 2007, **119**, 3093–3096, DOI: 10.1002/ange.200605224.
214 M. Grene and D. J. Depew, *The philosophy of biology : an episodic history*, Cambridge University Press, Cambridge, 2004.
215 V. Polshettiwar, C. Len and A. Fihri, *Coord. Chem. Rev.*, 2009, **253**, 2599–2626, DOI: 10.1016/j.ccr.2009.06.001.
216 S. Grätz, M. Oltermann, E. Troschke, S. Paasch, et al., *J. Mater. Chem. A*, 2018, DOI: 10.1039/C8TA03684E.
217 M. J. O'Neil, *The Merck index : an encyclopedia of chemicals, drugs, and biologicals.*, Royal Society of Chemistry, Cambridge, 2013.
218 M. Ballester, C. Molinet and J. Castañer, *J. Am. Chem. Soc.*, 1960, **82**, 4254–4258, DOI: 10.1021/ja01501a035.
219 G. A. Hiegel, G. Pozzi and AnuMahadevan, in *Encyclopedia of Reagents for Organic Synthesis*, John Wiley & Sons, Ltd, Chichester, UK, 2013.
220 J. K. Crandall, Y. Shi, C. P. Burke and B. R. Buckley, in *Encyclopedia of Reagents for Organic Synthesis*, John Wiley & Sons, Ltd, Chichester, UK, 2012.
221 T. Friščić, *J. Mater. Chem.*, 2010, **20**, 7599–7605, DOI: 10.1039/c0jm00872a.
222 N. Durairaj, S. Kalainathan and M. V. Krishnaiah, *Mater. Chem. Phys.*, 2016, **181**, 529–537, DOI: 10.1016/j.matchemphys.2016.06.090.

9 APPENDIX

9.1 SUPPLEMENTARY DATA

9.1.1 Schiff Base Polycondensation

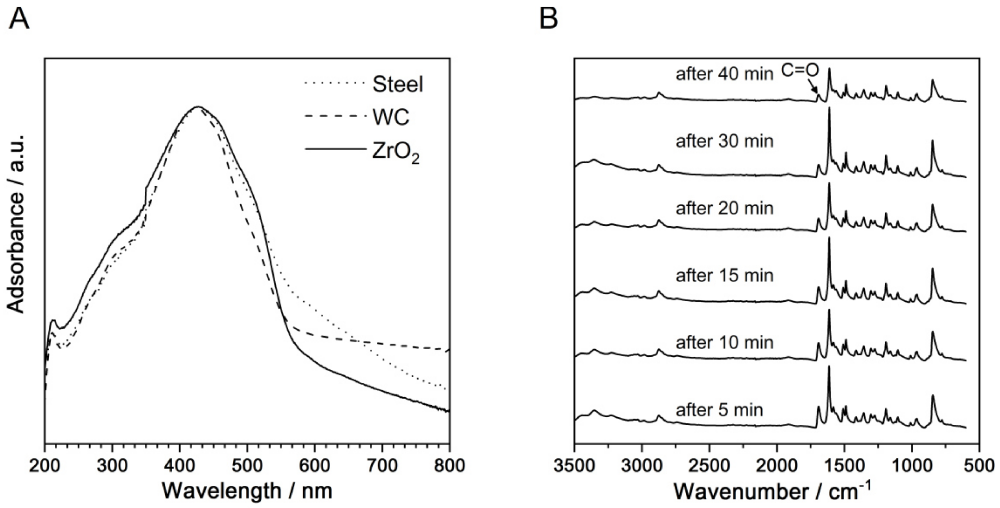

Figure Appendix 1 A: Influence of the milling material on the UV/Vis spectrum of the PA. 10 mm milling balls and 40 min of reaction time have been utilized in all cases. **B:** IR spectra taken at different times during the milling with 10 mm zirconium dioxide milling balls.

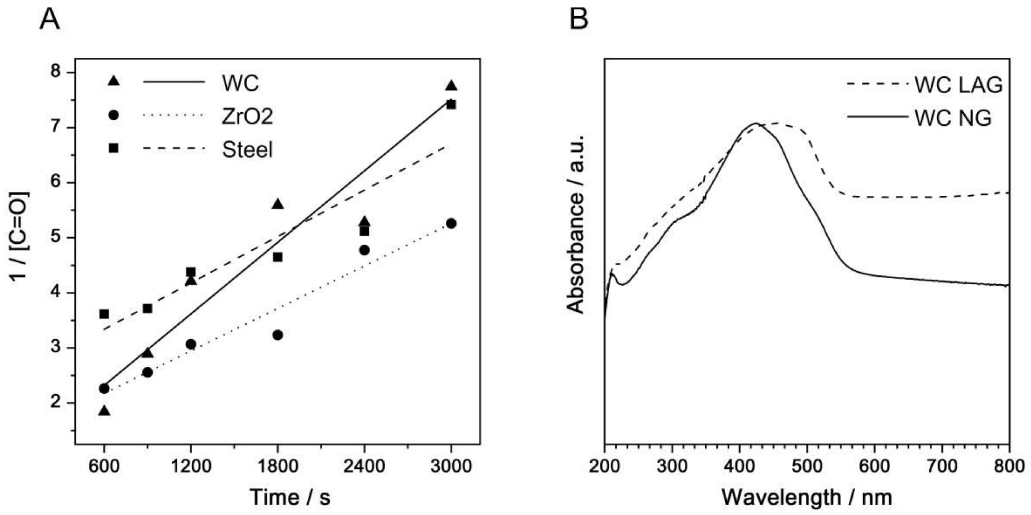

Figure Appendix 2 A: 2nd order rate law fits with the different milling materials. **B:** Differences in the solid-state UV/Vis spectrum of the samples milled with tungsten carbide for 40 min, with (LAG) and without (NG) the addition of ethanol.

9.1.2 Suzuki Polycondensation

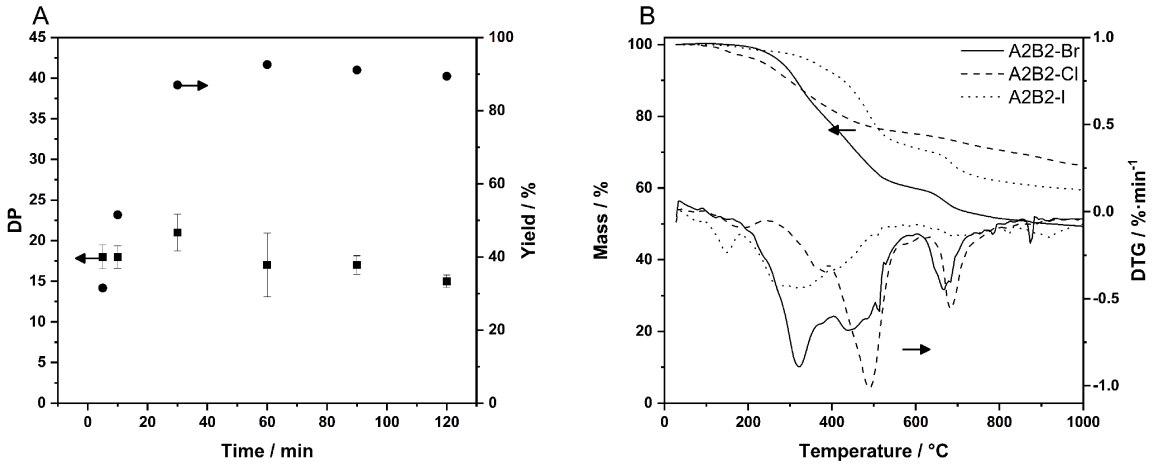

Figure Appendix 3 A: Preliminary experiments, DP (squares) and yield (circles) of the linear PPP vs time. **B:** Comparison of the TGA curves of A2B2 polymers synthesised out of A2 monomers with different halogen functions.

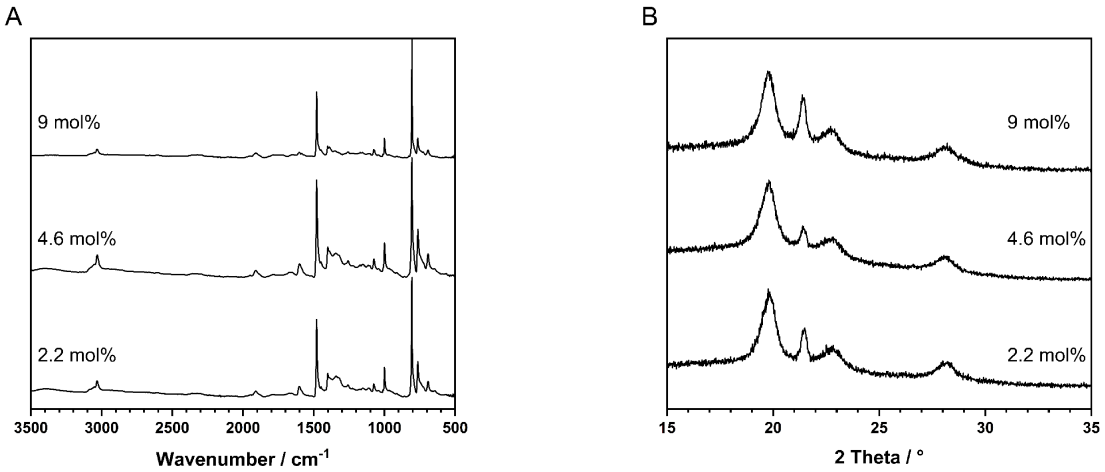

Figure Appendix 4 A: Comparison of the IR spectra of A2B2 polymers synthesized with different catalyst concentrations. **B:** Comparison of the XRD diffractograms of A2B2 polymers synthesized with different catalyst concentrations.

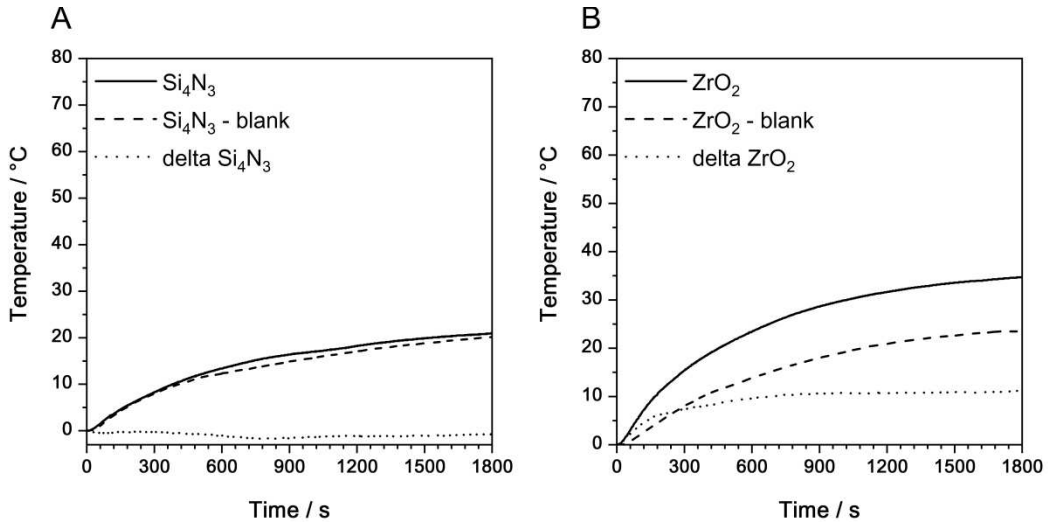

Figure Appendix 5 Comparison of the temperature increase during milling for different milling materials. **A:** Si_4N_3 and **B:** ZrO_2. Blank corresponds to a milling vessel filled only with the base. The dotted line is the difference between blank and polymerization experiment.

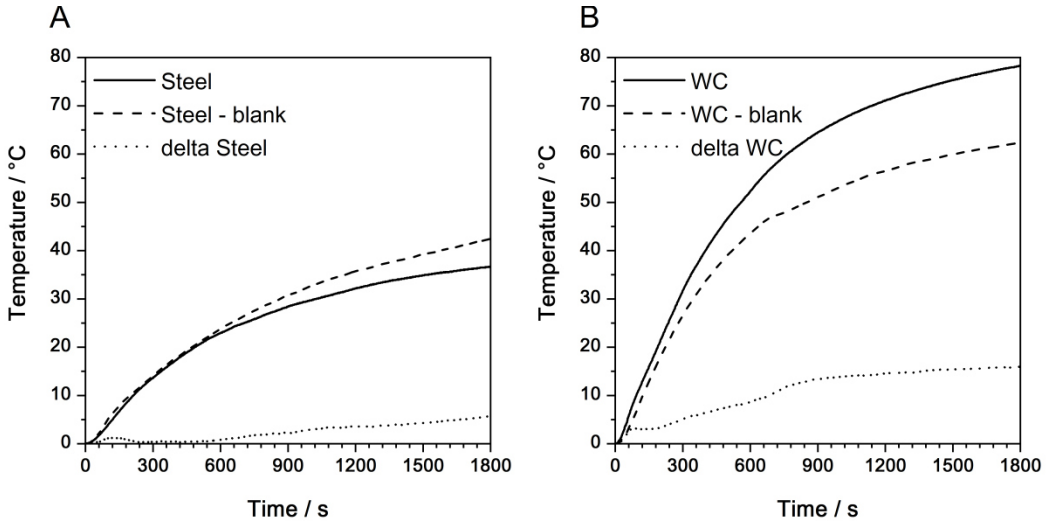

Figure Appendix 6 Comparison of the temperature increase during milling for different milling materials. **A:** Steel and **B:** WC. Blank corresponds to a milling vessel filled only with the base. The dotted line is the difference between blank and polymerization experiment.

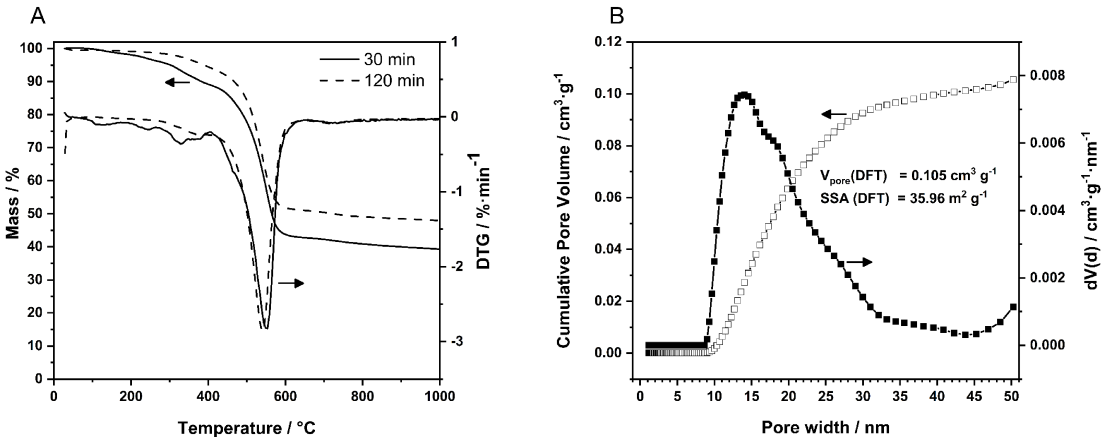

Figure Appendix 7 A: Comparison of the TGA curves of A2B1 after different polymerization times. **B:** Pore size distribution calculated from nitrogen physisorption experiments via QSDFT.

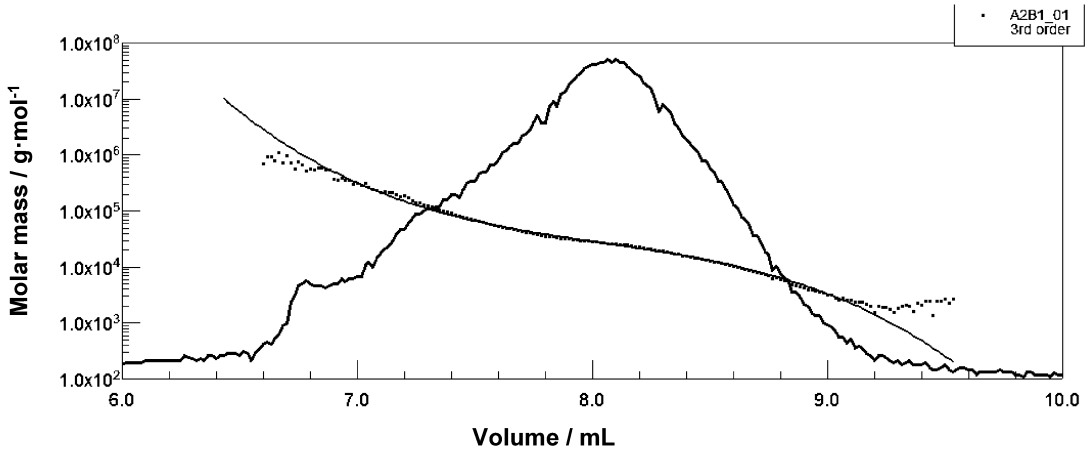

Figure Appendix 8 A: GPC results of A2B1-300; Molar mass calibration curve with 3rd order fit.

9.1.3 Oxidative Polymerization

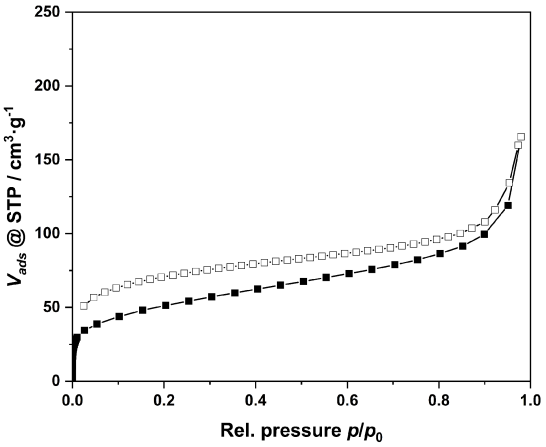

Figure Appendix 9 Low pressure argon physisorption isotherm of the solution-based reference MPT-1-ref, exhibiting a way lower surface area than the mechanochemical procedure and showing the typical swelling behavior.

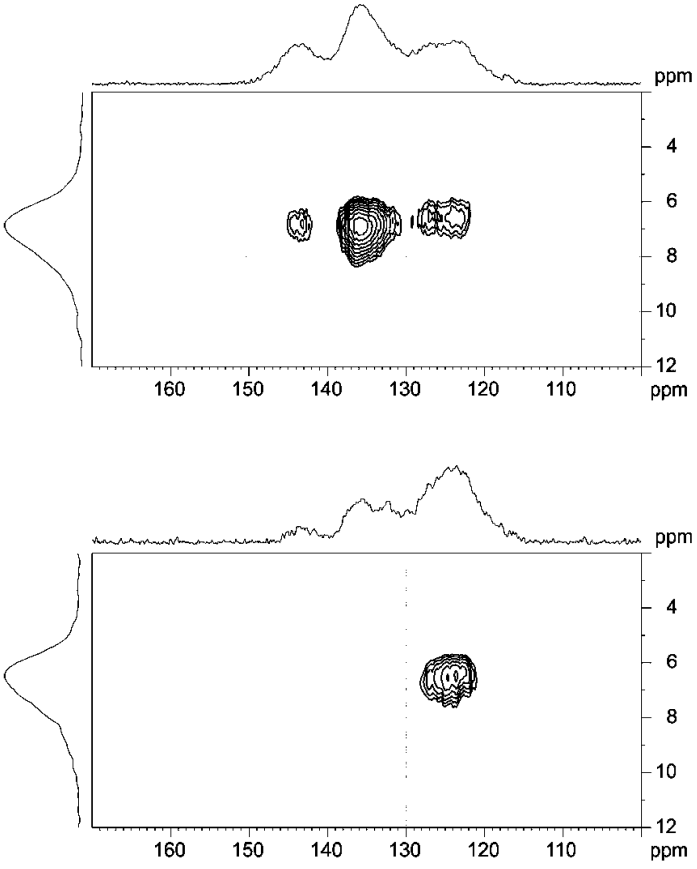

Figure Appendix 10 ^{1}H-^{13}C HETCOR NMR spectra of MTP-1 at contact times of 4 ms (Top) and 0.7 ms (Bottom). These experiments confirm the peak assignment for MTP-1 provided in Fig.3. At the long contact time (4 ms), correlations between all carbon atoms and protons (quaternary C´s and CH groups) appear whereas at a short contact time of 0.7 ms, only CH groups show up in the spectrum.

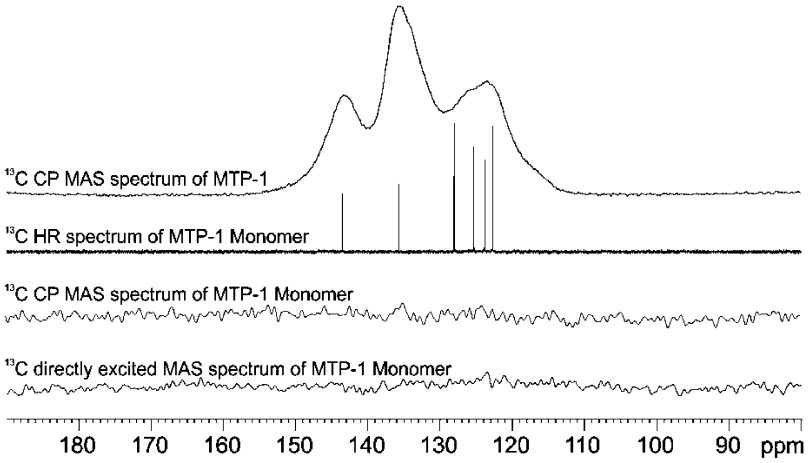

Figure Appendix 11 Comparison of the ^{13}C CP MAS NMR spectrum of MTP-1 (black) with the ^{13}C NMR spectra of the MTP-1 monomer. The red spectrum is the ^{13}C High-Resolution (HR, liquid state) NMR spectrum measured for MTP-1 monomer dissolved in $CDCl_3$. The solid-state NMR spectra (green, blue) of the monomer only show extremely broad lines for both, ^{1}H-^{13}C cross polarization (CP) and direct excitation. This can be explained by disorder of the solid-state of the monomer. Both, static and dynamic disorder (thermal mobility) can in principle contribute to this extreme line broadening.

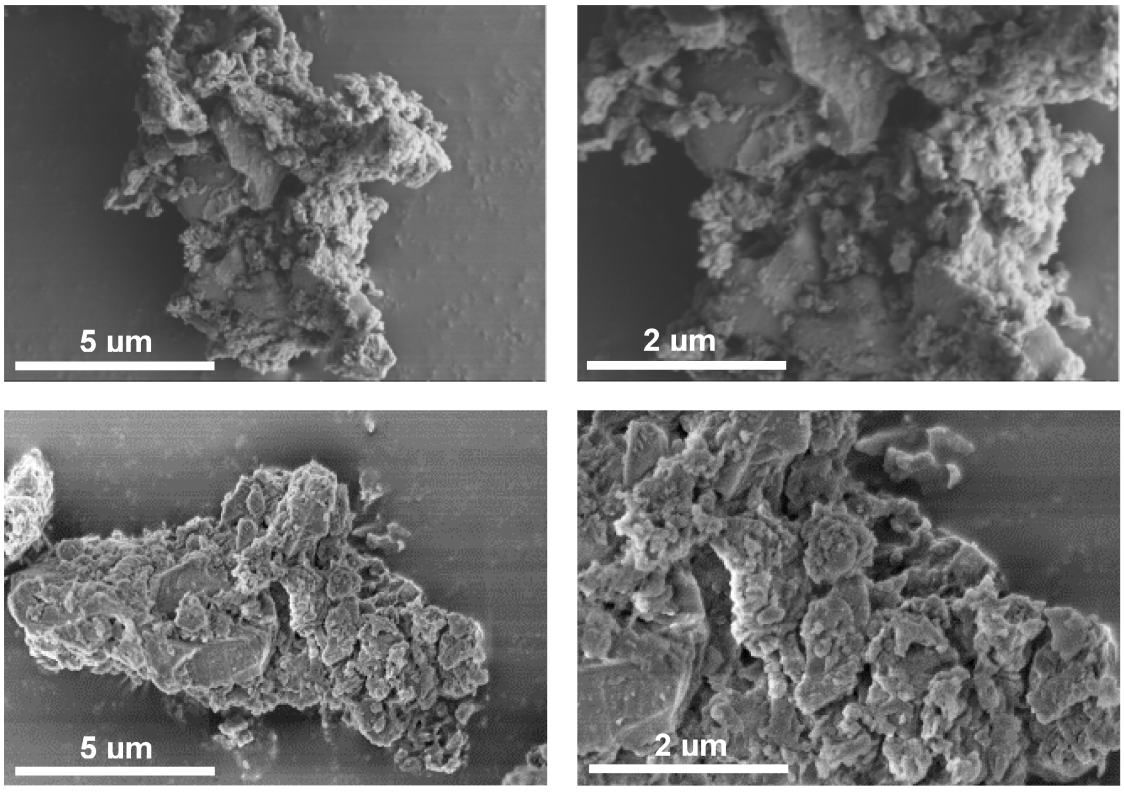

Figure Appendix 12 SEM images of two different particles and magnifications of MPT-1. Larger flakes are agglomerated with smaller unevenly shaped particles to form big agglomerates.

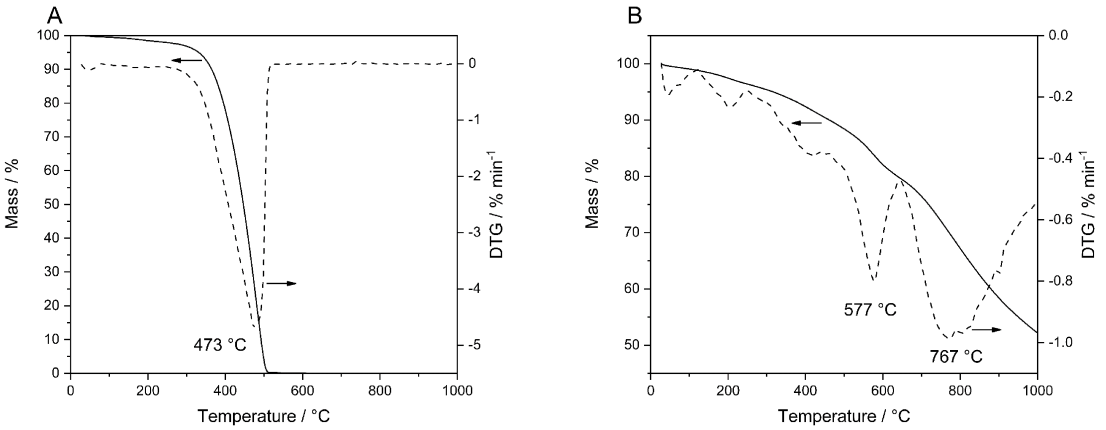

Figure Appendix 13 A:TGA curve of MTP-1 under air showing one major degradation step with a peak at 473 °C as visible by the DTG plot (dashed). The complete degradation also hints towards no contamination with either the oxidant or milling material. **B:** TGA curve of MTP-1 under argon showing several smaller degradations step as visible by the DTG plot (dashed).

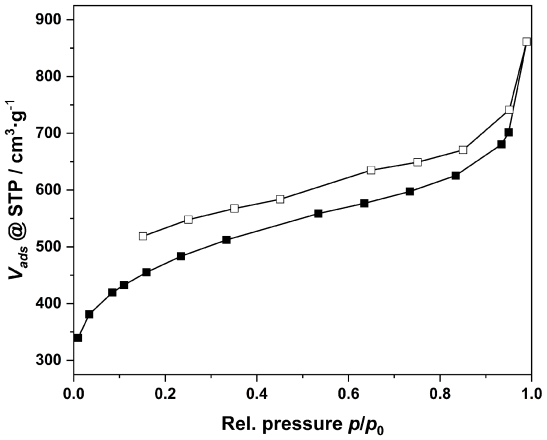

Figure Appendix 14 Nitrogen physisorption isotherm of the carbazole-based polymer MCP-1.

9.1.4 Scholl reaction

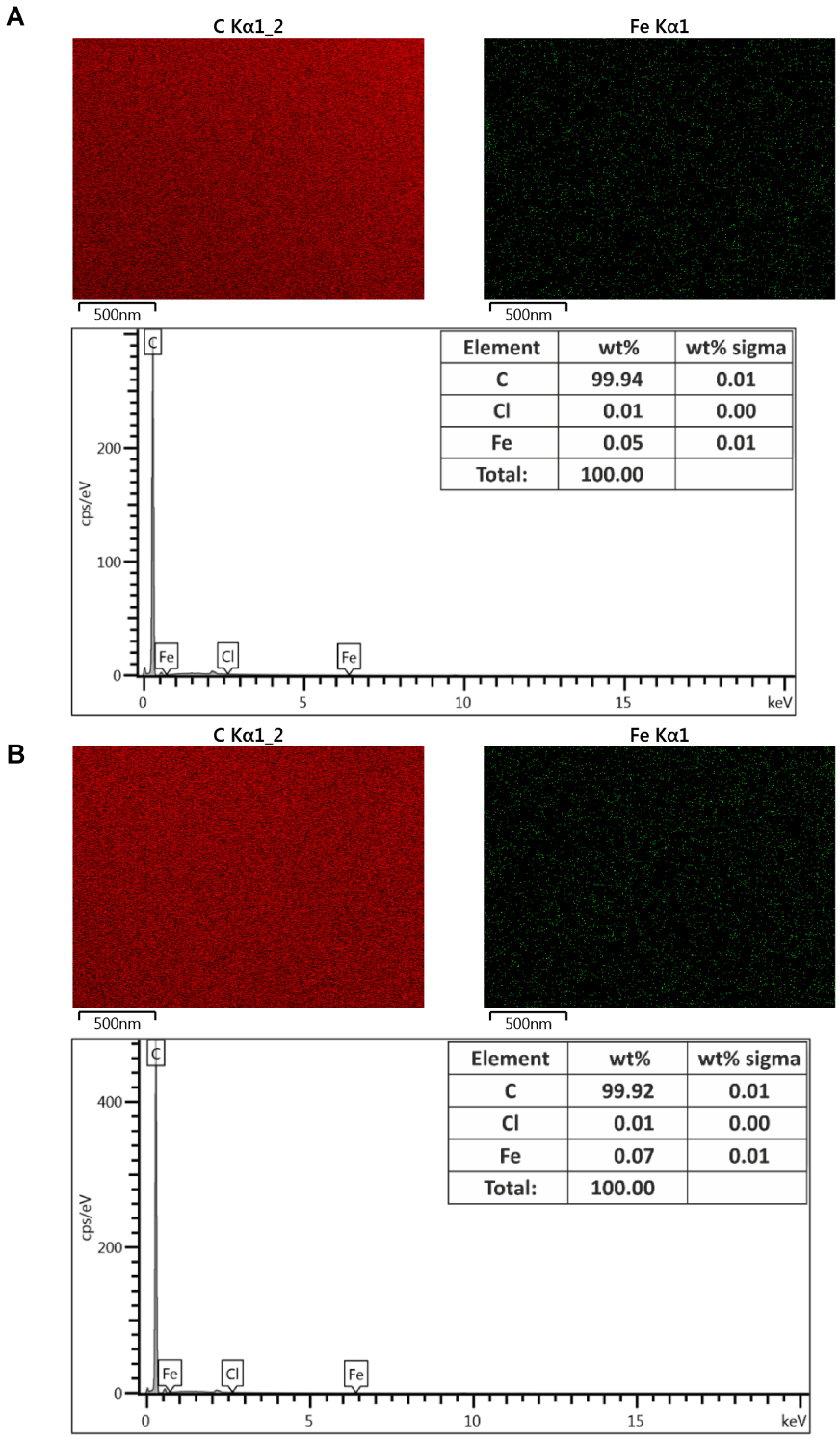

Element	wt%	wt% sigma
C	99.94	0.01
Cl	0.01	0.00
Fe	0.05	0.01
Total:	100.00	

Element	wt%	wt% sigma
C	99.92	0.01
Cl	0.01	0.00
Fe	0.07	0.01
Total:	100.00	

Figure Appendix 15 EDX mapping at two different spots of the sample milled for 30 min at 800 rpm with 22 zirconium dioxide balls. (**A** and **B**) revealing a neglectable amount of iron in the sample. The mapping data is calculating 0.05 wt% (A) and 0.07 wt% (B) of iron respectively which is below the limit of detection for this method. No zirconium was detected at all. This confirms the purity of these samples. Gold used for sputtering was excluded from the quantification.

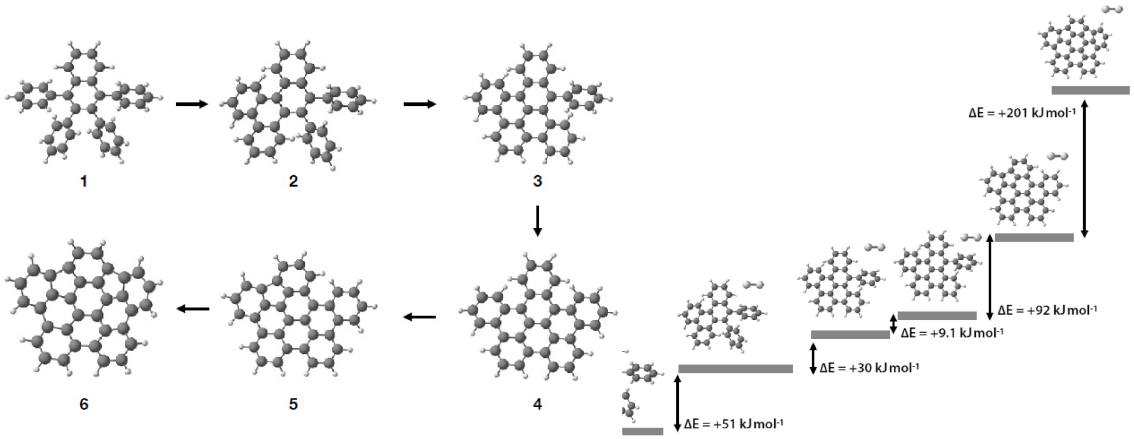

Figure Appendix 16 DFT calculations for the Scholl reaction of 1,2,3,4-tetraphenyl naphthalene. The First sequence for the formation of the 6-rings seems to be similar in a similar cascading fashion as for HBC. The five-ring formation, however, seems to be a very high energy step. The density functional theory simulation with PBE0 functional and TZVP basis set with Grimme D2 correction. Structures were optimised with default convergence criteria using Crystal14 software.

9.1.4.1 ^{1}H NMR Spectra of the Precursors

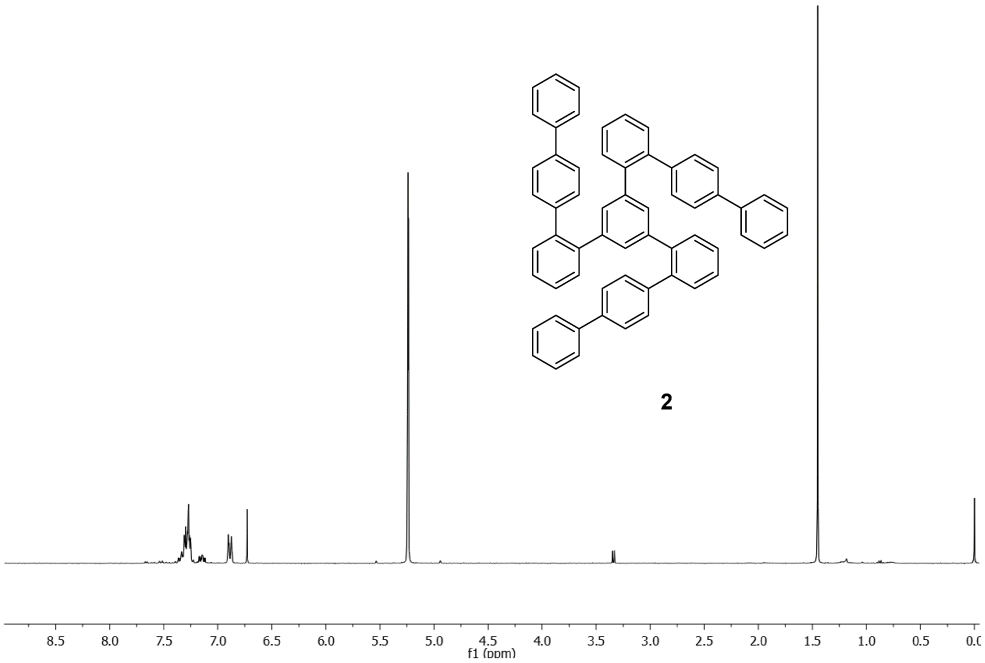

Figure Appendix 17 ^{1}H NMR spectrum of **2**.

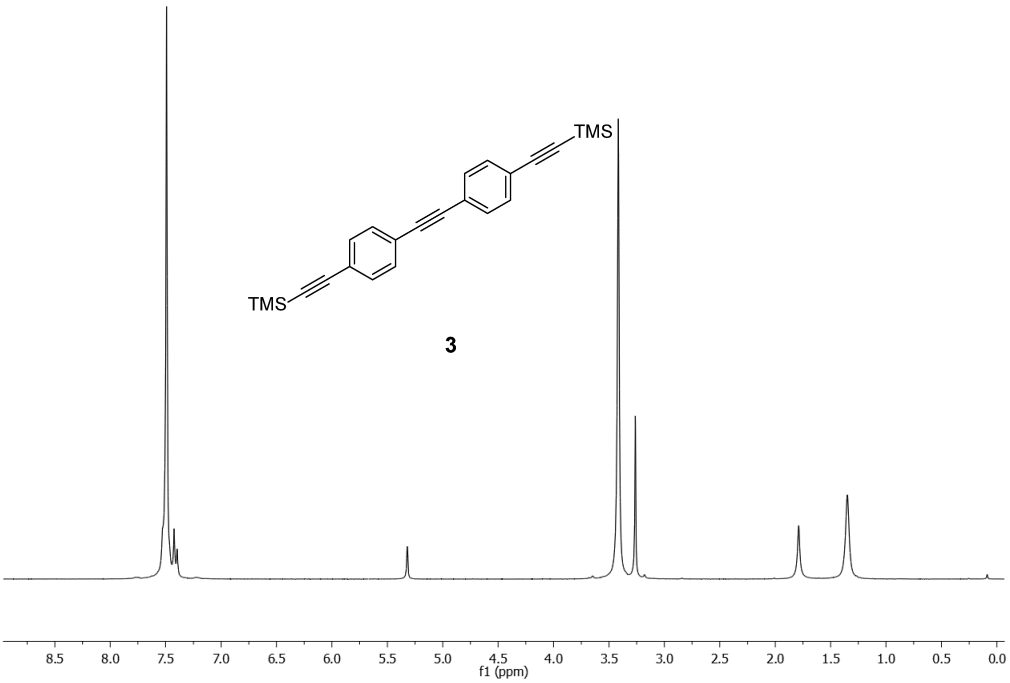

Figure Appendix 18 ^{1}H NMR spectrum of **3**.

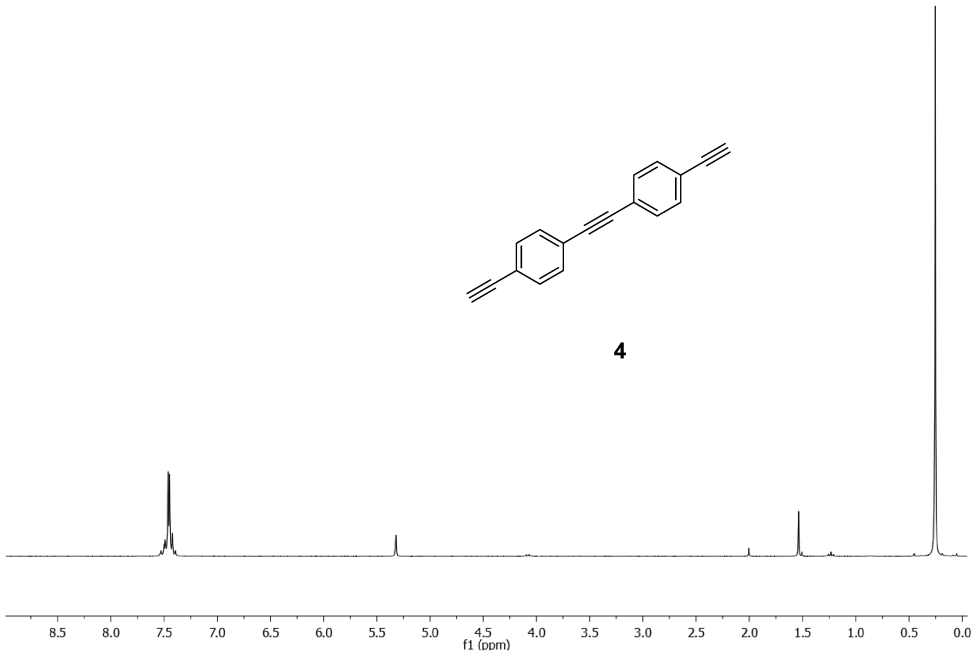

Figure Appendix 19 ^{1}H NMR spectrum of **4**.

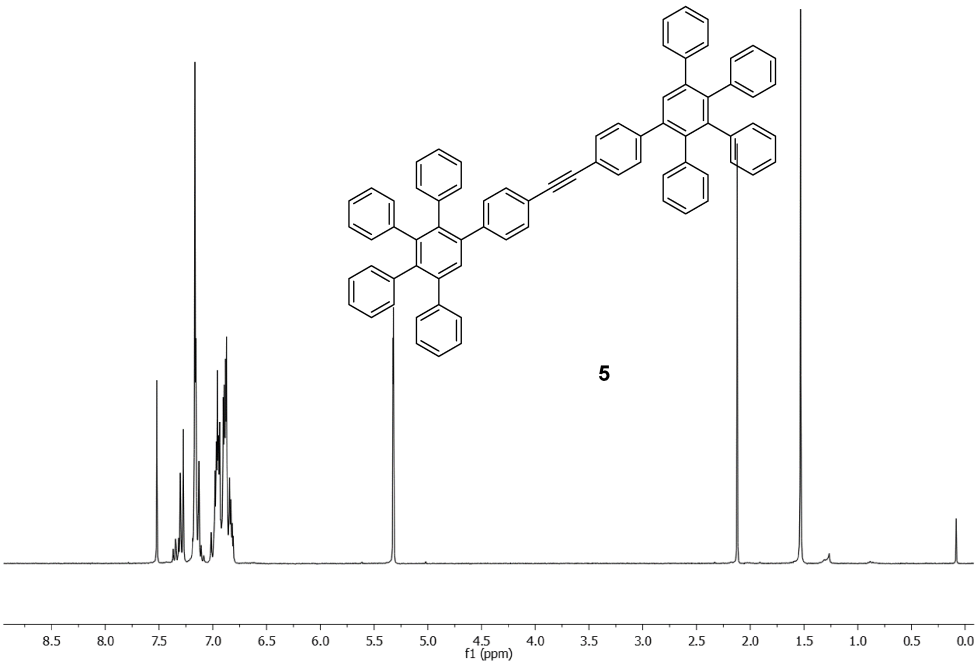

Figure Appendix 20 ^{1}H NMR spectrum of **5**.

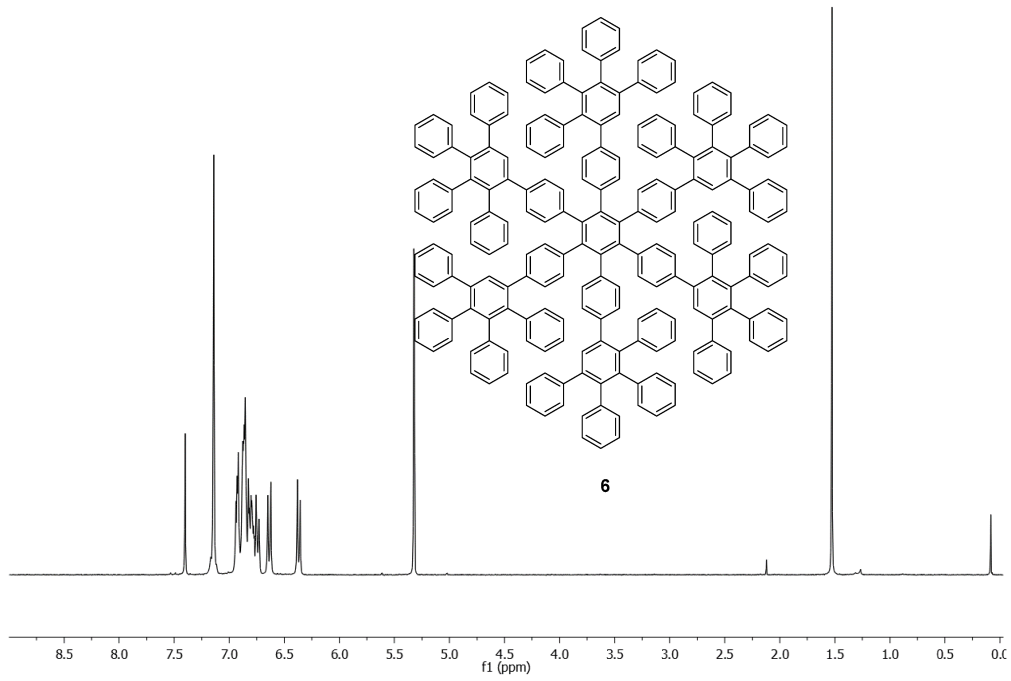

Figure Appendix 21 ^{1}H NMR spectrum of **6**.

9.1.4.2 Complete MALDI-TOF Spectra of the Nanographenes

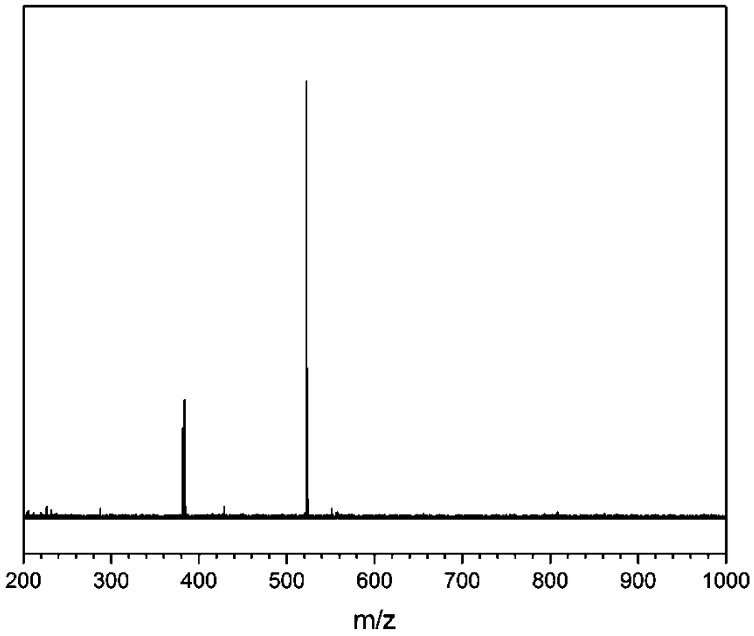

Figure Appendix 22 Complete MALDI-TOF spectrum of HBC.

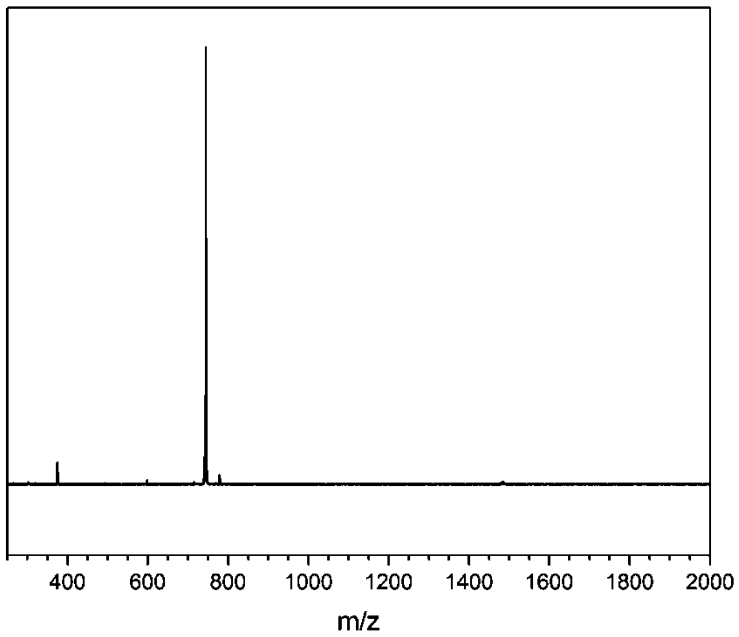

Figure Appendix 23 Complete MALDI-TOF spectrum of C_{60} (Triangolen).

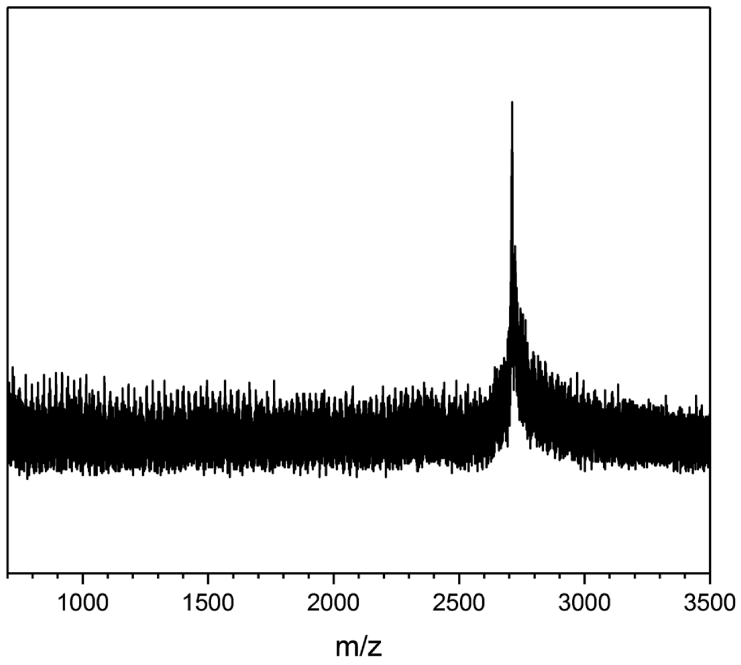

Figure Appendix 24 Complete MALDI-TOF spectrum of C_{222}.

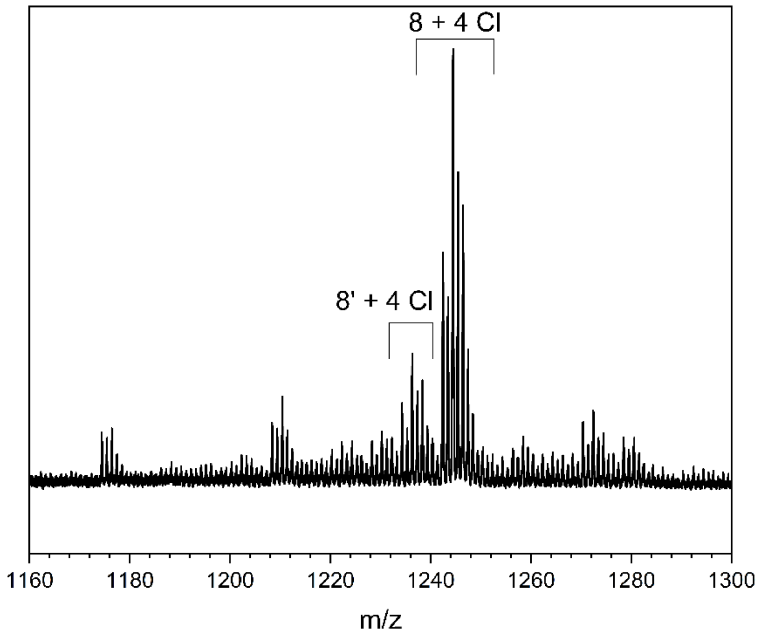

Figure Appendix 25 MALDI-TOF spectrum of extended HBC showing the main product as the fully closed species with 4 chlorine atoms and the moiety with four closed five-member-rings and four chlorine atoms.

9.1.5 Edge Chlorination

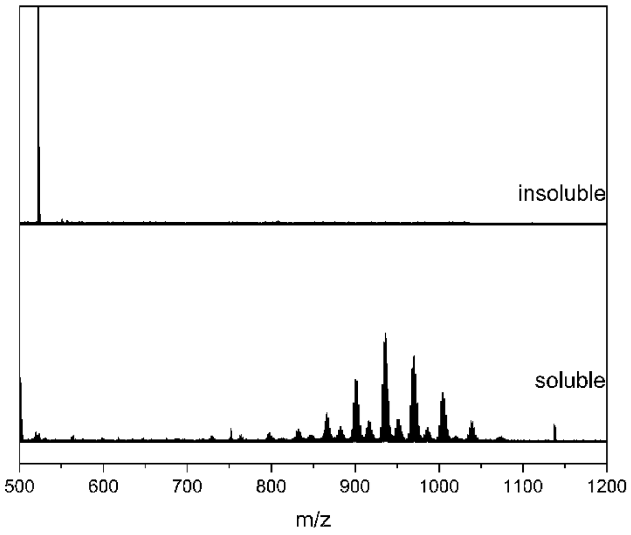

Figure Appendix 26 MALDI-TOF spectra of the edge-chlorination conducted with $FeCl_3$.

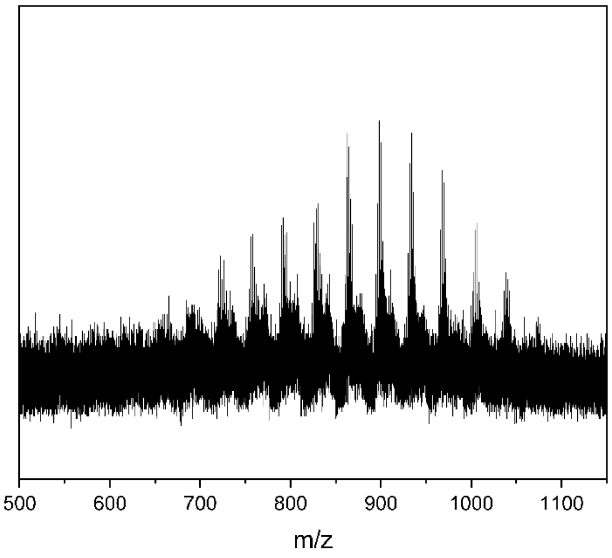

Figure Appendix 27 MALDI-TOF spectra of the edge-chlorination conducted with ICL, $AlCl_3$.

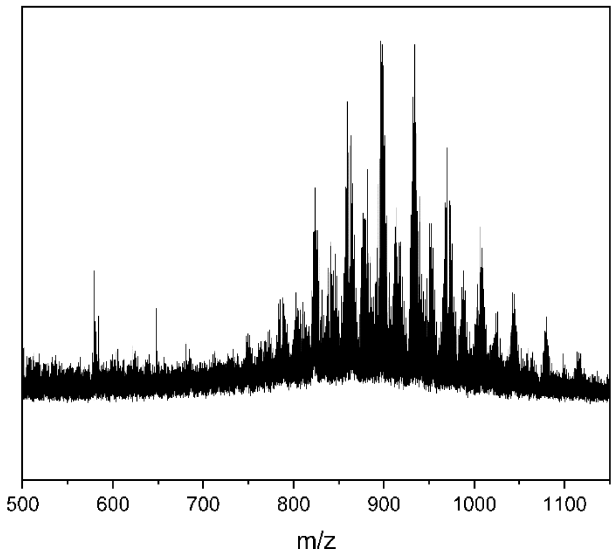

Figure Appendix 28 MALDI-TOF spectra of the edge-chlorination conducted with $C_3Cl_3N_3O_3$.

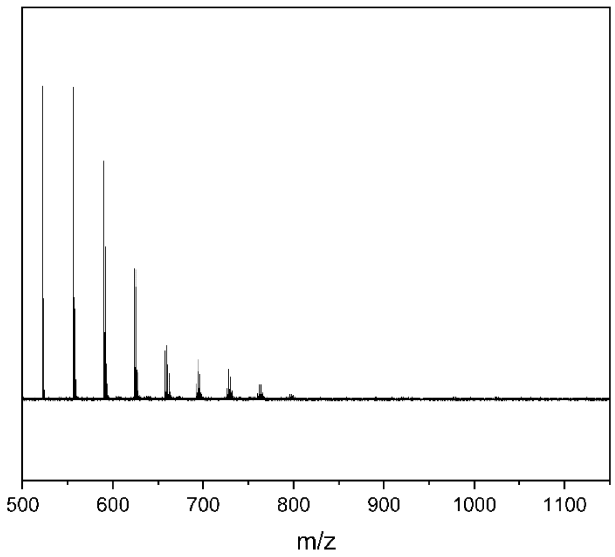

Figure Appendix 29 MALDI-TOF spectra of the edge-chlorination conducted with NCS.

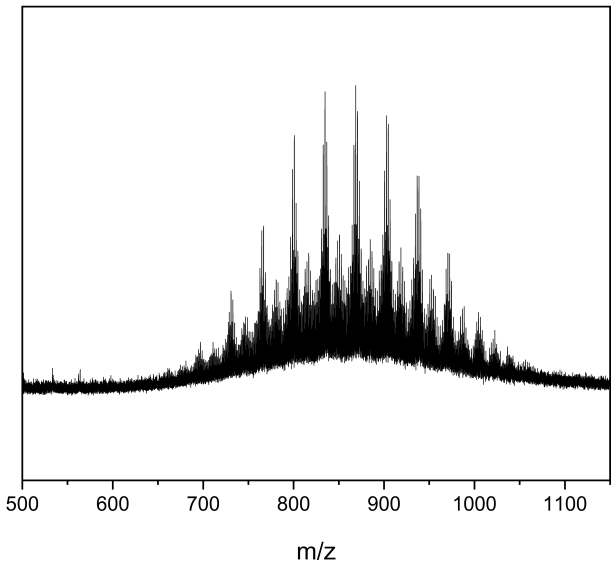

Figure Appendix 30 MALDI-TOF spectra of the edge-chlorination conducted with Oxone.

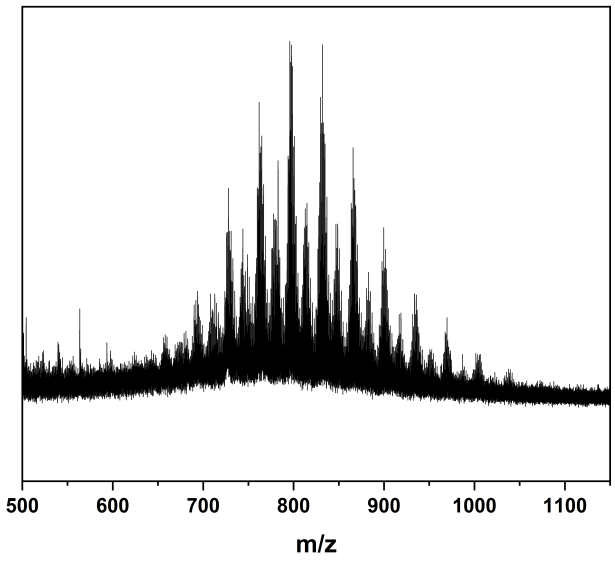

Figure Appendix 31 MALDI-TOF spectra of the one-pot edge-chlorination conducted with $C_3Cl_3N_3O_3$.

9.2 TABLE OF FIGURES

9.3 TABLE OF TABLES

10 CURRICULUM VITAE

Education

10/2015–(09/2018)	Technical University of Dresden, Dresden (Germany) PhD candidate in the group of Professor Kaskel • Mechanochemical synthesis of carbon materials and polymers • *In-situ* investigation of the formation of methane hydrate in carbon materials (XRD, SANS)
11/2014–09/2015	Leibniz-Institut für Polymerforschung Dresden e.V, Dresden (Germany) Research placement and Master thesis in the group of Professor Voit • Synthesis and characterization of cyanate esters from poly(pentadienone) derivates
09/2012–09/2015 (France)	European School for Chemistry, Polymers and Material Sciences (ECPM), Strasbourg German-French double diploma program • Specialized in polymer chemistry and engineering • Obtained a Bachelor equivalent and a Diplôme d'ingénieur (engineering diploma)
10/2010–09/2015	Technische Universität Dresden, Dresden (Germany) Bachelor and Master of Science in chemistry • Lectures: Inorganic, organic, physical, analytic, bio and polymer chemistry, toxicology, law • Lab work supporting the lectures covered about 50% of the time
2004–2008	Abitur (A-Levels) at the Georgius-Agricola-Gymnasium in Chemnitz (Germany) • Grade: 1.7 (B grade)

Experience

10/2015–(03/2019)	Technical University of Dresden, Dresden (Germany) Research assistant in the group of Professor Kaskel • Supervised seminars and lab work on a Bachelor and Master level • Supervised Bachelor and Master theses • Was in charge of the ball mills, DLS and physisorption devices
06/2013–08/2013	Dow Europe GmbH, Horgen (Switzerland) Work placement in the R&D-department for hot-melt adhesive for hygiene products • Benchmarked commercial adhesives and developed new adhesive formulations • Conducted and interpreted tensile, viscosity and DSC measurements • Developed a screening test for the optimization of mechanical properties
06/2013–08/2013	Ritz Instrument Transformers GmbH, Ottendorf-Okrilla (Germany) Work placement in the R&D-department of casting resin containing fillers • Analysed the influence of the method of agitation on the material properties
04/2011–07/2012	Technical University of Dresden (Germany) Student research assistant in the research group of Professor Kaskel • Synthesized porous carbon with hierarchical porosity
07/2008–06/2010	German Armed Forces National service and training as reserve officer, lieutenant of the reserve • Led a group of 14 recuts through basic training • Completed training as an engineer officer in charge of a platoon (around 40 people)

Languages

German	native speaker
English	fluent (CEFR–C2; TOEIC 990/990)
French	intermediate (CEFR–B2, TFI 775/990)
Russian	beginner (CEFR-A2)

Computer skills

Origin (incl. LabTalk), ChemDraw 12.0, SciFinder, Webdesign (HTML/PHP), C++ (Basics), Mendeley, Reaxys

Interests

Handball	Have been playing in a team since 1998 with only brief interruptions
Inline Skating	Have participated in the Berlin marathon in 2011,2012 and 2017
Winter sports	Have been skiing and snowboarding since 1996
Gardening	Enjoy relaxing in my garden, growing fruits and vegetables

11 LIST OF PUBLICATIONS OF SVEN GRÄTZ M.SC.

11.1 PEER-REVIEWED JOURNAL PUBLICATIONS

1.) Borchardt, L., Oschatz, M., Graetz, S., Lohe, M. R., Rümmeli, M. H., & Kaskel, S. (2014). A hard-templating route towards ordered mesoporous tungsten carbide and carbide-derived carbons. Microporous and Mesoporous Materials, 186, 163-167.

2.) Grätz, S., & Borchardt, L. (2016). Mechanochemical polymerization–controlling a polycondensation reaction between a diamine and a dialdehyde in a ball mill. RSC Advances, 6(69), 64799-64802.

3.) Nichterwitz, M., Grätz, S., Nickel, W., & Borchardt, L. (2017). Solvent-free hierarchization of zeolites by carbochlorination. Journal of Materials Chemistry A, 5(1), 221-229.

4.) Troschke, E., Grätz, S., Borchardt, L., Haubold, D., Senkovska, I., Eychmueller, A., & Kaskel, S. (2017). Salt templated synthesis of hierarchical covalent triazine frameworks. Microporous and Mesoporous Materials, 239, 190-194.

5.) Grätz, S., Wolfrum, B., & Borchardt, L. (2017). Mechanochemical Suzuki polycondensation–from linear to hyperbranched polyphenylenes. Green Chemistry, 19(13), 2973-2979.

6.) Troschke, E., Grätz, S., Lübken, T., & Borchardt, L. (2017). Mechanochemical Friedel–Crafts alkylation—A sustainable pathway towards porous organic polymers. Angewandte Chemie, 129(24), 6963-6967.

7.) Zhang, E., Hao, G. P., Casco, M. E., Bon, V., Grätz, S., & Borchardt, L. (2018). Nanocasting in ball mills–combining ultra-hydrophilicity and ordered mesoporosity in carbon materials. Journal of Materials Chemistry A.

8.) Leistenschneider, D., Zürbes, K., Schneidermann, C., Grätz, S., Oswald, S., Wegner, K., ... & Borchardt, L. (2018). Mechanochemical Functionalization of Carbon Black at Room Temperature. C, 4(1), 14.

9.) Grätz, S., Beyer, D., Tkachova, V., Hellmann, S., Berger, R., Feng, X., & Borchardt, L. (2018). The mechanochemical Scholl reaction–a solvent-

free and versatile graphitization tool. Chemical Communications, 54(42), 5307-5310.

10.) Grätz, S., Oltermann, M., Troschke, E., Paasch, S., Krause, S., Brunner, E., & Borchardt, L. (2018). Solvent-Free Synthesis of a Porous Thiophene Polymer by Mechanochemical Oxidative Polymerization. Journal of Materials Chemistry A.

11.) Casco, M. E., Badaczewski, F., Grätz, S., Tolosa, A., Presser, V., Smarsly, B., & Borchardt, L. (2018). Mechanochemical synthesis of porous carbon at room temperature with a highly-ordered sp 2 microstructure. Carbon.

12.) Leistenschneider, D., Schneidermann, C., Hippauf, F., Grätz, S., & Borchardt, L. (2018). The „In-situ electrolyte" concept – Using activation chemicals as electrolytes for carbon-based supercapacitors. Advanced Sustainable Systems, accepted

11.2 Book Contributions

2018 "Handbuch Chemische Reaktoren: Grundlagen und Anwendungen der Chemischen Reaktionstechnik" W. Reschetilowski
Springer, Germany 2018
Chapter: "Reaktoren für spezielle technisch-chemische Prozesse: Tribochemische Reaktoren"
L. Borchardt, S. Grätz

11.3 Conference Contributions

11.3.1 Oral Presentations as Presenting Author

23.-28.07.2017 The World Conference on Carbon 2017, Melbourne, Australia
Title: „Mechanochemical Suzuki Polycondensation – from Linear to Porous Carbonaceous Polymers"
S. Grätz, B. Wolfrum, L. Borchardt

26.-29.06.2018 8th Graphene Conference 2018, Dresden, Germany
Title: „Nanographenes by Solvent-free Syntheses – The Mechanochemical Scholl Reaction"
S. Grätz, S. Beyer, V. Tkachova, S. Hellmann, R. Berger, X. Feng, L. Borchardt

01.-06.07.2018 The World Conference on Carbon 2018, Madrid, Spain
Keynote Lecture
Title: „Nanographenes by Solvent-free Syntheses – The Mechanochemical Scholl Reaction"
S. Grätz, S. Beyer, V. Tkachova, S. Hellmann, R. Berger, X. Feng, L. Borchardt

11.3.2 **Poster Presentations as Presenting Author**

11.-15.09.2016	6th European Chemistry Congress, Sevilla, Spain Title: „Mechanochemical Polymerization–Controlling a Polycondensation Reaction in a Ball Mill" S. Grätz, L. Borchardt
01.-03.03.2017	29th German Zeolite Conference, Frankfurt am Main, Germany Title: „Solvent-free hierarchization of zeolites by carbochlorination" S. Grätz, M. Nichterwitz, L. Borchardt
14.-17.05.2017	2nd Green & Sustainable Chemistry Conference, Berlin, Germany Title: „Mechanochemical Suzuki Polycondensation – from Linear to Porous Carbonaceous Polymers" S. Grätz, B. Wolfrum, L. Borchardt
23.-28.07.2017	The World Conference on Carbon 2017, Melbourne, Australia Title: „Mechanochemical Friedel-Crafts-Alkylation – a sustainable pathway towards porous organic polymers" E. Troschke, S. Grätz, T. Lübken, M. Casco, L. Borchardt
29.08.2017	Workshop: Chemistry of 2D Materials, Dresden, Germany Title: „A Solid-State Pathway towards Covalent Organic Frameworks Polymerization Reactions in Planetary Ball Mills" S. Grätz, E. Troschke, B. Wolfrum, L. Borchardt
28.02-02.03.2018	30th German Zeolite Conference, Kiel, Germany Title: „Mechanochemical Oxidative Polymerization towards Microporous Polymers" S. Grätz, M. Oltermann, E. Troschke, L. Borchardt

11.4 PATENTS

L. Borchardt, D. Leistenschneider, S. Grätz, C. Schneidermann: „Kohlenstoffkompositformteil, Verfahren zu dessen Herstellung und Verwendung des Kohlenstoffkompositformteils in einem elektrochemischen Energiespeicher“ Deutsche Patentanmeldung 2018, DE102018001617

12 Erklärung gemäß §5 Abs. 1 Punkt 5

§5 Abs. 1 Punkt 5a

Versicherung

Hiermit versichere ich, dass ich die vorliegende Arbeit ohne unzulässige Hilfe Dritter und ohne Benutzung anderer als der angegebenen Hilfsmittel angefertigt habe; die aus fremden Quellen direkt oder indirekt übernommenen Gedanken sind als solche kenntlich gemacht. Die Arbeit wurde bisher weder im Inland noch im Ausland in gleicher oder ähnlicher Form einer anderen Prüfungsbehörde vorgelegt.

§5 Abs. 1 Punkt 5b

Die vorliegende Arbeit wurde am Institut für Anorganische Chemie der Technischen Universität Dresden im Zeitraum von Oktober 2015 bis September 2018 als eingeschriebener Promotionsstudent und unter wissenschaftlicher Betreuung von Herrn Dr. L. Borchardt und Herrn Prof. Dr. S. Kaskel angefertigt.

Datum, Unterschrift